Overview: On the transport and transformation of pollutants in the outflow of major population centres - observational data from the EMeRGe European intensive operational period in summer 2017

M. Dolores~~D.~~ Andrés Hernández[1], Andreas Hilboll[2,†], Helmut Ziereis[3], Eric Förster[4], Ovid O. Krüger[5], Katharina Kaiser[6,7], Johannes Schneider[7], Francesca Barnaba[8], Mihalis Vrekoussis[2,18], Jörg Schmidt[9], Heidi Huntrieser[3], Anne-Marlene Blechschmidt[1], Midhun George[1], Vladyslav Nenakhov[1,*], Theresa ~~Klausner[3]~~Harlass[3], Bruna A. Holanda[5], Jennifer Wolf[3], Lisa Eirenschmalz[3], Marc Krebsbach[10], Mira L. Pöhlker[5,**,~~,~~] Anna Beata K. Hedegaard[3,2]~~B. Hedegaard[2]~~, Linlu Mei[1], Klaus Pfeilsticker[11], Yangzhuoran Liu[1], Ralf Koppmann[10], Hans Schlager[3], Birger Bohn[12], Ulrich Schumann[3], Andreas Richter[1], Benjamin Schreiner[11], Daniel Sauer[3], Robert Baumann[3], Mariano Mertens[3], Patrick Jöckel[3], Markus Kilian[3], ~~—~~Greta Stratmann[3,***,~~,~~~~**,~~] Christopher Pöhlker[5], Monica Campanelli[8], Marco Pandolfi[13] Michael Sicard[14,15], José ~~J.~~L. Gómez-Amo[16], Manuel Pujadas[17], Katja Bigge[11], Flora Kluge[11], Anja Schwarz[9], Nikos Daskalakis[2], David Walter[5], Andreas Zahn[4], Ulrich Pöschl[5], Harald Bönisch[4], Stephan Borrmann[6,7], Ulrich Platt[11], and John Phillip Burrows[1]. ~~,~~ ~~*and the EMeRGe community.*~~

[1]Institute of Environmental Physics, University of Bremen, Bremen, Germany
[2]Laboratory for Modeling and Observation of the Earth System, Institute of Environmental Physics, Bremen, Germany.
[3]Deutsches Zentrum für Luft- und Raumfahrt (DLR), Institut für Physik der Atmosphäre, Oberpfaffenhofen, Germany
[4]Karlsruhe Institute of Technology, Institute of Meteorology and Climate Research, Karlsruhe, Germany
[5]Multiphase Chemistry Department, Max Planck Institute for Chemistry, Mainz, Germany
[6]Institute for Atmospheric Physics, Johannes Gutenberg University, Mainz, Germany
[7]Particle Chemistry Department, Max Planck Institute for Chemistry, Mainz, Germany
[8]National Research Council of Italy, Institute of Atmospheric Sciences and Climate (CNR-ISAC), Roma, Italy
[9]Leipzig Institute for Meteorology, Leipzig University, Leipzig, Germany
[10] Institute for Atmospheric and Environmental Research, University of Wuppertal, Wuppertal Germany
[11]Institute for Environmental Physics, University of Heidelberg, Heidelberg, Germany
[12]Institute of Energy and Climate Research IEK-8, Forschungszentrum Jülich, Jülich, Germany
[13]Institute of Environmental Assessment and Water Research, Barcelona, Spain
[14]CommSensLab, Dept. of Signal Theory and Communications, Universitat Politècnica de Catalunya, Barcelona, Spain
[15]Ciències i Tecnologies de l'Espai-Centre de Recerca de l'Aeronàutica i de l'Espai/Institut d'Estudis Espacials de Catalunya), Universitat Politècnica de Catalunya Barcelona, Spain
[16]Dept. Earth Physics and Thermodynamics, University of Valencia, Burjassot, Spain
[17]Centro de Investigaciones Energéticas, Medioambientales y Tecnológicas (Ciemat), Madrid, Spain
[18]Climate and Atmosphere Research Center (CARE-C), The Cyprus Institute, Nicosia, Cyprus
*now at Flight Experiments, Deutsches Zentrum für Luft- und Raumfahrt (DLR), Oberpfaffenhofen, Germany
** now at Faculty of Physics and Earth Sciences, Leipzig Institute for Meteorology, University of Leipzig/ Experimental Aerosol and Cloud Microphysics Department, Leibniz Institute for Tropospheric Research, Leipzig, Germany

*****now at Deutsches Elektronen-Synchrotron DESY, Notkestr. 85, 22607 Hamburg, Germany
† deceased

Correspondence to: M.D.Andrés Hernández (lola@iup.physik.uni-bremen.de)

Abstract. Megacities and other major population centers (MPCs) worldwide are major sources of air pollution, both locally as well as downwind. The overall assessment and prediction of the impact of MPC pollution on

tropospheric chemistry are challenging. The present work provides an overview of the highlights of a major new contribution to the understanding of this issue based on the data and analysis of the EMeRGe (**E**ffect of **Me**gacities on the transport and transformation of pollutants on the **R**egional to **G**lobal scal**e**s) ~~is an~~ international project. EMeRGe focuses ~~focusing~~ on atmospheric chemistry, dynamics and transport of local and regional pollution originating in ~~megacities and other major population centres (~~MPCs.~~).~~ Airborne measurements, taking advantage of the long range capabilities of the ~~HALO research platform (~~High altitude~~Altitude~~ and long~~Long~~ range research aircraft (HALO, www.halo-spp.de), are a central part of the ~~research~~ project. The synergistic use and consistent interpretation of observational data sets of different spatial and temporal resolution (e.g. from ground-based networks, airborne campaigns, and satellite measurements) supported by modelling within EMeRGe, provides a unique insight to test the current understanding of MPC pollution outflows.

In order to provide an adequate set of measurements at different spatial scales, two field experiments were positioned in time and space to contrast situations when the photochemical transformation of plumes emerging from MPCs is large. These experiments were conducted in summer 2017 over Europe and in the inter-monsoon period over Asia in spring 2018. The intensive observational periods (IOP) involved HALO airborne measurements of ozone and its precursors, volatile organic compounds, aerosol particles and related species as well as coordinated ground-based ancillary observations at different sites. Perfluorocarbon (PFC) tracer releases and model forecasts supported the flight planning, ~~and~~ the identification of pollution plumes, and the analysis of chemical transformations during transport.

This paper describes the experimental deployment and scientific questions of the IOP in Europe~~, which comprised 7 HALO research flights with aircraft base in Oberpfaffenhofen (Germany) for a total of 53 flight hours~~. The MPC targets London (Great Britain), Benelux/Ruhr area (Belgium, The Netherlands, Luxembourg and Germany), Paris (France), Rome and Po Valley (Italy), Madrid and Barcelona (Spain) were investigated during 7 HALO research flights with aircraft base in Germany for a total of 53 flight hours.~~.~~ An in-flight comparison of HALO with the collaborating UK-airborne platform FAAM took place to assure accuracy and comparability of the instrumentation on-board.

Overall, EMeRGe unites measurements~~Generally, significant enhancement~~ of near~~-trace gases~~ and far-field~~aerosol particles are attributed to~~ emissions, and hence deals with complex air masses ~~originating in MPCs at distances~~ of local and distant sources. Regional transport~~hundreds~~ of several European MPC outflows was successfully identified and measured. Chemical processing of the MPC emissions was inferred~~kilometres~~ from airborne observations of primary and secondary pollutants and the ratios between species having ~~the sources. The proximity of~~ different chemical lifetimes. Photochemical processing of aerosol and secondary formation or organic acids was evident during the transport of MPC ~~MPCs over Europe favours the mixing of~~ plumes. Urban ~~of different origin and level of processing and hampers the unambiguous attribution of the MPC sources. Similarly, urban~~ plumes mix efficiently with natural sources as mineral~~desert~~ dust and with biomass burning emissions from vegetation and forest fires. This confirms the importance of wildland fire emissions in Europe and indicates an important but discontinuous contribution to the European emission budget that might be of relevance in the design of efficient mitigation strategies.

~~The synergistic use and consistent interpretation of observational data sets of different spatial and temporal resolution (e.g. from ground-based networks, airborne campaigns, and satellite measurements) supported by modelling within EMeRGe, provides a unique insight to test the current understanding of MPC pollution outflows.~~ The present work provides an overview of the most salient results ~~and scientific questions~~ in the

European context, these being addressed in more detail within additional dedicated EMeRGe studies. The deployment and results obtained in Asia will be the subject of separate publications.

1 Introduction

In recent decades, the number and size of major population centres (MPCs) have increased dramatically. The term MPC describes a single metropolitan area or converging urban conurbations with a population exceeding 10 million inhabitants. In 1950, New York and Tokyo were the only two megacities in the world (Gardi, 2017) whereas for 2018 the United Nations reported 33 megacities and 48 urban agglomerations of 5 to 10 million inhabitants (UN, 2019). One cause of the recent growth of the number of MPCs is the rapid industrialisation of some parts of the world, in particular East Asia.

The economic consequences of urbanisation, the spatial growth of MPCs, and, in particular, the environmental and economical sustainability of megacities, have been a focus of recent discussion (ESPAS, 2018; Melchiorri et al., 2018; Hoole et al., 2019; Odendahl et al., 2019). The MPC has occasionally been presented as a favourable urban model~~,~~ because the concentration of resources and services and the development of more effective mitigation strategies make it potentially less harmful for the environment than other more dispersed population distributions (Grimm, 2008; Dodman, 2009). Nevertheless~~However~~, the agglomeration of emissions from fossil fuel combustion~~power required~~ for transport, industrial and domestic purposes~~, which is mostly generated from fossil fuel combustion~~, makes MPCs a growing and globally significant emission source of trace gases and aerosol particles for the troposphere. The current knowledge on local and regional impacts of MPC pollution outflows is still limited. Decoupling the pollutant input upwind from the MPC emissions remains essential to establish accurate source-receptor relationships and effective control and mitigation policies.

The EMeRGe (Effect of Megacities on the transport and transformation of pollutants on the Regional to Global scales) project has as an overarching objective the improvement of the current understanding of photochemical and heterogeneous processing of MPC plumes along expected transport pathways. EMeRGe began in 2016 in the framework of the Priority Program of the German Research Foundation (DFG: Deutsche Forschungsgemeinschaft, www.halo-spp.de) to exploit the High Altitude and Long range research aircraft (HALO) for atmospheric science.

EMeRGe has a focus on airborne measurements and fostered cooperation with an international research partnership (hereinafter referred to as EMeRGe international) to facilitate the delivery and comprehensive analysis of a unique set of data from aircraft-, ground- and satellite-based sensors. The institutions currently involved in EMeRGe and EMeRGe international are listed in the supplementary information (see S1 and S2).

Europe and Asia are regions of the world with a differing heritage of pollution control strategies and notable differences in the number, size and proximity of MPCs as well as in the nature of emissions. For this reason, two field experiments were designed in EMeRGe to investigate the transport and transformation processes of pollution plumes originating from European and Asian MPCs. The first intensive observational period (IOP) was carried out in Europe from 10 to 28 July 2017 with special focus on the study of active plume processing close to emission sources. The second IOP aimed at the investigation of long-range transport (LRT) of MPC outflows from the Asian continent to the Pacific during the spring inter-monsoon period and took place with HALO base in Taiwan from 10 March to 9 April 2018.

The present article describes the experimental design and specific objectives of the IOP of EMeRGe in Europe. It highlights key research questions and some of the scientific results, which are further explored in dedicated publications.

2 Background

High levels of urbanisation are associated with severe air pollution events which lead to adverse effects on human health (Lelieveld et al., 2015, 2020). ~~Frequent exposure to poor air quality affects the respiratory, cardiovascular and neurocognitive systems, and is associated with cancer and premature death. The World Health Organisation has reviewed (WHO, 2013) the scientific evidence for the health risk from particulate matter (PM), and trace gases such as ozone (O_3), carbon monoxide (CO), nitrogen dioxide (NO_2), sulphur dioxide (SO_2), metals (e.g. arsenic, lead and mercury) and polycyclic aromatic hydrocarbons (PAH).~~ The effects of pollution originating from MPCs and the development of adequate control strategies are receiving growing attention as the public concern about air quality and the interaction of pollution and climate on a warming planet increases (e.g., Jacob and Winner, 2009). In that respect, the MPC emissions of environmental interest are aerosol particles, which contain sulphate (SO_4^{2-}) and nitrate (NO_3^-), particulate organic matter (POM), black carbon (BC), and ammonium (NH_4^+), carbon monoxide (CO) and long-lived greenhouse gases (GHG) such as carbon dioxide (CO_2) and methane (CH_4). The net radiative effect of the aerosol particles largely depends on the size and chemical composition which determine their scattering and absorption capabilities (e.g., Haywood and Boucher, 2000). As cloud condensation nuclei (CCN) they have an additional effect on the optical properties and lifetime of clouds (e.g. Andreae and Rosenfeld, 2008; Campos Braga et al., 2017; Rosenfeld et al., 2008). Short-lived constituents of smog, such as nitrogen oxides (NO_x, i.e., NO and NO_2), volatile organic compounds (VOC), and sulphur dioxide (SO_2), react to produce ozone (O_3)~~produce~~O_3 and secondary aerosol particles and also have a climatic effect (UNEP, 2011; Mar, 2021).

~~The impact of aerosol particles on climate change has been investigated in detail (e.g. Pöschl, 2005; IPCC report, 2014). The aerosol net radiative effect largely depends on the size and chemical composition of the aerosol particles which determine their scattering and absorption capabilities (e.g., Haywood and Boucher, 2000). Furthermore, aerosol particles act as cloud condensation nuclei (CCN) and modify the optical properties and lifetime of clouds. Anthropogenic aerosol is known to increase the number of cloud droplets while decreasing their sizes (e.g. Andreae and Rosenfeld, 2008; Campos Braga et al., 2017 and references therein). This results in extended cloud lifetimes, suppressing precipitation (Rosenfeld et al., 2008). Consequently, an accurate representation of mass and number concentration, size distribution and chemical composition of particles in models is essential to assess climatic change (Reddington et al., 2013).~~

Primary MPC emissions are transported and transformed into secondary pollutants such as O_3 or secondary ~~organic~~ aerosols (organic and inorganic~~SOA~~) and lead to smog episodes downwind of the source. Modelling studies using artificial aerosol tracers and estimations of deposition potentials, indicate that about 50% of MPC emitted particles with diameter ≤2.5 μ~~-~~m ($PM_{2.5}$) deposit more than 1000 km from their source (Kunkel et al., 2012). Chemical and physical processing of MPC emitted pollutants can in turn be affected by mixing with natural, biogenic and other anthropogenic emissions from regional sources or long-range transported from other areas (Lawrence et al., 2007, Monks et al., 2009, Lawrence and Lelieveld, 2010, and references therein).

The specific impact of the plumes from MPCs, therefore, depends not only on the type of emission sources (e.g. industry, transportation~~traffic~~, domestic heating, and generation of electricity) but also on the variability of trace constituent emissions, the local meteorology and topography. ~~The impact of MPC pollution on the atmospheric~~

composition has been summarised by Zhu et al., (2012). In spite of the growing number of measurements campaigns, improved monitoring and modelling capabilities and the results achieved in the last decades, this review identifies important unresolved issues which limit the assessment of the impact of megacities on air quality and climate. Some examples are:

- the inaccurate modelling of the global effect of MPCs on anthropogenic emissions resulting from the current inconsistent local and regional MPC emission inventories (Denier van der Gon et al.; 2011, Mayer et al., 2000; Butler and Lawrence, 2009), Modelling
- the insufficient sub-grid parametrisation of MPCs in models,
- the inadequate characterisation of pollution transport patterns, and,
- the inaccurate prediction of cumulative pollution events observed in downwind regions of MPCs (Zhang et al., 2007; Kunkel et al., 2012).

In addition, modelling studies indicate that the combined effect of near-surface wind speeds and convection leads to significant latitudinal differences in regional to hemispheric dispersion characteristics (Lawrence et al., 2007 and references therein; Cassiani et al., 2013).2013). Plumes emitted at higher latitudes are probably subject to faster transport than outflows from tropical or sub-tropical MPC, travel larger distances and for time-scales exceeding ten days. Transport and transformation of MPC outflows are affected by the general weather patterns such as frontal passages and the frequency and duration of stagnation episodes, which are important for pollutant ventilation. In The predicted changes in these patterns indicate that future air quality in MPCs will generally be less influenced by local emission sources than by the last decades, improved monitoringmixing of anthropogenic and modelling capabilitiesnatural emissions outside the MPC (Butler et al., 2012).

In summary, the overall assessment and a growing number of measurements campaigns have provided essential information about the prediction of the impact of MPC pollution emitted by MPCs on the atmospheric composition (see review by Zhu et al., 2012). However, capturing the combined influence of emissions,tropospheric chemistry are challenging. Medium and dynamics for specific locations is still a big challenge. In particular, inconsistencies in long-term effects of anthropogenic emissions and their interaction with natural and biogenic emissions in the local and regional MPC inventories (e.g. surroundingsDenier van der Gon et al.; 2011, Mayer et al., 2000; Butler and Lawrence, 2009), and limitations in the prediction capabilities of pollution transport patterns and cumulative pollution events in downwind regions of MPCs (Zhang et al., 2007; Kunkel et al., 2012) require ongoing attention. Furthermoreindividual MPCs are poorly understood and imprecisely quantified. In addition, controlling policies, changes in land cover and climate continue to evolve and is expected tomight substantially modify the relation between anthropogenic emissions and both natural aerosol and trace gases, as predicted by e.g., Butler et al., (2012), and recently reported for East Asia (Fu et al., 2016; Silver et al., 2018 and references herein; Leung et al., 2018). Decoupling the pollutant input upwind from the MPC emissions remains essential to establish accurate source-receptor relationships and effective control and mitigation policies. The current knowledge on all these aspects is still insufficient.

1.1 Overarching objective of EMeRGe and methodology

The EMeRGe (Effect of Megacities on the transport and transformation of pollutants on the Regional to Global scales) project began in 2016 and is part of the Priority research program of the German Research Foundation (DFG: Deutsche Forschungsgemeinschaft, www.halo-spp.de) to exploit the High Altitude and Long range research aircraft (HALO) for atmospheric science. EMeRGe has as an overarching objective the improvement of

~~the current understanding of photochemical and heterogeneous processing of MPC plumes along expected transport pathways. This knowledge is required to assess the local and regional impacts of MPC outflows.~~

~~EMeRGe has a focus on airborne measurements and fostered cooperation with an international research partnership (hereinafter referred to as EMeRGe international) to facilitate the delivery and comprehensive analysis of a unique set of data from aircraft-, ground- and satellite-based sensors. The institutions currently involved in EMeRGe and EMeRGe international are listed in the supplementary information (see S1 and S2).~~

~~Europe and Asia are regions of the world with a differing heritage of pollution control strategies and notable differences in the number, size and proximity of MPCs as well as in the nature of emissions. For this reason, two field experiments were designed in EMeRGe to investigate the transport and transformation processes of pollution plumes originating from European and Asian MPCs. The first intensive observational period (IOP) was carried out in Europe from 10 to 28 July 2017 with special focus on the study of active plume processing close to emission sources. The second IOP aimed at the investigation of long-range transport (LRT) of MPC outflows from the Asian continent to the Pacific during the spring inter-monsoon period and took place with HALO base in Taiwan from 10 March to 9 April 2018.~~

~~EMeRGe aims to identify emission signatures and pollution hot spots by relating observations of pollutants to simulations and air mass trajectories. Chemical processing of the MPC emissions during transport is evaluated from the measurement of aerosol particles and trace gases. In particular O_3 and its precursors provide information about the photochemical activity and the transformation of primary into secondary pollutants within the MPC outflows. Furthermore, measurements at different altitudes downwind of selected MPCs are required for the identification of plume transport. Mixing of MPC plumes with biomass burning (BB) and mineral dust transport events and / or convection processes might have an impact in the processing of the MPC outflows. Finally, the accuracy and suitability of atmospheric chemistry models is investigated by comparing EMeRGe observations with dedicated simulations from state-of-the-art global and regional atmospheric chemistry models.~~

~~The present article describes the experimental design and specific objectives of the IOP of EMeRGe in Europe. It highlights key research questions and some of the scientific results, which are further explored in~~ 2018).

In Europe, the level of urbanisation~~forthcoming papers.~~

~~2 EMeRGe in Europe~~

~~2.1 MPC pollution in Europe~~

~~The level of urbanisation in Europe~~ is presently ~ 74% and is expected to further increase by 10% up to the middle of this century (UN, 2019). Large urban conurbations are ~~a~~ more abundant in Europe~~European urban phenomena~~ than megacities, of which there are a few. According to the European Environment Agency (EEA), the emission of air pollutants and precursors has decreased across Europe from the year 2000 to the present, partly as a result of the EU air quality legislation. Emissions of CO, BC, NO_x and non-methane VOCs have been reduced by around 30% and those of sulphur oxide (SO_x, primarily SO_2) up to 77%. Nevertheless, the daily and annual O_3 and PM limit concentrations for protection of human health are often exceeded in several areas of the continent (EEA, 2019). Significant differences in pollution and photochemical episodes between Northern and Central Europe and the Mediterranean region are regularly observed, in particular due to the differences in solar actinic radiation (Kanakidou et al., 2011).

European~~Europe~~ air quality is frequently influenced by LRT of North American pollution as captured by airborne measurements and investigated in several model studies (e.g. Stohl et al., 2003; Huntrieser and Schlager, 2004; Huntrieser et al., 2005). Some evidence of LRT of Asian pollution to the Mediterranean has also been documented (Lawrence and Lelieveld, 2010; Lelieveld et al., 2002). The chemical signatures of LRT of pollutants vary depending on pollutant lifetime and mixing. Some recent modelling studies infer that the impact of non-European pollution on the European surface O_3 annual average is larger than previously expected (Jonson et al., 2018).

In recent years, large European projects such as MEGAPOLI (http://megapoli.dmi.dk) and CityZen (Megacity-Zoom for the Environment; http://www.cityzen-project.eu), provided comprehensive theoretical and experimental data about MPCs in Europe. The MEGAPOLI field campaign was conducted in Paris in summer 2009 and winter 2010 (Beekmann et al., 2015) and investigated source apportionment and photochemical processing of emitted gaseous and particulate substances using several ground-based stations and measurement vehicles (Crippa et al., 2013; Freutel et al., 2013; von der Weiden-Reinmüller et al., 2014). Beekmann et al., (2015) estimated the impact of the urban emissions from the Paris megacity to be relatively low in comparison to other external industrial sources of pollution. Aircraft measurements were restricted to the near-field outflow (up to 200 km) in the boundary layer below 700 m asl (Brands et al., 2011; Freney et al., 2014). In comparison, EMeRGe focuses on the impact of different MPCs in Central~~middle~~ and Southern Europe and investigates atmospheric pollution plumes over much larger geographical extent~~latitudinal and longitudinal scales~~.

CityZen (2008-2011) studied air pollution in and around selected megacities and emission hotspots by using in-situ and satellite observations (Hilboll et al., 2013; Vrekoussis et al., 2013) as well as a series of different scale models (Colette et al., 2011; Im et al., 2012). The project focused on selected MPCs such as the Eastern Mediterranean, the Po Valley, the Benelux region, and the Pearl River Delta for intensive case studies but, in contrast to EMeRGe, did not conduct measurements of the photochemical evolution in the outflow of the studied regions.

The above studies focused on trace gases linked to air quality and provided relatively sparse information on GHGs. Long-lived greenhouse gases such as CH_4 and CO_2 emitted from individual European urban areas have been investigated in airborne and ground-based studies, e.g. for London (O'Shea et al., 2014; Helfter et al., 2016; Pitt et al., 2019), Paris (Bréon et al., 2015; Lian et al., 2019), Cracow (Kuc et al., 2003; Zimnoch et al., 2019), Berlin (Klausner et al., 2020) and Rome (Gioli et al., 2014). Collectively, they report on inconsistencies between the current emission inventories and measurements. This indicates the need for further experimental investigation of the GHG budget in Europe.

~~The capability of chemistry transport models (CTMs) to reproduce the variability in air quality of major anthropogenic emission hot spots in Europe has been evolving and investigated (e.g. Colette et al., 2011, 2012). State-of-the-art models reasonably captured trends of primary species but the modelling of O_3 changes and projected exposure to O_3 pollution in Europe is still challenging.~~

Overall, the proximity of most European MPCs results in the mixing of different pollution plumes during their transport. This hampers the identification of the air mass origin. The impact of biomass burning (BB) and mineral dust events ~~have, moreover, a variety of impact~~ on the total European burden of atmospheric aerosol and trace gases is, moreover, variable. Particularly in Southern Europe, BB and mineral dust plumes occur frequently and can significantly affect the chemical processing of MPC pollution plumes. BB events from agriculture or wildland fires have a strong seasonal pattern and related impacts in Europe (Barnaba et al., 2011). Wildfires emit

similar to MPC large amounts of pollutants, e.g. PM, NO_x, CO, VOC and PAH (Andreae, 2019). The number and severity of wildfires are expected to increase in Europe under warmer and drier conditions as a co-effect of climate change (Forzieri et al., 2017; Guerreiro et al., 2018; Turco et al., 2018). Desert dust episodes of different intensity originating in North Africa frequently affect air mass composition and atmospheric stratification over the Mediterranean particularly in spring and summer (e.g. Barnaba and Gobbi, 2004; (Kalivitis et al., 2007; Gkikas et al., 2013; Pey et al., 2013; Pikridas et al.; 2018).), ~~in spring and in summer (Barnaba and Gobbi, 2004; Gkikas et al., 2013; Pey et al., 2013)..~~

3~~2.2~~ Specific scientific questions and characteristics of the~~relevant to~~ EMeRGe IOP in Europe

3.1 Specific scientific questions

EMeRGe in Europe focuses on three primary scientific goals addressing a series of related specific questions:

I. Identification of emission signatures in MPC plumes over Europe

- Are there individual MPC emission signatures identifiable in pollution plumes measured over Europe?
- Is it possible to unambiguously identify MPC plumes after transport times of hours or days by tagging the air masses in the source regions with passive tracers released at the surface and using airborne sensors downwind?
- Can the effect of plumes from different emission sources (e.g., anthropogenic, BB, and/or a mixture of them) on the oxidation potential of the atmosphere be inferred from changes in the NO/NO_y and NO/VOC ratios in airborne measurements?
- Can airborne measurements detect signatures of urban and other emission sources of CH_4 in Europe adequately?
- How abundant are organic acids in European MPC plumes relative to inorganic acids and what are their main sources?
- Are satellite measurements of aerosol and trace gases capable of supporting the identification of MPC plumes and dominant transport paths?

II. Investigation and assessment of chemical processing in MPC pollution outflows

- Is the photochemical activity of MPC plumes readily related to changes in concentrations of radicals and their precursors measured by the HALO sensors?
- Is the photochemical ageing of MPC plumes well described by the chemical clocks inferred from the airborne measurements of trace gases and aerosol particles?
- Can the O_3 production efficiency and NO_x -and VOC-sensitive regimes in MPC plumes be determined? How do these change with respect to the plume age and mixing with background air?
- Can the importance of the role of formaldehyde (HCHO) as an intermediate product in the oxidation of VOCs, and glyoxal ($C_2H_2O_2$) and methylglyoxal ($C_3H_4O_2$) in secondary aerosol formation be inferred from their airborne measurement in MPC pollution plumes?
- Which processes control the heterogeneous formation of HONO in polluted air masses of MPC origin in the BL and lower troposphere over Europe?

III. Assessment of the relative importance of MPCs as sources of pollution over Europe

- How important are BB and dust emissions to MPC plume photochemistry over Europe in the summer 2017?

- How do the regional CH_4 urban emission distributions in Europe compare with previous observations in the same areas?
- Is it possible to assess the relative role of primary and secondary pollutants in the proximity and in the outflow of MPCs?
- Are state-of-the-art chemical models capable of adequately simulating transport and transformation of European MPC outflows?

~~2.~~3.2 Selection of MPC targets and measurement strategy

The dominant source of NO_x and CO in the planetary boundary layer (PBL) in Europe is anthropogenic activity, primarily fossil fuel combustion and BB.~~biomass burning.~~ Cloud free monthly average tropospheric composites of NO_2 columns retrieved from GOME2-B and OMI instruments on-board the MetOp-B and Aura satellites were used to identify the major MPCs in Europe during July in the EMeRGe study. Due to its short lifetime, NO_2 is a good indicator of the origin of emission sources. The tropospheric NO_2 columns retrieved in July 2016 during the campaign preparation showed enhanced NO_2 concentrations over the megacities London, Moscow and Paris ~~megacities~~, over large urban agglomerations such as the Benelux/Ruhr metropolitan area in Central Europe and the Po Valley in Northern Italy, and over the conurbations in Southern Europe such as Rome, Naples, Madrid and Barcelona. The satellite observations during the EMeRGe IOP in 2017 confirmed the NO_2 hot spots identified (Fig. 1). ~~The differences observed are most likely related to the special weather situation in 2017, as described in Sect. 3.1.~~

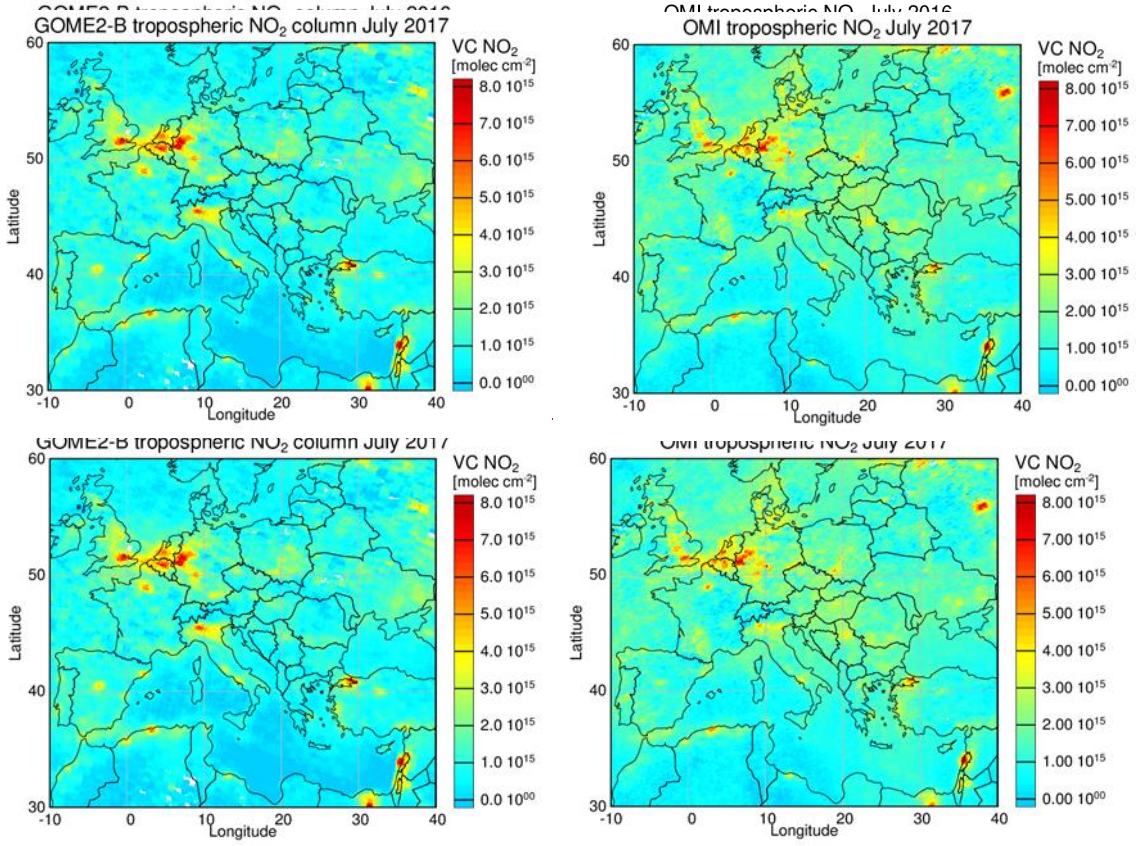

Figure 1: Satellite tropospheric NO_2 columns retrieved from GOME2-B (left panel, overpass at 9:30 h local time), and OMI (right panel, overpass at 12:45 h local time) instruments for ~~a) July 2016, a year before the EMeRGe IOP in Europe (top), and b)~~ the IOP period in July 2017. ~~(bottom).~~

CO was used in dispersion calculations to identify anthropogenic pollution from combustion. CO is a suitable tracer for transport pathways due to its relatively long atmospheric lifetime which is primarily determined~~loss~~ by the reaction with the OH radical and varies between a few weeks and a few months. To address the EMeRGe scientific objectives, the day-to-day flight planning focused on the identification of the location of the plumes from the targeted MPC outflows during potential flights. For this, the following forecast tools were exploited:

i) ECMWF (European Centre for Medium-Range Weather Forecasts, https://www.ecmwf.int/) and NCEP (National Center for Environmental Prediction, https://www.ncep.noaa.gov/) weather forecasts,

ii) NOAA (National Oceanic and Atmospheric Association) HYSPLIT (Hybrid Single Particle Lagrangian Integrated Trajectories, https://www.arl.noaa.gov/hysplit/) model for forward dispersion calculations using CO as a tracer of pollution. These forecasts, carried out by DLR (Deutsches Zentrum für Luft- und Raumfahrt), assume MPCs to be continuous emission sources and provide snap shots as well as horizontal and vertical cross sections of the selected outflows at certain times.

iii) Tailor-made CO and stratospheric ozone tracer simulations provided by CAMS (Copernicus Atmosphere Monitoring Service, http://atmosphere.copernicus.eu) through its field campaign support (see also Flemming et al., 2019).

A list of model simulations and satellite observations used for flight planning is given in Tables 1a and 1b. These are described in more detail in the supplement (see S3). The dedicated mission support tool (MSS, Mission Support System; Rautenhaus et al., 2012) provided additional assistance in the flight planning.

Table 1a: Model simulations used for flight planning during EMeRGe in Europe

Name	Type	Resolution of model output	Institution
CAMS-global (CIFS-TM5)	CTM	0.4° x 0.4°; 60 vertical levels	ECMWF
CAMS-regional ensemble	Median of 7 regional CTMs	0.1°x 0.1°; surface, 50, 250, 500, 1000, 2000, 3000, 5000 km	ECMWF
EMEP	regional CTM	0.25° E x 0.125° N; 20 vertical levels	Norwegian Meteorological Institute
HYSPLIT	Lagrangian trajectory model	0.1° x 0.1°; 20 vertical levels	NOAA/DLR
FLEXPART	Lagrangian trajectory model	1min /10 days back ECMWF-ERA5; 0.25° horizontal	NILU

Table 1b: Satellite observations used during EMeRGe in Europe

Sensor name	Satellite	Equator crossing time	Footprint	Institution
GOME-2	MetOp-B	10:30 LT	40 x 80 km^2	IUP Uni-Bremen

OMI	EOS-Aura	13:30 LT	13 x 24 km^2	IUP Uni-Bremen
SEVIRI	MSG	Geostationary	3 x 3 km^2	ICARE

The flight track and patterns available to HALO were constrained by a) flight restrictions from the air traffic authorities and special military used airspaces (SUA), and b) the unstable meteorological conditions dominating in Central Europe during the measurement period (see Sect. 3.4). ~~1).~~

Flight tracks to investigate the plumes from the MPC targets, London (Great Britain), Benelux/Ruhr area (Benelux countries and Germany, hereinafter referred to as BNL/Ruhr), Paris (France), Rome and Po Valley (Italy), and Madrid and Barcelona (Spain) were selected. It was possible to fly these flight tracks under favourable conditions typically more than once during the EMeRGe IOP, improving somewhat the representativeness of the measurements.

The HYSPLIT dispersion forecast indicated that the MPC pollution plumes targeted by EMeRGe resided predominantly below 3000 m. Consequently, the flights over Europe made use of the HALO long-endurance capabilities to fly in the PBL and incorporated vertical shuttles. Shuttles are defined here as a ~~The flight pattern involve the~~ descent or climb pattern between holding altitudes~~, coupled with long flight tracks at a given flight altitude.~~ Typically, three flight levels (FL), upwind or downwind of the target MPCs were~~are~~ part of the shuttle. Some of the MPC outflows were tagged by a coordinated release of a perfluorocarbon (PFC) tracer at the ground (see S5).. Details about flight tracks and flight regions are provided in Sect. 3.6.~~Sect. 2.4.2).~~

3.3 EMeRGe instrumentation

~~All HALO flights started from the DLR base Oberpfaffenhofen (OP), located Southwest of Munich in Germany. The flights are named E-EU-FN, where E stands for EMeRGe, EU for Europe and FN are the two digits of the flight number. Details about flight tracks and flight routes are provided in Sect. 3.3.~~

~~2.4 EMeRGe instrumentation~~

~~The pollutant measurements made aboard HALO were enhanced during the EMeRGe IOP in Europe by coordinated flights with other airborne sensors, complementary ground based measurements and model predictions. In this manner, the EMeRGe international cooperation provided additional aircraft-, satellite- and ground based observations and modelling studies during the preparation and execution phases of the EMeRGe IOP in Europe, as described in the following sections.~~

~~2.4.1 HALO payload~~

A key element of the EMeRGe data are the airborne measurements made on-board HALO, a Gulfstream G550 business jet modified and specifically equipped for scientific research (see www.halo.dlr.de). The HALO payload for EMeRGe comprises a set of state-of-the-art instrumentation for the measurement of trace gases and aerosol particles. Table 2 summarises target species and parameters measured by the instruments installed on-board HALO, which are complemented by the HALO ancillary measurements (BAHAMAS, see S4 in the supplement) during the EMeRGe campaign in Europe. The pollutant measurements made aboard HALO were

enhanced with tracer experiments using perfluorocarbon compounds (PFCs). Details are provided in the supplement (see S5).

During the EMeRGe IOP in Europe the EMeRGe international cooperation provided additional coordinated aircraft-, satellite- and ground-based observations and modelling studies during the preparation and execution phases of the EMeRGe IOP in Europe, as described in the supplement (see S6). To assure the accuracy and comparability of the instrumentation on-board one research flight on 13 July 2017 was dedicated to common and simultaneous measurements of HALO and the Facility for Airborne Atmospheric Measurements (FAAM, www.faam.ac.uk) from the UK Natural Environment Research Council in a so-called blind intercomparison exercise (see S7 in supplement).

Table 2: HALO instrumental payload for EMeRGe: PeRCA: Peroxy Radical Chemical Amplification; CRDS: Cavity Ring-Down Spectroscopy; HVS: High Volume Sampler; GC-C-IRMS: Gas Chromatography Combustion Isotope Ratio Mass Spectrometry; PTR-MS: Proton-Transfer-Reaction Mass Spectrometer; CI-ITMS: Chemical Ionisation Ion Trap Mass Spectrometry; GC-MS: Gas chromatography-mass spectrometry analysis; PAN: Peroxyacetyl nitrate; $\delta^{13}C(CH_4)$: Isotopic signature of methane; PFC: Perfluorinated carbon chemicals; DOAS: Differential Optical Absorption Spectrometry; AT-BS: Adsorption Tube and Bag air Sampler; TD-GC-MS: Thermal Desorption Gas Chromatography and Mass Spectrometry; ToF-AMS: Time of Flight- Aerosol Mass Spectrometry; SP2: Single Particle Soot PhotometerPhotometry; CCNC: Cloud Condensation Nuclei CounterNucleus Counting; MI: Multi Impactor for aerosol off-line analysis; CPC: Condensation Particle CounterCounting; DMA: Differential Mobility AnalyserAnalysis; OPC: Optical Particle CounterCounting; PSAP: Particle Soot Absorption PhotometerPhotometry. See details and HALO ancillary measurements in the supplement. The instrument details are given in the quoted literature.

Trace gas-in situ measurements				
Species/parameters	Acronym	Institution	Technique/Instrument	Reference
$RO_2^* = HO_2 + \sum RO_2$	PeRCEAS	Univ. Bremen	PeRCA + CRDS	George et al., 2020
VOC/C isotope ratios	MIRAH	Univ. Wuppertal	HVS/GC-C-IRMS	Wintel et al., 2013
OVOC	HKMS	KIT Karlsruhe	PTR-MS	Brito and Zahn, 2011
O_3	FAIRO	KIT Karlsruhe	UV-Photometry/ Chemiluminescence	Zahn et al., 2012
O_3, CO	AMTEX	DLR-IPA	UV-Photometry/ VUV-Fluorimetry	Gerbig et al, 1996
NO, NO_y	AENEAS	DLR-IPA	Chemiluminiscence/ Gold converter	Ziereis et al., 2004
SO_2, HCOOH	CI-ITMS	DLR-IPA	CI-ITMS	Speidel et al., 2007
a) CO_2 and CH_4	CATS	DLR-IPA	a) CRDS	Chen et al., 2010
b) PAN			b) GC-MS	Volz-Thomas et al., 2001
c) $\delta^{13}C(CH_4)$			c) GC-IRMS	Fisher et al., 2006
PFC tracer	PERTRAS	DLR-IPA	AT-BS/TD-GC-MS	Ren et al., 2015
Trace gas- remote sensing measurements				
Species/parameters	Acronym	Institution	Technique/Instrument	Reference
NO_2, HONO, BrO, CH_2O, $C_2H_2O_2$, $C_3H_4O_2$, SO_2, IO	mini-DOAS	Univ. Heidelberg	DOAS / UV-nIR; 2D optical spectrometer	Hüneke et al., 2017
NO_2, CH_2O, $C_2H_2O_2$, H_2O, SO_2, BrO, O_3	HAIDI	Univ. Heidelberg	DOAS / 3x2D-imaging spectrometers	General et al., 2014
Aerosol measurements				
Species/parameters	Acronym	Institution	Technique/Instrument	Reference
Particle composition	C-ToF-AMS	MPIC Mainz & Univ. Mainz	ToF-AMS	Schulz et al., 2018
BC, CCN, microscopic properties	CCN-Rack	MPIC Mainz	SP2	Holanda et al., 2020
			CCNC, MI	Wendisch et al., 2016
Particle size distribution/number concentration	AMETYST	DLR-IPA	CPC, OPC, PSAP, DMA	Andreae et al., 2018
Other parameters				
Species/parameters	Acronym	Institution	Technique/Instrument	Reference
Spectral actinic flux density (up/down) Photolysis frequencies	HALO-SR	FZ Jülich	CCD spectro- radiometry	Bohn and Lohse, 2017
Basic aircraft data	BAHAMAS	DLR -FX	various	Mallaun et al., 2015

3

~~2.4.2 Perfluorocarbon tracer experiments~~

~~Tracer experiments were performed during EMeRGe using perfluorocarbon compounds (PFC). PFCs are suitable tracers as they are chemically inert, do not interact with aerosol and clouds, have very low background in the atmosphere (~10 ppqv), and can be detected at mixing ratios as low as 1 ppqv. The tracer experiments involved the release of a mixture of PFCs at a site close to the centre of an MPC. These experiments establish Lagrangian connections between MPC centres and HALO measurements downwind. They support the studies on the formation of secondary gases and aerosol particles from the primary emissions in the pollution plumes. In addition, tracer experiments were used to test the dispersion parametrisations in transport models.~~

~~During the EMeRGe IOP in Europe, PMCH (C_7F_{14}, 350 amu) was the PFC used to tag polluted air masses at the release sites. The tracer was sampled on sorption tubes on board and subsequently analysed in the laboratory, as described in Ren et al., (2013, 2015). The limit of detection (LOD) and limit of quantification (LOQ) of the PFC analysis system are 0.7 ppqv and 2 ppqv, respectively, for sorption tube samples loaded for 3 min. The precision and accuracy are 6% and 11%, respectively. Three tracer releases were performed two in the city centre of London at the Imperial College on 17 and 26 July 2017 and one in the Ruhr region, at the University of Wuppertal on 26 July 2017 in Germany. The HALO flights and pattern for the tracer sampling in the plumes downstream were optimised with respect to the time of the tracer releases by using HYSPLIT tracer dispersion forecasts. Post campaign comparisons of the tracer measurements were performed with HYSPLIT and FLEXPART. More details of the EMeRGe tracer experiments are described in Schlager et al. (2021, in preparation).~~

~~2.4.3 Other airborne observations~~

~~The Facility for Airborne Atmospheric Measurements (FAAM, see www.faam.ac.uk) from the UK Natural Environment Research Council (NERC) joined the EMeRGe IOP in Europe. It made a set of flights around London in the Southeast of England in the UK.~~

~~To assure the accuracy and comparability of the instrumentation on board, one research flight on 13 July 2017 was dedicated to common and simultaneous measurements of HALO and FAAM in a so called blind intercomparison exercise. The two research aircraft flew in close formation for 1.6 hours around noon in the northern part of a restricted airspace. In total, 24 instruments were operated on the two aircraft and provided data for the comparison. The data obtained were uploaded under blind conditions and evaluated by an external referee. In addition, observational data were collected from the German~~ Meteorological **conditions** ~~Service at the observatory Hohenpeissenberg (47°48'N, 11°01'E) located downwind of the aircraft track, and model results were generated from 6 models and interpolated along the common flight path. A summary of the measured and modelled data available for direct comparisons is provided in the supplement (S5). Overall, about half of the data pairs from the sets of measurements on the two aircraft differ less than their combined error estimates. In most cases, the differences between the measurements are smaller than the deviations between the model results. For some instruments, the comparison led to significant data analysis improvements. The root mean square deviations between the measurements on FAAM and HALO were less than estimated errors for temperature, relative and absolute humidity, CO_2, benzene, vertical and horizontal wind components, and methane. The~~

~~largest discrepancies were found for some VOCs, sulphate aerosol and black carbon mass and number concentrations. The instrumental accuracy assessment from the comparison results in Schumann (2020).~~

In this subsection, a brief overview of the general meteorological situation over Europe is given. A summary of the meteorological conditions during individual flights is provided later in Sect. 3.6.

~~The Italian Sky Arrow Environmental Research Aircraft (Gioli et al., 2009) from the National Research Council of Italy (CNR) undertook additionally two research flights up to 2000 m over the city of Rome (Italy) concurrently with the HALO overpass flight on 11 July 2017. The aircraft was equipped with instrumentation targeting some aerosol parameters (total number and size distribution), gas concentrations (CO_2, O_3, H_2O) and key meteorological data (temperature, pressure and wind).~~

~~2.4.4 Collocated ground-based observations~~

~~EMeRGe was supported by measurements from a variety of ground-based stations which complemented the HALO observations. These measurements were also used for the planning of subsequent HALO flights and occasionally for in-flight manoeuvres.~~

~~For example, the European Aerosol Research Lidar Network, EARLINET (Pappalardo et al., 2014), a key component of the Aerosols, Clouds and Trace gases Research Infrastructure ACTRIS, joined as an EMeRGe international partner and provided coordinated, ground-based lidar measurements. Additional support was provided from other non-EARLINET lidar stations. Altogether, 19 stations supported the EMeRGe IOP in Europe. The specifications and location of the operated lidars as well as the coordinated measurements for each HALO flight are included in the supplement (S6).~~

~~In addition, measurements from several ceilometer networks contributed to EMeRGe, in particular the German Ceilonet of DWD (Deutscher Wetterdienst), the Italian ALICEnet (Automated Lidar Ceilometer network) and the ceilometers of the Belgian RMI (Royal Meteorological Institute of Belgium). The RMI also provided ozone soundings from Uccle three times per week. Additional ground-based and in-situ measurements were provided from ACTRIS stations, and sun photometer measurements from AERONET (Aerosol Robotic Network, Holben et al., 1998)~~

~~Two ground-based field campaigns deploying both remote sensing and in-situ measurements concurred with the EMeRGe IOP: ACTRIS-2 in the Po Valley, Italy (see http://actris-cimone.isac.cnr.it/), and HOUSE (High Ozone, Ultrafine particles and Secondary aerosol Episodes in urban and regional backgrounds) in Northeast Spain (see https://www.idaea.csic.es/egar/portfolio-items/house/). These data were made accessible for the analysis in the framework of EMeRGe international.~~

~~2.4.5 Satellite observations~~

~~Near real-time tropospheric NO_2 columns from the GOME-2 instruments on MetOp-A (GOME2-A; 40 km x 40 km resolution) and MetOp-B (GOME2-B; 80 km x 40 km resolution) as well as OMI (13 km x 24 km resolution at nadir) on NASA Aura were provided in July and August 2017 to support flight planning and quick-look interpretation of the EMeRGe IOP observations. NO_2 columns are calculated using the method described in Richter et al., (2005, 2011), and Hilboll et al., (2014). The retrievals use GOME-2 lv1 data provided by EUMETSAT and OMI lv1 data provided by NASA. They are not official GOME-2 / OMI data products. The plots were usually available 6 hours after measurement (https://www.iup.uni-bremen.de/doas/emerge.htm).~~

In addition, daily values of the aerosol optical thickness (AOT) at 0.55 µm were retrieved from the Spinning Enhanced Visible and Infrared Imager (SEVIRI) on board the Meteosat Second Generation (MSG) satellite. The spatial and temporal resolutions for the SEVIRI AOT product are 3 km at nadir and 15 minutes, respectively. The SEVIRI AOT product over land (SMAOL_AOT.v1.3.6) and ocean (SEV_AER_OC_L2.v1.04) (Thieuleux et al., 2005; Bréon et al., 2011) are merged and post-processed by using the eXtensible Bremen Aerosol/cloud and surfacE parameters Retrieval (XBAER) algorithm to minimise potential cloud contamination (Mei et al., 2017a, 2017b).

3 Characteristics of the EMeRGe IOP in Europe and its conditions

The EMeRGe IOP in Europe took place from 10 July 2017 to 28 July 2017. The results obtained are analysed considering the prevailing meteorological conditions in Europe during this period and the characteristics of the deployment in the different flight legs.

3.1 Meteorological conditions

The month of July was selected for the EMeRGe investigation because the summer period in Europe usually offers frequent events of high temperature and high insolation, which result in active photochemical processing of the air masses.

The monthly average weather conditions of July 2017 were evaluated by comparing 500 hPa geopotential height, temperature, wind and precipitable water with a 30-year (1981-2010) reference climatology using NCEP reanalysis data (Kalnay et al., 1996). As shown in Fig. 2, stagnation events, high temperatures and insolation dominated Southern Europe similar to the average of the 30-year climatology. At the ground, the summer 2017 was characterised by a number of heatwaves, which contributed to the propagation of frequent fire events especially on the Iberian Peninsula (EEA, 2018). Several EMeRGe flights were affected by such fires in the southern Mediterranean area as summarized later in Sect. 3.6. Furthermore, in Sect.4.4 more details are given on how the emissions from these fires frequently interacted with anthropogenic and other natural emissions.In contrast, during the EMeRGe period Northern Europe was influenced by a pronounced negative an upper-level negative pressure and temperature anomaly. was located over Northern Europe. The polar front was positioned further southwards than usually and accompaniedis usual with anomalously high upper-level wind speeds over Central Europe. These conditions favoured the passage of upper-level troughs associated with mid-latitude cyclones and enhanced precipitation over Central Europe. A cut-off low located over Great Britain during approximately the last ten days of the campaign led to a pronounced deviation ofaffected the average weather conditions in July. Thunderstorms frequently developed near the Alps over Southern Germany and Northern Italy. Due to the various meteorological conditions in Central and Southern Europe, the photochemical processing of the investigated polluted air masses proceeded highly differently as described in more detail in Sect. 4.5.

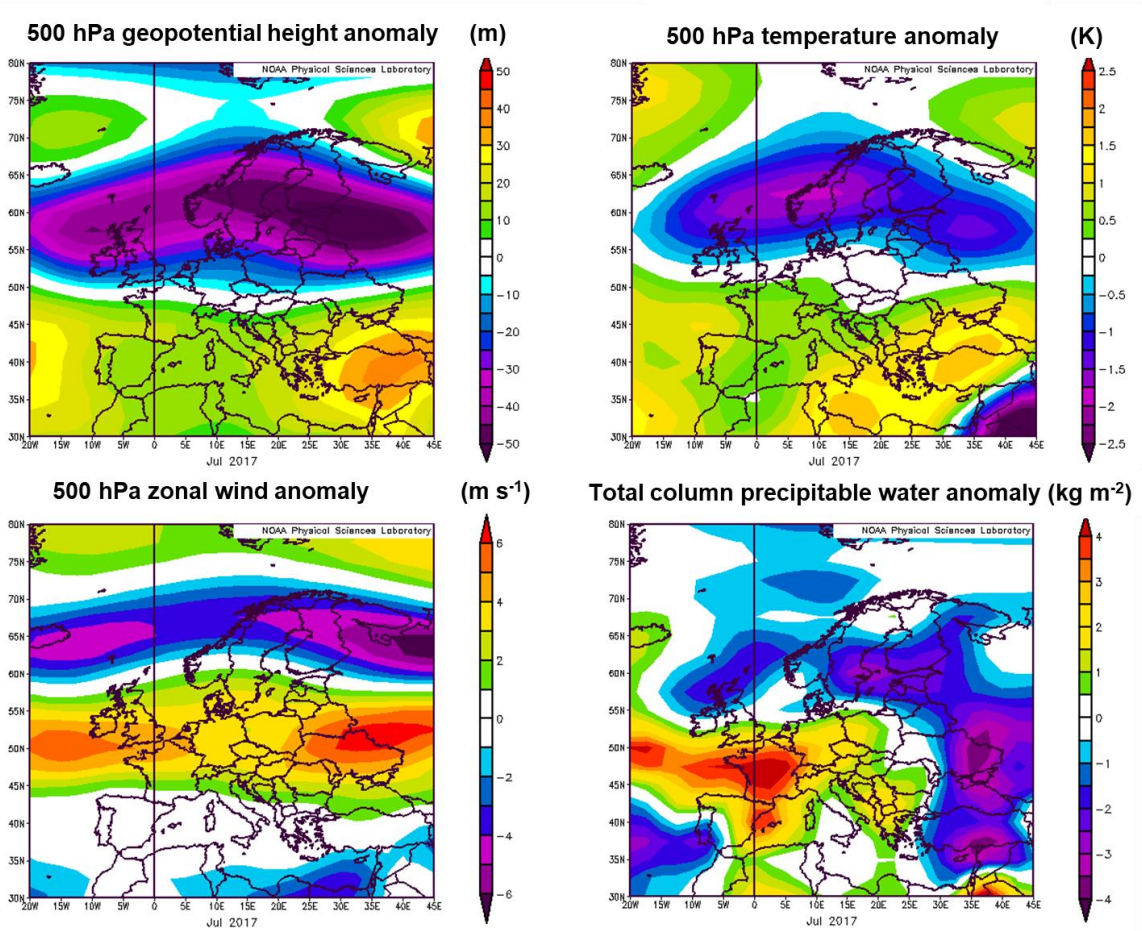

Figure 2: Mean anomalies of the 500 hPa geopotential height (top left panel), temperature (top right), zonal wind (bottom left) and total column precipitable water (bottom right) for July 2017 with respect to a 1981-2010 July climatology based on NCEP reanalysis data (Kalnay et al. 1996). Total column precipitable water is the amount of water potentially available in the atmosphere for precipitation from the surface to the upper edge of the troposphere. NCEP reanalysis data and images provided by the NOAA/ESRL Physical Sciences Laboratory, Boulder Colorado (http://psl.noaa.gov/).

3.5~~2~~ Aerosol optical depth

The aerosol load in the target regions during the EMeRGe IOP in July 2017 was investigated. Monthly averages of aerosol optical depths (AODs) measured in July 2017 at 17~~14~~ AERONET ~~sun-sky photometer~~ sites (AERONET, 2020) covering the ~~), in all six~~ EMeRGe target regions ~~(see S7 in the supplement)~~ were compared to the relevant climatology (i.e., the 19~~10~~-year "~~AOD~~ July AOD mean"~~average~~ between 2001~~2009~~ and 2019). These AERONET~~. Throughout this study, only version 3~~ level 2.0 AOD climatological data ~~were considered~~ (Giles et al., 2019~~). The measurements at 1020 nm presented here have the largest data coverage (139 data points). Data for other wavelengths (500 nm, 118 data points; and 675 nm, 132 data points~~) are visualized~~shown~~ in ~~the supplement.~~ Figure 3, referring to 500 nm wavelength. The results show that~~ displays the derived AODs. The AODs measured~~ in July 2017 the aerosol load was generally lower than the relevant climatological value in each target region. For the BNL/Ruhr area (Brussels, Cabauw, Lille, Jülich), Rome (Rome La Sapienza, Rome Tor Vergata), ~~close to~~ Paris (Palaiseau, Paris), and the Po Valley (Ispra, Modena, Sirmione) the relative deviations of the AODs from the mean values are similar and of the order of -30%. In Rome and the Po Valley the July-2017 AOD is outside the range of the climatological mean and standard deviations. For Eastern Spain (Barcelona, Burjassot, Monsec, Palma) and~~in~~ Southern Great Britain (Bayfordbury, Chilbolton), the aerosol load is closer to the relevant climatology,~~are very similar in the period 2009 to 2019. The AODs are within the~~

~~standard deviation of the 10-year average for the majority of the other stations~~ with relative deviations of 7% and 15%, respectively~~ranging from 10% to 14%. In contrast, the AOD observed in the Rome region was 22% lower than the 10-year average~~.

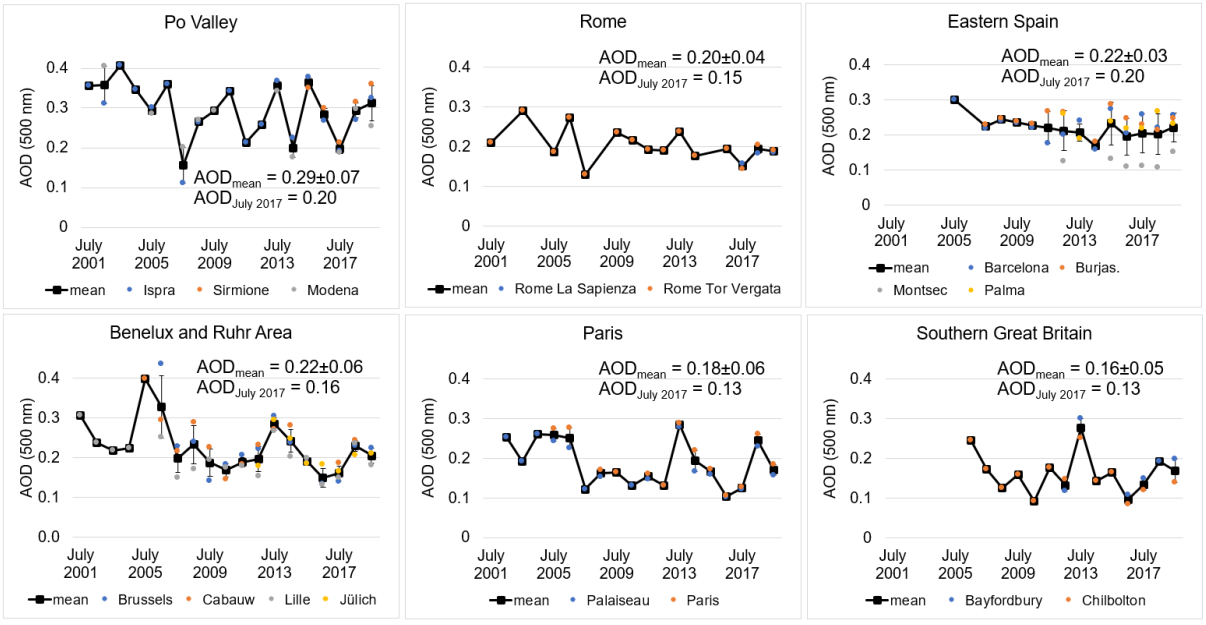

Figure 3: Monthly mean AOD values at 500 nm for July (years 2001-2019) in each of the EMeRGe target regions (black squares and standard deviations). These were obtained as mean of the multiple site monthly means (selected sites in colour, see legends). Note that for those AERONET instruments not having the 500 nm filter, the AOD values are interpolated using the Angstrom coefficient between the two closer wavelengths. The values of the climatological- and July-2017- AOD are also reported in the plot insets.

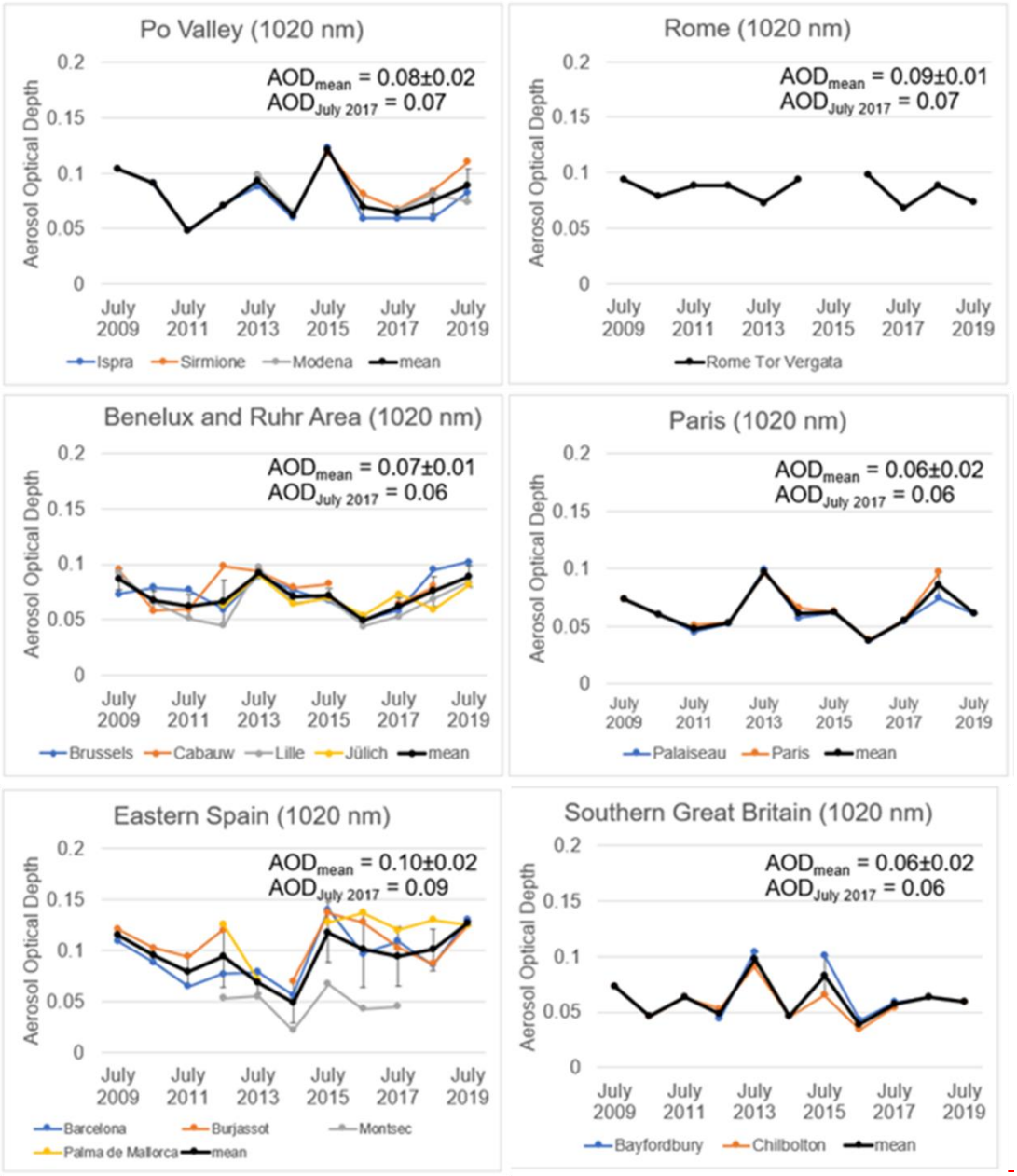

~~**Figure 3:** AODs derived at 1020 nm for AERONET stations in all six target regions of EMeRGe in Europe. Black lines show mean AOD values. The AODs derived for July 2017 and the 2009 to 2019 average are shown on each diagram. The AODs from July 2017 are representative of the average AODs from 2009 to 2019.~~

3.~~6~~3 Flight regions~~routes~~ and HALO flight tracks

The EMeRGe IOP in Europe comprised seven HALO flights ~~from 11 July 2017 to 28 July 2017,~~ for a total of 53 flight hours. All HALO flights started from the DLR base Oberpfaffenhofen (OP), located Southwest of Munich in Germany. The flights are named E-EU-FN, where E stands for EMeRGe, EU for Europe and FN are the two digits of the flight number. ~~As mentioned in Sect. 2.3, all HALO flights started from OP in Germany.~~ The flight tracks are shown in Fig. 4 and Table 3 summarises the corresponding flight times and targets.

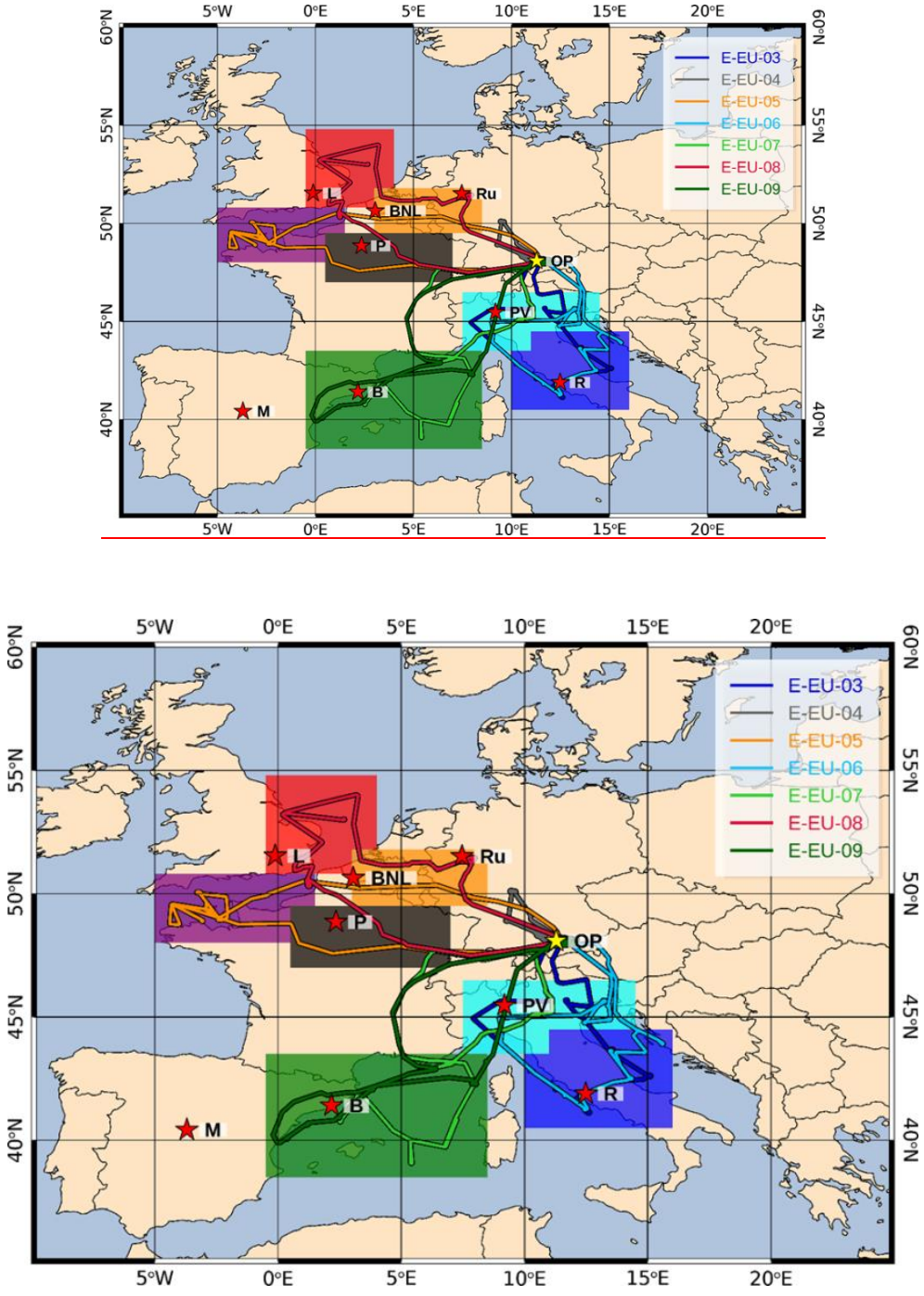

Figure 4: HALO flight tracks during the EMeRGe campaign in Europe on 11, 13, 17, 20, 24, 26 and 28 July 2017 (E-EU-03 to E-EU-09, respectively, colour coded). The specific flight times are presented in Table 3. MPC target areas are colour coded by shading: English Channel (purple) North Sea (red) Benelux/Ruhr (orange), Paris (black), Po Valley (cyan), Central Italy (blue), East Mediterranean (green).Distinctive locations/regions are marked with red stars, M: Madrid, B: Barcelona, P: Paris, L: London; BNL: Benelux; Ru: Ruhr area; PV: Po Valley, R: Rome. The coordinates of the MPC areas can be found in the supplement (S8). The position of the HALO base at DLR in Oberpfaffenhofen (OP) is also indicated by a yellow star for reference.

Overall, 60% of the HALO measurements during EMeRGe in Europe were performed below 3000 m to probe fresh and transported outflows of selected MPCs (see Fig. 5 for the distribution of HALO flight altitudes during the EMeRGe IOP).

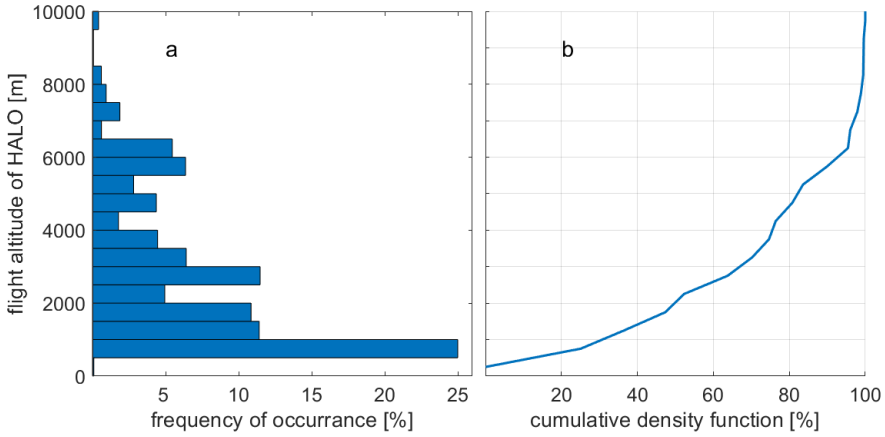

588

589 **Figure 5:** Frequency of occurrence of flight altitudes during EMeRGe in Europe in bins of 500 m, a) cumulated
590 frequencies of flight altitudes from the ground to 10000 m b) cumulative density function.

591

Table 3: Characteristics of the HALO flights carried out in Europe during EMeRGe. FR: flight route. Note that E-EU-01 and E-EU-02 were technical flights and are not considered in the present work.

Flight number	Day/ Month	Start/ End time (UTC)	FR	MPC emission and transport targets	Other features
E-EU-03	11/07	10:00/16:30	1	Rome, Po Valley; convection over Alps and Apennines	Mineral dust from Northern Africa; Fires in Southern Italy. Flights Sky Arrow over Rome
E-EU-04	13/07	10:40/15:00	2	Central Europe; Intercontinental transport	HALO-FAAM blind comparison Canada fires
E-EU-05	17/07	10:30/18:30	2	London, BNL/Ruhr, English Channel and Central Europe	FAAM flights over London PFC tracer release
E-EU-06	20/07	9:00/17:30	1	Rome, Po Valley; Convection over Alps and Apennines	Mineral dust from Northern Africa; Fires in Southern Italy and Croatia
E-EU-07	24/07	9:45/18:15	3	Po Valley, South France, Barcelona; West Mediterranean	Dust transport from Northern Africa, fires in Southern Europe
E-EU-08	26/07	7:45/15:20	2	London, BNL/Ruhr, Paris; English Channel and Central Europe	PFC tracer releases London, Wuppertal
E-EU-09	28/07	10:00/18:30	3	Po Valley, South France, Madrid, Barcelona; West Mediterranean	Fires in Southern France and Portugal

Different flight routes were selected to optimise the identification and measurement of outflows of target MPCs under the prevailing meteorological conditions. Taking the measurement objectives, the flight constraints and the prevailing meteorological weather conditions into account, three flight regions routes were selected for the identification and measurement of outflows of target MPCs during the EMeRGe IOP:

a) Flight region route 1: Southern Europe - Italy

b) Flight region route 2: London and Central Europe

c) Flight region route 3: Southwestern Europe

a) Flight region route 1: Southern Europe- Italy

The flight region route 1 was selected for the HALO flights E-EU-03 (S9, Fig. S9.1) and E-EU-06 (Fig. 6) on the 11 and 20 July 2017, respectively.

The synoptic situation in Europe during these days was characterised by a high-pressure system over the Mediterranean region and a cut-off low over the British Islands associated with the rapid passage of low-pressure systems over Great Britain and Scandinavia. As a result, a Southwest flow with a trough approaching from the West and a short wave passage dominated. These conditions were suitable for the investigation of the MPC targets in Italy (Po Valley and Rome) and of the transport of pollution over the Alps and Apennines.

Along the flight route, cloud formation in the Po Valley and thunderstorms in Southern Germany in the afternoon after 15 UTC were observed on both days.

During these flights, BB emissions from forest and intentional fires in Southern Italy, particularly in the Naples area, and along the coast of Croatia were detected. In addition, the transport of mineral dust from Northern Africa to the central Mediterranean and the Italian west coast was observed.

The E-EU-03 and E-EU-06 flights were carried out over approximately the same geographical area. Initially HALO flew over the Alps, then along the Po Valley to the Mediterranean coast of Italy. During E-EU-06 the vertical and horizontal distribution of pollutants was investigated in more detail by shuttles before entering the Po Valley and flying at lower altitudes. The tracks followed the Tyrrhenian Sea heading to the South and crossing the Italian Peninsula from West to East towards the Adriatic coast after a shuttle upwind of Rome. Along the Adriatic coast, shuttles were made while flying to the North. Finally, the flights crossed over the Alps back to OP. The E-EU-06 flight track details are summarised in Fig. 6.

Table 3: Characteristics of the HALO flights carried out in Europe during EMeRGe. FR: flight region. Note that E-EU-01 and E-EU-02 were technical flights and are not considered in the present work.

Flight number	Day/ Month	Start/ End time (UTC)	FR	MPC emission and transport targets	Other features
E-EU-03	11/07	10:00/16:30	1	Rome, Po Valley; convection over Alps and Apennines	Mineral dust from Northern Africa; Fires in Southern Italy. Flights Sky Arrow over Rome
E-EU-04	13/07	10:40/15:00	2	Central Europe; Intercontinental transport	HALO-FAAM blind comparison Canada fires
E-EU-05	17/07	10:30/18:30	2	London, BNL/Ruhr, English Channel and Central Europe	FAAM flights over London PFC tracer release
E-EU-06	20/07	9:00/17:30	1	Rome, Po Valley; Convection over Alps and Apennines	Mineral dust from Northern Africa; Fires in Southern Italy and Croatia
E-EU-07	24/07	9:45/18:15	3	Po Valley, South France, Barcelona; West Mediterranean	Dust transport from Northern Africa, fires in Southern Europe
E-EU-08	26/07	7:45/17:30	2	London BNL/Ruhr, Paris; English Channel and Central Europe	PFC tracer releases London, Wuppertal
E-EU-09	28/07	10:00/18:30	3	Po Valley, South France, Madrid, Barcelona; West Mediterranean	Fires in Southern France and Portugal

During E-EU-03 the HALO airborne measurements were complemented by two circuits around Rome by the Sky Arrow aircraft and its payload (see S6 in the supplement)~~,~~ starting at 8 UTC and at 12 UTC, respectively. Each circuit comprised three vertical spirals from 200 m to 1800 m altitude approximately. ~~In addition, ground-based measurements of trace gases and aerosol particles are available at selected sites (see S6 in the supplement).~~ The interpretation of these airborne ~~and ground-based~~ observations in combination with ground-based and in-situ data is discussed in Barnaba et al. (2021, in preparation).

Whole air samples for VOCs and their carbon isotope ratios were collected at the ground in evacuated canisters to determine a representative VOC fingerprint for Rome and Milan. To account for emission variations on the ground during the day, air samples were taken around 9 to 10 and 14 h local time.

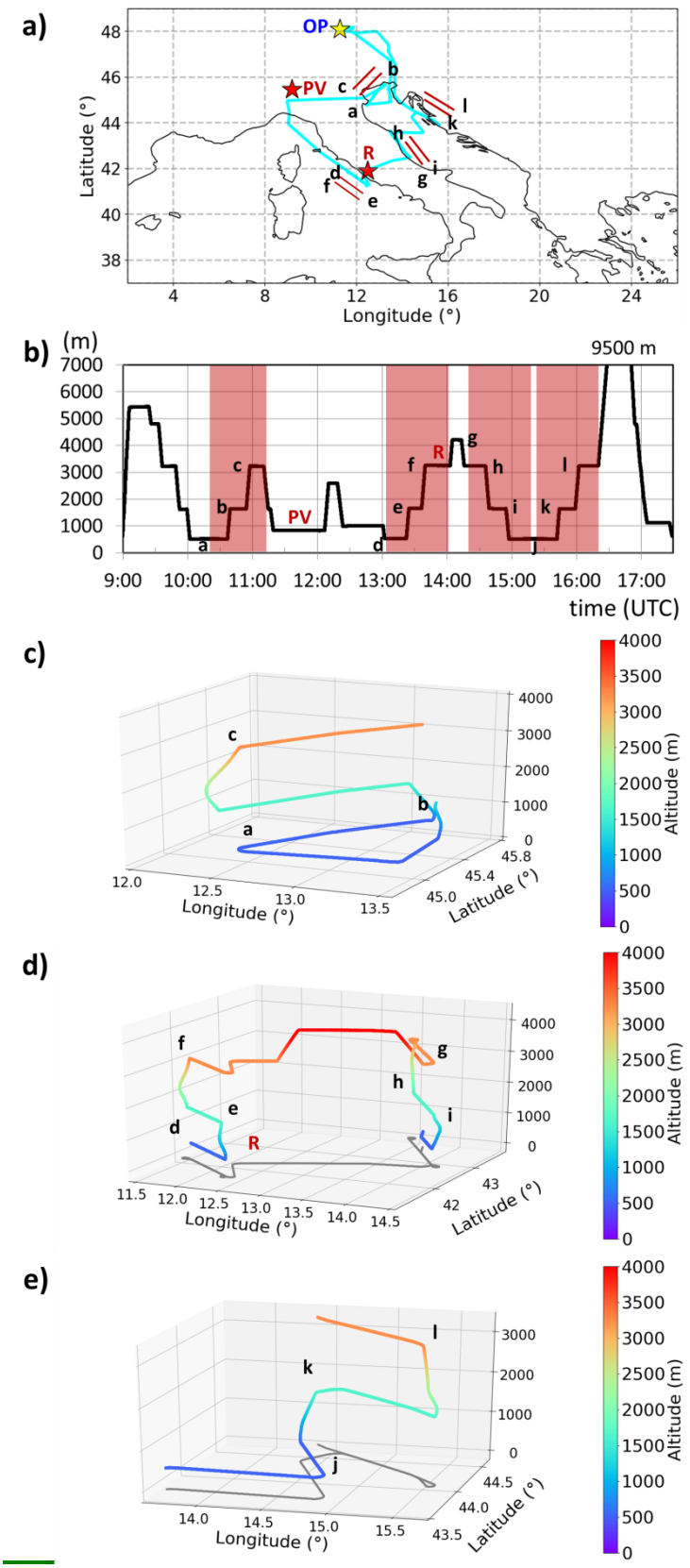

~~**Figure 6:** Details of the E-EU-06 flight on the 20 July 2017. Three shuttles took place downwind of the Po Valley (PV), upwind of Rome (R) and along the Adriatic coast and are marked with red lines on the map in a) as red shaded areas on the altitude diagram in b), and as a 3-D depiction in c), d) and e). The flight tracks during the shuttles d) and e) are shown in grey. The flight track in a) is coloured as in Fig. 4 and the EMeRGe MPC targets in red. Main changes in course and altitude are marked (a–l) on the graphs for reference. OP indicates the position of the HALO base.~~

b) Flight region~~route~~ 2: London and Central Europe

~~Flight route 2 was selected to study the London and BNL/Ruhr outflows with a scientific focus on their transport and interaction over Central Europe. As mentioned in Sect. 3.1, July 2017 had an unsettled weather in the UK and Central Europe with heavy, persistent rain at times and only brief hot spells. This made the selection of optimal flight tracks for this investigation challenging. The precise flight route 2 was tailored for the meteorological conditions prevailing during the E-EU-05, and E-EU-08 flights, which took place on 17 July and 26 July 2017 respectively, to optimally cover different aspects of the target outflows.~~

Flight region 2 was selected to study the London and BNL/Ruhr outflows with a scientific focus on their transport and interaction over Central Europe. As mentioned in Sect. 3.4, July 2017 had an unsettled weather in the UK and Central Europe with heavy, persistent rain at times and only brief hot spells. This made the selection of optimal flight tracks for this investigation challenging. The precise flight route 2 was tailored for the meteorological conditions prevailing during the E-EU-05, and E-EU-08 flights, which took place on 17 July and 26 July 2017 respectively, to optimally cover different aspects of the target outflows.

The flight E-EU-05 (S9, Figure S9.3) took advantage of a short high-pressure ridge that formed behind a trough over Scandinavia on 17 July 2017. The outflow of the MPC London was predicted to travel to the English Channel and the Northern coast of France. This area is regularly used by the UK and French air forces whose activities in the SUAs constrained the original flight options and the flight track were optimised during the flight route. Over the area of interest, HALO flew at different altitudes within the PBL. On the way back to OP, the outflow of Paris was probed South of Orly. On that day, the FAAM platform carried out two complementary circuits around London at 8:00 and 13:30 UTC.

On 26 July 2017, the synoptic situation changed slightly as a cut-off low moved eastwards over Germany while a trough approached from the West. In the period after the cut-off low and before the passage of the warm front over London, the route of E-EU-08 was chosen such that the outflow of London close to the East coast of England and its mixing with the BNL/Ruhr outflow over the European continent were probed (see Fig. 7). Cloudy conditions predominated throughout the day. This flight is studied in more detail in Sect. 4.3. ~~2.~~

The identification of the London outflow was confirmed by the on-board measurement of a PFC tracer released in the centre of London for both flights. During E-EU-08, a second tracer release was carried out in Wuppertal in the afternoon to identify the BNL/Ruhr outflow. In addition, information on the isotopic fingerprints in VOCs representative for London and Ruhr MPC air were obtained by collecting whole air samples at the tracer release sites before, during and after the release, and in the afternoon (see Sect. 4.5).~~2.).~~

The E-EU-04 flight track on 13 July 2017 is a particular case that also covered Central Europe (see S8~~S9~~ in the supplement). The first part of the flight was dedicated to the blind instrumental intercomparison between the HALO and FAAM platforms described in S7~~2.4.3~~ (see Schumann, 2020). A weak high-pressure ridge over Germany dominated. The main objective for the rest of the flight was to probe intercontinental pollution transport between 5000 and 7000 m altitude with signatures of fires originating in Canada.

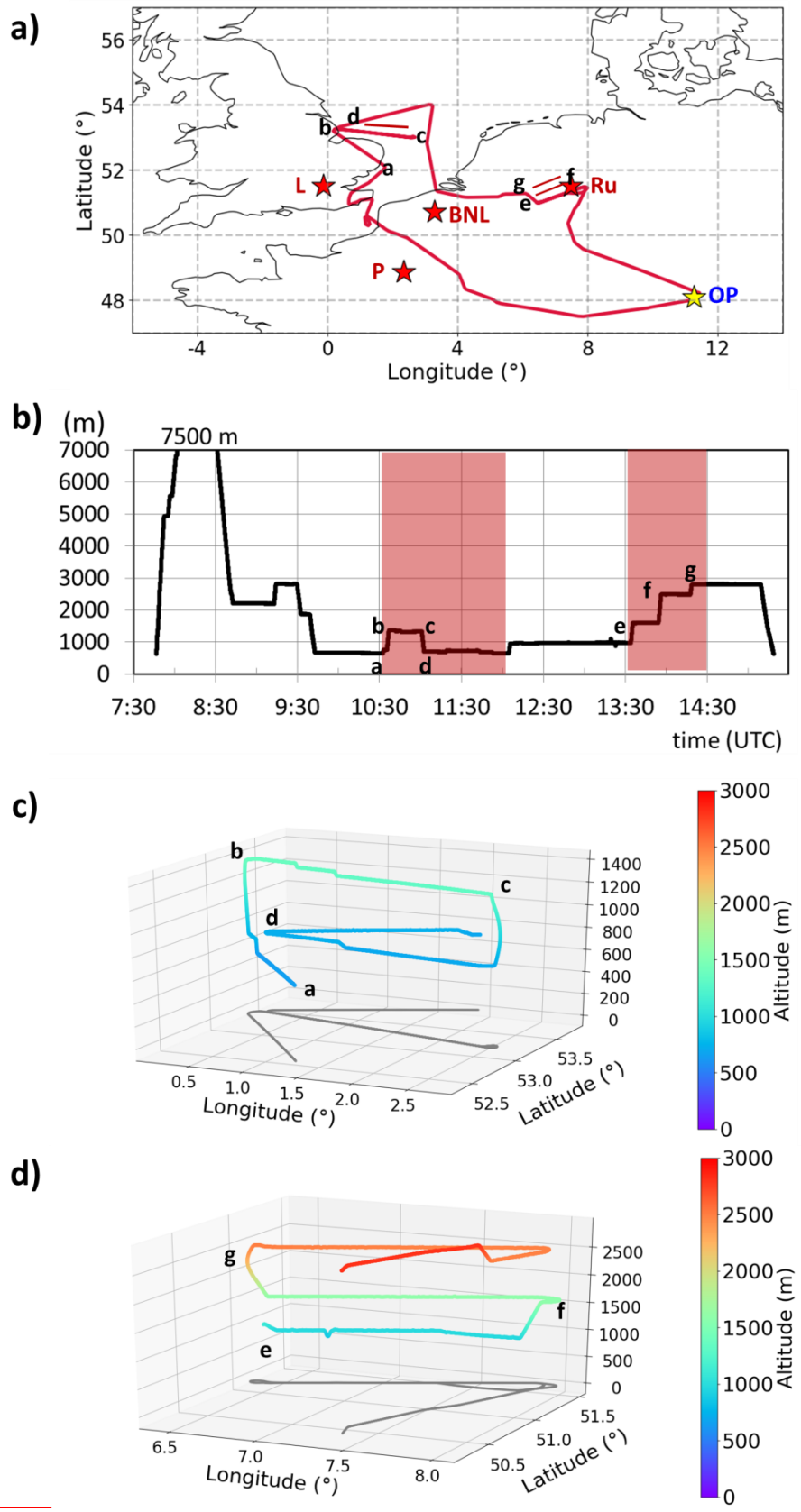

~~**Figure 7:** Details of the E-EU-08 flight on the 26 July 2017. The position of the shuttles downwind from London and the BNL/Ruhr area are indicated in red on the map in a), marked by the red shaded areas in b), and as a 3-D depiction in c) and d). The flight tracks during the shuttles are shown in c) and d) in grey. In a) the EMeRGe MPC targets are shown in red and the flight track coloured as in Fig. 4. Main changes in course and altitude are marked (a-g) on the graphs for reference. OP indicates the position of the HALO base.~~

~~c)a)~~ ~~c)~~ **Flight ~~route 3: Southwestern Europe~~**

c) ~~The objective of flight route 3 was to investigate the transport of Southern European MPC outflows into the Western Mediterranean.~~ **region 3: Southwestern Europe**

The objective of flight route 3 was to investigate the transport of Southern European MPC outflows into the Western Mediterranean. This flight region~~route~~ was selected for the E-EU-07 and E-EU-09 flights on the 24 and 28 July 2017, respectively.

The meteorological situation on 24 July 2017 over Europe was characterised by the eastwards displacement of a cut-off low leaving the British Islands. This was associated with a Southwest flow during the passage of a trough over Spain and France. Dust transport from Northern Africa, thunderstorms in the Po Valley and fires in the South Mediterranean coast of France and Corsica prevailed. The E-EU-07 flight track crossed the Po Valley and focused on the measurement of the predicted outflow of pollution from Southern France and Barcelona into the Mediterranean. Three shuttle flight patterns downwind from Marseille, Barcelona and close to the western coast of Sardinia were carried out (see S9 in the supplement).

On 28 July 2017, a short wave trough with a weak cold front passed over France. This situation led to a prevailing westerly flow and suitable conditions for the E-EU-09 flight over Southern Europe. Two shuttle flight patterns were carried out downwind of Marseille and Barcelona. Features of interest during this flight were the transport of the Madrid and Barcelona outflows in stratified layers into the Mediterranean and the transport of forest fire emissions originating in Southern France and Portugal. This is described in more detail in Sect. 4.3~~.2~~.

Further details on all the flight tracks and shuttles are given in the supplement (S9).

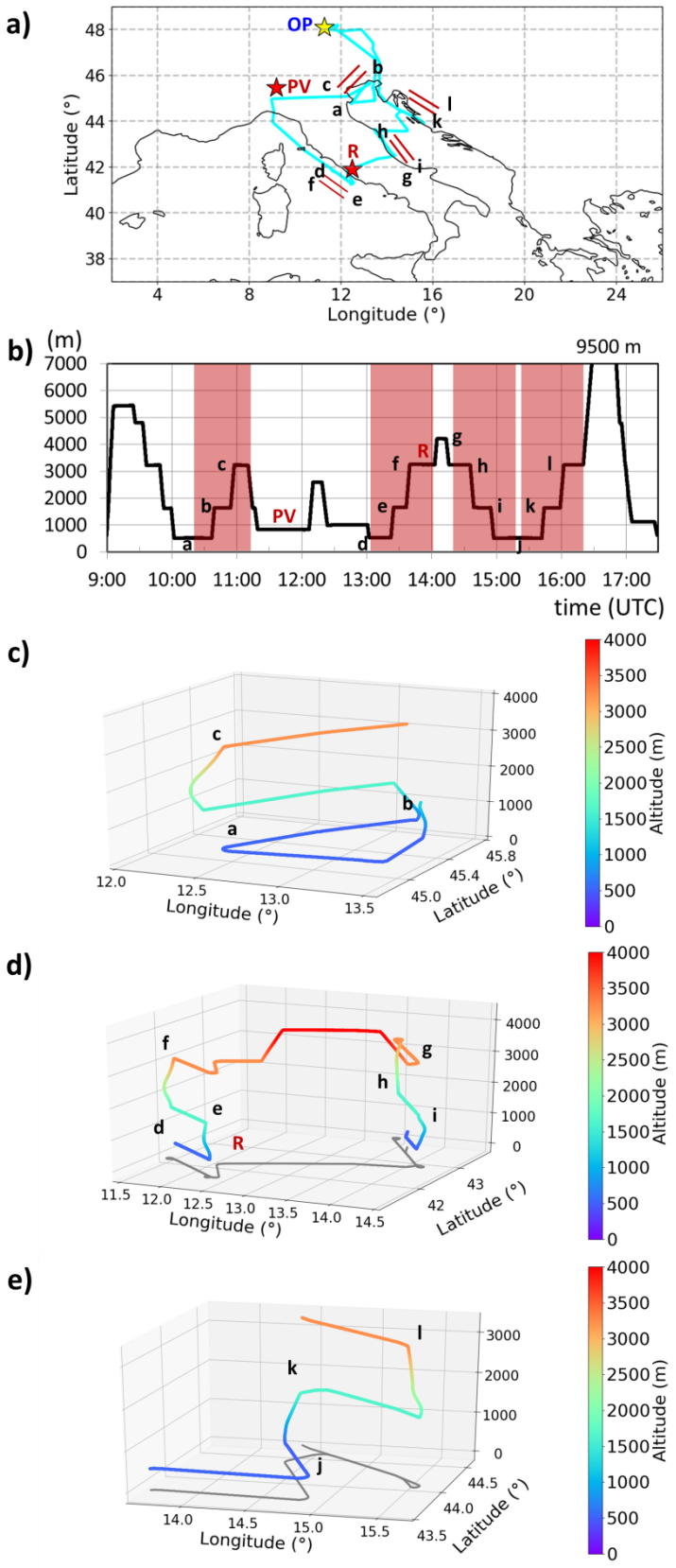

~~3.4~~

Figure 6: Details of the E-EU-06 flight on the 20 July 2017. Three shuttles took place downwind of the Po Valley (PV), upwind of Rome (R) and along the Adriatic coast and are marked with red lines on the map in a), as red shaded areas on the altitude diagram in b), and as a 3-D depiction in c), d) and e). The flight tracks during the shuttles d) and e) are shown in grey. The flight track in a) is coloured as in Fig. 4 and the EMeRGe MPC targets in red. Main changes in course and altitude are marked (a-l) on the graphs for reference. OP indicates the position of the HALO base.

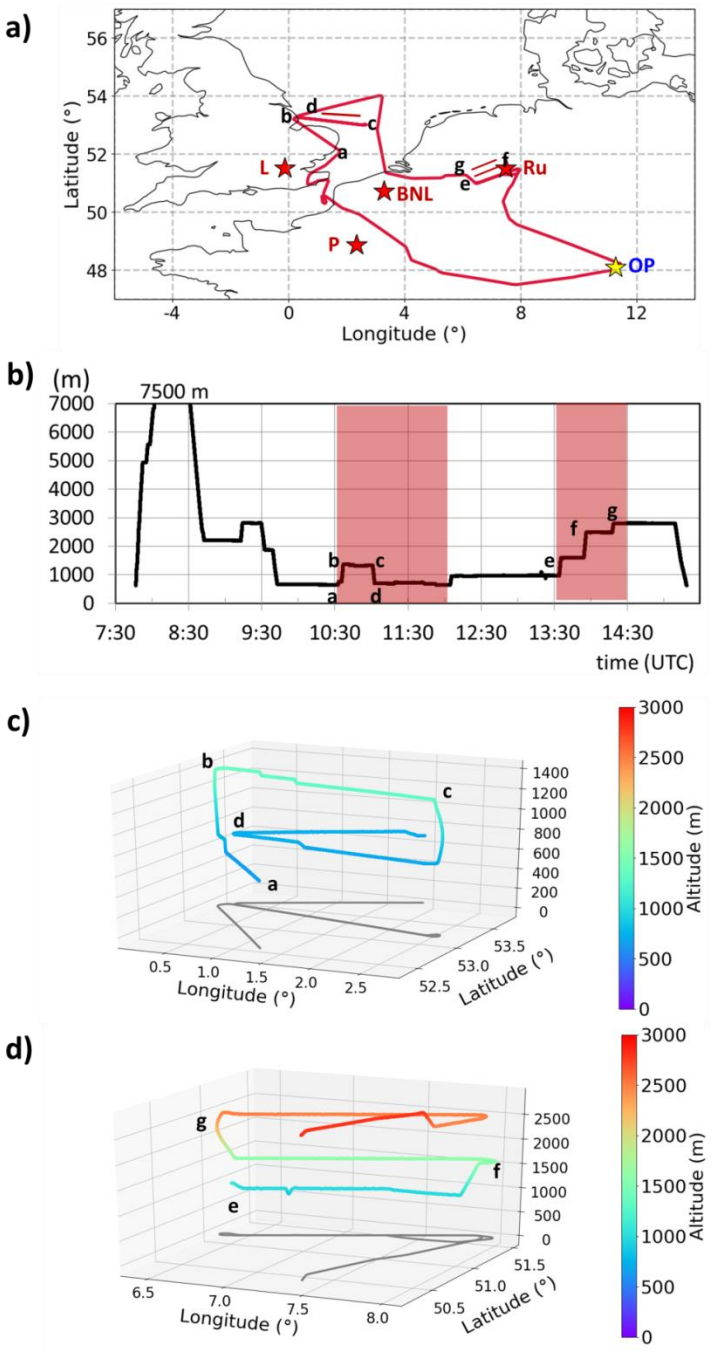

710

711 **Figure 7:** Details of the E-EU-08 flight on the 26 July 2017. The position of the shuttles downwind from London and the
712 BNL/Ruhr area are indicated in red on the map in a), marked by the red shaded areas in b), and as a 3-D depiction in c) and
713 d). The flight tracks during the shuttles are shown in c) and d) in grey. In a) the EMeRGe MPC targets are shown in red and
714 the flight track coloured as in Fig. 4. Main changes in course and altitude are marked (a-g) on the graphs for reference. OP
715 indicates the position of the HALO base.

716

3.7 Model predicted pollution transport patterns

CAMS global model data (see S3 for the model description) are~~were~~ used here to identify and characterise prominent~~evaluate characteristic~~ pollution transport patterns during the EMeRGe IOP over Europe. ~~CAMS operational near real time (NRT) simulations with full emissions and chemistry were incorporated in the analysis. A stratospheric O_3 tracer as a proxy for stratospheric tropospheric transport was also used. In addition, passive CO tracers (i.e., no chemical loss or production) provided through the CAMS field campaign support (https://atmosphere.copernicus.eu/scientific-field-campaign-support) were used with either a) only emissions from EMeRGe target cities switched on in the simulations (CO city tracer), or b) only BB emissions switched on in the simulations.~~

Figures 8 to~~,~~ 10 ~~and 11~~ show composite average maps of ~~12 h~~ CAMS-global forecasts at 12 UTC~~forecast~~ for the EMeRGe flights to the North (Flight region~~route~~ 2: E-EU-05 and E-EU-08) and to the South of Europe (Flight regions~~routes~~ 1 and 3: E-EU-03, E-EU-06, E-EU-07, and E-EU-09; see Fig.4 and Table 3 for description). A division into southwards and northwards flights is meaningful, as pollution transport patterns during individual flights in the two subgroups mainly resemble each other. Comparison of the~~The model was initialised at 00 UTC, for the forecast at 12:00 UTC. The~~ CO city tracer simulations at 500 and 925 hPa (see Fig. 8) indicates~~indicate~~ that the largest part of the anthropogenic MPC emissions remained close to the surface within the PBL. The emissions from the MPCs in the North (e.g. London, Paris) were~~are expected to be~~ frequently transported eastwards due to the dominant west-southwesterly winds (Figure 8, top left). Emissions~~. In contrast, emissions~~ from MPCs South of the polar front, such as Madrid, rather remained in the proximity of the emission sources~~spread in all directions~~ due to variable weak winds (Figure 8, bottom left). Emissions from~~. In~~ the highly polluted Po Valley~~, the emissions~~ were often transported to the Northeast and lifted over the high mountains of the Alps (Figure 8, bottom right).~~.~~

During flights towards the South, higher~~Higher~~ temperatures and dry conditions in Southern Europe ~~during the EMeRGe IOP~~ favoured O_3 production and smog events (~~. This was the case for flights to the South of Europe, as indicated by the simulations at 925 hPa (see~~ Fig. 10, bottom left~~8 and Fig. 11~~). These meteorological conditions supported the propagation of multiple and mostly intentionally started fires in the Mediterranean area. Average~~Figure 9 shows average~~ fire radiative power observed by MODIS (MODerate resolution Imaging Spectroradiometer, http://modis-fire.umd.edu/) and assimilated within CAMS-global over Europe in July 2017 is included in~~. In~~ the supplement (S10). Fire~~target area, fire~~ hot spots are visible around the Mediterranean ~~(e.g., Southern Italian Peninsula, Sicily, Sardinia, Croatia, France around Marseille, North Africa)~~ and in Portugal.

Further evaluation of the CAMS simulations shows that CO emitted by fires around the Mediterranean mainly remained ~~at altitudes~~ below approximately 700 hPa. In contrast, CO resulting from the LRT of North American fire emissions was observed around 500-700 hPa over Europe. The average fields show that CO from North American fires was expected to be more pronounced during flights to the North (see Fig. 9~~10~~), than to the South (see Fig.10~~11~~) with a maximum in the average fields over Great Britain.

The stratospheric O_3 tracer indicates that stratospheric intrusions ~~over the flight domain during the campaign~~ concurred with ~~the~~ LRT of North American fire emissions initially lofted by warm conveyor belts or deep convection. ~~The LRT of fire emissions towards Europe is associated with mid-latitude cyclones crossing the Atlantic.~~ Dry air masses rich in O_3 were~~ then~~ transported downwards to comparably low altitudes. In the average fields of stratospheric O_3 for flights towards the North (see Fig. 9, bottom~~10, lower~~ right), a~~ panel), the~~ stratospheric intrusion over Europe stretches broadly from Southern Greece and Southern Italy to the Northeast.

The latter is associated with the cut-off low which developed on 20 July 2017 over UK and dominated the weather conditions over Europe for approximately one week~~started to move eastwards on 26 July 2017~~.

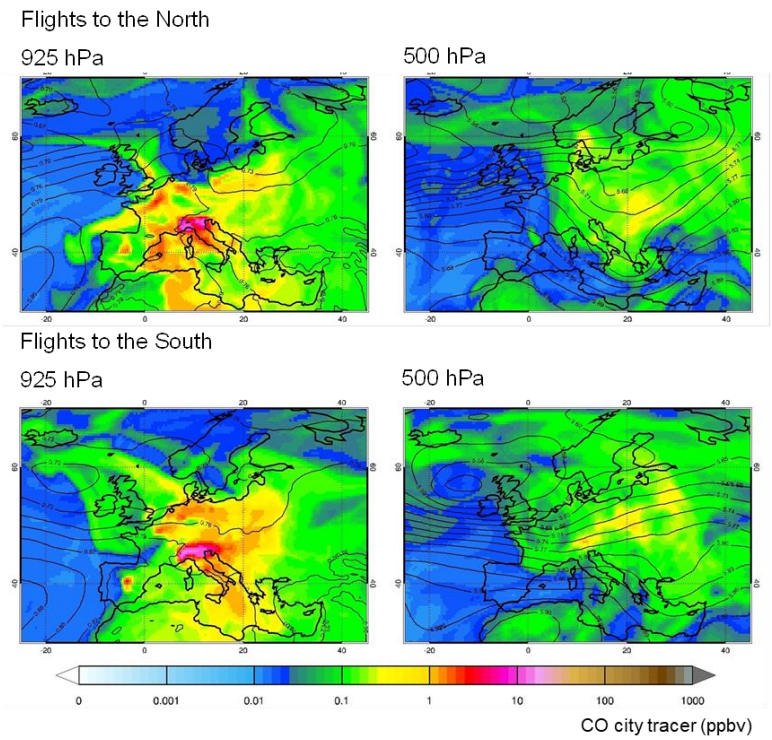

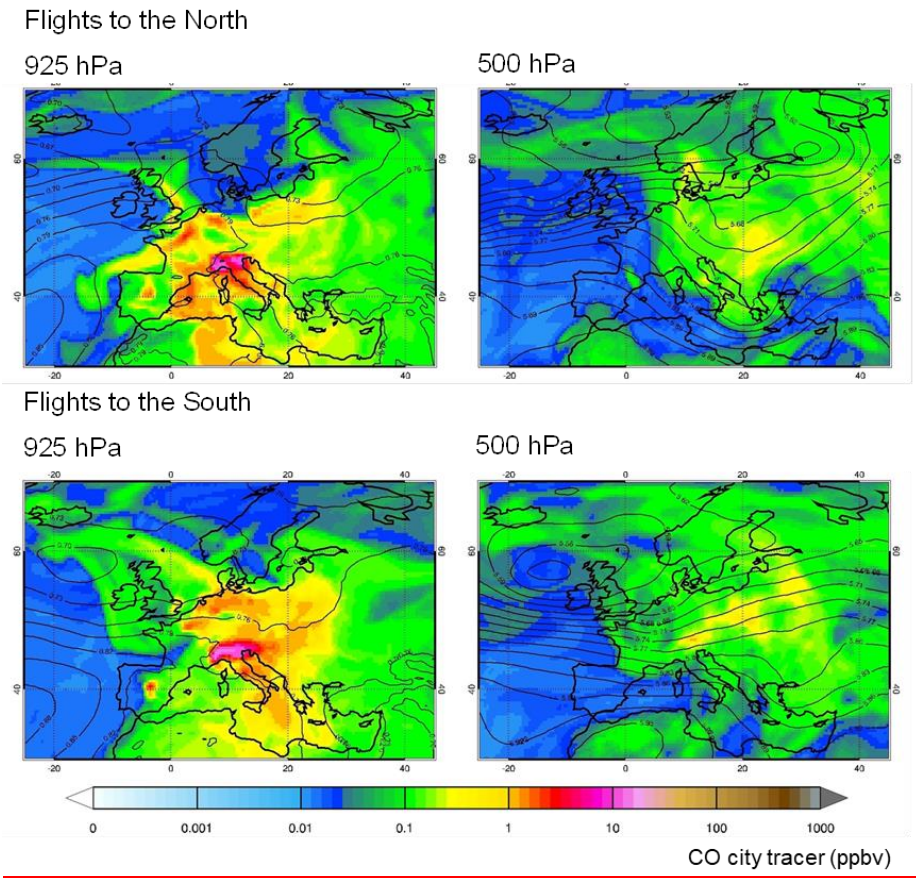

Figure 8: Coloured shadings of composite averages of CAMS-global city tracer forecasts of CO (ppbv) at 925 hPa (left) and 500 hPa (right) and 12:00 UTC for days of flights to the North ((E-EU-05, E-EU-08, top) and South (E-EU-03, E-EU-06, E-EU-07, E-EU-09, bottom) of Europe. Black contours show corresponding averages of geopotential height (km) from the ECMWF-Integrated Forecasting System (IFS).

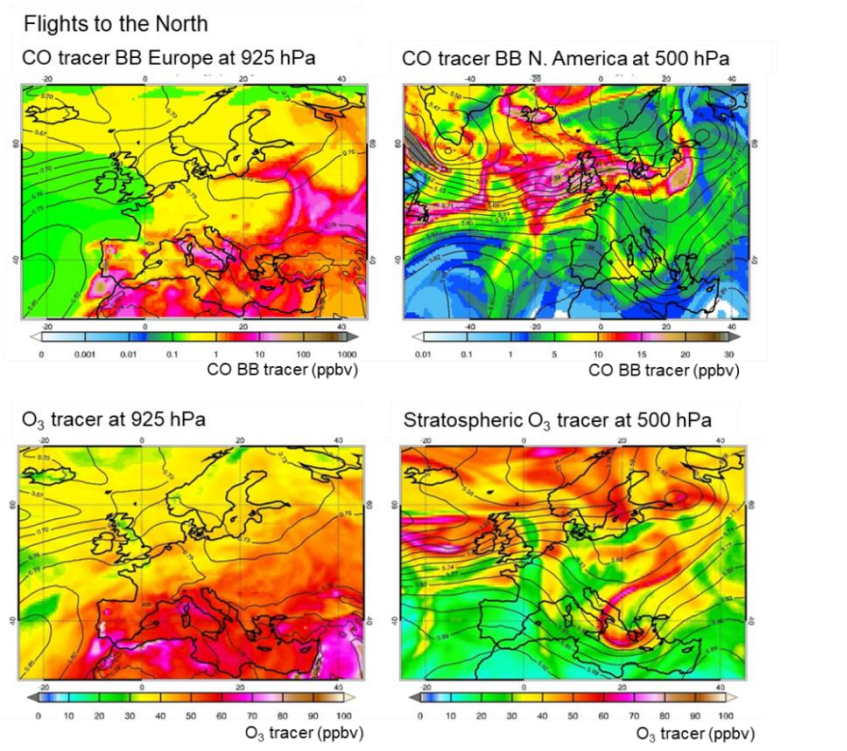

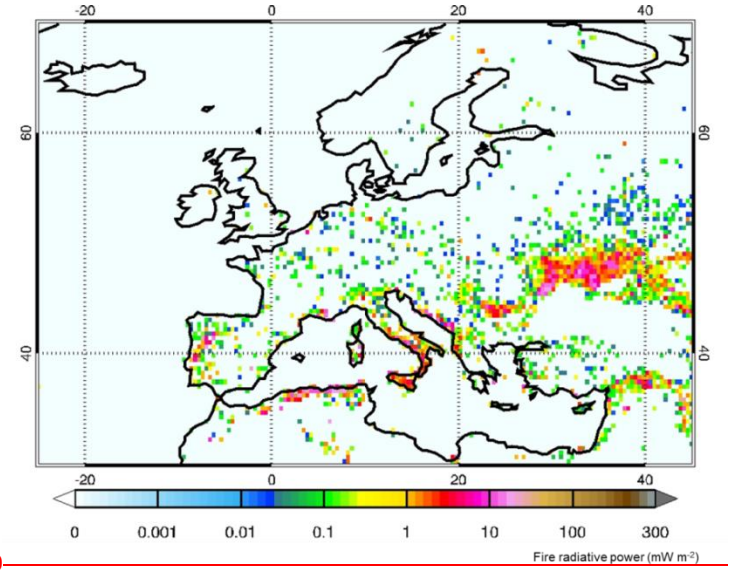

Figure 9

~~**Figure 9:** Average fire radiative power (mW m^{-2}) as observed by MODIS over Europe in July 2017. Data from the CAMS Global fire assimilation system (GFAS). https://www.ecmwf.int/en/ forecasts /dataset/global-fire-assimilation-system-gfas) fire emission database (Kaiser et al., 2012).~~

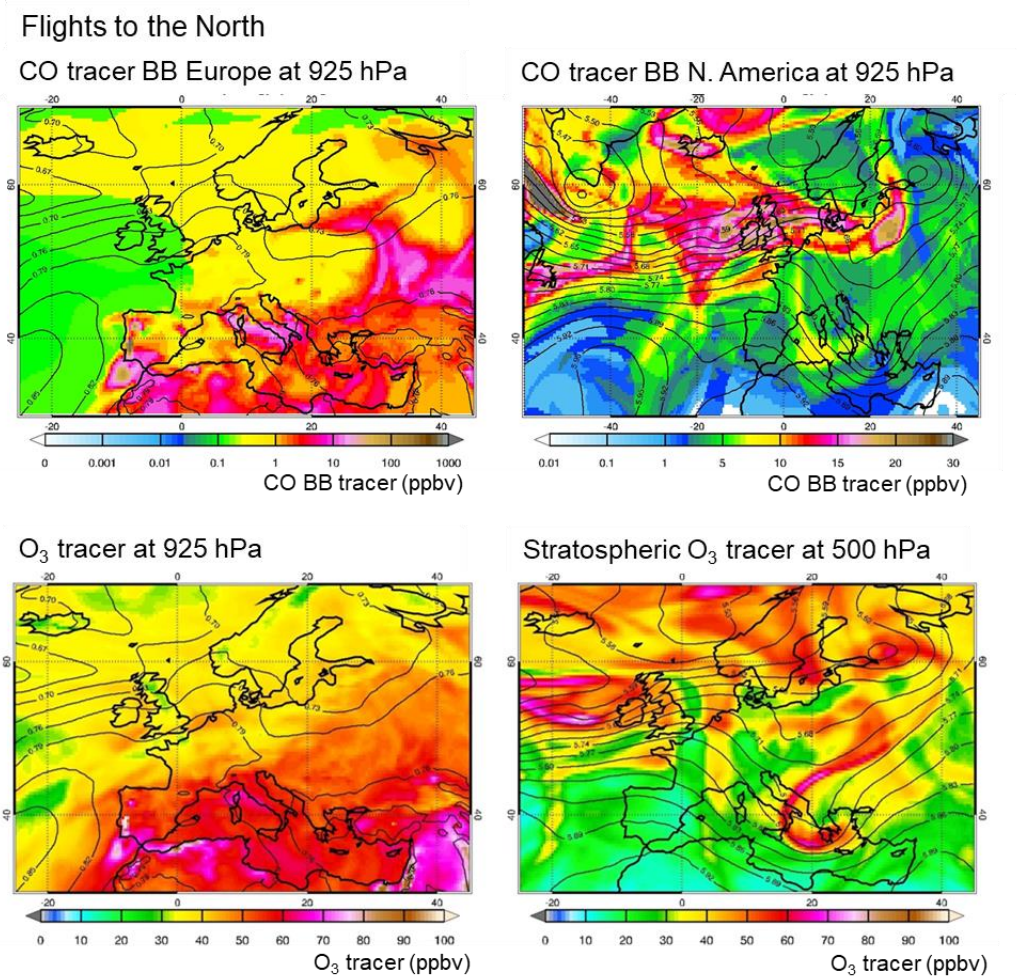

~~Figure 10~~: Coloured shadings of composite averages of CAMS-global forecasts at 12:00 UTC for flights to the North (E-EU-05, E-EU-08): BB CO tracer (ppbv) from Europe at 925 (top left), and from North America at 500 hPa (top right)~~;) at 925 hPa;~~ O_3 (ppbv) at 925 hPa (bottom left), and stratospheric ozone tracer (ppbv) at 500 hPa (bottom right). Black contours show averages of geopotential height (km) from ECMWF-IFS. Note the different scales. The BB tracer from North America (top right) is shown on a larger map than the other CAMS forecasts in this image.

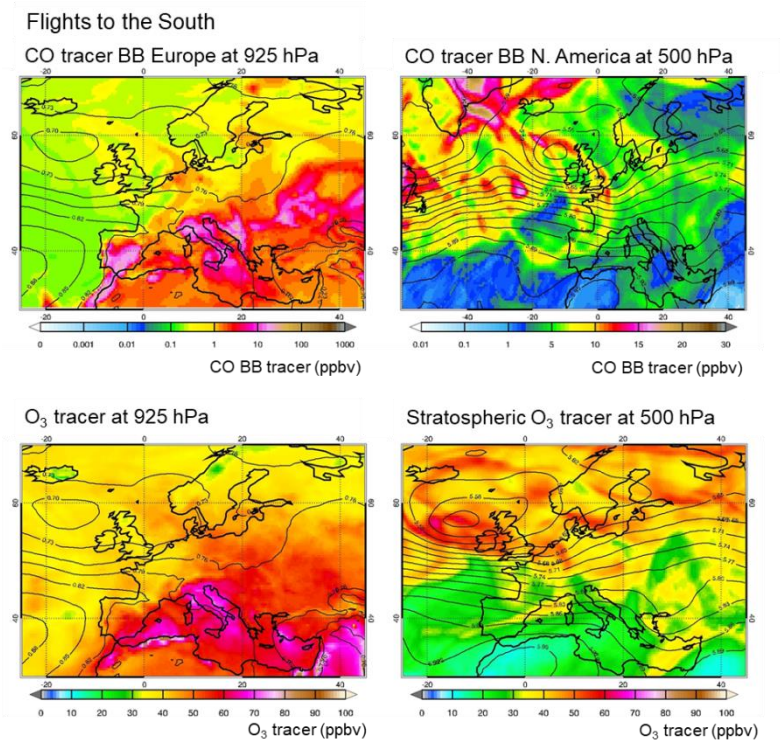

781

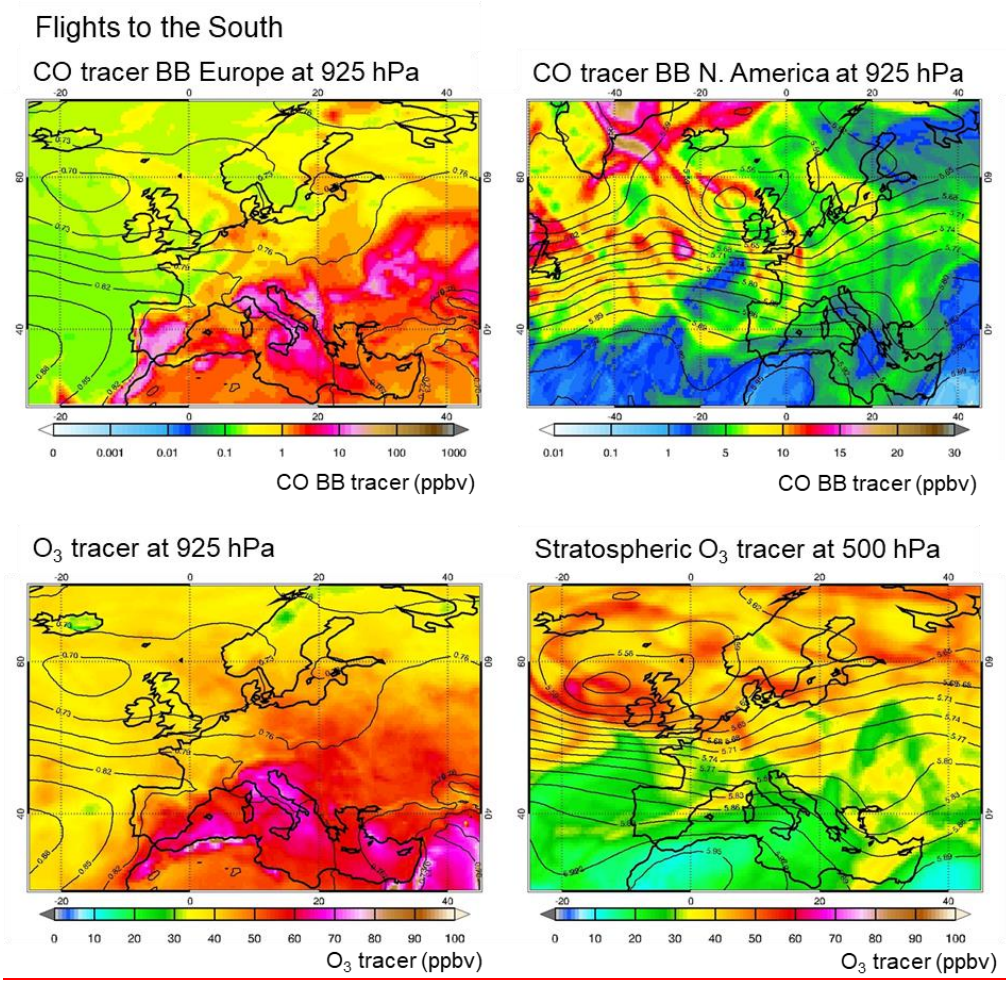

782

783 **Figure 10~~11~~:** Coloured shadings of composite averages of CAMS-global forecasts as in Fig.10, but for flights to the
784 South (E-EU-03, E-EU-06, E-EU-07 and E-EU-09). Note that

785

~~**3.5 Measured amount and distribution of trace gases and aerosol particles**~~

~~The chemical composition and~~ the BB tracer from North America (top right) is shown on a larger map than ~~extent of photochemical activity of~~ the other CAMS forecasts in this image.

4 Transport and transformation of pollution plumes ~~air masses probed~~ during the EMeRGe IOP in Europe

The EMeRGe campaign in Europe focused on ~~were different for~~ the identification and measurement of plumes of pollution from selected MPCs, i.e. their emissions, transport and transformation. EMeRGe achieved its measurement objectives by exploiting the unique capabilities of the HALO research platform to probe these plumes over a relatively large geographical coverage and by the use of forecasting models and tools. The analysis and publication of EMeRGe results is expected to provide new insights into the transport and transformation of pollution plumes over Europe during the IOP in July 2017. In that respect, general findings are summarised in the following sections

4.1 Observations

EMeRGe provides a unique set of in-situ and remote sensing airborne measurements of trace gases and aerosol particles along~~different~~ flight routes and regions in the lower troposphere over Europe. The interpretation of the HALO measurements during the EMeRGe IOP in Europe is facilitated by the use of collocated ground-based and satellite measurements. In that respect, EMeRGe enhances previous pollution studies in Europe by adding an extensive experimental data set in the PBL. The composition of the sampled air masses is highly variable throughout~~tracks. This is to be expected as a result of the large geographical coverage of~~ the flights, which cover large geographical areas of heterogeneous topography, under~~the~~ different solar insolation conditions and ~~the flight path of the air masses, the heterogeneous topography and the~~ proximity to~~of~~ pollution sources. To illustrate this variability, average, median and quartiles values of selected species measured during the EMeRGe flights are included in the supplement (S11). ~~of different types.~~

- Pollution hotspots were identified by using the spatial distribution of trace gases and aerosol particles observed over the flight tracks. A detailed analysis of the complexity of the air masses measured and the variations encountered in individual flights is beyond the scope of the present work and will be presented in dedicated publications. Figure 11 shows as an example the CO, NO, O_3, CH_3COCH_3, CH_4, and the organic aerosol mass concentrations measured during the EMeRGe flights in Europe. CO, total reactive nitrogen (NO_y) and its most reactive forms NO and NO_2, are key species in the identification of anthropogenic pollution. As can be seen in Fig.11, the highest NO concentrations were found in the vicinity and downwind of major pollution sources like London, the BNL/Ruhr region and the Po Valley. The Alps and Apennines on the Italian Peninsula lead to the transport of the Po Valley outflow southwards along the Italian Adriatic coast which is the geographic opening of the Po Valley (Finardi et al., 2014). High NO concentrations are indicative of recent or "fresh" anthropogenic emissions. The NO_y lifetime of a few days enables a more reliable identification of aged polluted air masses further out from the source regions. Maximum NO_y values as large as 12 ppbv (not shown) were measured over Europe. Elevated CO and NO_y accompanied by low NO, as measured in the proximity of Barcelona, indicate that there has been a significant amount of processing of the pollution plumes sampled. Emission hot-spots can be hardly identified in the spatial distribution of O_3 as expected from its non-linear secondary formation. Maximum O_3 mixing ratios were generally observed at a distance downwind of MPCs. Organic aerosol has strong anthropogenic sources such as combustion (traffic, fossil fuel combustion, industrial activity, BB), and showed similar behaviour to CO and NO, in that larger mass concentrations were closer in time and space to MPCs such as London, Po Valley, and BNL. The lifetime of aerosol particles in the PBL is in the order of a few days, which explains the high variability observed. Additionally, aerosol particle concentrations presented a strong gradient above the PBL (see Fig.12).
- Signatures of urban sources of long-lived greenhouse gases like CH_4 and CO_2 were identified in the airborne measurements close to the MPC regions in Europe. The identification of plumes of GHG and the quantification of the MPC contributions to the regional GHG budget are challenging. This is caused by the long lifetime of these gases which yields a well-mixed and large atmospheric background. As can be seen in Fig. 11, the highest and most distinctive CH_4 mixing ratios in the PBL were encountered in the Po Valley (up to 2.4 ppm), downwind of London and across the BNL/Ruhr region (up to 2 ppm). Slightly lower mixing ratios were detected downwind of Barcelona (up to 1.94 ppm). The CH_4 mixing ratios were higher than the global mean ground level mixing ratio of around 1.85 ppm for July 2017. At large downwind distances from the MPC regions the CH_4 emissions are diluted and/or mixed with pollution from surrounding sources. Although the contribution of BB emissions to total global anthropogenic CH_4 is on the order of a few percent (Saunois et al., 2019) mixing ratios of CH_4 comparable to those in urban plumes were occasionally measured in BB events that strongly influenced the local GHG distribution, as during E-EU-07 (not shown). For the assignment of the GHG enhancements to their source region, supporting model simulations and complementary measurements of shorter-lived species with smaller background concentrations and thus better signal-to-background ratios are therefore needed (Klausner, 2020).

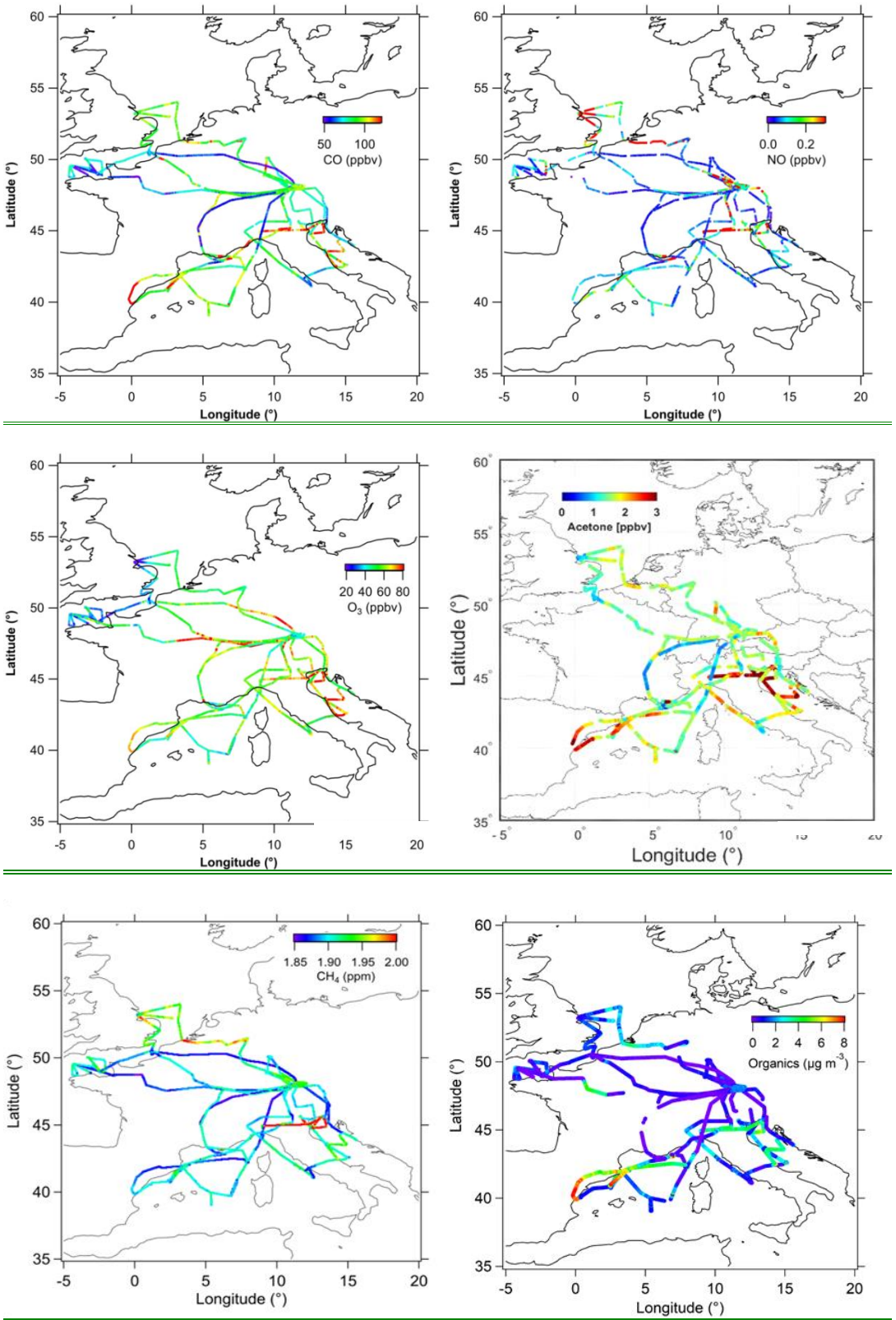

Figure 11: Mixing ratios of CO, NO, O_3, CH_3COCH_3, CH_4, and organic aerosol mass concentrations measured along all EMeRGe flights in Europe. To increase colour contrast, 50 ppbv has been set as lower limit for CO, and 0.5 ppbv and 80 ppbv as upper limit for NO and O_3, respectively. These limits are representative for more than 95% of all measurements. CH_4 mixing ratios are in 0.05 x 0.05° bins as in Klausner (2020). Organic aerosol mass concentrations are plotted for the original time resolution of 30 sec. Note that mixing ratios measured at different altitudes in the shuttle areas are not distinguishable in the figure.

- Large amounts of HONO detected in the moderately polluted upper boundary layer (several 100 ppt) and in the lower free troposphere (several 10 ppt) often exceeded mixing ratios expected from known gas-phase reactions as indicated by comparisons with model simulations. Potential mechanisms for the heterogeneous HONO formation are explored using theoretical studies in combination with the gas-phase, aerosol composition and radiation observations. These measurements indicate that additional HONO is likely formed by a suite of different heterogeneous processes in the residual layer and lower free troposphere, in agreement with many near surface observations in the polluted environment. This additional HONO may contribute significantly to the oxidation capacity of these polluted air masses.
- Elevated concentrations of pollutants were typically observed below the top of the BL and occasionally after being transported over long distances. Curtain maps showing the latitudinal and vertical distributions of selected species supported the classification of the air masses, especially in the lower 2000 m of the troposphere. Differences observed North and South of the Alps are e.g. evident in Fig. 12, showing a reasonable agreement in the geospatial distribution of the cloud condensation nuclei (CCN) and CO which has been documented as a nearly linear relationship within the PBL by Pöhlker et al. (2016, 2018). CO is a good tracer for relatively fresh combustion (e.g. Andreae, 2019). The CO emitted by open BB exceeds concentrations from anthropogenic sources. Thus, the good agreement for CCN and CO in the lower troposphere for the peak concentrations (color-coded in red in Fig. 12) implies BB to be the source of CCN. Elevated CO observations not related to increases in CCN indicate aerosol removal by cloud processing (e.g. Fig. 12 above 4000 m between 41 and 44°N) .

The vertical and latitudinal distribution of the CCN number concentration (N_{CCN}) showed a strong vertical gradient. Generally, N_{CCN} was highest in and above the PBL, up to ~2000 m a.s.l. The N_{CCN} depends strongly on the particular air mass, its photochemical history and the source of pollution as shown in Fig. 12b. In Northern Europe, (50 to 55 °N), N_{CCN} up to 1200 cm^{-3} were measured in the London outflow over the North Sea and over the BNL/Ruhr region. Below 46 °N, N_{CCN} often exceeded 1500 cm^{-3} above the MPC in the Po Valley, Rome, Marseille and Barcelona, the highest concentrations being observed in the Po Valley. An interesting observation was the distinct layer of BB smoke measured above the PBL between 2000 and 3500 m altitude, close to Marseille and Barcelona (40 to 42 °N). The high N_{CCN} due to BB are episodic in nature, whereas the CCN emissions from anthropogenic activity are produced daily with probably a weekend modulation. The vertical profile in Fig. 12b is a composite of all data but clearly shows that altitudes below 2000 m have the highest N_{CCN}. The increased values between 2000 and 4000 m are associated with air masses, which either come from Po Valley air being lifted up the Alps (e.g. Diemoz et al. 2019a, b), or from BB events upwind flowing into the Mediterranean.

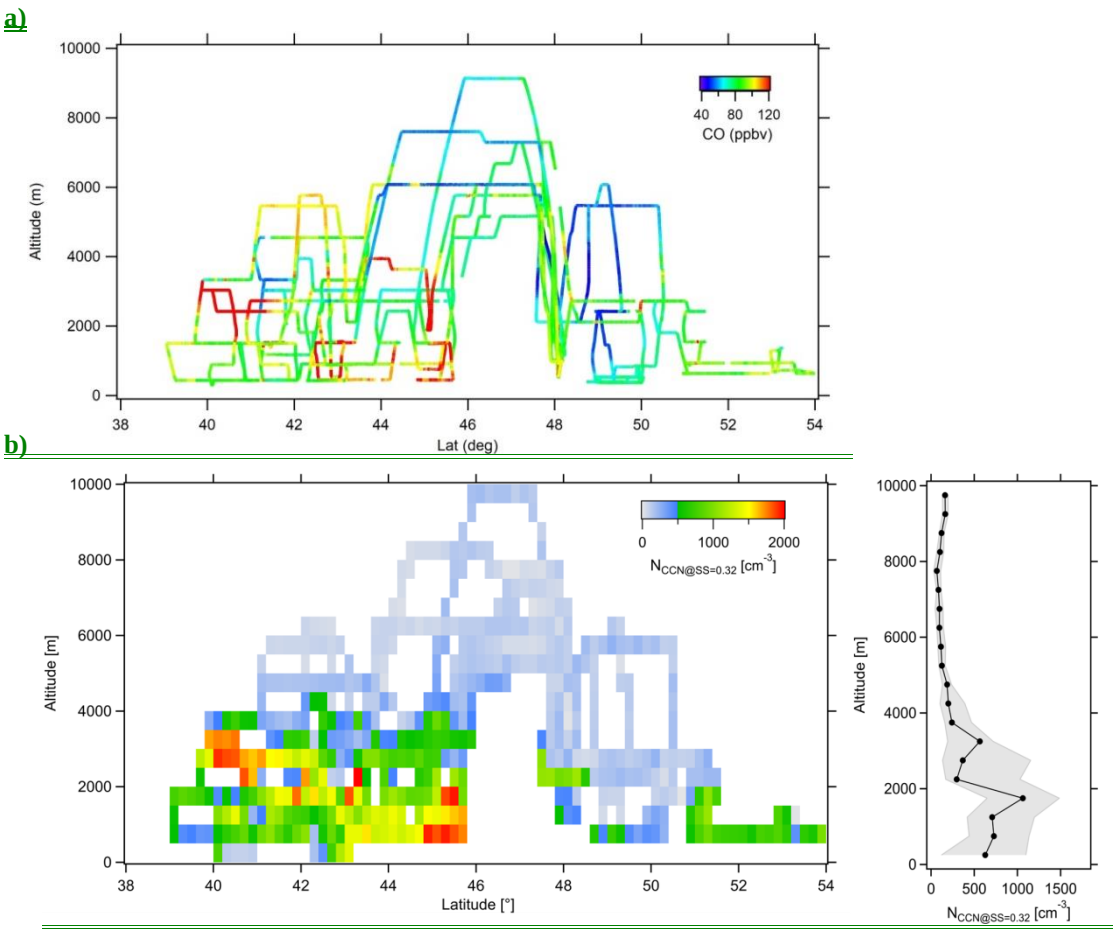

Figure 12: Vertical and latitudinal distribution observed during the EMeRGe IOP of a) CO mixing ratios, and b) CCN number concentration at a supersaturation (*S*) of 0.32 % (except for E-EU-04, due to instrumental failure). The CCN curtain plot on the left is made with latitude- (0.2°) and altitude-binned (500 m) CCN number concentrations. On the right, the median vertical N_{CCN} (*S*=0.32 %) profile is represented by a solid black line and the interquartile range by a grey shaded area. CCN data is STP corrected.

~~Table 4 shows the average, median and quartiles values of selected species measured during E-EU-08 and E-EU-06 as examples of flights in Northern and Southern Europe, respectively. The mean values and variability of most of the species are of the same order of magnitude in both flights and generally higher for E-EU-06 below 2000 m except for NO. Higher temperatures and insolation in the South are associated with higher O_3 and RO_2^* as for example observed in E-EU-06 below 2000 m. The higher SO_2 and CH_3CN mean values are associated to the plumes measured in the Po Valley and to the fires dominating in the South during the IOP, respectively. The average concentrations measured for the rest of the EMeRGe flights are included in the supplement (S10).~~

~~**Table 4:** Mean concentrations (mean), median (med) and quartiles (25^{th}-75^{th}) of selected measured trace gases and aerosol particles for E-EU-08 and E-EU-06 as examples of flights in Northern and Southern Europe. n.a. non available. *HCHO: HCHO from PTRMS measurements; *HCHO: HCHO from miniDOAS measurements; N_{CN}: $N_{D>250nm}$ particle with D> 10 nm, and D>250 nm, respectively (inlet cut-off 1.5 to 3 µm depending on height); BCm: black carbon mass concentration; BCn: black carbon number concentration; OA: Organic aerosol. Note that NCN, N_D, BCm, BCn, OA, NO_3^-, SO_4^{2-}, NH_4^+ and Cl^- are given for standard temperature and pressure conditions.~~

E-EU-08	<2000 m				2000-4000 m				>4000 m				
species	mean	med	25th	75th	mean	med	25th	75th	mean	med	25th	75th	Unit
O_3	43	45	37	49	51	53	49	55	64	63	56	73	ppbV
CO	98	96	92	102	90	91	85	93	94	93	92	96	ppbV
NO	407	225	155	450	138	77	60	108	109	102	82	131	pptV
NO_y	3734	3039	2075	4018	1991	1302	720	1777	4619	3765	2652	5761	pptV
HONO	n.a.	n.a.	n.a.	n.a.	n.a.	n.a.	n.a.	n.a.	n.a.	n.a.	n.a.	n.a.	pptV
NO_2	n.a.	n.a.	n.a.	n.a.	n.a.	n.a.	n.a.	n.a.	n.a.	n.a.	n.a.	n.a.	pptV
*HCHO	n.a.	n.a.	n.a.	n.a.	n.a.	n.a.	n.a.	n.a.	n.a.	n.a.	n.a.	n.a.	pptV
RO_2^*	20	21	10	29	31	28	21	37	19	13	0	35	pptV
SO_2	193	99	68	169	55	54	43	64	55	52	38	68	pptV
N_{CN}	4514	3186	2066	4551	1041	790	582	1245	2900	1635	728	3935	cm^{-3}
$N_{D>250nm}$	119.2	111.5	61.1	161.1	18.2	12.3	6.2	21.8	7.7	4.4	2.3	9.2	cm^{-3}
BCm	0.14	0.12	0.07	0.18	0.02	0.01	0.01	0.03	0.01	0.00	0.00	0.01	$\mu g\ m^{-3}$
BCn	71	68	42	92	10	8	4	13	4	3	2	6	cm^{-3}
OA	1.80	1.88	1.21	2.37	0.58	0.51	0.34	0.71	0.49	0.50	0.36	0.63	$\mu g\ m^{-3}$
NO_3^-	1.21	0.96	0.60	1.68	0.10	0.07	0.05	0.11	0.07	0.06	0.05	0.08	$\mu g\ m^{-3}$
SO_4^{2-}	0.85	0.73	0.56	0.97	0.20	0.18	0.13	0.23	0.09	0.09	0.07	0.11	$\mu g\ m^{-3}$
NH_4^+	0.80	0.65	0.46	1.08	0.16	0.13	0.10	0.19	n.a.	n.a.	n.a.	n.a.	$\mu g\ m^{-3}$
Cl^-	0.09	0.08	0.05	0.12	0.03	0.02	0.01	0.03	0.03	0.03	0.02	0.03	$\mu g\ m^{-3}$
C_3H_6O	1517	1543	1347	1705	1384	1404	1312	1495	1602	1614	1534	1707	pptV
CH_3CN	94	95	80	106	130	126	113	140	130	131	116	147	pptV
C_5H_8	80	68	56	89	61	57	50	65	69	65	56	71	pptV
C_6H_6	64	63	47	78	33	29	25	36	30	27	24	38	pptV
C_7H_8	45	35	25	55	29	24	18	33	22	19	17	24	pptV
^{x}HCHO	1234	1165	937	1461	642	637	538	733	411	407	290	496	pptV
$C_2H_2O_2$	n.a.	n.a.	n.a.	n.a.	n.a.	n.a.	n.a.	n.a.	n.a.	n.a.	n.a.	n.a.	pptV
$C_3H_4O_2$	n.a.	n.a.	n.a.	n.a.	n.a.	n.a.	n.a.	n.a.	n.a.	n.a.	n.a.	n.a.	pptV

E-EU-06	<2000 m				2000-4000 m				>4000 m				
species	mean	med	25th	75th	mean	med	25th	75th	mean	med	25th	75th	Unit
O_3	69	71	58	77	52	51	50	52	58	56	53	64	ppbV
CO	111	113	94	125	78	77	73	81	77	78	70	82	ppbV
NO	189	123	84	205	71	56	47	66	483	42	23	136	pptV
NO_y	3321	2542	1701	4104	737	581	465	939	2006	366	283	490	pptV
HONO	15	13	0	27	3	0	0	9	0	0	0	0	pptV
NO_2	454	378	238	531	169	174	115	199	191	172	43	303	pptV
*HCHO	1408	1219	996	1731	709	690	627	748	588	597	580	599	pptV
RO_2^*	49	52	36	63	41	44	30	53	31	38	16	44	pptV
SO_2	673	514	289	877	136	131	113	152	120	85	73	100	pptV
N_{CN}	6136	2943	2052	4823	1493	1291	1147	1496	914	803	603	1185	cm^{-3}
$N_{D>250nm}$	174.2	150	85.8	224.3	49	48.5	41.1	54.9	22.2	16.3	7	30.7	cm^{-3}
BCm	0.30	0.28	0.14	0.40	0.09	0.07	0.05	0.10	0.04	0.02	0.01	0.04	$\mu g\ m^{-3}$
BCn	127	127	65	176	34	33	28	39	11	7	4	18	cm^{-3}
OA	3.12	3.25	2.02	3.92	1.07	1.00	0.73	1.32	0.45	0.34	0.28	0.51	$\mu g\ m^{-3}$
NO_3^-	0.69	0.15	0.09	0.62	0.07	0.06	0.05	0.08	0.07	0.05	0.04	0.08	$\mu g\ m^{-3}$
SO_4^{2-}	1.64	1.49	0.98	1.93	0.59	0.61	0.55	0.68	0.27	0.20	0.11	0.44	$\mu g\ m^{-3}$
NH_4^+	0.82	0.67	0.46	1.04	0.28	0.29	0.24	0.32	0.17	0.17	0.09	0.22	$\mu g\ m^{-3}$
Cl^-	0.04	0.04	0.02	0.05	0.02	0.02	0.01	0.02	0.03	0.03	0.03	0.03	$\mu g\ m^{-3}$
C_3H_6O	2444	2434	1935	2937	1645	1656	1514	1799	1476	1452	1316	1605	pptV
CH_3CN	140	131	115	152	129	131	118	138	135	132	123	145	pptV
C_5H_8	98	78	59	112	62	57	50	64	73	67	55	83	pptV
C_6H_6	109	94	56	152	36	34	25	41	32	30	22	37	pptV
C_7H_8	57	42	25	77	35	25	22	51	32	30	26	37	pptV
^{x}HCHO	1843	1651	1088	2374	891	875	748	993	641	616	491	782	pptV
$C_2H_2O_2$	220	192	132	276	182	103	49	260	101	63	8	111	pptV
$C_3H_4O_2$	1496	1275	1075	1577	1351	790	574	1622	817	571	296	756	pptV

~~The transport, transformation and radiative impact of pollutants depend on their vertical distribution. During the EMeRGe IOP the maximum concentrations of trace gases and aerosol species were typically measured below 2000 m. Figure 12 shows the vertical distribution of CO, O_3, NO_y and PAN mixing ratios for all HALO observations made during the EMeRGe IOP, averaged over altitude bins of 500 m. CO, total reactive nitrogen~~

~~(NO_y) and its most reactive forms NO and NO_2, are key species in the identification of anthropogenic pollution.~~

4.2 Identification, classification and characteristics of pollution plumes

Anthropogenic and biogenic signatures were identified in the pollution plumes by using enhancements in the concentration of selected species, such as CO, NO_y and VOCs measured on-board HALO. Measured large pollution plume events were initially categorised into a) anthropogenic pollution (AP), b) biomass burning (BB), c) mixed and d) biogenic plumes, by using enhancements of CH_3CN, C_6H_6 and C_5H_8 over 184 ppt, 49 ppt and 85 ppt thresholds, respectively. These thresholds take into consideration three times the instrumental noise over the limit of detection (LOD) or the individual atmospheric background values. Anthropogenic polluted air masses were e.g. identified by the enhancements of C_6H_6 and absence of CH_3CN in contrast with the unpolluted background air in the absence of both chemical tracers. Similarly, CH_3CN enhanced plumes in the absence of C_6H_6 were identified as pure or aged BB events (see S12 for details). ~~During daylight, NO and NO_2 are typically in or close to a photostationary state that is established in the order of minutes. Further photochemical reactions convert NO and NO_2 into longer lived reservoirs such as PAN or HNO_3. PAN has major implications for the global distributions of O_3 and OH as it can release NO_2 at higher tropospheric temperatures far from the sources of pollution (e.g. Fischer et al., 2014). On average, changes of CO with altitude were not pronounced except below 2000 m and above 8000 m. This is consistent with the relatively long lifetime of CO and a well mixed troposphere in summer. As the lifetime of NO_y is much shorter than that of CO, the distance from the source has a stronger influence on NO_y than on CO observations. NO_y shows a pronounced height dependence and variability which is reflected in the large standard deviations and the differences between mean and median values (not shown). The PAN measurements made up to 3000 m altitude have a similar behaviour. The high NO_x/NO_y ratios occasionally observed at high altitudes are attributed to NO_x production by lightning and more rapid transport.~~

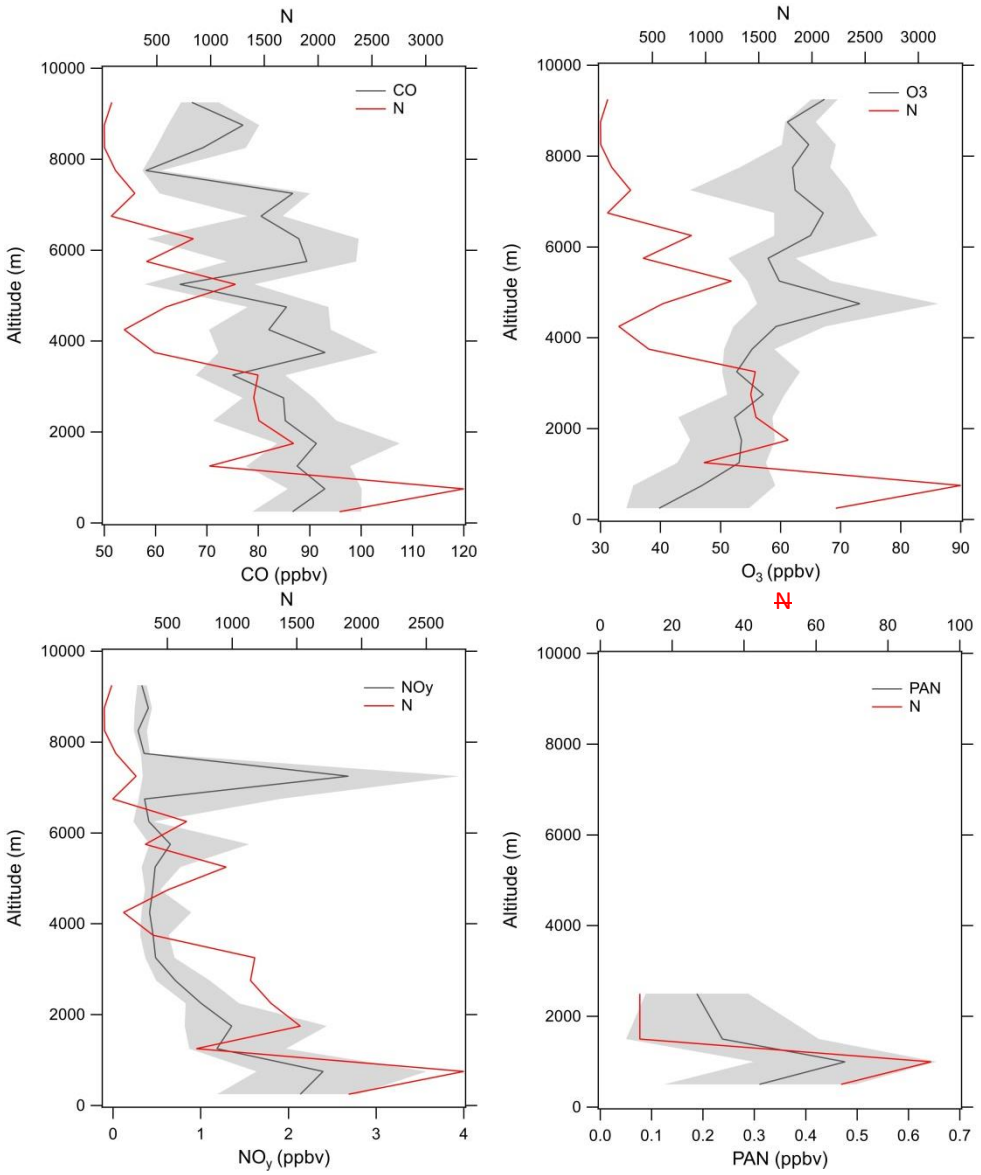

~~**Figure 12:** Variation of CO, O_3, NO_y and PAN volume mixing ratios versus altitude during EMeRGe over Europe. Solid lines represent the medians averaged over altitude bins of 500 m and the shaded areas are the quartiles. The number of measuring points (N) is shown in red.~~

- Figure 13 illustrates the result of applying this procedure to the flight E-EU-08 on 26 July 2017, which investigated the London and BNL/Ruhr MPC outflows (see Sect.4.3).

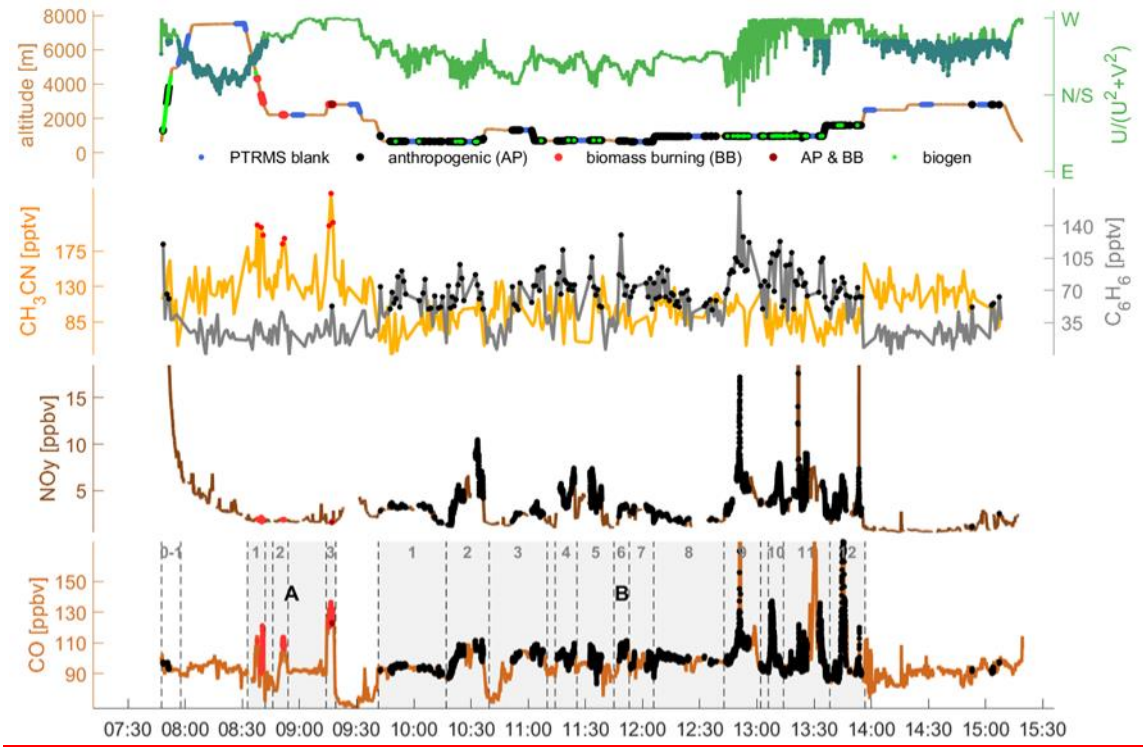

Figure 13: Time series for E-EU-08 on the 26 July 2017 used for the categorisation of plumes based on VOC measurements: altitude, wind direction, CH_3CN, C_6H_6 and NO_y as refinement. The wind direction (green line and axis) is given as $U/(U^2+V^2)$, -1 is east wind (E), +1 is west wind (W), values around zero have North or South components (N/S). South components are marked with dark green colour. Altitude (brown line, top panel) is colour-coded in green during C_5H_8 enhancements, in red during CH_3CN enhancements, in black during C_6H_6 enhancements and in dark red during both, CH_3CN and C_6H_6 enhancements. Additionally, blue colour-coded blank measurements of CH_3CN, C_6H_6 and C_5H_8 are given. In the bottom panel, final numbering of structures and plumes according to concentration enhancements are shown for CO. Colour-coding indicates CH_3CN enhancements (red), C_6H_6 enhancements (black), and both, CH_3CN and C_6H_6 enhancements (brown).

- Anthropogenic polluted air presented distinctive features in contrast to background air in Europe. These are summarised as follows:

a) Maximum concentrations of trace gases and aerosol species of anthropogenic origin were typically measured below 2000 m during the EMeRGe IOP.

As an example, Fig.14 shows median vertical distributions of observed major primary and secondary VOCs. ~~observed during the EMeRGe IOP in Europe.~~ Longer lived VOCs were as expected well mixed in the troposphere and those with anthropogenic sources showed higher variability and highest mixing ratios below 2000 m. Benzene (C_6H_6) and toluene (C_7H_8) are primarily of anthropogenic origin. HCHO and acetaldehyde (C_2H_4O) have anthropogenic BB and significant biogenic sources. They are also generated downwind by the oxidation of transported VOCs. ~~In contrast, benzene (C_6H_6) and toluene (C_7H_8) are primarily of anthropogenic origin.~~ These species have a short lifetime as they are oxidised quickly in the lower layers of the troposphere. As a result, the concentrations observed above 2000 m were close to the LOD.~~instrumental limit of detection.~~ The same is true for isoprene (C_5H_8) and xylene (C_8H_{10}) which have lifetimes in the order of some hours.

~~Acetonitrile (CH_3CN) and acetone (CH_3COCH_3) are typically well mixed in the troposphere due to their longer lifetimes, which are in the order of months.~~ This~~As a recognised tracer for BB, the increase of median CH_3CN with altitude identifies the LRT of BB emissions from North America and the local transport of BB events in Europe. The averaged~~ vertical distribution is not as evident in~~of methanol (CH_3OH), having ~ 12 days lifetime,~~

~~might result from the convective mixing of a variety of ground sources which in the summer are largely of biogenic origin.~~

~~Known sources of~~ glyoxal ($C_2H_2O_2$) and methylglyoxal ($C_3H_4O_2$) which result from~~are~~ the oxidation of C_5H_8 and BB. $C_2H_2O_2$ is also an oxidation product of acetylene (C_2H_2) which is of anthropogenic origin. $C_3H_4O_2$ is produced in the oxidation of CH_3COCH_3, which is thought to have a dominant biogenic source (Andreae, 2019; Wennberg et al., 2018). Both gases are also formed during the oxidation of other VOCs, particularly alkenes, aromatics, and monoterpenes (Myriokefalitakis et al., 2008; Fu et al., 2008; Taraborrelli et al., 2020) and are present both as primary or secondary pollutants during BB events (e.g., Vrekoussis et al., 2009; Alvarado et al., 2020).

Acetonitrile (CH_3CN) and acetone (CH_3COCH_3) are typically well mixed in the troposphere due to their longer lifetimes, which are in the order of months. The increase of median CH_3CN with altitude identifies the LRT of BB emissions from North America and the local transport of BB events in Europe.

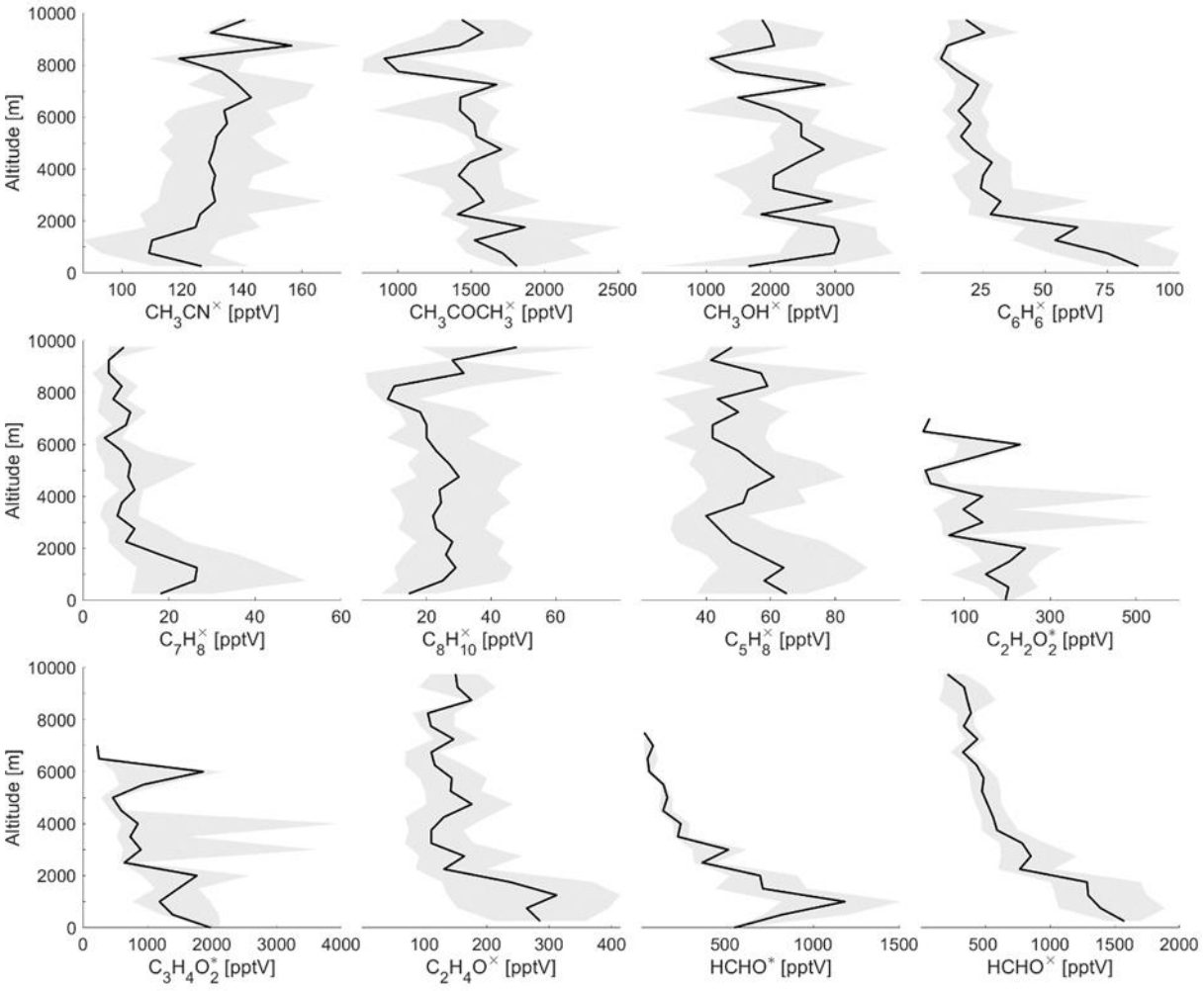

Figure 14~~13~~: Variation of VOC versus altitude measured by the HKMS (labeled with ×) and the miniDOAS (labeled with *) instruments during EMeRGe over Europe. Shaded areas are the quartiles, solid lines represent median concentrations.

During EMeRGe, HCHO was measured by the in-situ HKMS and the mini-DOAS remote sensing instruments (see Table 2). These instruments probed slightly different air masses due their instrument characteristics (for averaging kernel of the mini-DOAS instrument see S11 in the supplement), and did not operated at strictly the same data rate and for the same times. For example, unlike HKMS, mini-DOAS did not probe the polluted air

masses during aircraft ascent and descent from OP. Despite differences in sampling volume, rate and time, the instrument specific average vertical distribution of HCHO measured on-board HALO by both instruments illustrates in a similar manner the differences in trace gas concentrations encountered in polluted and background air during the EMeRGe IOP (see Fig. 15).~~The HCHO mixing ratios measured by the in-situ PTRMS (HKMS) and the remote sensing miniDOAS instruments~~ In the air masses classified as polluted the HCHO results from direct emission and oxidation of VOC precursors and is discernibly higher than the lower boundary of the measurements. The HCHO in the less polluted or background air in Europe is then attributed to be predominantly released from CH_4 oxidation.

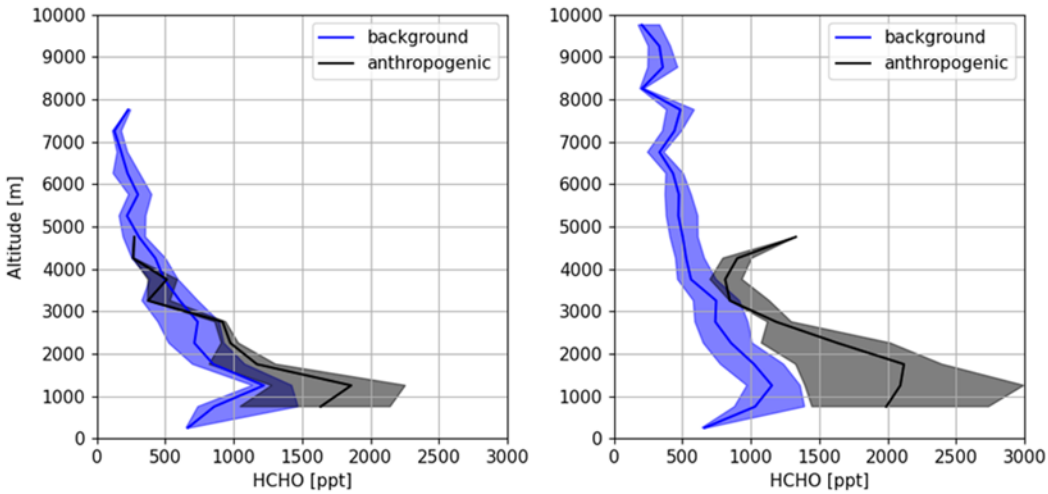

Figure 15: Vertical profiles of HCHO (miniDOAS left, HKMS right) for pure anthropogenic emissions (C_6H_6 enhancement in absence of CH_3CN) and background air (in the absence of C_6H_6 and CH_3CN). Shaded areas are the quartiles, solid lines represent median concentrations.

The HCHO mixing ratios measured during the IOP in Europe are consistent with previous remote sensing observations over South East Asia (Burrows et al., 1999) and North America in summer (Kluge et al., 2020; Chance et al., 2000; Dufour et al., 2009; Boeke et al. 2011; De Smedt et al., 2015; Kaiser et al., 2015; Chan Miller et al., 2017, and references therein). They are also in the same range as those measured in the Po Valley (Heckel et al., 2005).

The HCHO mixing ratios observed in the PBL and middle troposphere during EMeRGe are somewhat lower than all summer~~the~~ North American mixing ratios previously measured (see Fig. 16). The~~14). This might be related to the fact that several EMeRGe flight tracks were carried out far from emission sources over the North and the Mediterranean Seas. In addition, the~~ emissions of HCHO and its VOC precursors have been reported in previous studies to be lower in Europe than in North America (e.g. Dufour et al., 2009; De Smedt et al., 2015). However, as several EMeRGe flight tracks were carried out far from emission sources over the North and the Mediterranean Seas, this difference might be related to a larger marine influence to the air masses analysed over Europe.

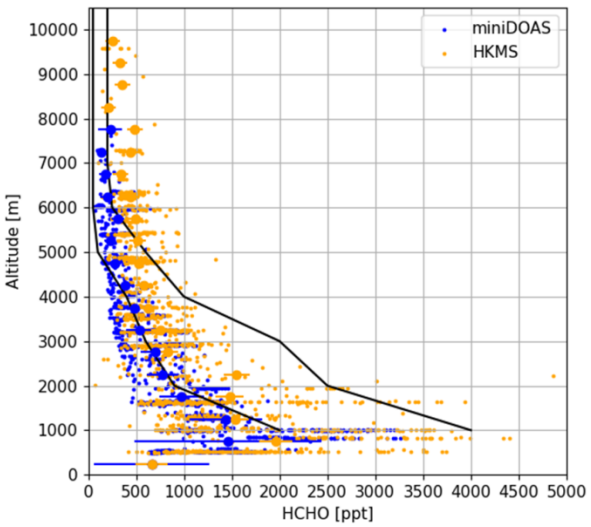

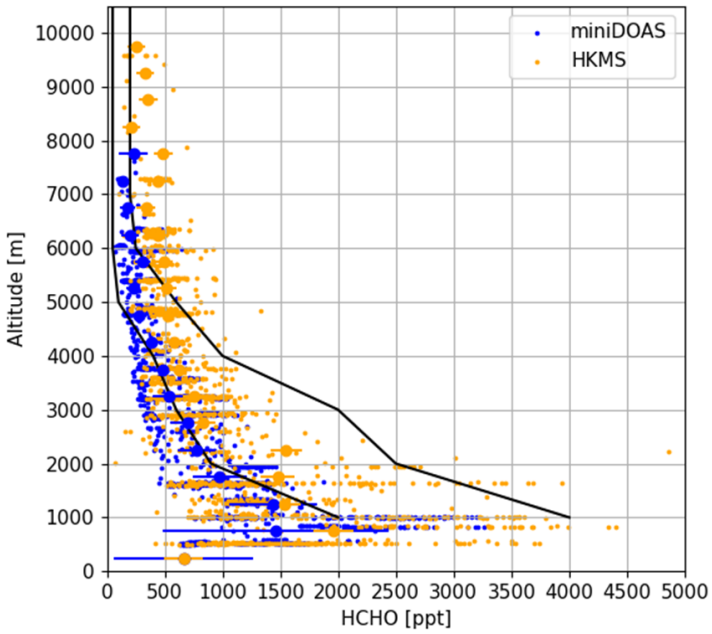

Figure 16~~14~~: HCHO measurements by the HKMS (in orange) and the miniDOAS instruments (in blue). Mean values (bigger dots) and the respective accuracies (horizontal bars) are also shown. The black lines indicate the range of previous HCHO measurements over North America in summer (Kluge et al., 2020). Note that HKMS and miniDOAS agree within their accuracies in spite of having different air sampling volumes, which did not perfectly overlap.

Inside pollution plumes small particles in the diameter range 0.01 to 3 µm dominated. In the ~~The~~ vertical ~~profiles shown in Fig. 14 are averages from the measurements taken along all flights at variable distances from various source regions and under different meteorological conditions. In a next step, pollution hotspots are identified by using the spatial~~ distribution of ~~trace gases and aerosol particles observed over the flight tracks. Figure 15 shows as an example the CO NO, O_3, CH_3COCH_3, CH_4, and the organic aerosol mass concentrations measured during the EMeRGe flights in Europe.. A detailed analysis of the complexity of the air masses measured and the variations encountered in individual flights is beyond the scope of the present work and will be presented in dedicated publications.~~

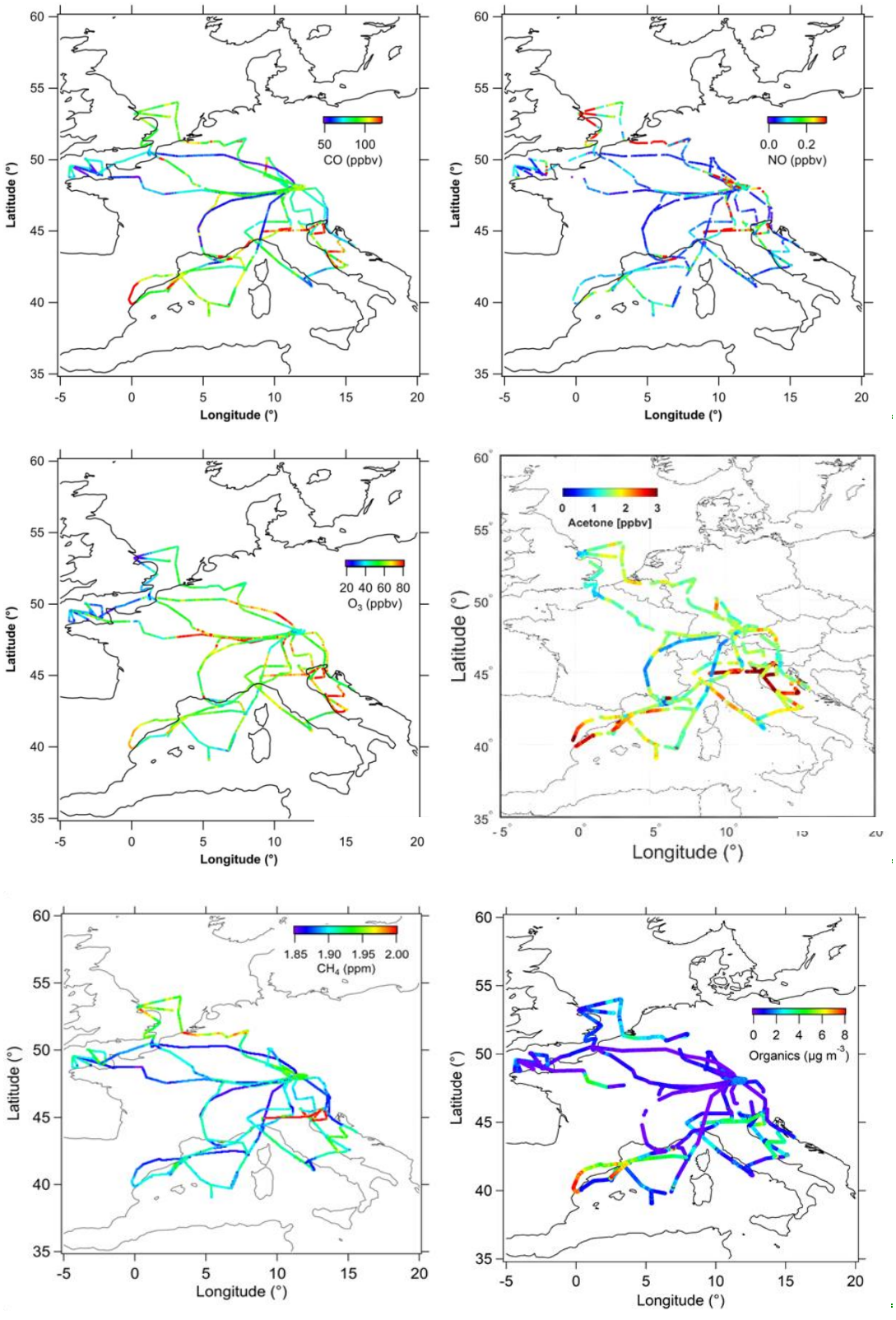

1033

1034

1035

1036 ~~**Figure 15:** Mixing ratios of CO, NO, O_3, CH_3COCH_3, CH_4, and organic aerosol mass concentrations measured along all~~
1037 ~~EMeRGe flights in Europe. To increase colour contrast, 50 ppbv has been set as lower limit for CO, and 0.5 ppbv and 80~~
1038 ~~ppbv as upper limit for NO and O_3, respectively. These limits are representative for more than 95% of all measurements. CH_4~~
1039 ~~mixing ratios are in 0.05 x 0.05° bins as in Klausner (2020). Organic aerosol mass concentrations are plotted for the original~~
1040 ~~time resolution of 30 sec. Note that mixing ratios measured at different altitudes in the shuttle areas are not distinguishable in~~
1041 ~~the figure.~~

1042 ~~During the EMeRGe IOP in Europe, the highest NO concentrations were found in the vicinity and downwind of~~
1043 ~~major pollution sources like London, the BNL/Ruhr region and the Po Valley. High NO concentrations are~~

indicative of recent or "fresh" anthropogenic emissions. The NO_y lifetime of a few days enables a more reliable identification of aged polluted air masses further out from the source regions. Maximum NO_y values as large as 12 ppbv were measured. Elevated CO and NO_y, accompanied by low NO, as measured in the proximity of Barcelona, indicate that there has been a significant amount of processing of the pollution plumes sampled. Emission hot-spots can be hardly identified in the spatial distribution of O_3, as expected from its non-linear secondary formation. Maximum O_3 mixing ratios were generally observed at a distance downwind of MPCs, determined by O_3 production and loss in the plumes.

Organic aerosol has strong anthropogenic sources such as combustion (traffic, fossil fuel combustion, BB) and industrial activity, and shows similar behaviour to CO and NO, in that larger mass concentrations are closer in time and space to MPCs such as London, Po Valley, and BNL. The lifetime of aerosol particles in the PBL is a few days, which explains the high variability observed. Additionally, aerosol particle concentrations have a strong gradient above the PBL (see Sect. 4.1). As a result, the flight shuttles at different altitudes have large variability in the horizontal distribution.

The highest and most distinctive CH_4 mixing ratios in the PBL were likewise encountered in the Po Valley (up to 2.4 ppm), downwind of London and across the BNL/Ruhr region (up to 2 ppm). Slightly lower mixing ratios were detected downwind of Barcelona (up to 1.94 ppm). The mixing ratios were higher than the global mean ground level mixing ratio of around 1.85 ppm for July 2017. The emission plume signatures were generally more evident when shuttles were performed close to the respective MPC regions. At large downwind distances the CH_4 emissions are diluted and/or mixed with pollution from surrounding sources. For the assignment of the GHG enhancements to their source region, supporting model simulations and complementary measurements of shorter lived species with smaller background concentrations and thus better signal to background ratios are needed (Klausner, 2020).

The distribution of highly reactive species such as peroxy radicals, during the flights is determined by the rates of photochemical production and loss of HO_2 and organic peroxy radicals RO_2. The RO_2^{Σ} measured is the sum of $HO_2 + \sum RO_2$, R being an organic chain which produces NO_2 in its reaction with NO. Oxygenated VOC (OVOC) result from the oxidation of VOC emissions (e.g. CH_3COCH_3 or HCHO) and are strong sources of HO_2 and CH_3O_2. The RO_2* mixing ratios observed in EMeRGe are shown in Fig. 16. Mixing ratios up to 120 pptv RO_2^*, 3 ppbv of CH_3COCH_3 and 4 ppbv of HCHO were measured in the air masses probed. Provided insolation conditions (i.e. actinic fluxes) and amount of precursors are similar, the production of peroxy radicals is observed as long as plumes mix at any altitude. Generally, higher RO_2* were measured below 45°N. This is in part due to the higher insolation during the flights over the Mediterranean area, which accelerates photooxidation and the production of RO_2*. The O_3 production rates calculated from the RO_2^* measured on board are consistent with the values reported in urban pollution for NO<1 ppbv (e.g. Tan et al, 2017; Whalley et al, 2018, 2021). The photochemical activity of the air masses has been studied using the RO_2^*, the trace constituents and photolysis rates measured during the EMeRGe IOP (George et al., 2021, in preparation).

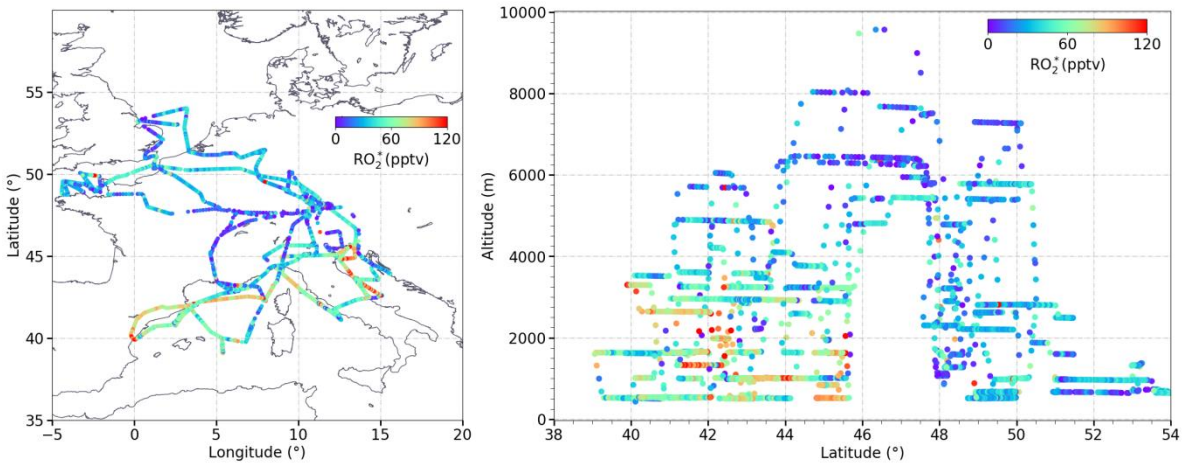

Figure 16: RO_2^* spatial and vertical distribution measured along all EMeRGe flights in Europe.

The identification of MPC outflows and the investigation of the pollution events benefits from knowledge of the mixing of anthropogenic, natural and biogenic sources during the EMeRGe flights. The curtain maps showing the latitudinal and vertical distributions of selected species help to classify the air mass mixtures, especially in the lower 2000 m of the troposphere. Differences observed North and South of the Alps are evident in Fig. 17, showing a reasonable agreement between the vertical distributions of CCN and CO which has been documented in earlier studies (e.g. Pöhlker et al. 2016, 2018).

The vertical and latitudinal distribution of the cloud condensation nuclei number concentration (N_{CCN}) shows a strong vertical gradient. Generally, N_{CCN} is highest in and above the PBL, up to ~2000 m a.s.l. The N_{CCN} depend strongly on the particular air mass, its photochemical history and the source of pollution as shown in Fig. 17b. In Northern Europe, (50 to 55 °N), N_{CCN} up to 1200 cm^{-3} were measured in the London outflow over the North Sea and over the BNL/Ruhr region. Below 46 °N, N_{CCN} often exceeds 1500 cm^{-3} above the MPC in the Po Valley, Rome, Marseille and Barcelona, the highest concentrations being observed in the Po Valley.

An interesting observation was the distinct layer of BB smoke measured above the PBL between 2000 and 3500 m altitude, close to Marseille and Barcelona (40 to 42 °N). The high N_{CCN} due to BB are episodic in nature, whereas the CCN emissions from anthropogenic activity are produced daily with probably a weekend modulation.. The vertical profile in Fig. 17b is a composite of all data but clearly shows that altitudes below 2000 m have the highest N_{CCN}. The peak between 2000 and 4000 m is associated with air masses, which either come from BB events upwind and flow into the Mediterranean, or are Po Valley air being lifted up the Alps.

a)

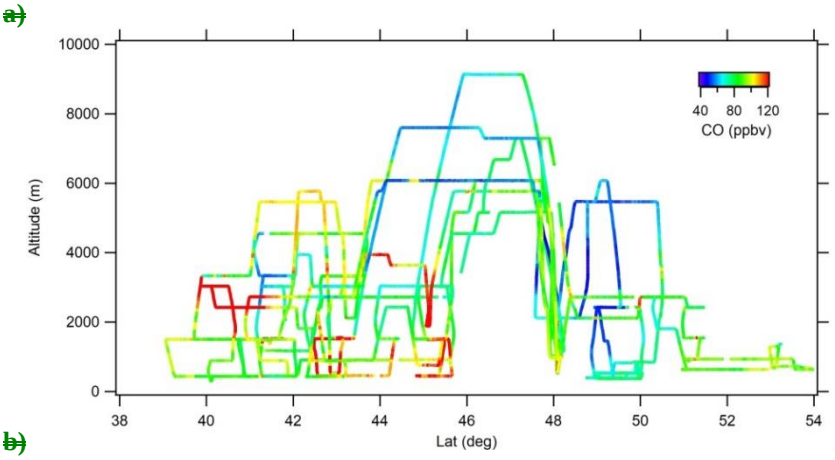

b)

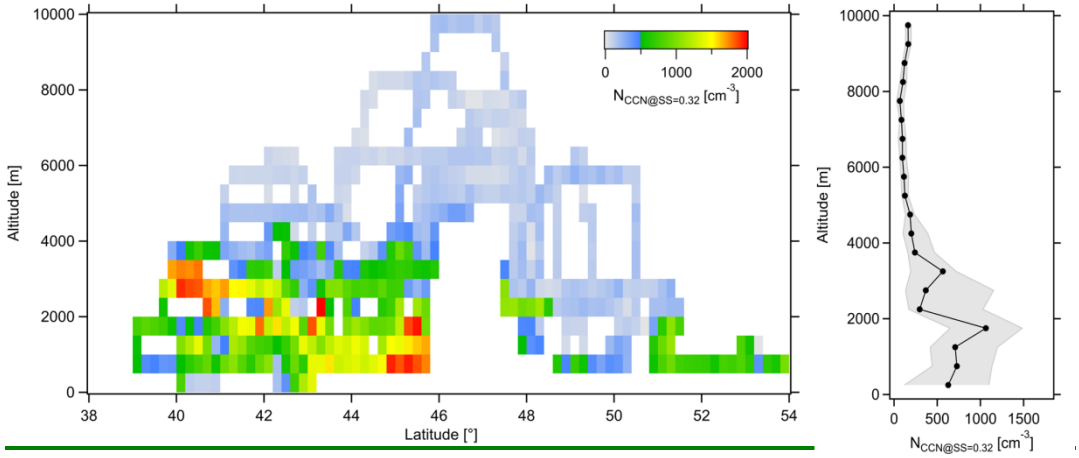

Figure 17: Vertical and latitudinal distribution observed during the EMeRGe IOP of a) CO mixing ratios, and b) CCN number concentration at a supersaturation (*S*) of 0.32 % (except for E-EU-04, due to instrumental failure). The CCN curtain plot on the left is made with latitude- (0.2°) and altitude-binned (500 m) CCN number concentrations. On the right, the median vertical N_{CCN} (*S*=0.32 %) profile is represented by a solid black line and the interquartile range by a grey shaded area. CCN data is STP corrected.

4 Identification of pollution outflows within the EMeRGe IOP in Europe

The investigation of transport and transformation of MPC outflows over Europe benefits from the unambiguous identification of individual MPC sources. With this objective, a series of complementary plume tagging or identification approaches were used in the EMeRGe IOP in Europe:

I) Enhancement in the concentration of selected atmospheric species

Periods in which large pollution plume events were measured on board HALO were initially categorised into the following: a) anthropogenic pollution (AP), b) biomass burning (BB) and c) mixed plumes, by using the presence and enhancements of VOCs in these plumes, which are characteristic for different sources. For example, CH_3CN is almost exclusively emitted from BB (de Gouw et al., 2003; Warneke et al., 2010) whereas C_6H_6 is emitted by traffic and petroleum- related industrial activities (Paz et al., 2015) as well as BB (Simpson et al., 2011; Andreae, 2019). Hence, C_6H_6 enhancements in the absence of CH_3CN can be used to identify relatively "pure" anthropogenic pollution. Similarly, CH_3CN enhanced plumes in the absence of C_6H_6 are identified as pure or aged BB events. Events with only CH_3CN can originate from mixed sources, as C_6H_6 may have decayed while CH_3CN remains, due to the different atmospheric lifetimes of these two tracers (CH_3CN ~ 6 month, C_6H_6 ~

10 days). When both VOCs are enhanced, the plumes are considered to have air masses from either BB and AP sources or only from recent BB. Additionally, enhanced C_5H_8 as short lived biogenic tracer is used as an indicator for recent contact with the PBL having biogenic sources (Förster et al., 2021, in preparation).

These large categorised pollution events were then further classified into single plumes by using altitude, water content, wind direction and enhancements in the concentrations of pollution tracers such as CO and NO_y measured on board HALO. Fine structures or signatures in individual plumes were numbered relative to the main plume event they belong to.

All plumes encountered are numbered using the notation E-EU-FN-S-PL similarly to the flight nomenclature mentioned in Sect. 2.3, i.e., E stands for EMeRGe, EU for the campaign in Europe, FN are 2 digits for the flight number, S is the letter assigned to the identified captured pollution event, and PL are two digits reserved for the plume number within each pollution event.

II) Backward trajectories: last contact with PBL

The origin and history of the plumes probed at each point of the flight track are traced by using highly resolved backward trajectories calculated by the kinematic trajectory model FLEXTRA (Stohl et al., 1995, 1999). Parameters calculated using FLEXTRA and meteorological fields are used to assign the origin of the observed plumes to the EMeRGe targets in different parts of the flight tracks. Typically, the last contact to the PBL (lcPBL), i.e., the time when the backward trajectory reaches the PBL the first time, and sensitivity trajectories which provide the probability of contact of a particular air mass with the lower meters of the PBL before the measurement are used. This information is cross checked with the estimated age of air masses based on HYSPLIT CO dispersion calculations in III). More details about trajectories and related parameters are given in S11 in the supplement.

III) Forward trajectories: dispersion of MPC outflows

In a similar approach to that used in the forecast procedures (see Sect. 2.3 and S3 in the supplement), the HYSPLIT dispersion model was used to calculate the dispersion of CO emissions using emission rates from the EDGAR HTAP V2 emission inventory. They are expressed as CO enhancement caused by the selected MPC outflow over the CO background. The performances of FLEXPART and HYSPLIT for the EMeRGe data are compared for the case studies within EMeRGe.

IV) Detection of released PFC tracers

Sampling of PMCH from a tracer release in the centre of London during E-EU-05, and from a tracer release in the centre of London and at the University of Wuppertal during E-EU-08, enabled the prediction of the dispersion and the mixing of the targeted MPC outflows in these flights to be compared. Details on the tracer experiments during the EMeRGe IOP over Europe are described in Schlager et al. (2021 in preparation).

4.1 Characterisation of polluted air masses by using chemical tracers

Initially, as described in I) in the previous section, in situ measurements of C_6H_6 and CH_3CN on board HALO (Förster et al., 2021, in preparation) were used to identify measurements of unpolluted background air (absence of both tracers) and of anthropogenic polluted air masses (enhancement of C_6H_6 and absence of CH_3CN).

In Fig. 18, the HCHO measured by the miniDOAS and HKMS instruments on board is shown. In the air masses classified as polluted the HCHO results from direct emission and oxidation of VOC precursors and is discernibly higher than the lower boundary of the measurements. The HCHO in the less polluted or background air in Europe is then attributed to be predominantly released from CH_4 oxidation.

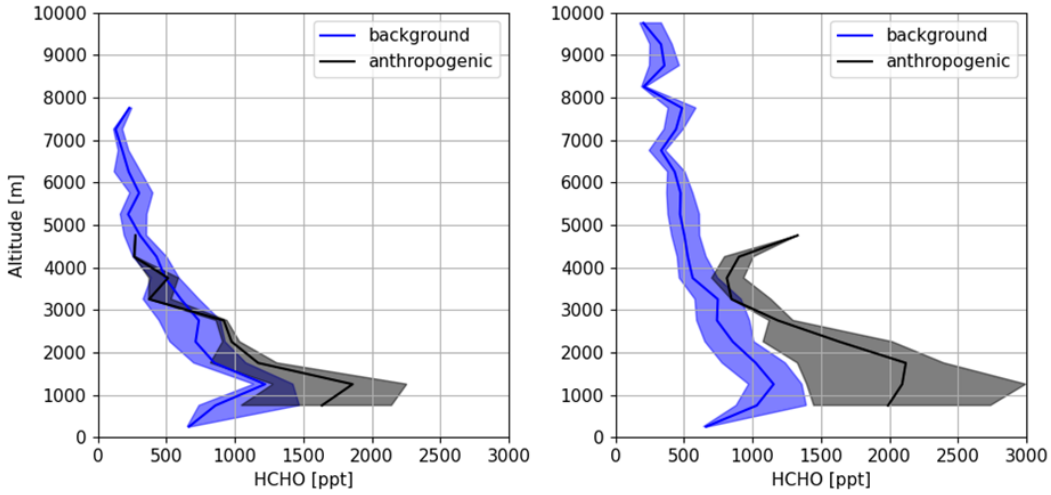

Figure 18: Vertical profiles of HCHO (miniDOAS left, HKMS right) for pure anthropogenic emissions (C_6H_6 enhancement in absence of CH_3CN) and background air (in the absence of C_6H_6 and CH_3CN). Shaded areas are the quartiles, solid lines represent median concentrations.

In a similar manner, the aerosol particle concentration and composition have been tagged for anthropogenic and background air masses (see Fig. 19).

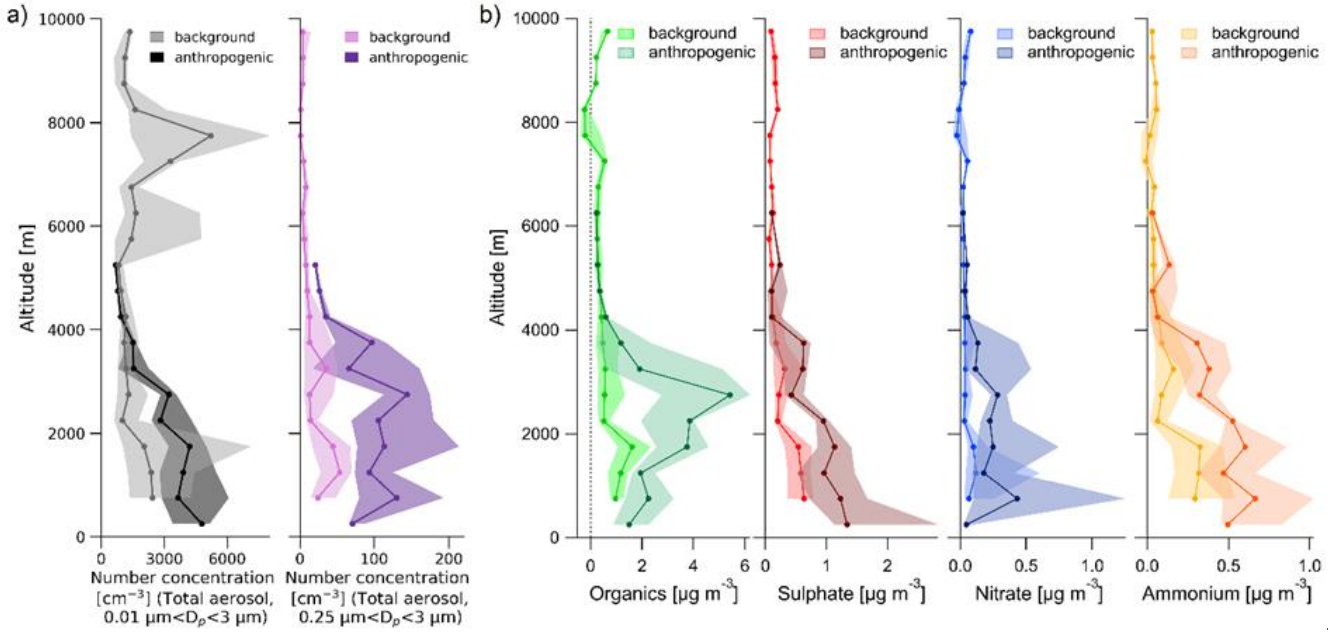

Figure 19: As in Fig. 18, for a) the total aerosol number concentrations for two different size ranges (0.01-3 µm and 0.25-3 µm) and b) organic, sulphate, nitrate and ammonium mass concentrations in the aerosol particles. The dots in the solid lines represent the medians averaged over altitude bins of 500 m and the shaded areas are the quartiles.

(Fig. 17a~~In the vertical distribution of the total aerosol number concentrations (Fig. 19a~~), the difference between anthropogenic and background air masses is more pronounced in the size range between 0.25 µm and 3 µm than in the size range between 0.01 µm and 3 µm. At altitudes below 4000 m the averaged total aerosol number concentrations show several maxima which are mainly caused by local pollution plumes. In contrast to all other profiles, there are two additional maxima in the number concentration compared to background aerosol for the size range 0.01 µm to 3 µm at around 6000 m and 7500 m. These maxima are not apparent in the profiles of particle larger than 0.25 µm. The corresponding sequences can be associated~~This is consistent~~ with ~~the attribution of LRT of~~ air masses from convective outflows giving rise to enhanced~~North America, where they had contact with BB emissions. New~~ particle concentrations in the sub-100 nm size range~~formation events cannot be excluded but are considered unlikely~~.

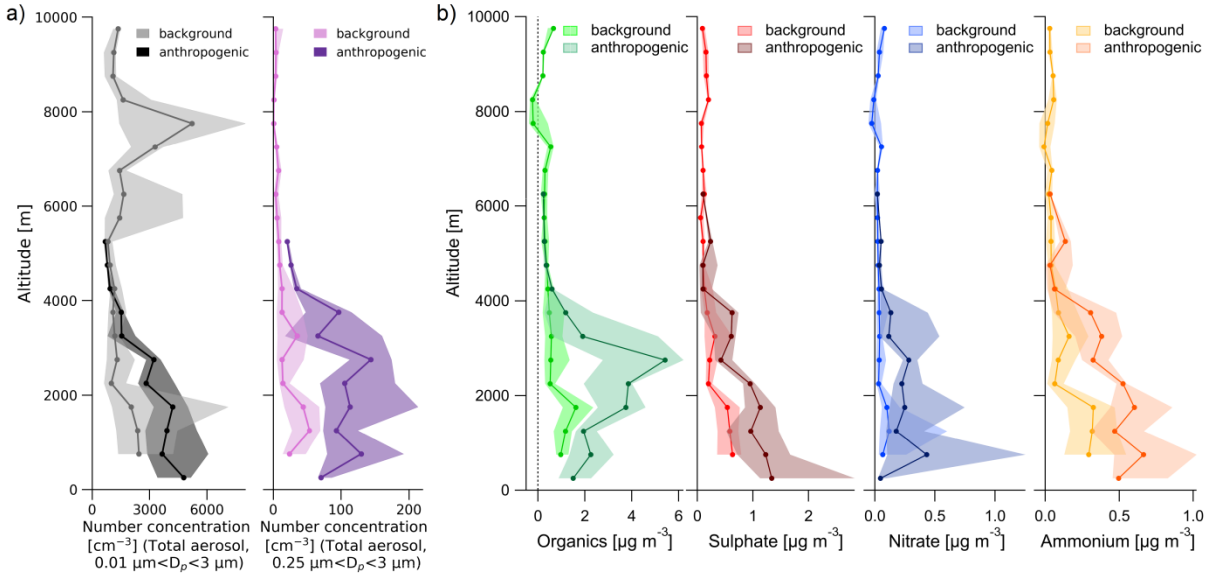

Figure 17: As in Fig. 15 but for a) the total aerosol number concentrations for two different size ranges (0.01-3 µm and 0.25-3 µm), and b) organic, sulphate, nitrate and ammonium mass concentrations in the aerosol particles. The dots in the solid lines represent the medians averaged over altitude bins of 500 m and the shaded areas are the quartiles.

Secondary organic aerosol (SOA) prevailed in the polluted air masses probed in Europe above 2000 m. In the free troposphere above 4000 m the direct effect of anthropogenic emissions on the organic and inorganic aerosol components is observed to be small. The vertical profiles of the chemically resolved aerosol mass concentrations in Fig. 17b~~19b~~ clearly show the enhanced concentrations in the anthropogenically influenced air masses compared to the background air masses. Differences in the median vertical profiles of the inorganic and organic aerosol (OA) suggest that organic aerosol in anthropogenic air masses is mainly formed by secondary processes. The OA maximum between 2000 and 4000 m observed in ~~As a result of~~ the anthropogenically influenced air masses can be explained~~time required~~ by one particular measurement period above Spain during flight E-EU-09. The trajectory analysis shows an uplift and transport of ~~the emitted precursor VOCs to be converted into secondary organic aerosol, the~~ anthropogenic influenced air masses from Madrid to the measurement location. Further possible reasons might also be lower temperature leading to enhanced SOA formation in this ~~organic aerosol concentration increases above 2000 m~~ altitude range, but also a longer conversion time of VOCs to SOA in comparison to the conversion time for inorganic aerosol precursor gases. In contrast, the inorganic components of the aerosol, especially ammonium and sulphate ions, show a steady decrease in the anthropogenically influenced air masses until up to about 4000 m. Above that altitude, the difference between background and anthropogenic profiles becomes small for both organic and inorganic aerosol components. This

is a very interesting finding, implying that the direct influence of anthropogenic emissions on the aerosol of the free troposphere over Europe is small.

4.3 Identification of MPC outflows

- The identification of individual MPC sources was possible~~Additional information is provided~~ by using a) enhancements in the concentration of selected atmospheric species, b) backward trajectories and the last contact with PBL, c) forward trajectories and dispersion of MPC outflows, and d) detection of released PFC tracers. Details about the plume identification and tagging approaches used during the EMeRGe IOP in Europe are given in the supplement (S12).
- MPCs were, as expected, identified as significant sources for reactive nitrogen species. The concentration of reactive nitrogen species within pollution plumes exceeded the background concentration by up to a factor of 10. With increasing distance to the MPC sources reactive nitrogen species were processed and finally removed~~vertical distribution of carbon isotope ratios obtained~~ from the atmosphere as indicated by correlations observed with CO.
- MPC outflows not sampled by in-situ instruments were identified during overpasses by the down-looking remote sensing instruments~~whole air samples taken~~ on-board HALO. Fig. 18 shows HAIDI measurements ~~and~~ at 8 km of the Milan outflow during E-EU-09. The measurements of HAIDI were used to estimate emissions and plume geometries, NO_2 being an important target species. The HAIDI instrument has three scanning telescopes pointed at nadir, 45° forward and 45° backwards direction. On the left side of Fig.18, the data from the nadir telescope scanner are shown at high spatial resolution (a pixel is ca.400x 400 m). The map shows a strong NO_2 plume Northeast of Milan. The plume substructures are also clearly visible. On the right side of the figure, the data from all three telescope scanners are plotted as a function of time at a lower spatial resolution. The time delay of about 80 s between the peak as seen in the forward and backward scanners indicates that this plume is close to the ground. Wind data from the lowest layer from the ECMWF ERA-5 reanalysis product [Copernicus Climate Change Service, 2017] implied a wind angle of 293°, which is consistent with this outflow from the urban area East of Milan. The uncertainty in the estimated NO_2 emission rate of 607± 67 kg/day may be increased due to the low wind speed (0.6 m/s), the complex plume shape and the small relative angle between the HALO flight track and the plume direction.

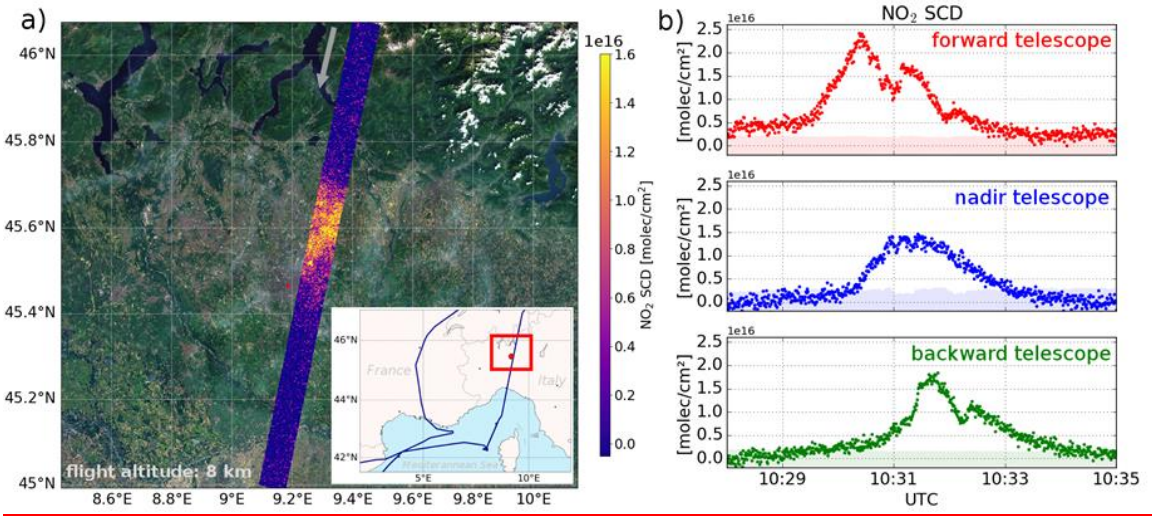

Figure 18: HAIDI measurement at 8 km altitude of the Milan outflow during the flight E-EU-09: a) pixel-resolved NO_2 slant column densities observed by the nadir camera (marked by the red square on the map). The grey arrow indicates the direction of the flight. An enhancement of up to 1.5×10^{16} molec/cm² over the background is observed Northeast of Milan (red coloured circle), b) NO_2 slant column densities averaged over the whole swath for all three telescopes: forward (top) nadir (middle)

and backward (bottom). The height of the plume centre is estimated from the time difference of the maxima. Sources of background imagery: ESRI, DigitalGlobe, GeoEye, i-cubed, USDAFSA, USGS, AEX, Getmapping, Aerogrid, IGN, IGP, swisstopo, and the GIS User Community.

Different ranges of $\delta^{13}C$ values in VOCs were determined and attributed to MPC sources for the first time, e.g. for C_6H_6 in the Po Valley and Rome. Atmospheric residence times of the MPC plumes measured on-board were retrieved from isotope measurements in VOC samples collected at MPC~~the~~ ground sites in London, Wuppertal, Milan and Rome and on-board HALO. The vertical distribution of ~~. The~~ $\delta^{13}C$ values in pentanal ($C_5H_{10}O$) and C_6H_6 are shown in Fig. 19,~~20 are~~ colour coded according to the different areas sampled, as given in the overview map in Fig. 4. In general, the $\delta^{13}C$ values are in the expected range reported by previous studies (e.g. Rudolph et al., 2000; Goldstein and Shaw, 2003).

The air samples taken during the EMeRGe IOP at ground stations exhibited different features in $\delta^{13}C$ values for the Southern and for the Northern European MPCs. Lower~~In general, lower~~ $\delta^{13}C$ values for $C_5H_{10}O$ and C_6H_6, indicative of fresh emissions, were generally observed below 2000 m altitude. On average, $C_5H_{10}O$ was~~is~~ less enriched in ^{13}C in the Rome and Milan (-32.6 ‰) than in the London and Wuppertal samples (-31.4 ‰), whereas it was~~is~~ the opposite for C_6H_6, i.e., (-27.3 ‰) and (-29.0 ‰), respectively. Moreover, the $\delta^{13}C$ ground values in Italy indicated~~indicate~~ more constant sources in $C_5H_{10}O$ and C_6H_6 as in the Northern MPCs, as was~~is~~ apparent from the standard deviations of 0.8 ‰ and 0.7 ‰ in contrast to 1.2 ‰ and 3.3 ‰, respectively.

The EMeRGe flights to the Southern MPCs in Europe covered a larger altitude range than the flights to the Northern MPCs. The upwind and downwind shuttles at different flight altitudes of the Rome MPC illustrated~~illustrate~~ a general increase in $\delta^{13}C$ in $C_5H_{10}O$ and C_6H_6 with increasing altitude. This implies that chemically processed air was encountered during the transits over the Apennines. In comparison to $C_5H_{10}O$, the enrichment in ^{13}C with altitude in C_6H_6 was~~is~~ not very pronounced. This is consistent with the longer lifetime of C_6H_6 and a well-mixed troposphere with a variety of ground sources mixed by convection (e.g. thunderstorms) in summer. Consequently, the values for $\delta^{13}C$ in $C_5H_{10}O$ represented~~represent~~ local conditions, whereas those in C_6H_6 provided~~provide~~ regional or LRT information. The isotopic signatures revealed~~reveal~~ a second layer with rather fresh emissions in the altitude region between 2000 and 3000 m which extended~~extends~~ to 4000 m in the Southern MPCs (e.g. Rome and Po Valley). These observations were~~are~~ consistent with the trace gases and aerosol measurements.

The location and position of the city plumes were typically well forecasted by the CAMS-global, MECO(n) regional and by HYSPLIT dispersion simulations using urban city tracers. Figure 20 shows an example with

results from E-EU-08 on 26 July 2017 as the London and BNL/Ruhr MPC outflows were investigated. The

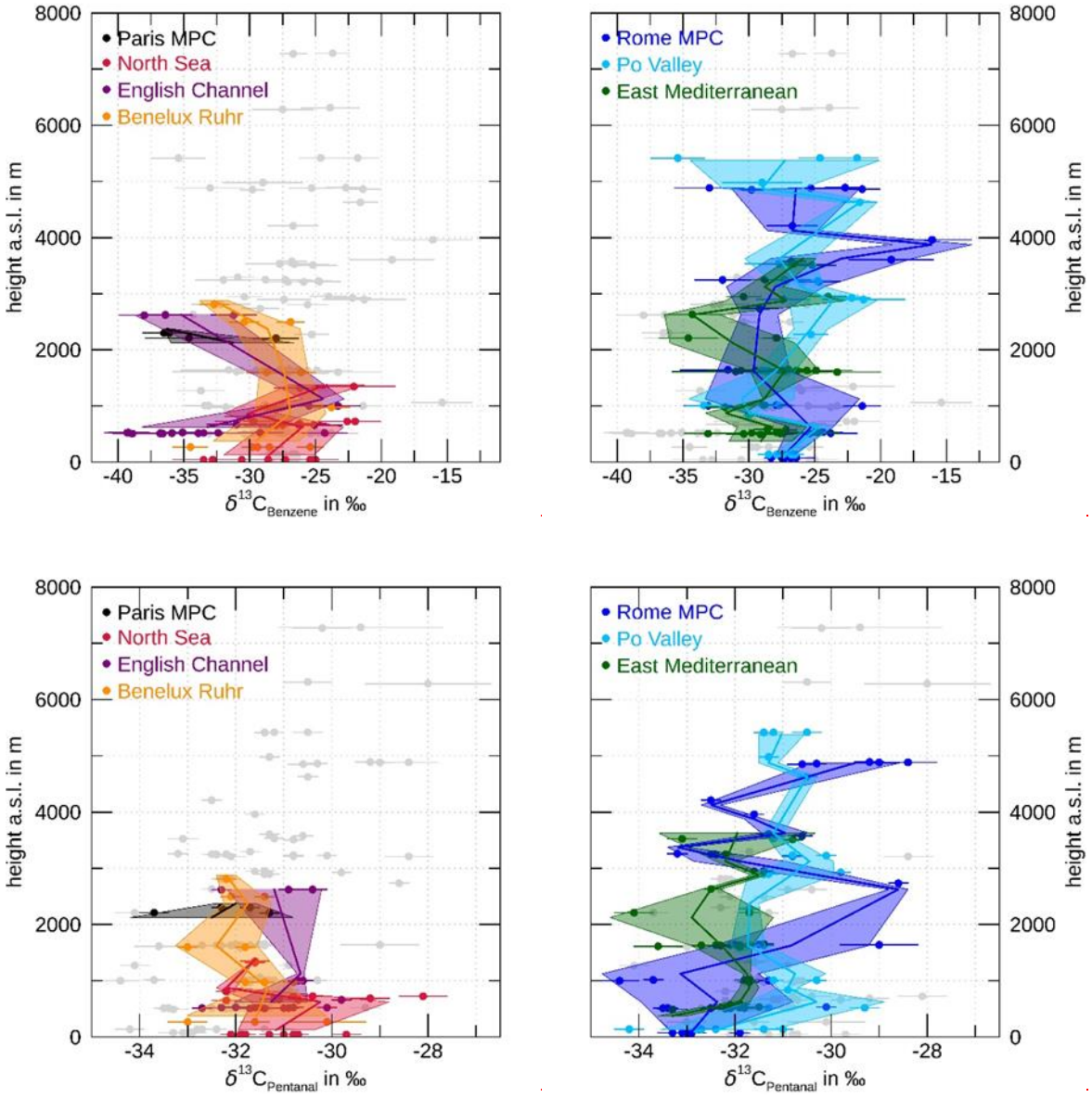

• ~~**Figure 20:** Vertical distribution of $\delta^{13}C$ values in $C_5H_{10}O$ (left) and C_6H_6 (right~~ HYSPLIT dispersion calculations of the CO city plumes were used to define the location of the outflows, which were measured along the Eastern UK coast between 10 and 12 UTC and over the European continent between 13:20 and 14:15 UTC approximately. The plumes identified using enhanced mixing ratios of selected atmospheric species, and the estimated air-mass transport times are summarised in S13 in the supplement. These plumes show mixtures of anthropogenic pollution (AP), BB and biogenic emissions (BIO). Overall, the HYSPLIT dispersion and FLEXTRA backward calculations agreed reasonably in identifying fresh emitted London plumes such as B-02 and B-04 (see Fig.13): the measured 22 and 19 ppbv CO increases over background are estimated by HYSPLIT as 25 and 22 ppbv (sum of all transport times). B-05 is a good example of significant mixing with aged plumes (12-24 h) which seem to dominate in B-06 and B-08 (see detail in Fig. 20). Plume B-09 is a good example of mixing of freshly emitted plumes from BNL/Ruhr (0-6 h) and aged emissions (>24 h) of London origin.

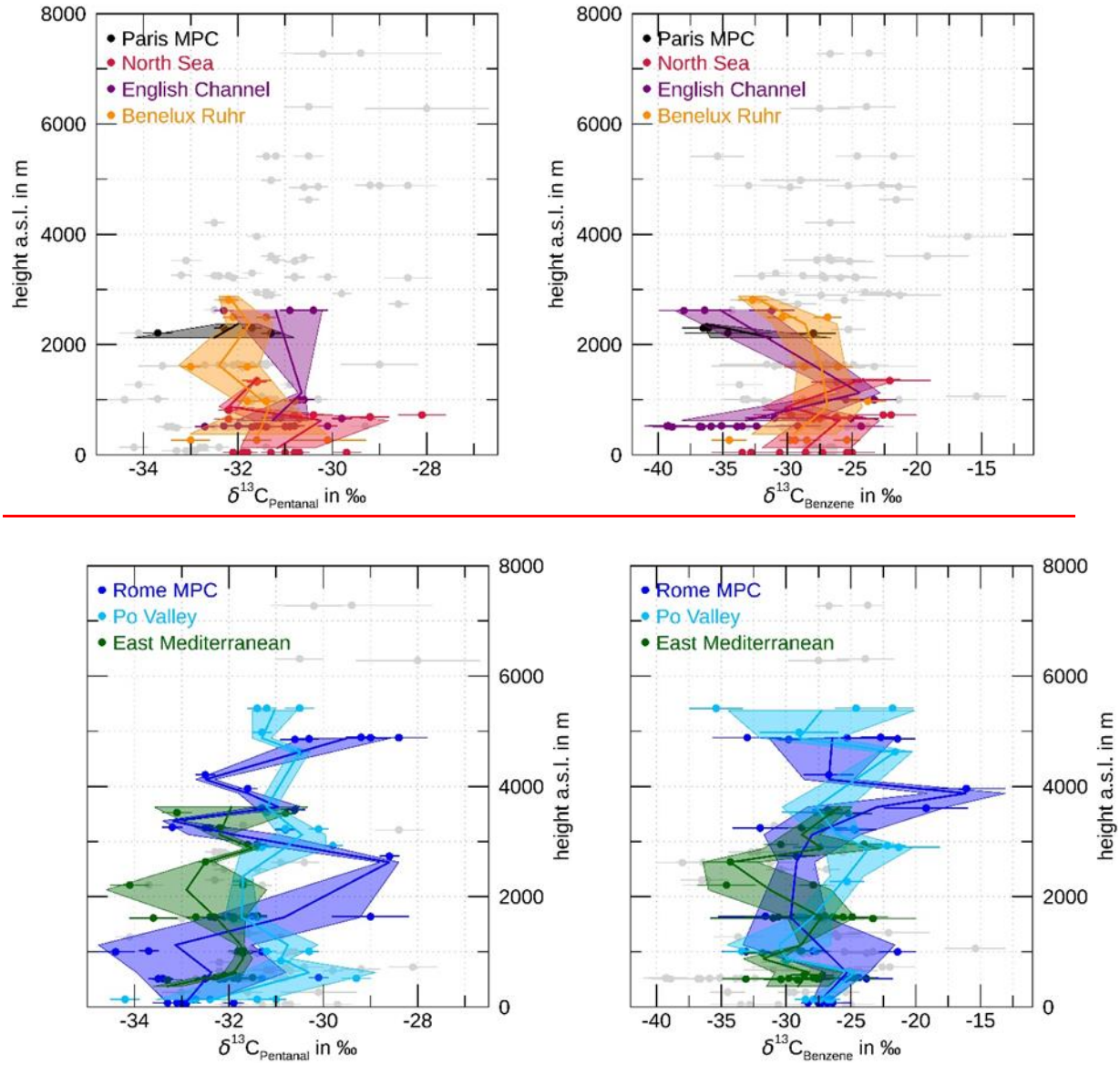

Figure 19: Vertical distribution of $\delta^{13}C$ values in $C_5H_{10}O$ (left column) and C_6H_6 (right column) in whole air samples taken on HALO and at the ground sites in London, Wuppertal, Milan and Rome. Data for northbound flights (top row~~left column~~) are colour coded for Paris MPC (black), North Sea (red), English Channel (violet), BNL/Ruhr (orange). Data for southbound flights (bottom row~~right column~~) are colour coded for Rome MPC (blue), Po Valley MPC (cyan) and East Mediterranean (green). The coloured shadings refer to the standard deviation of $\delta^{13}C$ values in altitude bins of 250 m. Mean $\delta^{13}C$ values of the respective altitude bins are represented as solid colour-coded lines. The $\delta^{13}C$ values at the lowest altitudes in each colour represent the results of air samples at the ground stations: London (red), Wuppertal (orange), Rome (blue) and Milan (cyan). Error bars in $\delta^{13}C$ are given for each sample value. Remaining data are shown in grey.

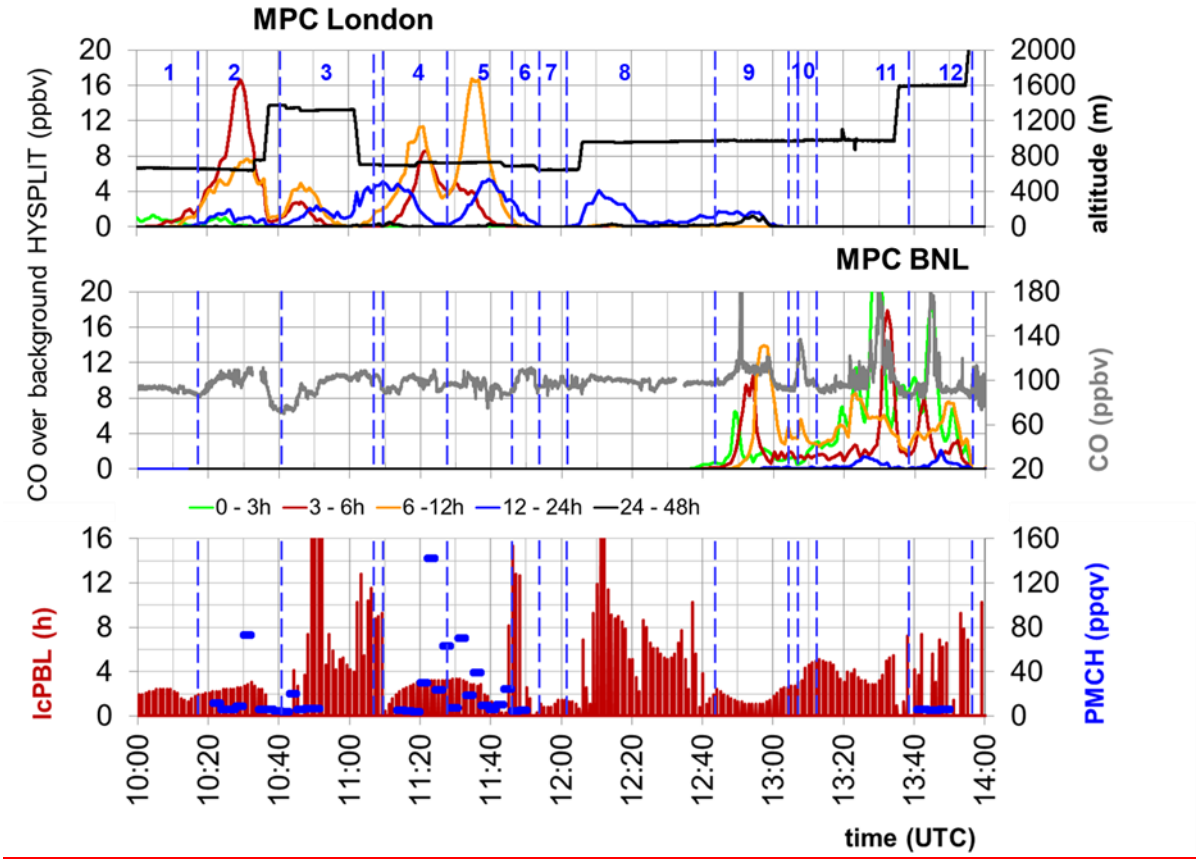

Figure 20: Detail of the MPC outflow of London (B-01 to B-09) and BNL/Ruhr (B-09 to B-12) probed with HALO along the E-EU-08 flight track. Numbering in blue corresponds with the classification in Fig. 13 ("B-0" is omitted for clarity). The position of the plumes is also indicated by the blue lines. Dispersion of CO emissions of target MPCs and the transport time of the air mass calculated by HYSPLIT are depicted in the middle panel. The last contact with the PBL (lcPBL) calculated using FLEXTRA is also shown. Elevated PMCH mixing ratios were measured for B-02, B-04 and B-05.

- MPC outflows were successfully and unambiguously identified after transport times of between 5 and 26 hours by tagging polluted air masses through ground-based releases of PFC tracers in the centre of MPCs. The aim of the PFC tracer experiments was to establish Lagrangian connections between polluted air masses in the center of selected cities and downstream measurements on-board HALO guided by HYSPLIT forecasts of the dispersion of the tracer plumes. In Fig. 20 the PMCH volume mixing ratios measured on-board during E-EU-08 are shown. For B-02, B-04 and B-05, enhanced tracer values above the 8.5 ppqv atmospheric background in Europe were clearly detected.
- The downwind impact of pollution from MPCs was identified by combining information from measurements on-board in selected areas with backward and sensitivity trajectories. Figure 21 shows an example of the density distribution for forward trajectories (FT) of MPC Rome outflows. The figure highlights the typical transport pattern towards the Adriatic coast and the representativeness of the HALO shuttles at different altitudes in the Mediterranean and along the Adriatic coast during the flights E-EU-03 and E-EU-06. The flight tracks for E-EU-03 and E-EU-06 are colour-coded with the BC mass, a good tracer for urban emissions. The elevated BC mass concentrations observed in the area of an increased FT density over the Adriatic indicates the measurement of urban emissions in the statistically expectable transport pattern for the urban outflow of Rome during the month of July. A comparison of the gases remote sensing observations on-board HALO with their columnar amounts observed by ground-based measurements in the Rome area in the framework of the PANDONIA

global network for air quality and atmospheric composition (https://www.pandonia-global-network.org/) is discussed in Campanelli et al. 2021 (in preparation 2021).

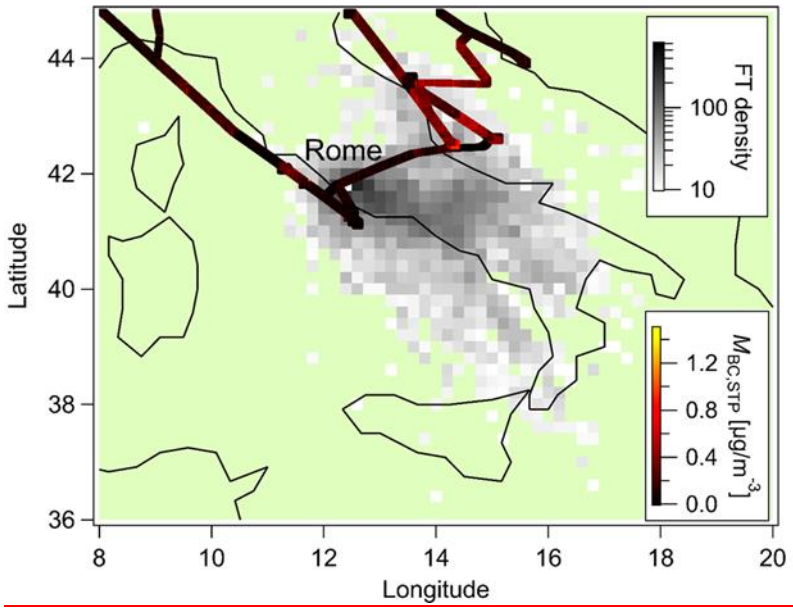

Figure 21: Forward trajectory (FT) density plot for air masses starting in Rome (100 m a.g.l.) in the month of July from multiple years (2017 to 2020). The grey scale represents the counts of FT points in each grid cell. The flight track of E-EU-03 and E-EU-06 is colour-coded with the BC mass concentration. The FT density distribution was calculated as explained in Pöhlker et al. (2019). The FT starts at 100 m above ground level for the month of July in a multi-year period (2017 until 2020) by using the HYSPLIT package (version 4, Revision 664, October 2014) (Stein et al., 2015; Rolph et al., 2017).

- Regional transport of several European MPC outflows was successfully identified and measured: a) London over the English Channel to Central Europe, b) Po Valley either North over the Alps or in a south-easterly direction towards the Adriatic, c) Rome over the Apennines into the Adriatic and d) Madrid and Barcelona into the Western Mediterranean.

The downwind impact of the MPC outflows during EMeRGe was explored in respect of the vertical and horizontal extension of the observed plumes. Information from transects and shuttles in selected areas was combined as shown in Fig. 22 for the B-01 to B-12 plumes during the E-EU-08 flight. The E-EU-08 track included a flight transect (a-b-c-d-e) at approximately 600 m altitude and a shuttle (600-1400 m) between b-c and c-d in the outflow of London from 10 UTC to 12 UTC. A second shuttle (g-h-i) at 900, 1500 and 2400 m was made in the BNL outflow from 13:20 UTC approximately. Relevant changes in the HALO course and altitude are marked by coloured circles and letters in Fig. 22. Backward trajectories indicated that the air measured at around 10:30 UTC at 600 m (blue circle), 11:00 UTC (point c at 1400 m and 600 m), 11:20 UTC (yellow circle) and 11:50 UTC at 600 m (pink circle) had passed over the MPC London a few hours before being probed at an altitude below 1000 m. Selected backward trajectories are shown in Fig. 22c. At these times, the measured enhancements in CO and NO_y and the NO/NO_y ratios were in reasonable agreement with the transport time predicted by HYSPLIT for the CO enhancement in the MPC London plumes in Fig. 20. For plume B-02, HYSPLIT predicted the London contribution to be a mixture of air masses transported in the previous 3 to 24 hours. The air probed had up to 10 ppb of NO_y and approximately 2 ppbv NO. The latter suppresses RO_2^*. OH and RO are produced but also react with NO and NO_2. These measurements confirm the predicted mixing of relatively fresh emissions with aged and more photochemically processed air masses.

The vertical distribution of CO in the plume during the shuttles is depicted in the 3D diagrams in Fig. 22b. The CO measured indicates that the plume B-03 is well mixed horizontally with the plume B-06 up to 1400 m altitude. According to the backward trajectories (not shown), the plume at 11:52 UTC is transported from the Northeast coast of UK and had no recent contact with the outflow of London. This is distinguishable by the high SO_2 mixing ratios measured. The plumes B-08 and B-09 measured over the continent at 900 m were predicted to have been in contact with emissions of the MPC London within the previous 24 hours (Fig.20 and Fig. 22c). From 12:50 UTC the air probed was expected to mix with recent emissions of the MPC BNL as indicated by the observed higher NO levels and enhancements in NO_y, SO_2 and C_6H_6 in Fig. 22a.

The composition of the air measured during the shuttle between the way points g and h in Fig. 22a at 13:30 and 13:45 UTC and the backward trajectories indicated that the outflow from the MPC BNL was sampled in a plume extending from 1000 m to 1500 m. This air mass was not detectable at 2500 m.

- Distinct pollution and aerosol layering were observed over some of the investigated MPCs. Collocated ground-based remote sensing instruments improved the understanding of the evolution of the airborne observed scenarios and the attribution of the vertical distribution of pollutants probed during the shuttles.

A particular case of interest was the vertical distribution of pollutants observed at the coast of Barcelona during E-EU-09. HYSPLIT CO dispersion simulations indicated that the Madrid outflow was transported over a long distance above the Iberian Peninsula to the North-Eastern coast at altitudes above 2000 m while in the lower layers the Barcelona outflow predominated, as illustrated in Fig. 23. In contrast with the air sampled at 500 m, the backward trajectories and HYSPLIT dispersion calculations indicated that the air probed from 15:15 to 15:25 UTC at 1600 m had passed over MPC Barcelona within 6-12 hour before sampling. There is no indication of fresh NO emissions, and NO_y, C_6H_6 and CO were significantly higher than at the lower altitude. The layering is attributed to be the result of the recirculation of emissions in the Barcelona outflow within the land-breeze regimes close to the coast. Later at this FL (green and red circles in Fig. 23), the backward trajectories and HYSPLIT estimations indicated sampling of regional emissions that had travelled along the coast from Valencia. This is consistent with the observed decreases in C_6H_6, NO_y and BC. In the upper FL at 15:45 UTC, NO_y, C_6H_6 and CO significantly increased in air transported from Portugal (as in the 36 h backward trajectories) across the Iberian Peninsula at altitudes above 2000 m, after PBL contact with the MPC Madrid below 1000 m the evening before. According to the pollution control network of Madrid, the average CO surface concentration exceeded 350 ppb on the 27 July 2017, the zonal wind direction was WSW and the average wind speeds were greater than 16 km/h. The observed mixing ratio decreased when this feature at 3000 m disappeared. Re-entering and stratification of plumes having different processing along the Spanish coast has also been documented in the past (e.g. Millán et al., 1997, 2000 and references therein).

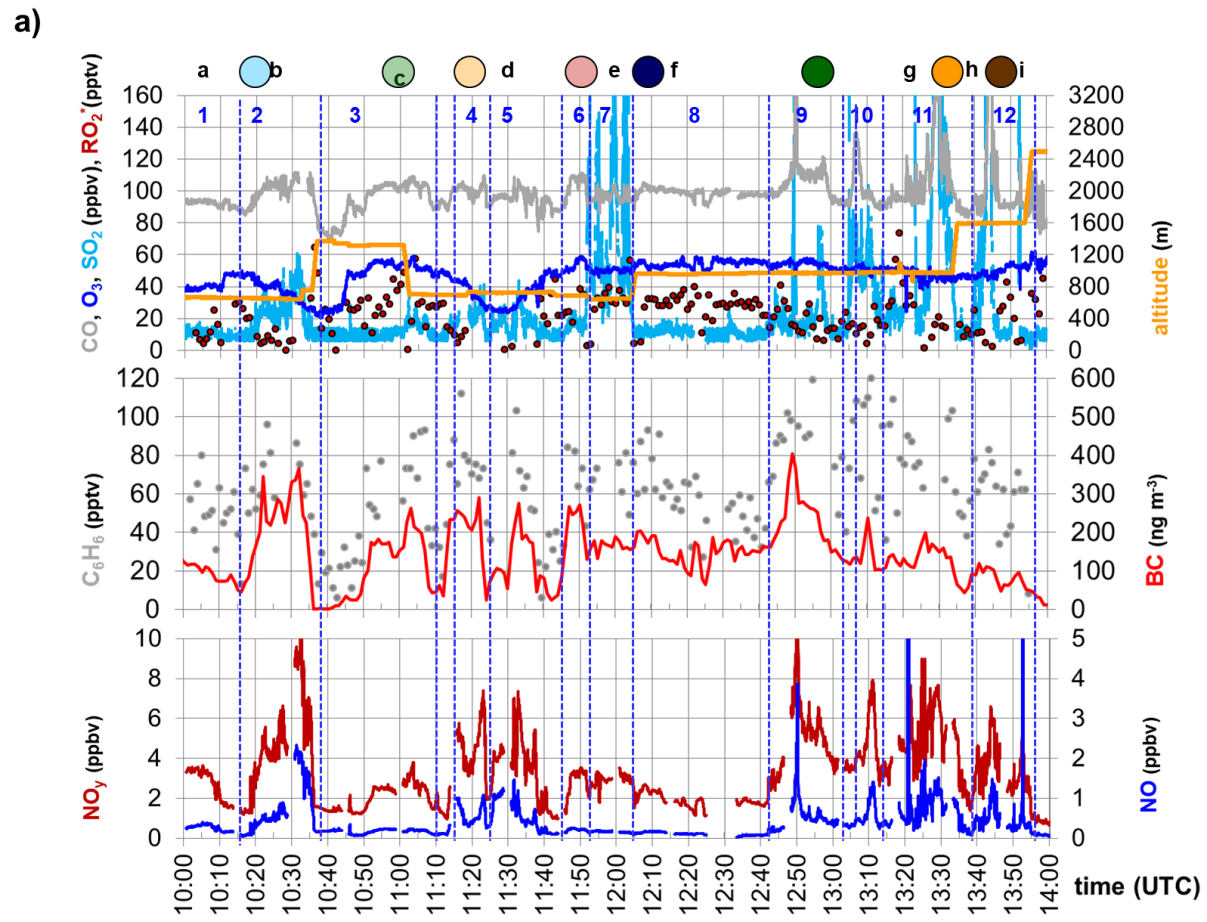

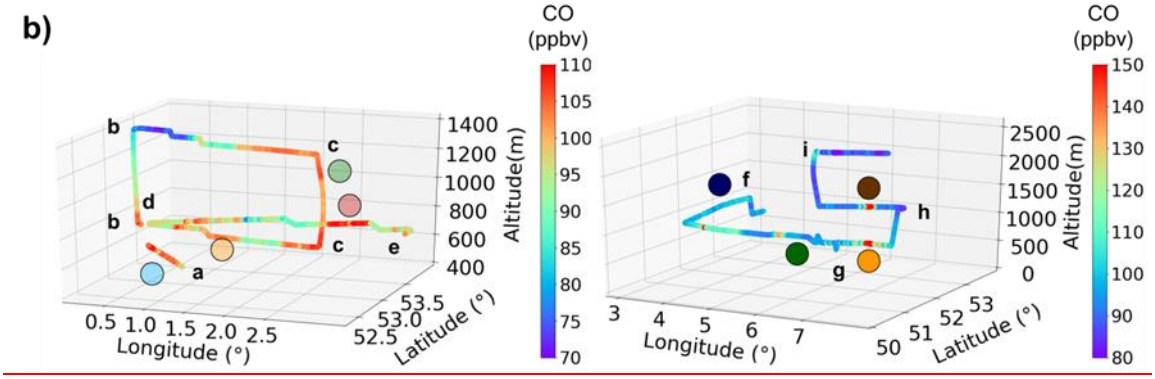

c)

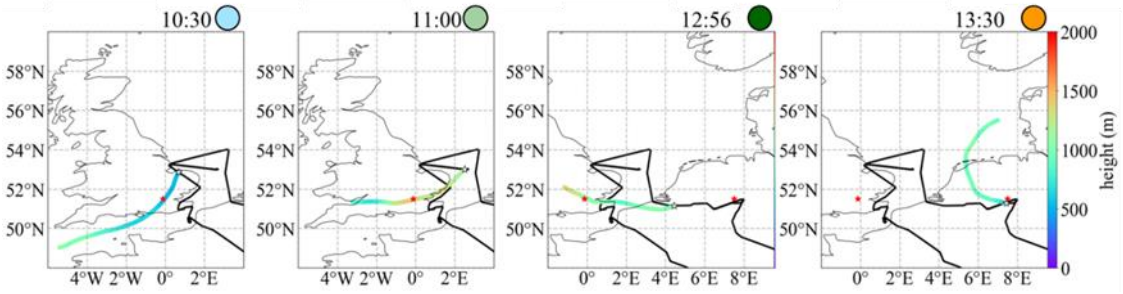

Figure 22: a) CO, O_3, SO_2, RO_2*, NO_y, NO, C_6H_6 and BC measured in the outflow of London and BNL during E-EU-08 on 26 July 2017. The position and numbering of the plumes are indicated by blue lines and numbers as classified in Fig. 22 ("B-0" is omitted for clarity), b) 3D shuttles colour coded with the CO mixing ratios observed. Relevant changes in the HALO course and altitude are marked by colour circles and letters (a-i). c) Selected backward trajectories (24h). The red stars indicate the position of the MPCs of interest.

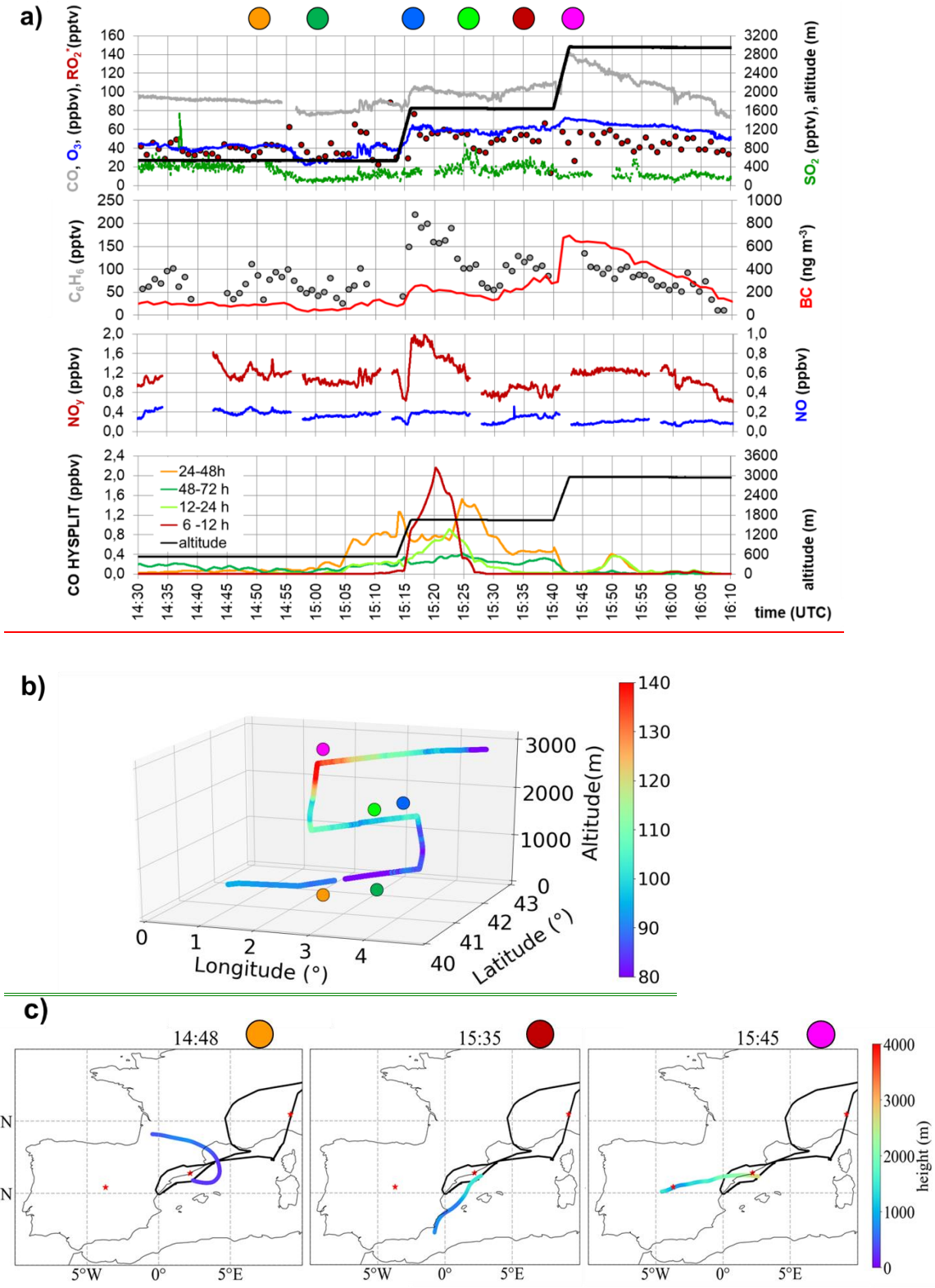

Figure 23: Stratified pollution layers along the Spanish coast during the E-EU-09 flight on the 28 July 2017, a) temporal variation of CO, O_3, RO_2*, NO_y, NO, SO_2, C_6H_6 and BC during the shuttle, b) 3D view of the shuttle colour coded with CO mixing ratios, c) selected backward trajectories (last 24h). Coloured circles marked the corresponding times. Red stars indicate the position of the MPCs of interest.

Data from the closest four ground-based remote sensing stations available in the framework of EMeRGe international enhanced the interpretation of the HALO measurements. These are data of a lidar in Barcelona (BRC) and three ceilometers in Montseny (MSY), on top of the Serra del Montsec (MSA) (Titos et al., 2019),

and in Burjassot (VLC) near Valencia. Figure 24 shows the location of the stations with respect to the HALO flight track. The stations MSY and MSA were approached at a flight altitude of 2600 m when HALO entered the air space above the Iberian Peninsula. Subsequently, HALO shuttles were carried out Northeast of Valencia at 500, 1000, 2000 and 2600 m and East of Barcelona at 500, 1600 and 3000 m.

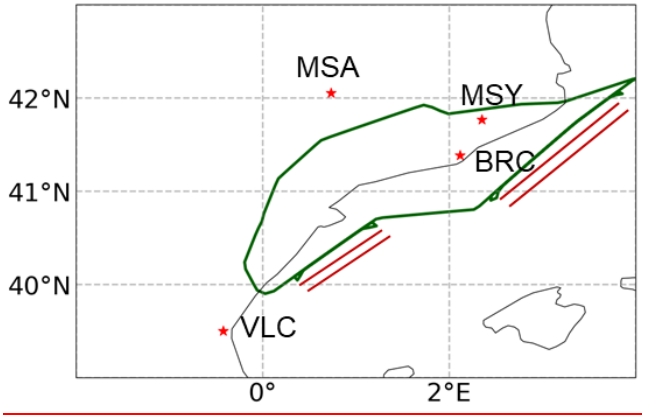

Figure 24: Detail of E-EU-F09 flight track (in green) and the ground-based stations with coordinated remote sensing measurements in the vicinity: Montseny (MSY), Sierra del Montsec (MSA), Burjassot (VLC) and Barcelona (BRC). Red lines indicate the position of the HALO shuttles.

The lofted aerosol layer observed at all ground-based remote sensing stations from above the PBL up to 4000 m altitude was also probed by HALO (see Fig. 25). The profiles of the backscatter coefficient derived at MSA, MSY, VLC and BRC on the 28 July 2017 are displayed in Fig. 26 and Fig. 27. The lofted aerosol layer in Fig. 25 corresponded with increased backscatter coefficients ranging from 0.4 to 1.9 $(Mm \cdot sr)^{-1}$.

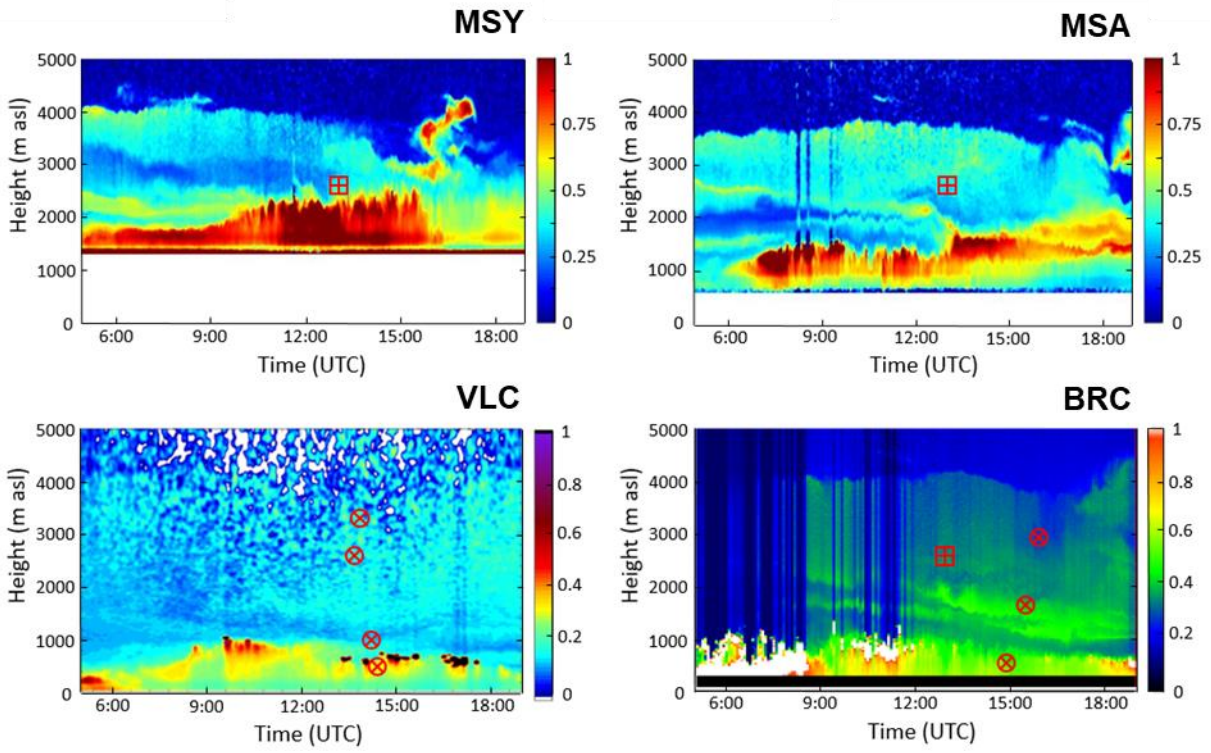

Figure 25: Time series of range-corrected lidar signals ground-based remote sensing measurements in MSY, MSA (both at a wavelength of 1064 nm), VLC (910 nm) and BRC (532 nm) on the 28 July 2017. Signal strengths relative to the maximum signal of the corresponding measurement are depicted. Red circles show time and altitude of the HALO overpasses used for comparison of airborne with ground-based remote sensing measurements (see Fig. 26 and Fig. 27). Red squares show further HALO overpasses.

The composition of PM1 particles (i.e., with diameter up to 1 µm) was retrieved from the HALO in-situ measurements at different altitudes during the shuttles. The observed PM1 composition near Burjassot is shown in Fig. 27. Although the ceilometer measurements refer to total aerosol and the in-situ data only to PM1, both revealed two distinct aerosol layers: a) a PBL below 1000 m altitude with enhanced concentrations of sulphate and ammonium and a backscatter coefficient between 2.0 and 2.7 $(Mm \cdot sr)^{-1}$, and b) a lofted aerosol layer between 1500 and 3500 m altitude with higher organic, nitrate and BC mass fraction. The difference in composition is likely related to different aerosol sources. While the boundary aerosol layer had a local origin, the lofted aerosol layer was influenced by the transport of regional emissions. This is consistent with the transport of the MPC Madrid outflow as indicated in Fig. 23.

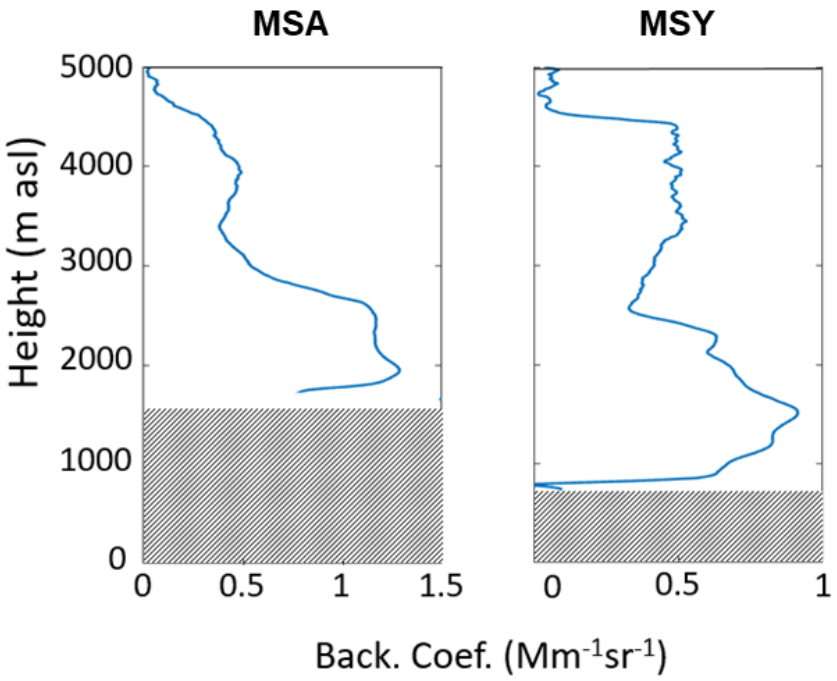

Figure 26: Profiles of the backscatter coefficient derived at 1064 nm in MSA and MSY for the 28 July 2017 from 12:50 to 13:20 UTC. The grey shadings indicate the height of the ceilometers.

Similarly, the lidar and in-situ measurements close to Barcelona revealed a different aerosol composition of the PBL below 900 m and a lofted aerosol layer above 2000 m. In addition, a third aerosol layer evolved between 1000 and 1800 m altitude with a backscatter coefficient up to 1.5 $(Mm \cdot sr)^{-1}$. The mass fractions of ammonium, sulphate and organic aerosol are between the values of those of the PBL and of the lofted aerosol layer above.

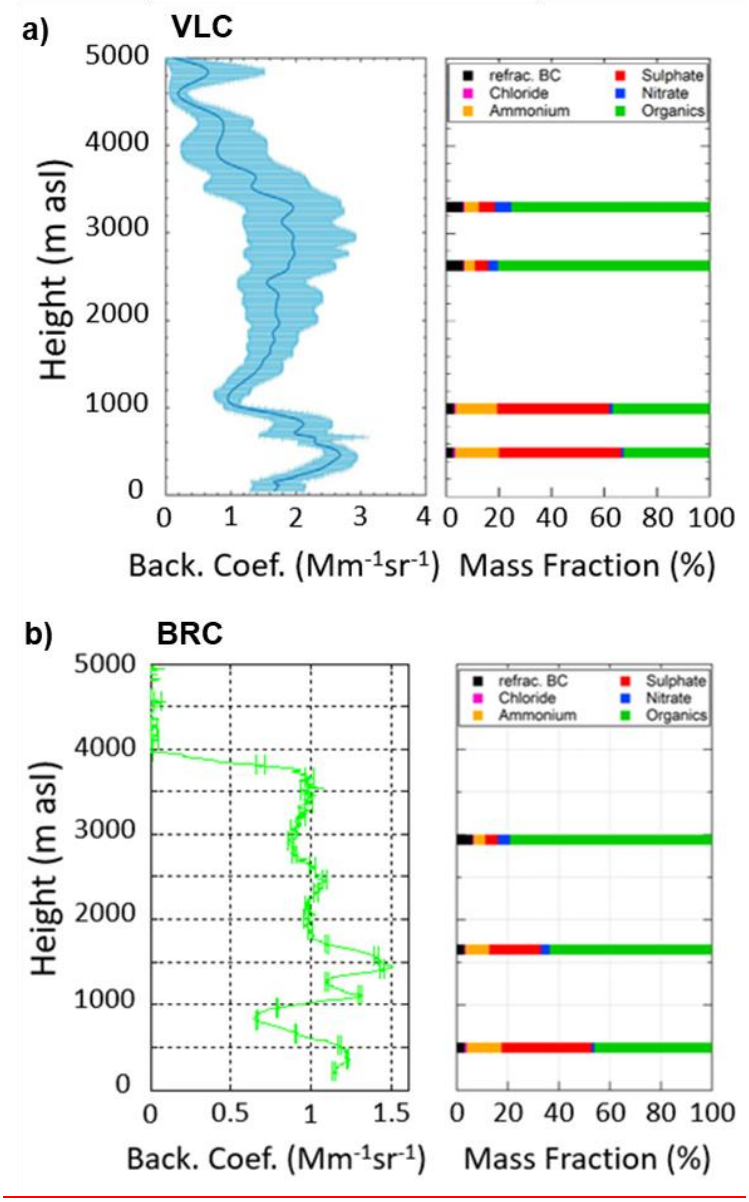

Figure 27: Distinct aerosol layers observed near Burjassot/Valencia and Barcelona. a) Profile of the backscatter coefficient derived at 910 nm for 13:30-14:30 UTC in VLC (left), and fractional composition of PM1 measured (SP2 and AMS) on-board HALO (right), b) the same derived in BRC at 532 nm for 14:45-15:45 UTC. The periods of comparison with the HALO data are 13:42-13:56 (9:30 min) at 3300 m; 13:34-13:40 (5:30 min) at 2630 m, 14:03-14:14(11:30 min) at 1000 m and 14:18-14:31 (23 min) at 500 m for VLC, and 15:43-16:00:(17:30 min) at 2940 m; 15:16-15:40 (24 min) at 1650 m, and 14:47-15:14 (27 min) at 500 m for BRC.

4.4 Mixing of MPC outflows with air masses of biogenic and natural origin: forest fires and dust

• Plumes~~Typically, plumes~~ of anthropogenic, ~~and~~ biogenic and natural origin were often mixed in the air probed over Europe during the~~. The~~ EMeRGe IOP.

The BB ~~was characterised by the~~ contribution of fresh wildfires in the Mediterranean area was substantial~~, which add BB signatures to the probed air masses, and mixed with anthropogenic plumes~~ as indicated by VOCs, ~~and~~ in particular ~~by the~~ CH_3CN, and aerosol observations. For particles emitted from BB, a frequently used tracer is levoglucosan which is identified using the m/z 60 ion ($C_2H_4O_2^+$) in aerosol mass spectrometry (Schneider et al., 2006; Alfarra et al., 2007). However, the~~The~~ photochemical degradation of levoglucosan is fast in summer (Hennigan et al., 2010, 2011; Lai et al., 2014), and in the BB aerosol observed during the IOP in Europe flight tracks it was generally processed too fast to be distinguished from other secondary aerosol.

A more robust indicator for particles from BB is BC. BC particles are formed in processes of incomplete combustion, and therefore are an important component of both BB and urban aerosol particles (Bond et al., 2013). The microphysical properties of BC give insights into the combustion sources and atmospheric ageing time of the pollution plumes (Liu, 2014, Laborde, 2012, Holanda et al., in preparation 2021). Figure 2821 shows an example of average BC mass size distributions ~~for different plumes~~ encountered during the E-EU-06 flight. A complex mixing of different open ~~(anthropogenic,~~ BB sources with lightly aged BB smoke from fires in Croatia was observed. Grassland~~,~~ and fires in Italy mostly from mixed forests and savannahs were the dominant combustion fuel.~~mixture).~~ The plumes were classified according to the VOC observations (see S12). This complex mix of biomass burning (BB, core diameter (Dc) = 200 nm) BC sources, got occasionally mixed with anthropogenic emissions (BB+AP, Dc = 210 nm). Rather pure anthropogenic urban haze (AP) with significantly smaller ~~as described in I) in Sect. 4. Larger BC cores were found in pure BB plumes and mixed BB and AP plumes, with~~ mean modal diameter (D_c = 170 nm) was additionally measured. The resulting sizes agree with literature~~) of 200 and 210 nm, respectively. Smaller BC cores, with mass size distribution peaking at D_c = 170 nm, were found in urban pollution, as a result of the different fuel burnt and combustion conditions. These~~ values ~~obtained during EMeRGe are consistent with previous aircraft observations~~ for urban haze and BB smoke (e.g. ~~plumes (~~Schwarz et al., 2008; Laborde et al., 2013; Liu et al., 2020; Holanda et al. 2020).~~)~~ During E-EU-06, the average total BC mass concentration was also substantially higher in relatively pure ~~BB and mixed~~ BB smoke and in the mixed conditions with urban haze (BB, ~~(~~0.61 ± 0.12 µg m^{-3} and BB+AP, 0.81 ± 0.35 µg m^{-3}, respectively) than in urban pollution (AP, 0.35 ± 0.15 µg m^{-3}).

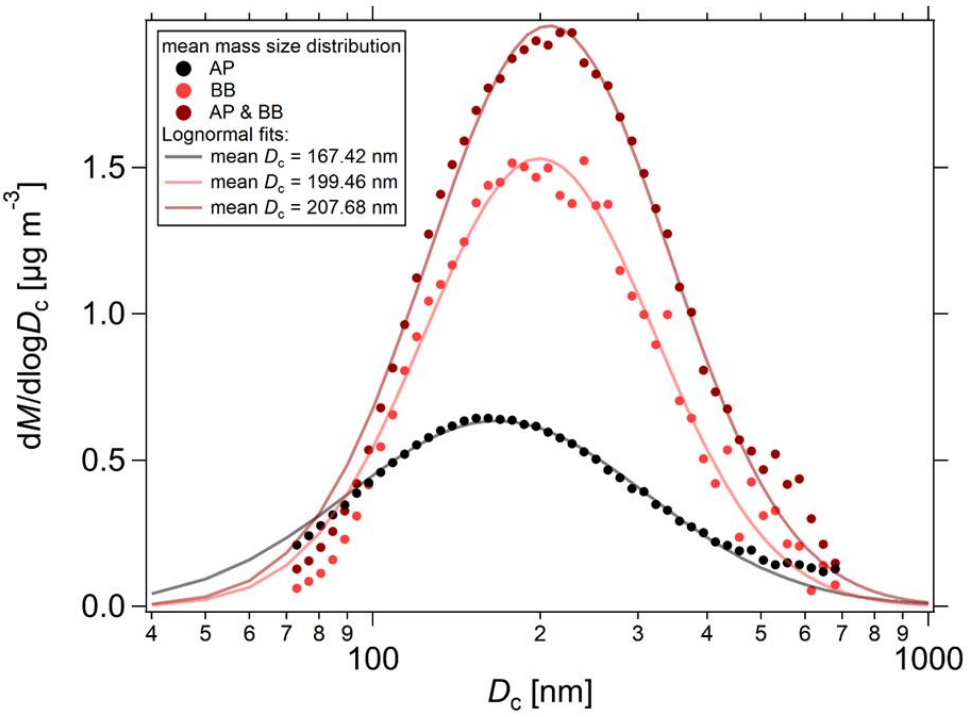

Figure 2821: Mean mass size distribution of black carbon particles measured in anthropogenic pollution (AP, black), BB (light red), pollution from anthropogenic/ BB mix (AP & BB, dark red) during E-EU-06 on 20 July 2017. Dc: refractive black carbon core diameter. Lognormal fits were applied to the mean size distributions for 100 < *Dc* < 300 nm.

Mineral dust events contributed significantly to some of the plumes measured over Europe during the EMeRGe IOP. Mineral dust was identified in the aerosol size distribution and the optical properties of air masses probed in Southern Europe above the PBL. An example of the impact of dust on the aerosol size

distributions observed close to the western coast of Italy is illustrated in Fig. 29.~~**4.2 Identification and classification of MPC outflows: London**~~

~~The flight E-EU-08 on 26 July 2017 has been selected to illustrate the procedure for the identification and classification of air mass origin and the different source contributions to the plumes. As briefly described in Sect. 3.3, the E-EU-08 investigated the London and BNL/Ruhr MPC outflows. HYSPLIT dispersion calculations of the CO city plumes were used to define the location of the outflows, which were measured along the Eastern UK coast between 10 and 12 UTC and over the European continent between 13:20 and 14:15 UTC approximately. Cloudy and rainy conditions prevailed throughout the flight reduced flight visibility and limited further tracing of the BNL/Ruhr outflow over Germany in the afternoon. However, the PMCH was observed from the two releases showing the success of this technique and the adequacy of the description of the transport in HYSPLIT.~~

~~4.2.1 Identification of pollution plumes~~

~~Figure 22 shows the time series of C_6H_6 and CH_3CN, their enhancements colour coded on the altitude and the identified plumes along the flight by using the time series of CO and NO_y, as described in I) in Sect. 4. Figure 23 summarises the result of applying the tagging tools II) and III) to the E-EU-08. Overall, the HYSPLIT dispersion and FLEXTRA backward calculations agree reasonably in identifying fresh emitted London plumes such as B-02 and B-04: the measured 22 and 19 ppbv CO increases over background are estimated by HYSPLIT as 25 and 22 ppbv (sum of all transport times). B-05 is a good example of significant mixing with aged plumes (12-24 h) which seem to dominate in B-06 and B-08 (see detail in Fig. 23). Plume B-09 is a good example of mixing of freshly emitted plumes from BNL/Ruhr (0-6 h) and aged emissions (>24 h) of London origin. The PFC tracer measured on board is also depicted in Fig. 23. For B-02, B-04 and B-05, enhanced PMCH volume mixing ratios above the 8.5 ppqv atmospheric background in Europe were clearly detected.~~

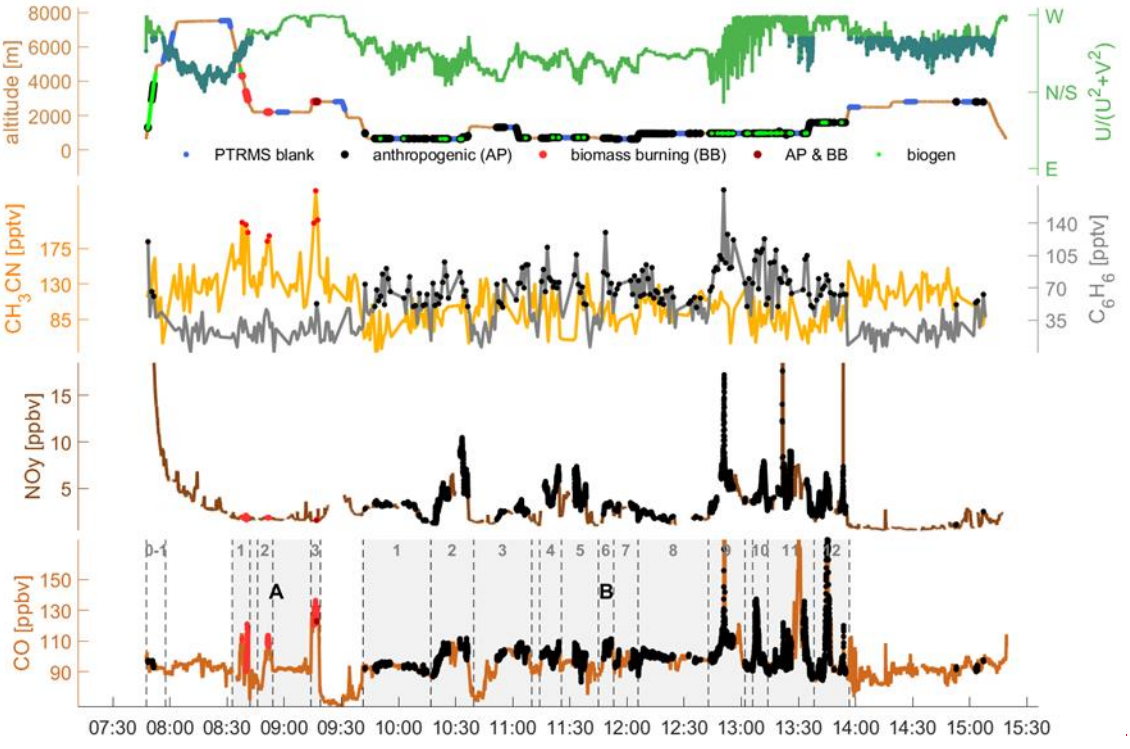

Figure 22: ~~Time series for E-EU-08 on the 26 July 2017 used for the categorisation of plumes based on VOC measurements: altitude, wind direction, CH_3CN, C_6H_6 and NO_y as refinement. The wind direction is given as~~

U/(U²+V²), -1 is east wind, +1 is west wind, values around zero have North or South components. South components are marked with dark green colour. Altitude is colour coded in light green during C_5H_8 enhancements, in light red during CH_3CN enhancements, in black during C_6H_6 enhancements and in dark red during both, CH_3CN and C_6H_6 enhancements. Additionally, blue colour coded blank measurements of CH_3CN, C_6H_6 and C_5H_8 are given. Final numbering of structures and plumes according to concentration enhancements are shown for CO. Colour coding indicates CH_3CN enhancements (light red), C_6H_6 enhancements (black), and both, CH_3CN and C_6H_6 enhancements (dark red).

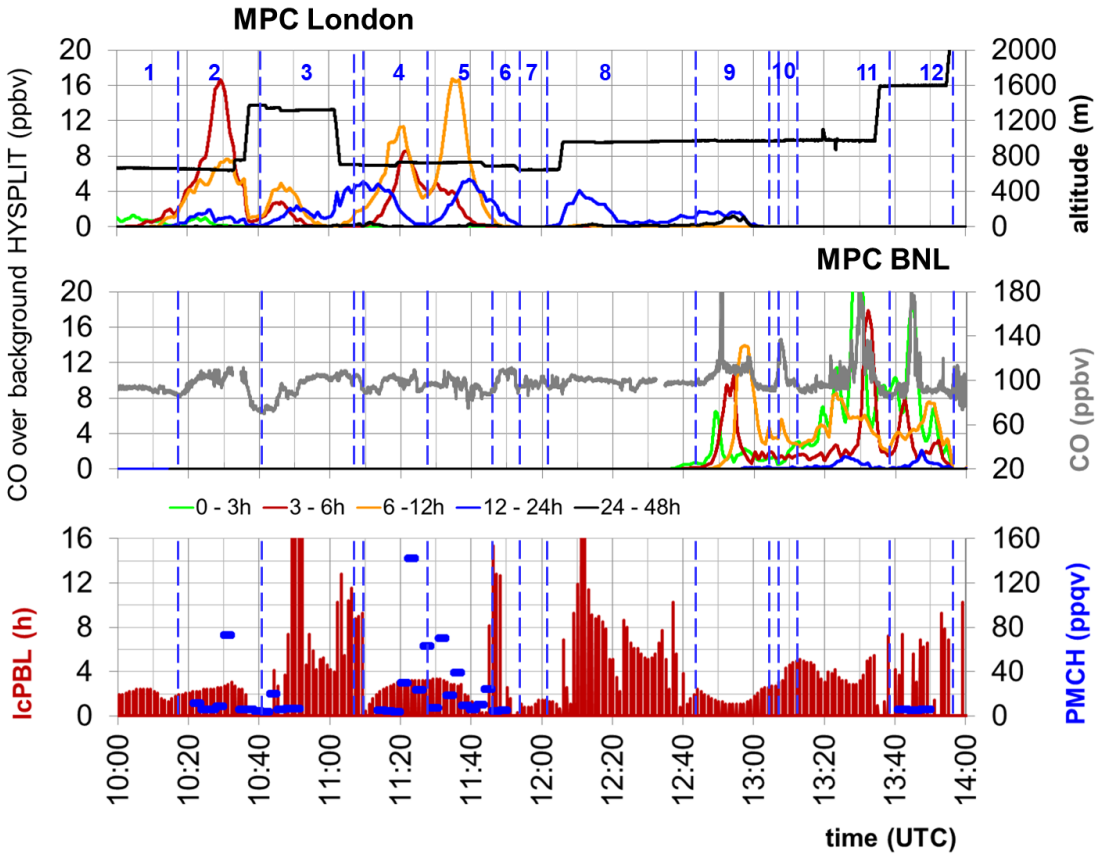

Figure 23: Detail of the MPC outflow of London (B-01 to B-09) and BNL/Ruhr (B-09 to B-12) probed with HALO along the E-EU-08 flight track. Numbering in blue corresponds with the classification in Fig. 22 (B is omitted for simplicity). The position of the plumes is also indicated by the blue lines. Dispersion of CO emissions of target MPCs and the transport time of the air mass calculated by HYSPLIT are depicted. The last contact with the PBL (lcPBL) calculated using FLEXTRA is also shown. Elevated PMCH mixing ratios were measured for B-02, B-04 and B-05.

The plumes identified using I), i.e., enhanced concentrations of mixing ratios of selected atmospheric species, and the MPC assigned outflow with the estimated air mass transport times are summarised in Table 5. These plumes show mixtures of anthropogenic pollution (AP), BB and biogenic emissions (BIO).

Table 5: Synopsis of identified structures (A and B) and plumes with anthropogenic (AP), biomass burning (BB) and biogenic signatures (BIO), MPC assignments and estimated transport times (Ttime) based on HYSPLIT and FLEXTRA for E-EU-08.

Notation	begin [UTC]	end [UTC]	signature	MPC origin	Ttime [h]
E-EU-08-0-01	07:47:34	07:57:40	BB, BIO		
E-EU-08-A-00	08:32:45	09:19:00			
E-EU-08-A-01	08:32:45	08:42:00	BB		
E-EU-08-A-02	08:46:00	08:54:00	BB		
E-EU-08-A-03	09:14:00	09:19:00	AP, BB		
E-EU-08-B-00	09:41:25	13:56:45			
E-EU-08-B-01	09:41:25	10:17:00	AP, BIO	London	0-3
E-EU-08-B-02	10:17:00	10:39:30	AP, BIO	London	0-3
E-EU-08-B-03	10:39:30	11:10:00	AP, BIO	London	6-24
E-EU-08-B-04	11:14:10	11:25:35	AP, BIO	London	3-6
E-EU-08-B-05	11:25:35	11:45:00	AP, BIO	London	3-6
E-EU-08-B-06	11:45:00	11:53:00	AP	London	12-24
E-EU-08-B-07	11:53:00	12:05:50	AP		
E-EU-08-B-08	12:05:50	12:42:45	AP	London	12-24
E-EU-08-B-09	12:42:45	13:02:00	AP, BIO	London/BNL/Ruhr	12-48/0-6
E-EU-08-B-10	13:06:00	13:14:00	AP, BIO	BNL/Ruhr	0-12
E-EU-08-B-11	13:14:00	13:38:15	AP, BIO	BNL/Ruhr	0-3
E-EU-08-B-12	13:38:15	13:56:45	AP, BIO	BNL/Ruhr	0-3

4.2.2 Characterisation of the MPC London outflow

The vertical and horizontal extension of the observed outflows during EMeRGe is investigated by combining the information from transects and shuttles in selected areas. Figure 24 shows, as an example, the CO, O_3, SO_2, RO_2*, NO_y, NO, C_6H_6 and BC observations made for the B-01 to B-12 plumes during the E-EU-08 flight. The E-EU-08 track included a flight transect (a-b-c-d-e) at approximately 600 m altitude and a shuttle (600-1400 m) between b-c and c-d in the outflow of London from 10 UTC to 12 UTC. A second shuttle (g-h-i) at 900, 1500 and 2400 m was made in the BNL outflow from 13:20 UTC approximately. Relevant changes in the HALO course and altitude are marked by coloured circles and letters in Fig. 24.

Backward trajectories indicate that the air measured at around 10:30 UTC at 600 m (blue circle), 11:00 UTC (point c at 1400 m and 600 m), 11:20 UTC (yellow circle) and 11:50 UTC at 600 m (pink circle) had passed over the MPC London a few hours before being probed at an altitude below 1000 m. Selected backward trajectories are shown in Fig. 24c. At these times, the measured enhancements in CO and NO_y and the NO/NO_y ratios are in reasonable agreement with the transport time predicted by HYSPLIT for the CO enhancement in the MPC London plumes in Fig. 23. For plume B-02, HYSPLIT predicts the London contribution to be a mixture of air masses transported in the previous 3 to 24 hours. The air probed had up to 10 ppb of NO_y and approximately 2 ppbv NO. The latter suppresses RO_2^*. OH and RO are produced but also react with NO and NO_2. These measurements confirm the predicted mixing of relatively fresh emissions with aged and more photochemically processed air masses. The vertical distribution of CO in the plume during the shuttles is depicted in the 3D diagrams in Fig. 24b. The CO measured indicates that the plume B-03 is well mixed horizontally with the plume B-06 up to 1400 m altitude. According to the backward trajectories (not shown), the plume at 11:52 UTC is

transported from the Northeast coast of UK and had no recent contact with the outflow of London. This is distinguishable by the significantly higher SO_2 mixing ratios measured.

The plumes B-08 and B-09 measured over the continent at 900 m are predicted to have been in contact with emissions of the MPC London within the previous 24 hours (Fig.23 and Fig. 24c). From 12:50 UTC the air probed is expected to mix with recent emissions of the MPC BNL as indicated by the observed higher NO levels and enhancements in NOy, SO_2 and C_6H_6 in Fig. 24a.

The composition of the air measured during the shuttle between the way points g and h in Fig. 24a at 13:30 and 13:45 UTC and the backward trajectories indicate that the outflow from the MPC BNL was sampled in a plume extending from 1000 m to 1500 m. This air mass was not detectable at 2500 m.

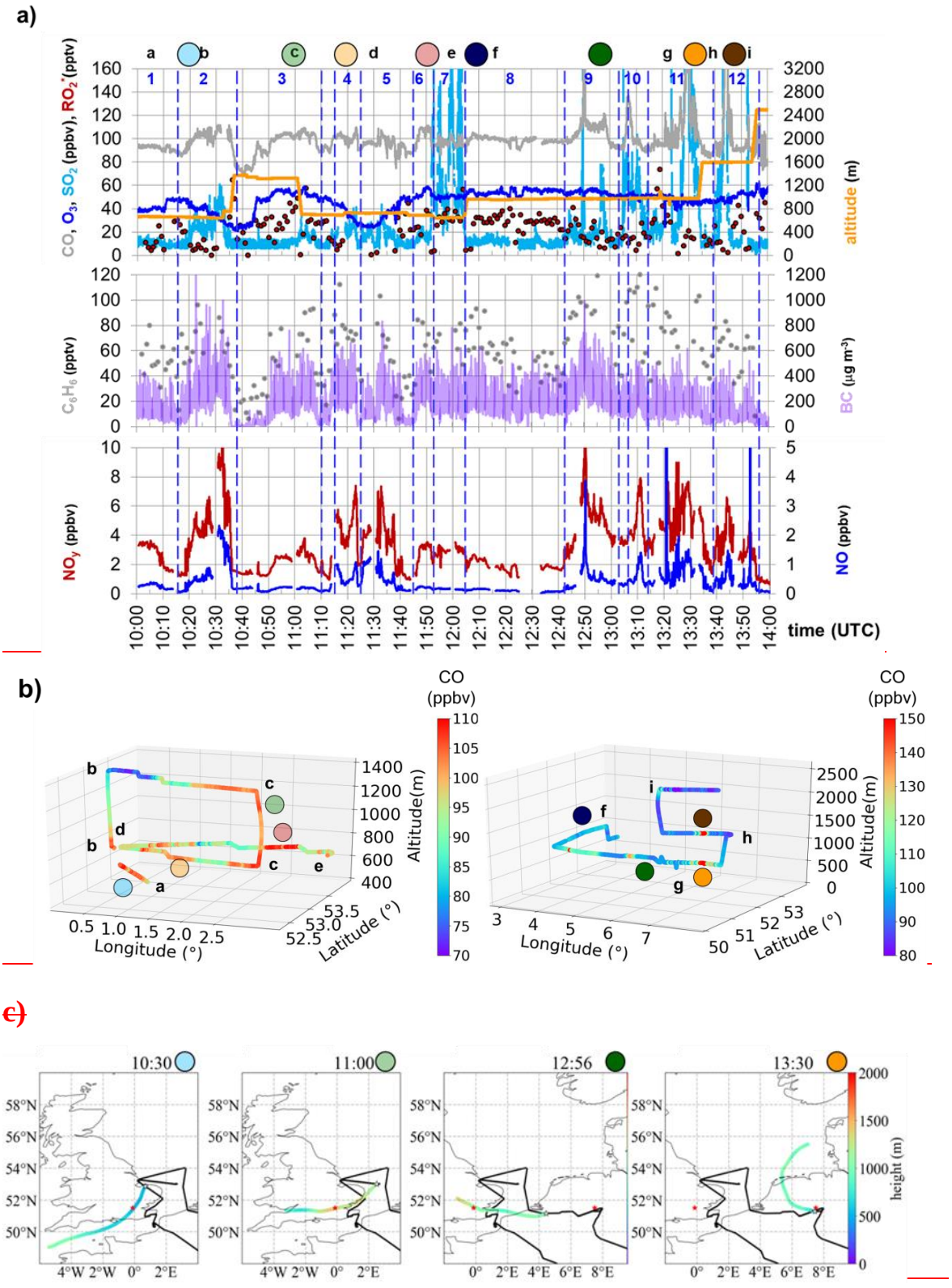

~~**Figure 24:** a) CO, O_3, SO_2, RO_2*, NO_y, NO, C_6H_6 and BC measured in the outflow of London and BNL during E-EU-08 on 26 July 2017. The position and numbering of the plumes are indicated by blue lines and numbers as classified in Fig. 22 (B is omitted for clarity), b) 3D shuttles colour coded with the CO mixing ratios observed. Relevant changes in the HALO course and altitude are marked by colour circles and letters (a-i). c) Selected backward trajectories (24h). The red stars indicate the position of the MPCs of interest.~~

- ~~Further information about the characteristics of the plumes is obtained from the air samples gathered with MIRAH on board HALO and on the ground sites in London and Wuppertal during the flight E-EU-~~

~~08. As stated in 4.1, lower~~ The concentration of particles with a diameter below 250 nm was analysed by the Differential Mobility Analyzer (DMA) in 6 steps of 30 s duration, resulting in a period of 3 minutes for each integrated measurement. The evaluated DMA data were then combined with the data from an Optical Particle Counter (OPC) for particles in the range from 0.25 to 3 µm. The first two sequences in Fig. 29 are taken at 2900 m and the third at 1300 m altitude during E-EU-03. The third period and lowest in altitude had the smallest total number concentration with a clear enhancement of the particles above 600 nm. According to FLEXTRA, HALO flew approximately 800 m above the PBL at the time of sampling. The increase in the coarse mode particles above the PBL implies mineral dust rather than sea salt. According to backward trajectories, the air mass probed had recent contact at altitudes below 1000 m with the dust plumes over the Mediterranean near Sardinia. In fact, both satellite- and ground-based observations indicated a Saharan dust event affecting the Central Mediterranean air masses measured during E-EU-03 on 11 July 2017. (see Fig.32 and the discussion below).

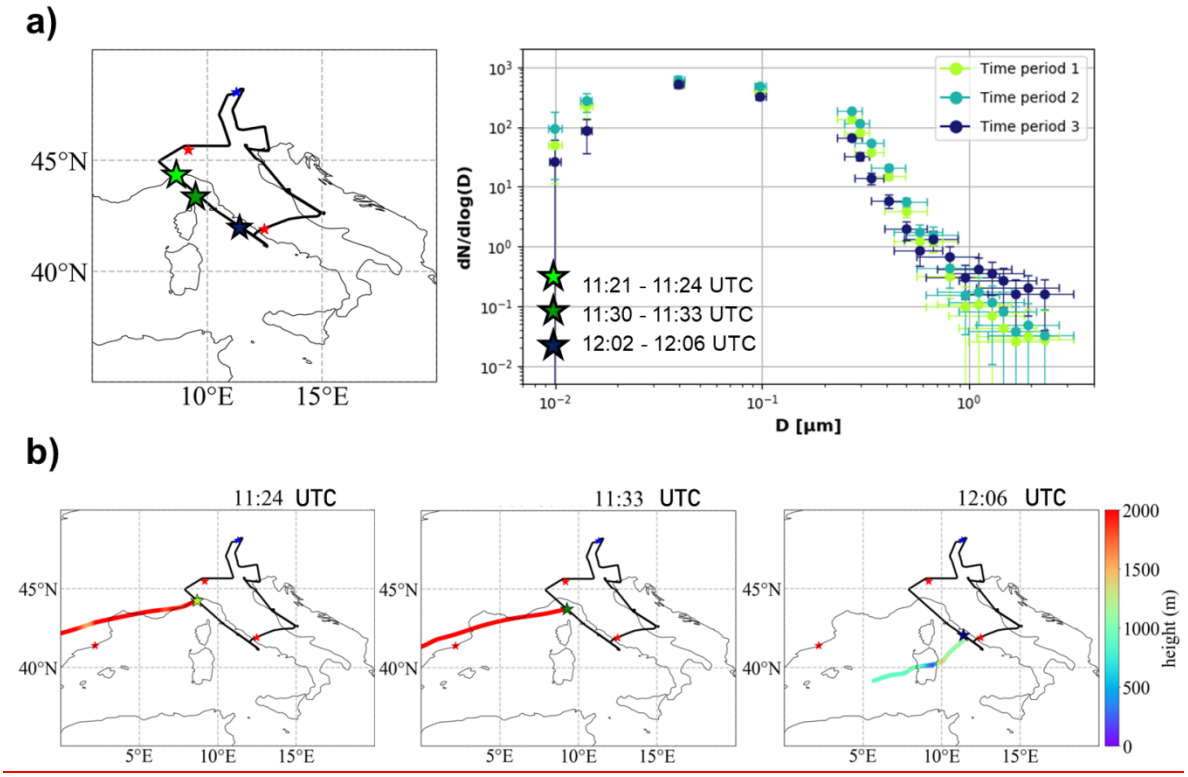

Figure 29: Example of the effect of dust plumes on the aerosol concentration during E-EU-03 on the 11 July 2017. a) Particle size distribution for 3 selected time periods (right) and position of the sample points in the flight track (left). The error bars on the y-axis are the standard deviations of the mean measured concentrations. The error bars in x-direction indicate the 16th and 84th percentile of the median diameters of the sensitivities of each size channel, b) 48h backward trajectories for the three periods selected. The red stars indicate the position of the MPCs of interest.

The presence of mineral dust on 11 July 2017 is also confirmed by the continuous aerosol profile measurements made over Rome by the automated lidar-ceilometer (ALC) .HALO overpassed the Rome area around midday. Figure 30 shows a lofted aerosol layer with increased depolarization indicative of the non-spherical mineral particles, at an altitude between 1000 and 2000 m from the morning. It then vertically mixed with local particles lifted by the PBL dynamics in the middle of the day, at the time of the DMA measurement. This indicates that HALO flew above a dust layer during the first two time-periods of the DMA measurement, thus probing rather low concentrations of large particles. Subsequently, in the time-period 3, HALO dived into the dust layer and this explains the increase of particles larger than 600 nm in the DMA measurements. Additionally to the coarse mineral particles, aerosol properties observed over Rome both on board the Sky Arrow aircraft and at the ground provide evidence for an important role of fine particle photo-nucleation in the MPC Rome, favoured by high radiation and temperatures (Campanelli et al., 2021; Barnaba et al., 2021 in preparation).

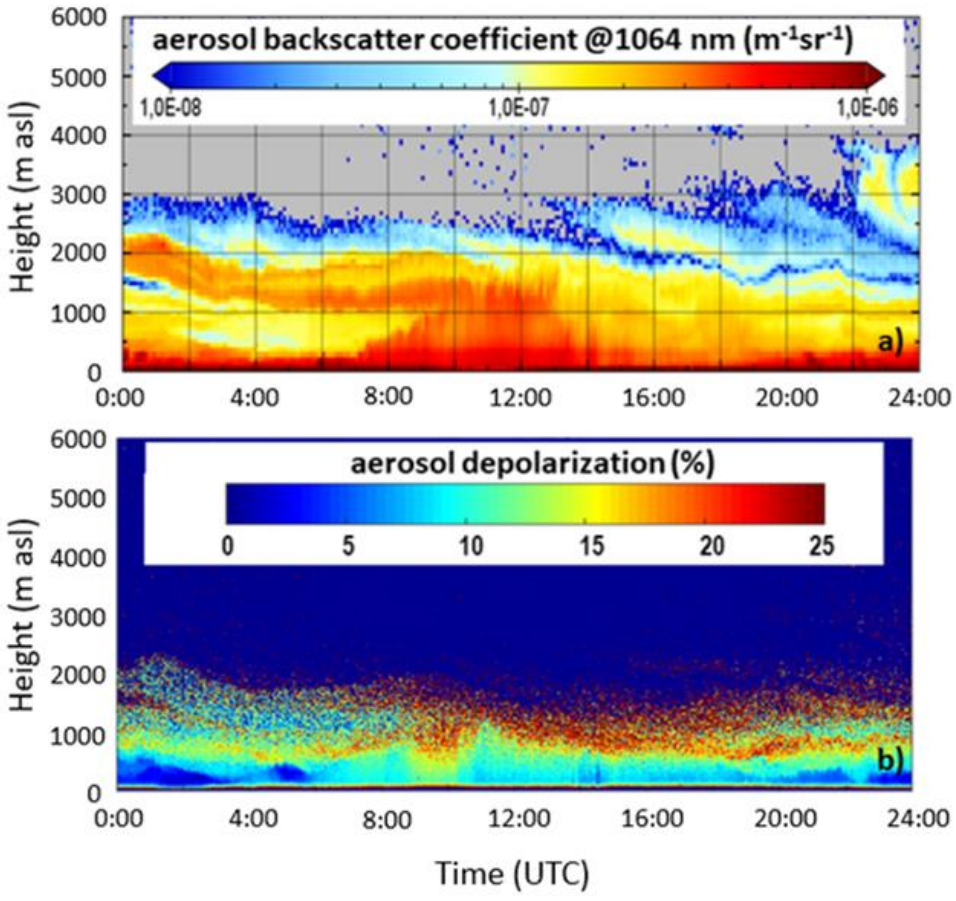

Figure 30: Aerosol profile measurements performed in Rome (Italy) on 11 July 2017 by the Automated Lidar-Ceilometer network (ALICENET). Aerosol backscatter coefficient (m^{-1} sr^{-1}) at 1064 nm (top), and aerosol depolarization in % (bottom).

- Transport of BB emissions from fires and mineral dust events were identified by combining HALO observations with remote sensing satellite retrievals

BB emission from fires was e.g. probed during the E-EU-07 flight downwind of Marseille. The plume transport eastwards from near Marseille is well-captured by SEVIRI with AOT values around 0.25 at 0.55 µm in the afternoon, as shown in Fig. 31. This plume was probed by HALO in-situ measurements at around 11:30 and 16:30 UTC. The BC mass concentrations depicted in the figure agree with the satellite data. The highest BC was measured at roughly 2000 m and exceeded 7 µg m^{-3}. In the PBL, measured BC mass concentrations were as high as 1 µg m^{-3}. The stratification of pollution plumes above the PBL is a commonly observed feature for BB emissions (Holanda et al., 2020).

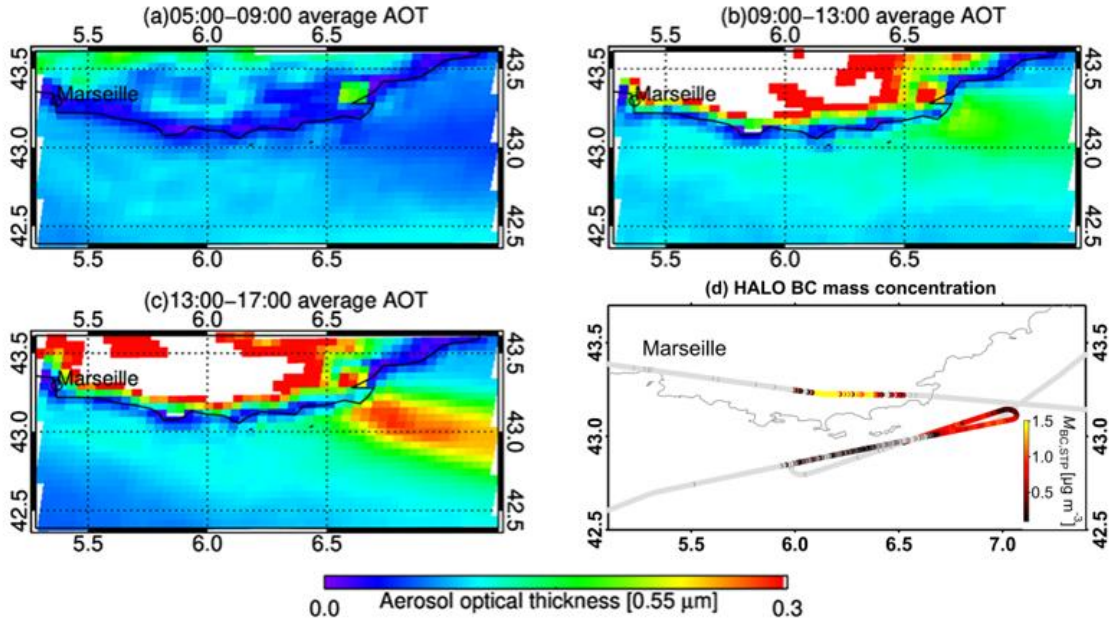

Figure 31: (a - c) Aerosol optical thickness at 0.55 µm as retrieved from SEVIRI from 05:00 to 17:00 UTC on 24 July 2017. (d) E-EU-07 flight track, colour-coded with BC mass concentration (M_{BC}). For a better contrast, the scale for M_{BC} ranges from 0.1 to 1.5 µg m^{-3}. Grey colour on the flight track indicates values below 0.1 µg m^{-3}. The mass concentration reached values up to 7 µg m^{-3} at the French coast.

A further example is the transport of the Saharan dust event affecting the air masses measured during E-EU-03 on 11 July 2017 as explained in Fig.29. Figure 32 shows the MODIS satellite RGB image at 10:30 UTC and the corresponding dust-related elevated AOT at 0.55 µm as retrieved from SEVIRI from 09:00 to 13:00 UTC.

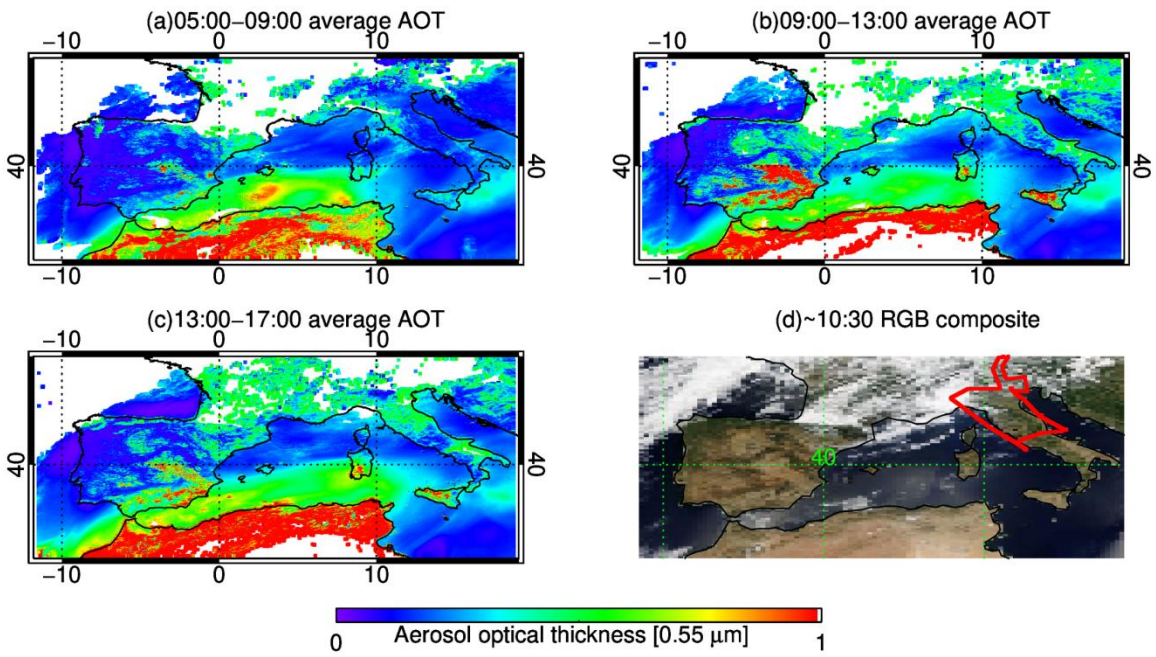

Figure 32: (a-c) Aerosol optical thickness at 0.55 µm as retrieved from SEVIRI from 05:00 to 17:00 UTC on 11 July 2017, (d) MODIS RGB composite figure showing corrected reflectance at 10:30 UTC (https://worldview.earthdata.nasa.gov/). The MODIS RGB composite is created combining red, green and blue bands into one picture. White areas are clouds. The E-EU-03 flight track (in red) is superimposed on (d).

4.5 Photochemical processing of polluted air masses during transport

- Photochemical processing of the MPC emissions during transport was substantial during EMeRGe as inferred from airborne observations of primary and secondary pollutants and the ratios between species having different chemical lifetime:

a) The **NO to NO_y ratio** provided information about the reactivity of the air mass but was not a reliable chemical clock due to the complex and rapid chemistry involved in the air masses investigated. Depending on the chemical and physical conditions, the lifetime of NO versus the formation of other reactive nitrogen compounds was of the order of a few hours or less. Internal transformation processes within the family of total reactive nitrogen NO_y do not alter their integrated concentration. However, the lifetime of NO_y, which varies between hours and days, is also controlled by loss processes such as washout and aerosol formation.

b) The **NO_y to CO ratio** was generally significantly higher for the processed polluted plumes than for the background air masses. For instance, during E-EU-08 the NO_y to CO ratio was of the order of 0.01 to 0.02 in the air sampled outside the outflow of London and increased up to 0.1 in the London outflow plumes, as the air mass was processed and mixed. This ratio is usually used to study ageing of an air mass with respect to ozone and nitrogen chemistry (e.g. Stohl et al., 2002). The CO lifetime varies between several weeks and months (e.g. Emmons et al., 2010) and the NO_y/CO ratio is expected to decline to background values within a few days, depending on the distance from the source as well as on the chemical and physical properties of the air mass.

c) The ratio between **VOCs** with comparable emission sources but significantly different chemical lifetimes such as C_7H_8/C_6H_6 was a good indicator for the presence of freshly or already processed anthropogenic emissions in the probed air within EMeRGe. This ratio is often used as a chemical clock to study emissions from gasoline-powered engines used in traffic and industry (Gelencsér et al., 1997; Shaw et al., 2015; Warneke et al., 2001). The atmospheric lifetime of these aromatic hydrocarbons, i.e., 1.9 and 9.4 days, respectively (Garzón et

al., 2015), is assumed to be controlled only by the reaction with OH radicals (Atkinson, 2000). Provided that the emission rates are known, the C_7H_8/C_6H_6 ratio is expected to decrease with increasing distance to the pollution source and can be used to estimate the photochemical age of the sampled air (Winkler et al., 2002; Warneke et al., 2007). However, the complex plume mixing before sampling and potential variations in the emission ratios of distinct VOC sources (e.g. Barletta et al., 2005) limited the use and feasibility of this chemical clock for the determination of the transport time of specific outflows in EMeRGe.

d) The combination of **C_7H_8/C_6H_6 and NO_y/CO ratios** with the simultaneous observations of **CO and organic ions in aerosol particles** enabled the discrimination of dilution and processing in the plumes. Figure 33 shows an example of photochemical processing of the gas and the aerosol phases in ageing London plumes as measured by the C-ToF-AMS during E-EU-08. Aerosol mass spectrometer data using organic ions containing oxygen, e.g. CO_2^+ (m/z 44) and $C_2H_3O^+$ (m/z 43), were used to assess photochemical oxidation. Observations from laboratory and field studies indicate that during photochemical processing the ion signal of m/z 43 decreases while that of m/z 44 increases (Ng et al., 2010; Lambe et al., 2011). This metric is used to infer the degree of photochemical processing of organic aerosol in the atmosphere (e.g., Ng et al., 2011; Schroder et al., 2018; de Sa et al., 2018). The data in Fig. 33 are plotted in *f*44-*f*43 space, where *f* denotes the ratio of the respective ion to the total organic ion signal. In these metric, atmospheric processing moves the data points towards the upper left corner of the triangle indicated by the dotted lines (Ng et al., 2010). Since photo-oxidation of fresh plumes is fast and mixing of aged plumes with the background occurs, the use of aerosol composition to assess photochemical processing requires complementary information from other measurements to be reliable. This is achieved by using simultaneous measurements of CO to indicate dilution, while inferring atmospheric processing from the C_7H_8/C_6H_6 and NO_y/CO ratios. Lower CO concentrations due to plume dilution along transport correspond to higher photochemical processing in the upper part of the triangle. As NO_y has a shorter lifetime than CO, the NO_y/CO ratio indicates that the processing is taking place in addition to dilution. Therefore, lower NO_y/CO and C_7H_8/C_6H_6 ratios in the upper part of the triangle indicate aged and processed air. In the case shown, the FLEXTRA backward trajectories revealed that the air masses identified as "background" were transported above the PBL and had no recent contact to the MPC London. The anthropogenically influenced air masses were a mixture of recent emissions and photochemically processed London outflow as mentioned in 4.3 (see also Fig. 36).

a)

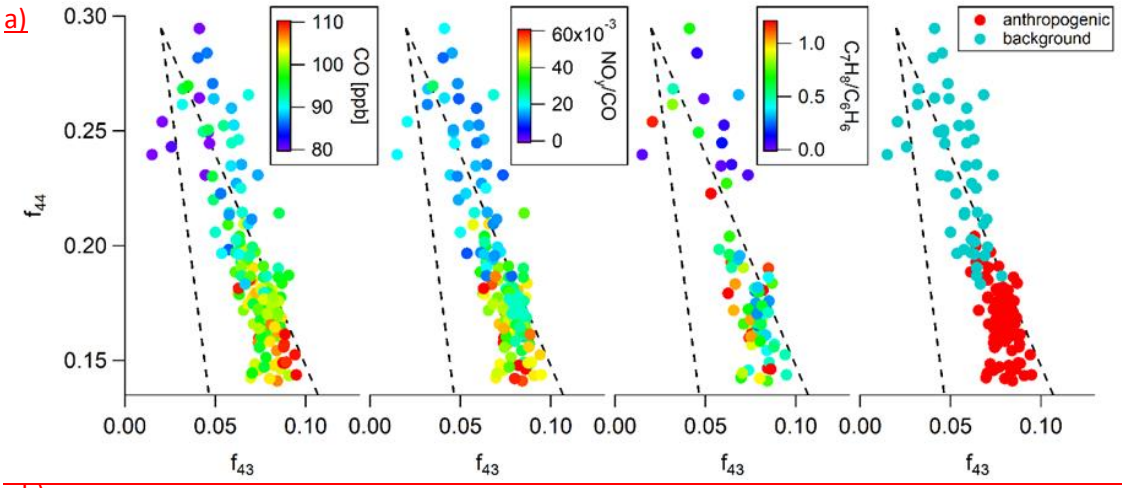

b)

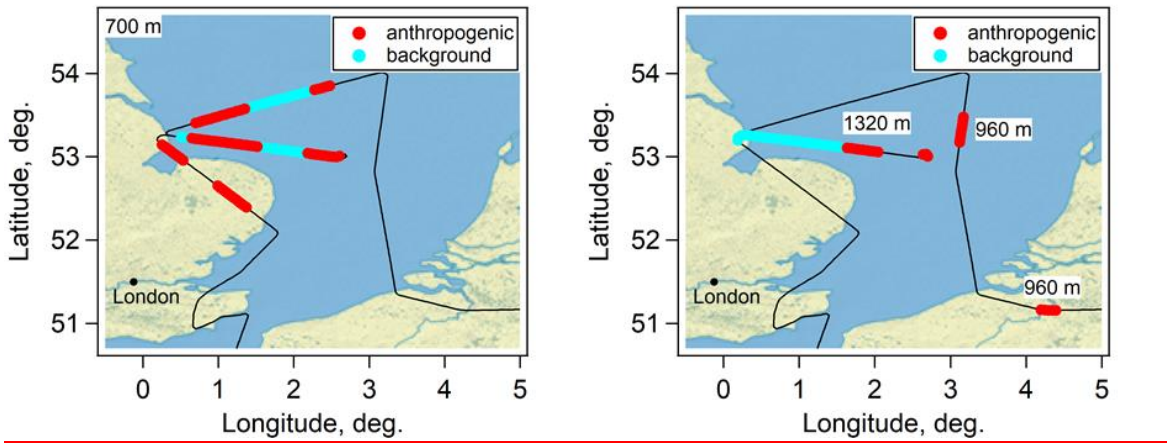

Figure 33: a) Scatter plots of C-ToF-AMS signal fractions at m/z 44 (f44) and m/z 43 (f43) of the London plume measured during the E-EU-08 on 26 July 2017 between 10:20 and 12:57 UTC. In this metric, the degree of photochemical processing increases to the upper left corner of the triangle which encompasses the range of typical atmospheric observations The colour code indicates dilution (CO) and processing of the gas phase (NO_y to CO and C_7H_8 to C_6H_6 ratios). The right panel shows the assignment to unpolluted background air and air masses of anthropogenic polluted origin as introduced in Sect. 4.2. b) Spatial distribution of the background and anthropogenic polluted air masses identified in a). The flight altitudes are indicated in the graphs.

- Photochemical processing of aerosol was evident during the transport of MPC plumes. Chemical processing was fast under European summer conditions and modified both the chemical properties and the partitioning between gas and particle phase in the air masses over Europe. The aerosol composition and mass loadings were to a large degree determined by the atmospheric dynamics, i.e. mass concentrations in the PBL were generally higher than above, and most of the MPC plumes were found to reside in the PBL. However, anthropogenically influenced air masses above the PBL were found to also contain higher aerosol mass concentrations than air masses not influenced by anthropogenic emissions. Plume air contained less oxygenated organic aerosol, but the transition to background air conditions was smooth, indicating that the aerosol oxidation was faster than the decay of benzene which was used for the plume tagging.

- The photochemical activity as indicated by the presence of free radicals varied widely in the plumes. The RO_2^* mixing ratios observed in EMeRGe are shown in Fig. 34. The RO_2^* measured is the sum of $HO_2 + \sum RO_2$, R being an organic chain which produces NO_2 in its reaction with NO. Mixing ratios up to 120 pptv RO_2^* were measured in the air masses probed. Provided that insolation conditions (i.e. actinic fluxes) and the amount of precursors are similar, peroxy radicals are expected to be produced as long as plumes mix at any altitude. Generally, higher RO_2^* were measured below 45°N and 3000 m. This was in part due to the higher insolation and temperatures prevailing during the flights over the Mediterranean area, which accelerated photooxidation and the production of RO_2^*. Rates of photochemical production and loss of HO_2 and RO_2 were estimated by using airborne measurements and photostationary steady state calculations. In particular the measured photolysis frequencies are important to quantify the primary production of radicals to elucidate the radical budget based on the measured RO_2^* concentrations. Overall, measured and estimated radical concentrations are in good agreement (George et al., 2021, in preparation). Up to 4000 m, O_3 photolysis was found to be the primary radical source (> 40 %) followed by HCHO photolysis in the air masses probed. HONO and HNO_3 formation and heterogeneous losses on the aerosol surface dominated the peroxy radical losses in the polluted plumes encountered. The O_3 production rates calculated from the RO_2^* measured on-board are consistent with the values reported in urban pollution for NO <1 ppbv (e.g. Tan et al, 2017; Whalley et al, 2018, 2021).

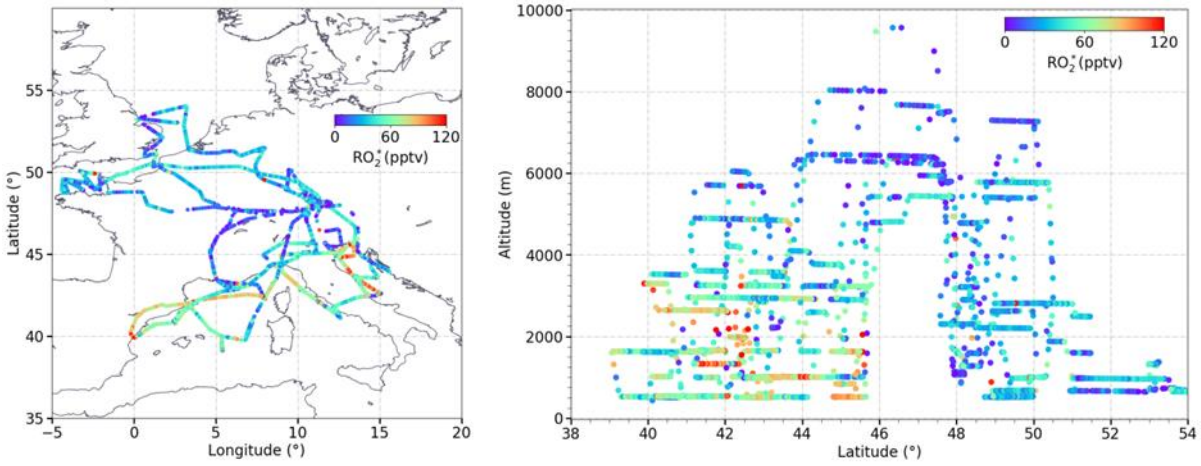

Figure 34: RO_2^* spatial and vertical distribution measured along all EMeRGe flights in Europe.

- The secondary photochemical formation of formic acid (HCOOH) was observed to be the main source of HCOOH in Europe in pollution plumes of major cities aged 24 to 48 hours.

Figure 35 shows HCOOH enhancements above ambient background relative to CO enhancements in different MPC plumes as a function of plume age. Here, ΔHCOOH and ΔCO are determined from the measurements, and the plume age from HYSPLIT simulations considering CO emissions from EDGAR and the dispersion of the plumes during transport. CO is used as an indicator of the strength of emissions from combustion in the individual MPC plumes and as tracer for the dilution of the plumes for the meteorological conditions during the measurements. Although HCOOH has primary sources, i.e., the emissions by fossil fuel combustion and BB, the secondary formation from gas-phase and aqueous photochemistry has been suggested to be dominant in the troposphere (Paulot et al., 2011). The ΔHCOOH to ΔCO ratios in Fig. 35 increase significantly with plume age indicating secondary formation of HCOOH to be the main source in the MPC plumes, mainly due to oxidation of C_5H_8 in the plume.

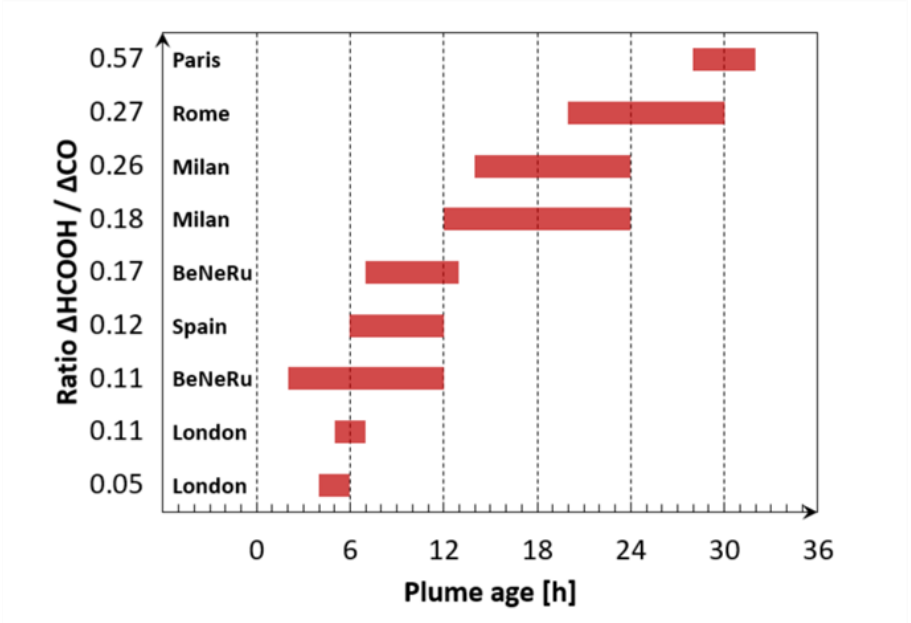

Figure 35: Observed enhancements of formic acid (ΔHCOOH) in MPC plumes relative to observed CO enhancements (ΔCO) as a function of plume age from HYSPLIT simulations. The corresponding city-plume is indicated next to the ratios.

Chemical ageing of MPC plumes was assessed from the isotope measurements in VOC samples collected at MPC ground sites and on-board HALO. Figure 36 shows an example of the measured $\delta^{13}C$ values of $C_5H_{10}O$ and C_6H_6 observed during the flight E-EU-08. Low carbon isotope ratios indicate fresh emissions, whereas higher values indicate an enrichment of the compound in ^{13}C, which is linked to chemical ageing.

~~In Fig. 25, the measured $\delta^{13}C$ values of $C_5H_{10}O$ and C_6H_6 are shown as examples.~~ The identified London outflow in Sect.4.3 is also evident in the carbon isotope ratios obtained from HALO samples taken between 10 and 11 UTC. The latter remain in the range of the representative source values from whole air samples collected at the ground station in London. The higher $\delta^{13}C$ values observed between 11:10 and 12:00 UTC indicate chemically-processed London outflow air.

Later in the flight, the $\delta^{13}C$ values measured over the BNL/Ruhr area are in the range of the source values in air samples collected in Wuppertal. The range in $\delta^{13}C$ values of ± 1.5 ‰ in $C_5H_{10}O$ (± 3.5 ‰ in C_6H_6) implies a mixture of slightly aged air and rather fresh emissions from the Ruhr area.

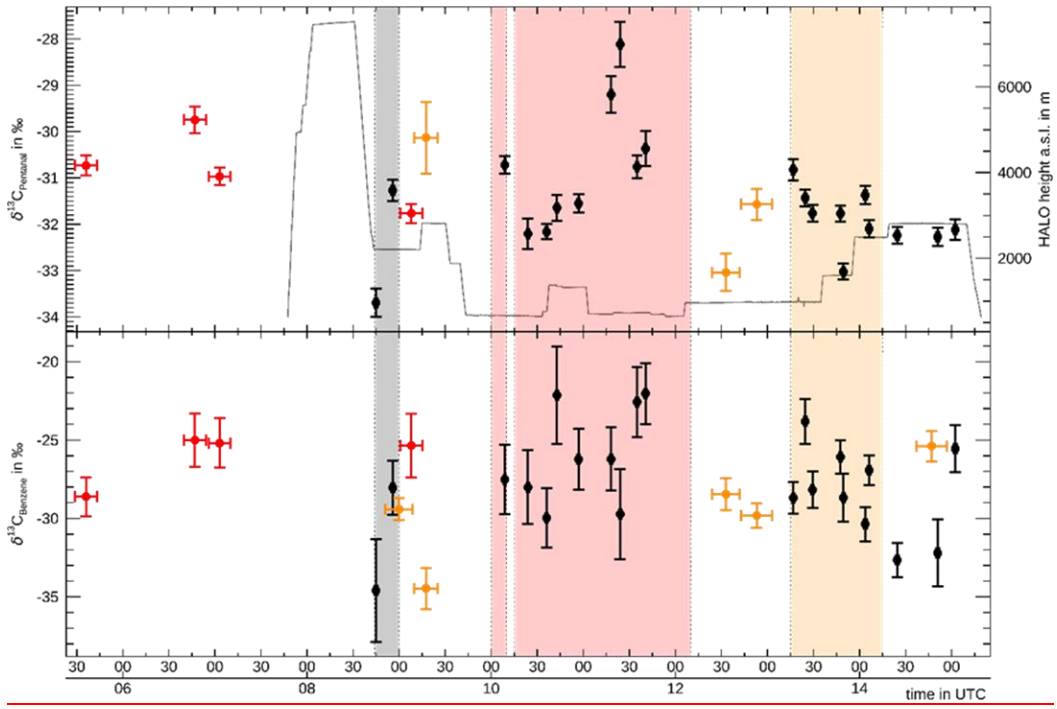

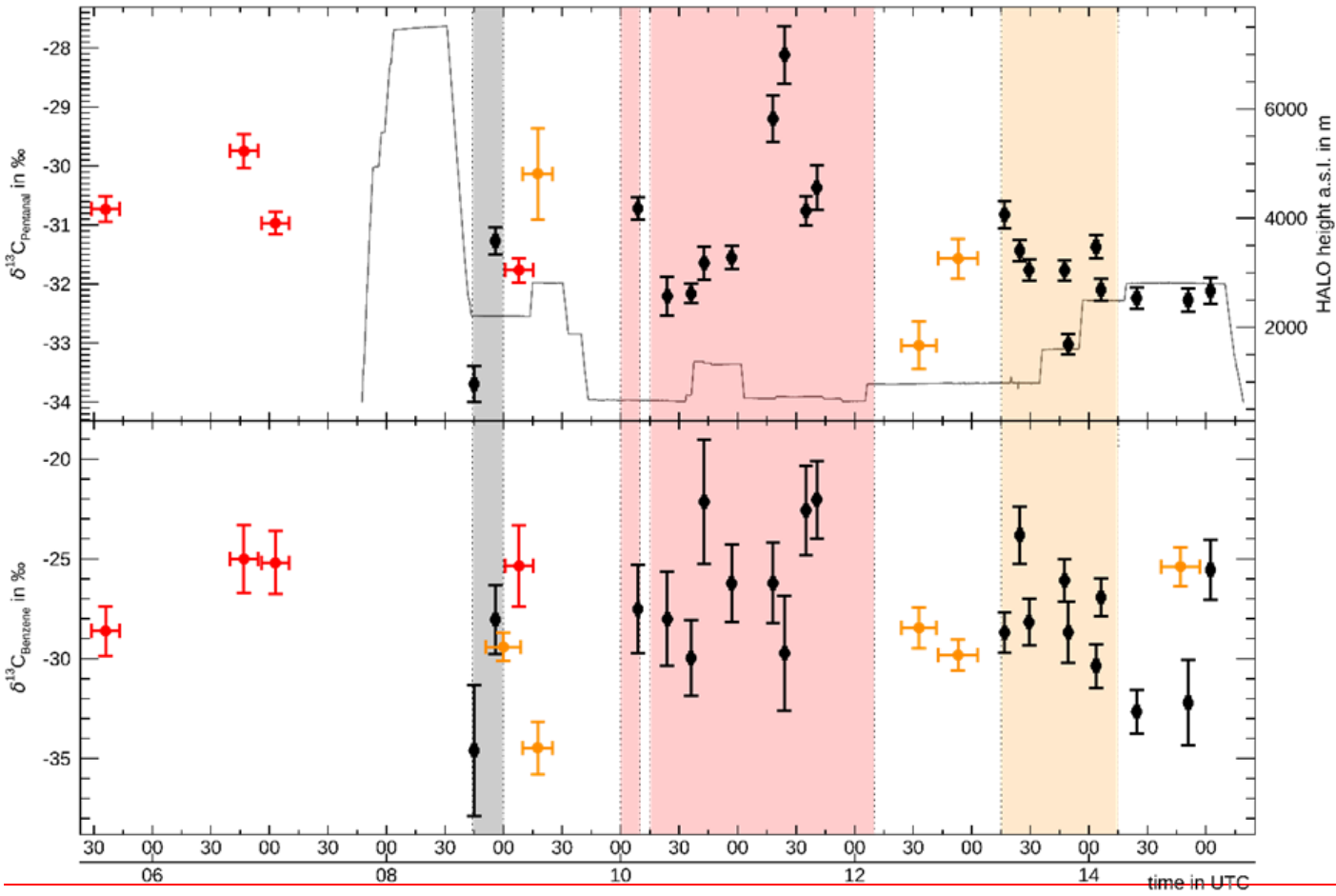

Figure 3625: $\delta^{13}C$ values in $C_5H_{10}O$ (top panel) and C_6H_6 (bottom panel) in whole air samples gathered with the whole air sampler MIRAH on the HALO aircraft (black) during E-EU-08 as well as on the ground sites in London (red) and Wuppertal (orange). The HALO flight altitude is given in grey on the top panel. Background shadings indicate different measurement regions during the flight according to Fig. 4: Paris (grey), South of London and North Sea region (red), BNL/Ruhr (orange).

~~Pollution plumes of the London MPC outflow were also assigned during E-EU-05. These were measured after transport over the English Channel and to the European continent. Similar to the study of Ashworth et al. (2020), the processing of the plumes from the emissions probed by the FAAM aircraft in the circuits around London will be addressed in separate publications. Observations of the released PFC tracer in London improved the definition of the plume in the area of measurement.~~

4.~~3 Specific case studies of MPC outflows~~

~~In addition to the plume from London, other MPC outflows were identified and analysed during the EMeRGe IOP in Europe by combining tagging and observational tools. Two representative case studies are briefly presented in the following. The corresponding detailed analysis is subject of separate publications.~~

~~4.3.1 MPC Po Valley and Rome~~

~~Shuttles at different altitudes upwind of Rome in the Mediterranean and along the Adriatic coast during the flights E-EU-03 and E-EU-06 provided information about the vertical distribution of trace gases at different distances from the sources of the MPC Po Valley and MPC Rome.~~

~~As for the MPC London case in Sect. 4.2., backward and sensitivity trajectories support the identification of plumes downwind from these MPCs. The density distribution for forward trajectories (FT) of MPC Rome~~

outflows in Fig. 26 highlights the typical transport pattern towards the Adriatic coast and the representativeness of the HALO measurements. The flight tracks for E-EU-03 and E-EU-06 are colour coded with the BC mass, showing a good agreement between the four-year FT analysis and the actual in-situ measurements. These results also strengthen the assumption of the HALO measurements being representative for the transport of air masses from the MPC Rome. The FT density distribution was calculated as explained in Pöhlker et al., (2019). The FT starts at 100 m above ground level for the month of July in a multi-year period (2017 until 2020) by using the HYSPLIT package (version 4, Revision 664, October 2014) (Stein et al., 2015; Rolph et al., 2017).

For the Rome MPC, the airborne measurements at low altitudes made by the Sky-Arrow research aircraft agree reasonably well with the columnar amounts of gases observed by the PANDONIA global network for air quality and atmospheric composition (https://www.pandonia-global-network.org/) and the remote sensing observations on board HALO. These data support the determination of the geographical extension and location of the Rome outflow (see Barnaba et al., Campanelli et al., in preparation 2021).

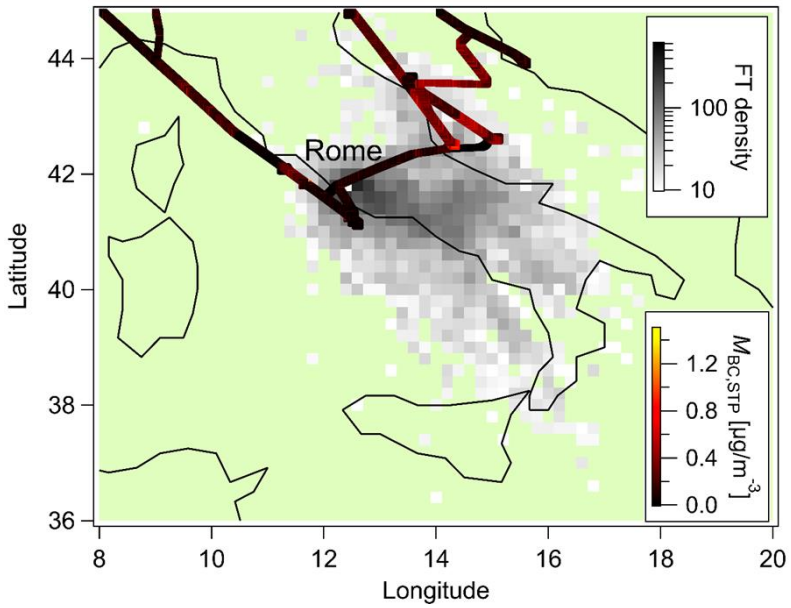

Figure 26: Forward trajectory (FT) density plot for air masses starting in Rome (100 m a.g.l.) in the month of July from multiple years (2017 to 2020). The grey scale represents the counts of FT points in each grid cell. The flight track of E-EU-03 and E-EU-06 is colour coded with the BC mass concentration.

The MPC Po Valley has surface emissions from the urban agglomeration over a relatively large area. It is a good example of a patchy and complex outflow that has largely been investigated as pollution hot spot in Europe. Several studies show the importance of the pollution transport from this area to the surrounding regions (e.g. Diémoz et al., 2019a, 2019b) and the complexity of chemical and dynamical processes within the Po Valley mixing layer (e.g. Curci et al., 2015). The Alps and Apennines on the Italian Peninsula lead to the transport of the Po Valley outflow southwards along the Italian Adriatic coast which is the geographic opening of the Po Valley (Finardi et al., 2014). In a dedicated study, the in-situ and remote instruments at ground based sites and airborne measurements from two aircrafts are combined to examine in detail the transport of pollutants during the EMeRGe IOP for the case Po Valley (Andrés Hernández et al., in preparation 2021).

When HALO flew over MPC outflows but did not sample them in situ, the down-looking remote sensing instruments on board enabled the identification of plumes as illustrated in Fig. 27 by using HAIDI measurements

at 8 km of the Milan outflow during E-EU-09. The measurements of HAIDI were used to estimate emissions and plume geometries, NO_2 being an important target species.

The HAIDI instrument has three scanning telescopes pointed at nadir, 45° forward and 45° backwards direction. On the left side of Fig.27, the data from the nadir telescope scanner are shown at high spatial resolution. The map shows a strong NO_2 plume Northeast of Milan. The plume substructures are also clearly visible. On the right side of the figure, the data from all three telescope scanners are plotted as a function of time at a lower spatial resolution. The time delay of about 80 s between the peak as seen in the forward and backward scanners indicates that this plume is close to the ground. Wind data from the lowest layer from the ECMWF ERA-5 reanalysis product [Copernicus Climate Change Service, 2017] implied a wind angle of 23.8°, which is consistent with this plume originating from the city of Milan. The estimated NO_2 emission rate of 607± 67 kg/day may have a higher uncertainty due to the low wind speed (0.6 m/s), the complex plume shape and the small relative angle between the HALO flight track and the plume direction.

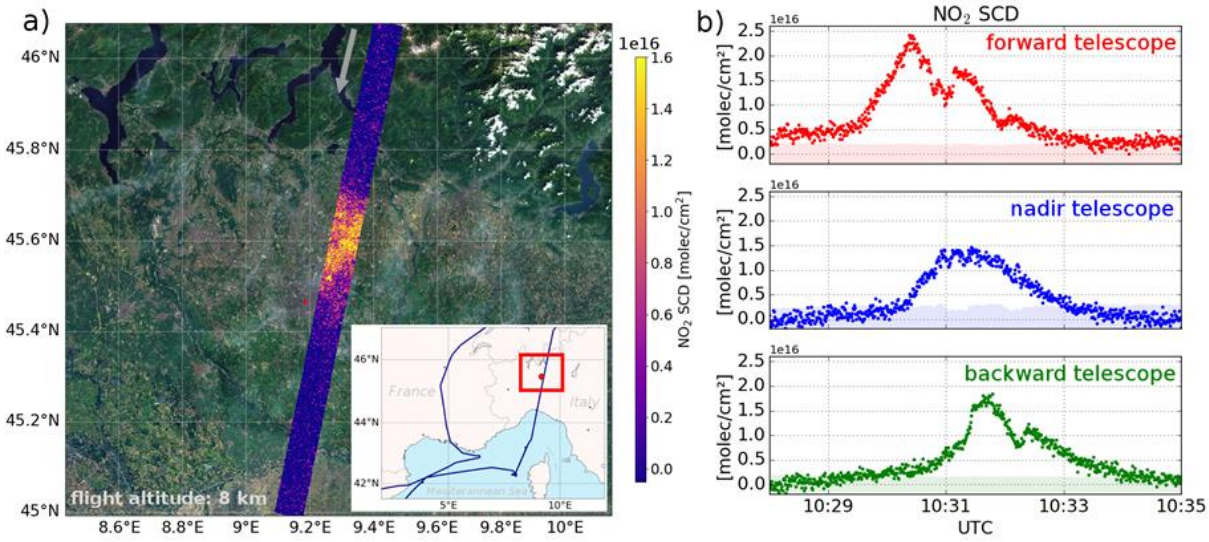

Figure 27: HAIDI measurement at 8 km altitude of the Milan outflow during the flight E-EU-09: a) pixel-resolved NO_2 slant column densities observed by the nadir camera (marked by the red square on the map). An enhancement of up to 1.5×10^{16} molec/cm² over the background is observed Northeast of Milan (red-coloured circle), b) NO_2 slant column densities averaged over the whole swath for all three telescopes: forward (top) nadir (middle) and backward (bottom). The height of the plume centre is estimated from the time difference of the maxima.

Model

~~**4.3.2 MPC Madrid and Barcelona**~~

~~The vertical distribution of pollutants observed at the coast of Barcelona during E-EU-09 is a particular case of interest for the study of vertical layering of pollution. HYSPLIT CO dispersion~~ simulations **of EMeRGe observations** ~~indicate that the Madrid outflow was transported over a long distance above the Iberian Peninsula to the North-Eastern coast at altitudes above 2000 m while in the lower layers the Barcelona outflow predominated, as illustrated in Fig. 28.~~

~~In contrast with the air sampled at 500 m, the backward trajectories and HYSPLIT dispersion calculations indicate that the air probed from 15:15 to 15:25 UTC at 1600 m had passed over MPC Barcelona within 6-12 hour before sampling. There is no indication of fresh NO emissions, and NO_y, C_6H_6 and CO are significantly higher than at the lower altitude. The layering is attributed to be the result of the recirculation of emissions in the Barcelona outflow within the land breeze regimes close to the coast. Later at this FL (green and red circles in Fig. 28), the backward trajectories and HYSPLIT estimations indicate sampling of regional emissions that had travelled along the coast from Valencia. This is consistent with the observed decreases in C_6H_6, NO_y and BC. In the upper FL at 15:45 UTC, NO_y, C_6H_6 and CO significantly increase in air transported from Portugal (as in the 36 h backward trajectories) across the Iberian Peninsula at altitudes above 2000 m, after PBL contact with the MPC Madrid below 1000 m the evening before. According to the pollution control network of Madrid, the average CO surface concentration exceeded 350 ppb on the 27 July 2017, the zonal wind direction was WSW and the average wind speeds were greater than 16 km/h. The observed mixing ratio decreases when this feature at 3000 m disappears. Re-entering and stratification of plumes having different processing along the Spanish coast has also been documented in the past (e.g. Millán et al., 1997, 2000 and references therein).~~

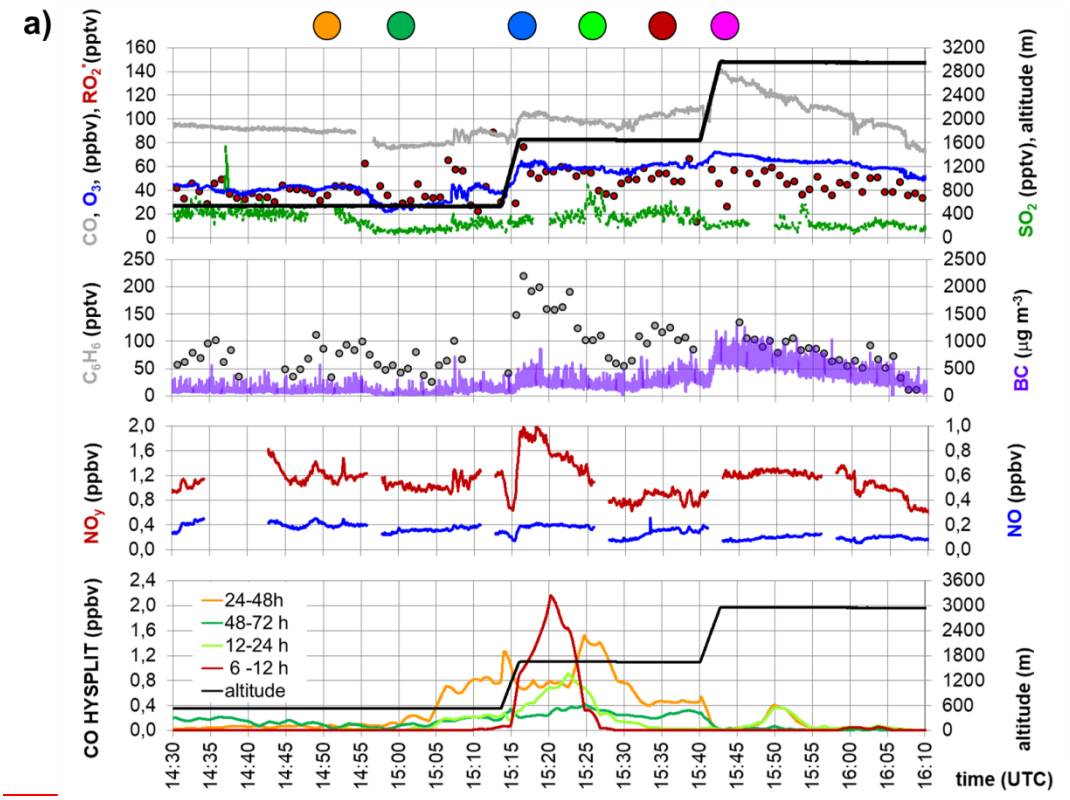

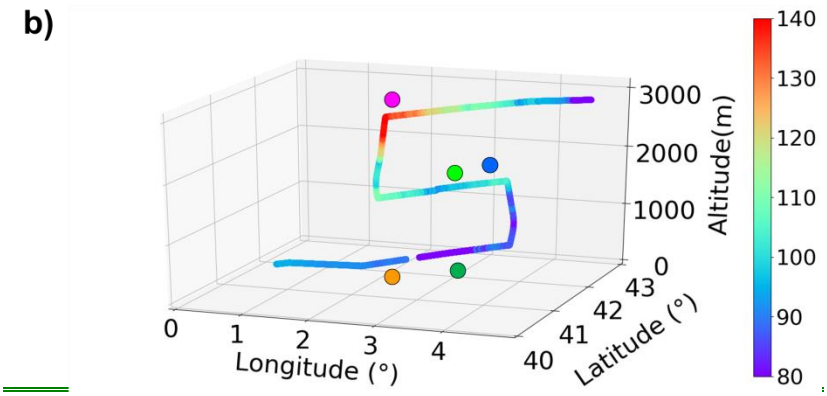

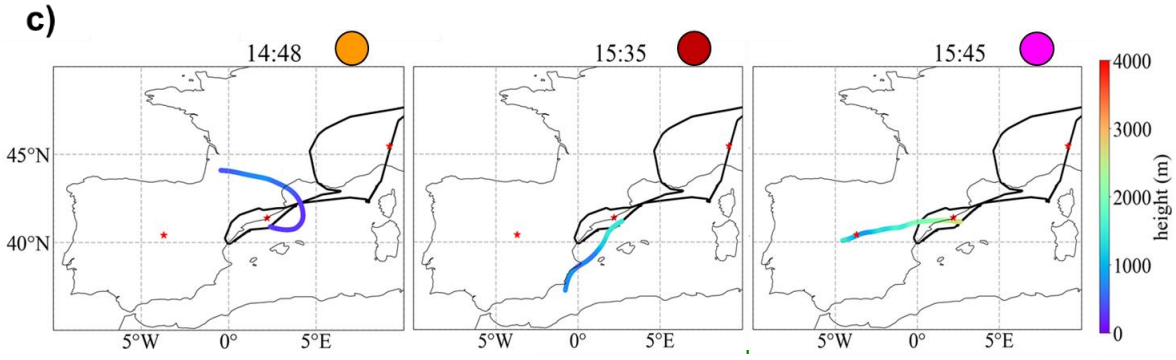

Figure 28: Stratified pollution layers along the Spanish coast during the E-EU-09 flight on the 28 July 2017, a) temporal variation of CO, O_3, RO_2*, NO_y, NO, SO_2, C_6H_6 and BC during the shuttle, b) 3D view of the shuttle colour coded with CO mixing ratios, c) selected backward trajectories (last 24h). Coloured circles marked the corresponding times. Red stars indicate the position of the MPCs of interest.

These HALO measurements are consistent with the long-term analysis of data from the closest four ground-based remote sensing stations available in the framework of EMeRGe international. These are data of a lidar in

Barcelona (BRC) and three ceilometers in Montseny (MSY), on top of the Serra del Montsec (MSA) (Titos et al., 2019) and in Burjassot (VLC) near Valencia. Figure 29 shows the location of the stations with respect to the HALO flight track. The stations MSY and MSA were approached at a flight altitude of 2600 m when HALO entered the air space above the Iberian Peninsula. Subsequently, HALO shuttles were carried out Northeast of Valencia at 500, 1000, 2000 and 2600 m as well as East of Barcelona at 500, 1600 and 3000 m, as presented in Fig. 28.

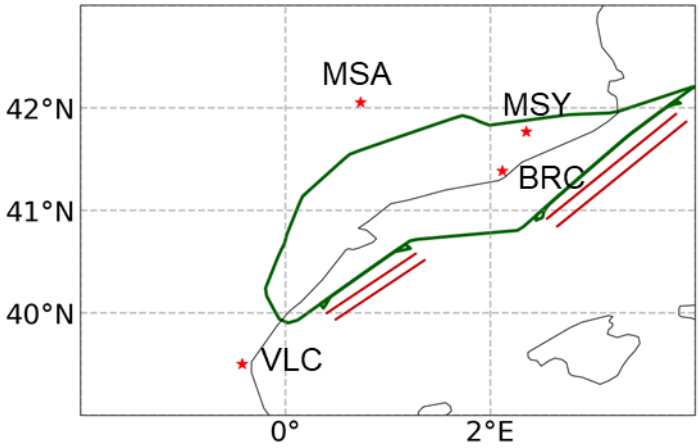

Figure 29: Detail of E-EU-F09 flight track (in green) and the ground-based stations with coordinated remote sensing measurements in the vicinity: Montseny (MSY), Sierra del Montsec (MSA), Burjassot (VLC) and Barcelona (BRC). Red lines indicate the position of the HALO shuttles.

A lofted aerosol layer from above the PBL up to 4000 m altitude was observed at all ground based remote sensing stations and also probed by HALO (see Fig. 30).

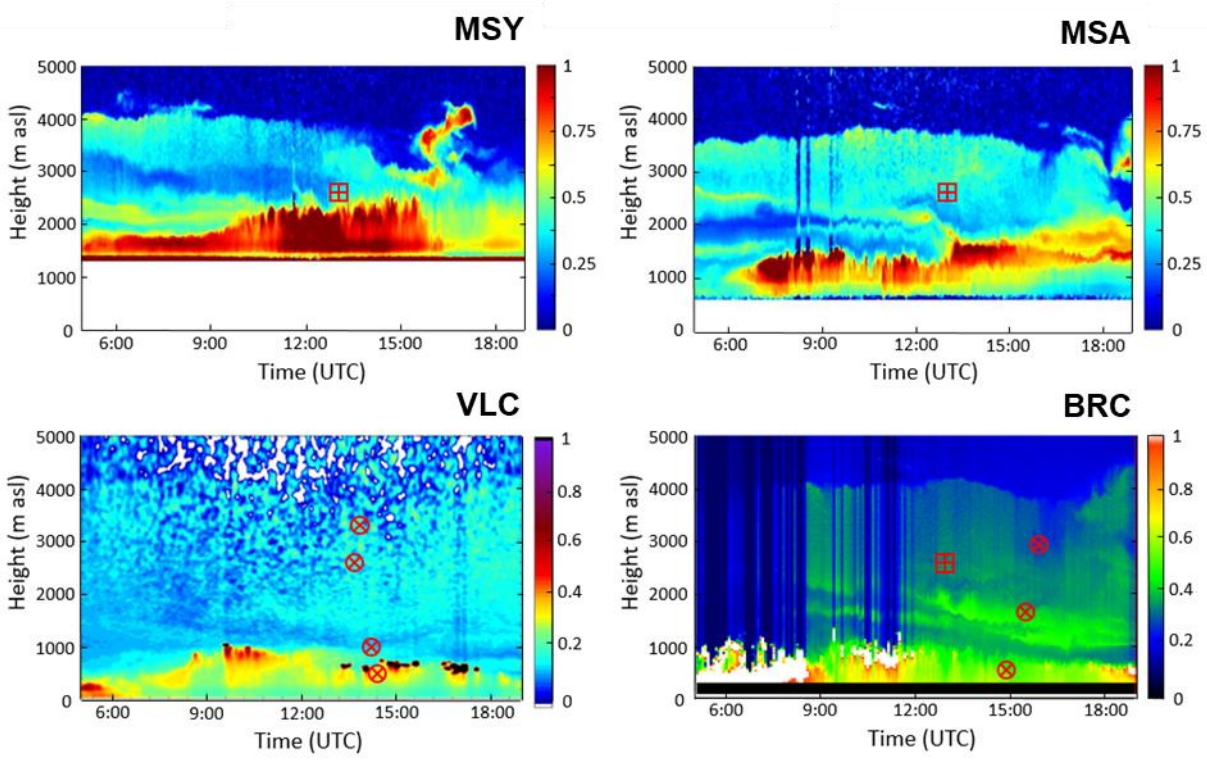

Figure 30: Time series of range-corrected lidar signals ground-based remote sensing measurements in MSY, MSA (both at a wavelength of 1064 nm), VLC (910 nm) and BRC (532 nm) on the 28 July 2017. Signal strengths relative to the maximum signal of the corresponding measurement are depicted. Red circles show time and altitude of the HALO overpasses used for comparison of airborne with ground-based remote sensing measurements (see Fig. 31 and Fig. 32). Red squares show further HALO overpasses.

The profiles of the backscatter coefficient derived at MSA, MSY, VLC and BRC on the 28 July 2017 are displayed in Fig. 31 and Fig. 32. These measurements illustrate the lofted aerosol layer shown in Fig. 30 with increased backscatter coefficients ranging from 0.4 to 1.9 $(Mm \cdot sr)^{-1}$. The composition of PM1 particles (i.e., with diameter up to 1 micron) was retrieved from the HALO in situ measurements at different altitudes during the shuttles. The observed PM1 composition near Burjassot is shown in Fig. 32. Although the ceilometer measurements refer to total aerosol and the in situ data only to PM1, both reveal two distinct aerosol layers: a) a PBL below 1000 m altitude with a backscatter coefficient between 2.0 and 2.7 $(Mm \cdot sr)^{-1}$ and enhanced concentrations of sulphate and ammonium, and b) a lofted aerosol layer between 1500 and 3500 m altitude with higher organic, nitrate and BC mass fraction. The difference in composition is likely related to different aerosol sources. While the boundary aerosol layer has a local origin, the lofted aerosol layer is influenced by the transport of regional emissions. This is consistent with the transport of the MPC Madrid outflow as indicated in Fig. 28.

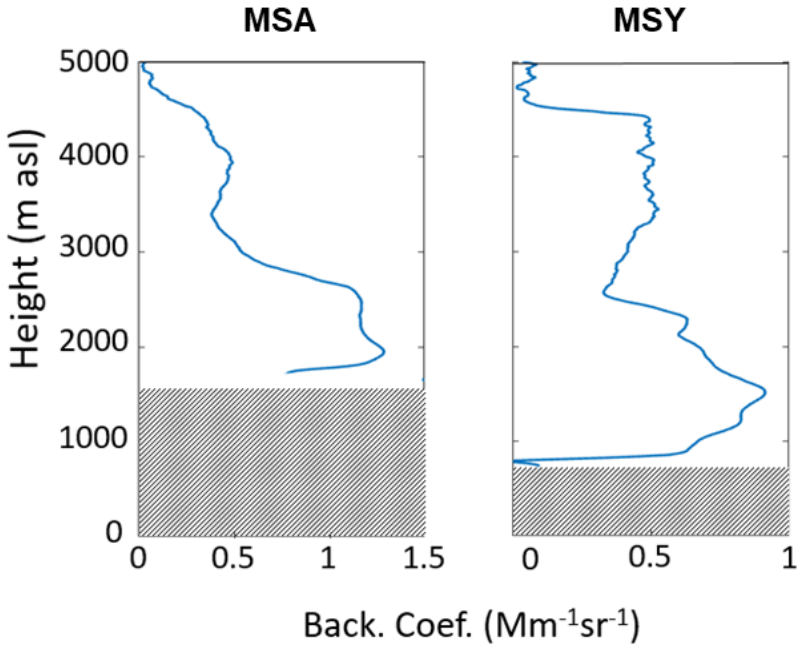

Figure 31: Profiles of the backscatter coefficient derived at 1064 nm in MSA and MSY for the 28 July 2017 from 12:50 to 13:20 UTC. The grey shadings indicate the height of the ceilometers.

Similarly, the lidar and in situ measurements close to Barcelona reveal a different aerosol composition of the PBL below 900 m and a lofted aerosol layer above 2000 m. In addition, a third aerosol layer evolved between 1000 and 1800 m altitude with a backscatter coefficient up to 1.5 $(Mm \cdot sr)^{-1}$. The mass fractions of ammonium, sulphate and organic aerosol are between the values of those of the PBL and of the lofted aerosol layer above.

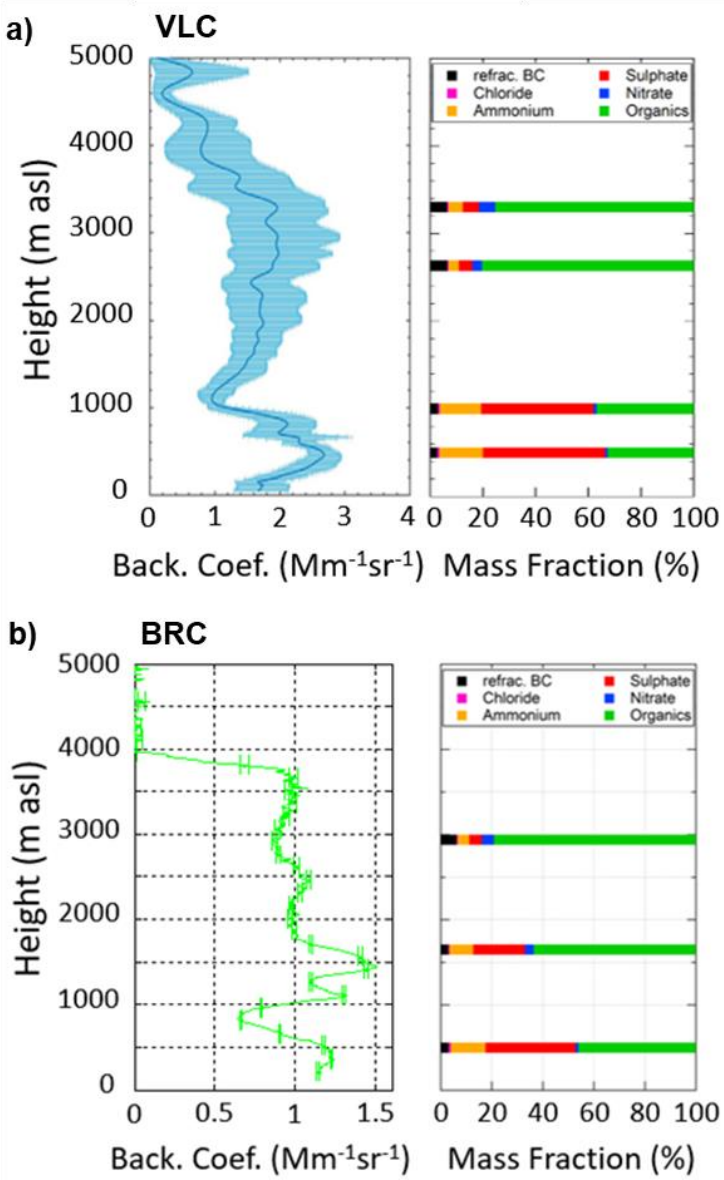

~~**Figure 32:** Distinct aerosol layers observed near Burjassot/Valencia and Barcelona. a) Profile of the backscatter coefficient derived at 910 nm for 13:30-14:30 UTC in VLC (left), and fractional composition of PM1 measured (SP2 and AMS) on-board HALO (right), b) the same derived in BRC at 532 nm for 14:45-15:45 UTC. The periods of comparison with the HALO data are 13:42-13:56 (9:30 min) at 3300 m; 13:34-13:40 (5:30 min) at 2630 m, 14:03-14:14(11:30 min) at 1000 m and 14:18-14:31 (23 min) at 500 m for VLC, and 15:43-16:00;(17:30 min) at 2940 m; 15:16-15:40 (24 min) at 1650 m, and 14:47-15:14 (27 min) at 500 m for BRC.~~

~~4.4 Specific case studies of mixing of MPC outflows with air masses of biogenic origin: forest fires and dust~~

~~Typically the composition of the measured pollution plumes indicated that emission came from sources other than of the targeted MPCs. These influence the photochemical oxidation and chemical reactions of the probed air masses. Supporting satellite and ground based measurements of forest fire and dust signals enable the identification of these sources.~~

BB emission from fires was e.g. probed during the E-EU-07 flight downwind of Marseille. The plume transport eastwards from near Marseille is well captured by SEVIRI with AOT values around 0.25 at 0.55 µm in the afternoon, as shown in Fig. 26. This plume was probed by HALO in situ measurements at around 11:30 and 16:30 UTC. As an example of the agreement between remote sensing satellite retrievals and HALO observations, BC mass concentrations are also depicted in the figure. The highest BC was measured at roughly 2000 m and exceeded 7 µg m^{-3}. In the PBL, measured BC mass concentrations were as high as 1 µg m^{-3}. The stratification of pollution plumes above the PBL is a typical feature for BB emissions (Holanda et al., 2020).

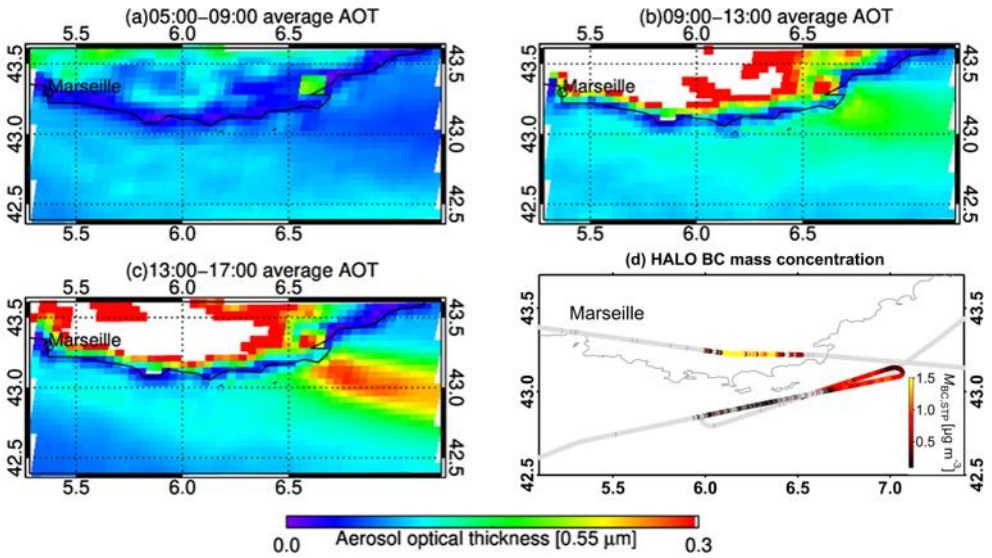

Figure 33: (a – e) Aerosol optical thickness at 0.55 µm as retrieved from SEVIRI from 05:00 to 17:00 UTC on 24 July 2017. (d) E-EU-07 flight track, colour-coded with BC mass concentration (M_{BC}). For a better contrast, the scale for M_{BC} ranges from 0.1 to 1.5 µg m^{-3}. Grey colour on the flight track indicates values below 0.1 µg m^{-3}. The mass concentration reached values up to 7 µg m^{-3} at the French coast.

Mixing ratios of CH_4 comparable to those in urban plumes were measured in this BB event during E-EU-07 (not shown). This distinct peak concentration strongly influences the local GHG distribution (Klausner, 2020), although the contribution of BB emissions to total global anthropogenic CH_4 is on the order of a few percent (Saunois et al., 2019).

Dust events were observed and contributed significantly to some of the plumes measured over Europe during the EMeRGe IOP. On 11 July 2017, there was a Saharan dust event affecting the air masses measured during E-EU-03, as indicated by both satellite- and ground-based observations. Figure 34 shows the MODIS satellite RGB image at 10:30 UTC and the corresponding elevated AOT at 0.55 µm as retrieved from SEVIRI from 09:00 to 13:00 UTC.

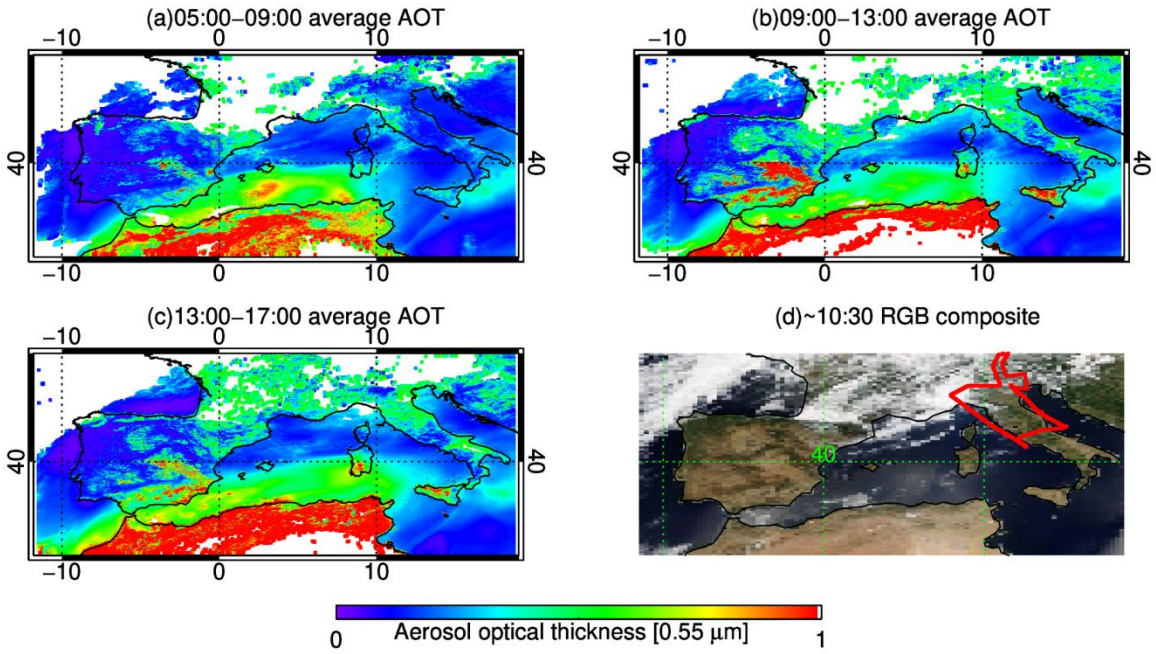

Figure 34: (a-c) Aerosol optical thickness at 0.55 µm as retrieved from SEVIRI from 05:00 to 17:00 UTC on 11 July 2017, (d) MODIS RGB composite figure showing corrected reflectance at 10:30 UTC (https://worldview.earthdata.nasa.gov/). The MODIS RGB composite is created combining red, green and blue bands into one picture. White areas are clouds. The E-EU-03 flight track (in red) is superimposed on (d).

The impact of dust on the aerosol size distributions observed on board HALO close to the western coast of Italy during E-EU-03 is illustrated in Fig. 35. The concentration of particles with a diameter below 250 nm was analysed by the Differential Mobility Analyzer (DMA) in 6 steps of 30 s duration, resulting in a period of 3 minutes for each integrated measurement. The evaluated DMA data points are then combined with the data from an Optical Particle Counter (OPC) for particles in the range from 250 nm to 3 µm. The first two sequences in Fig. 35 are taken at 2900 m and the third at 1300 m altitude. The third period and lowest in altitude had the smallest total number concentration with a clear enhancement of the particles above 600 nm. According to FLEXTRA, HALO flew approximately 800 m above the PBL at the time of sampling. The increase in the coarse mode particles above the PBL implies mineral dust rather than sea salt. According to backward trajectories, the air mass probed had recent contact at altitudes below 1000 m with the dust plumes over the Mediterranean near Sardinia shown by MODIS in Fig.34.

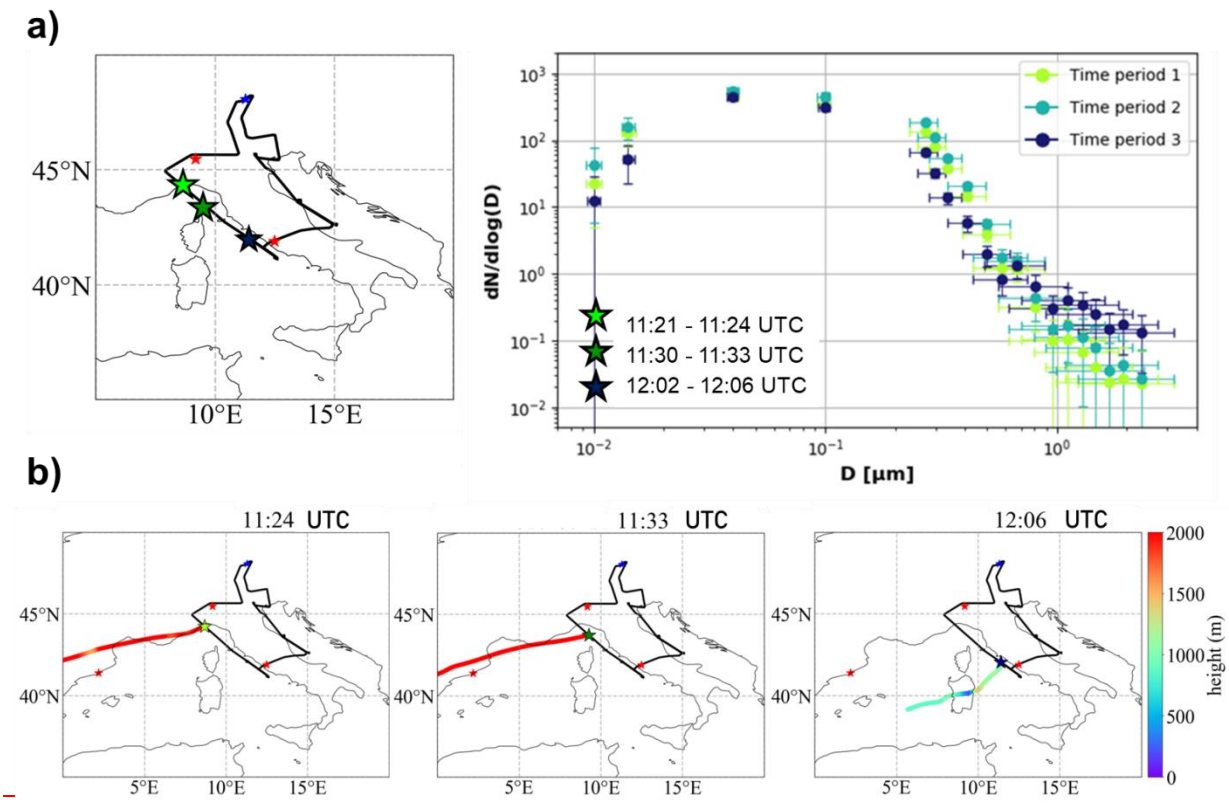

Figure 35: Example of the effect of dust plumes on the aerosol concentration during E-EU-03 on the 11 July 2017. a) Particle size distribution for 3 selected time periods (right) and position of the sample points in the flight track (left). The error bars on the y-axis are the standard deviations of the mean measured concentrations. The error bars in x-direction indicate the 16th and 84th percentile of the median diameters of the sensitivities of each size channel. b) 48h backward trajectories for the three periods selected. The red stars indicate the position of the MPCs of interest.

These observations agree with the measurement of the continuous automated lidar ceilometer (ALC) in Rome on 11 July 2017, which include the overpass by HALO in the Rome area (see Fig. 36). A lofted aerosol layer with increased depolarization was detected at an altitude between 1000 and 2000 m from the morning and mixed with local particles lifted by PBL dynamics in the middle of the day, at the time of the DMA measurement. This indicates that HALO flew above a dust layer during the first two periods of the DMA measurement. Thus, HALO probed rather low concentrations of large particles. Subsequently, HALO dived into the dust layer and this explains the increase of particles larger than 600 nm.

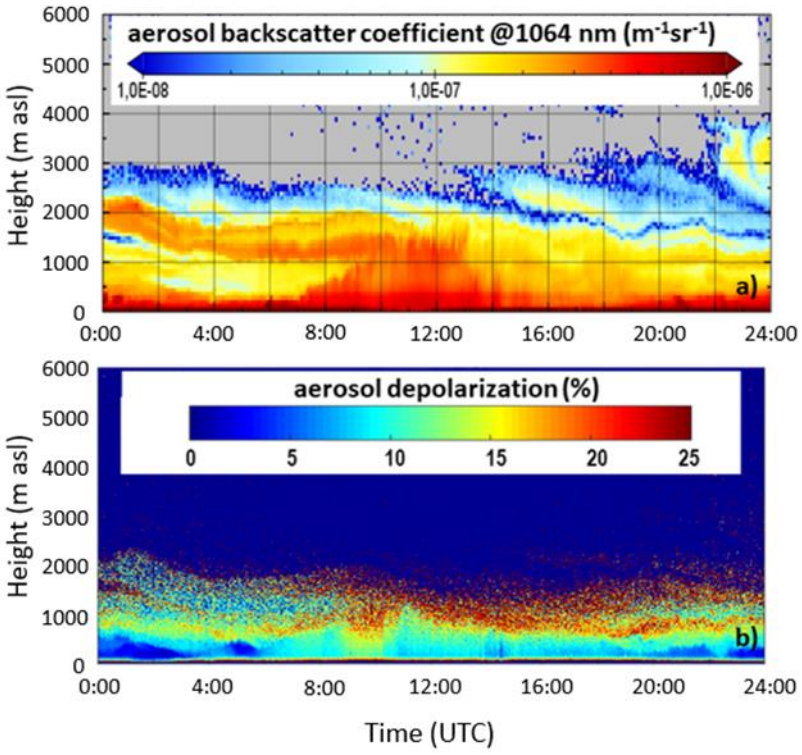

Figure 36: Aerosol profile measurements performed in Rome (Italy) on 11 July 2017 by the Automated Lidar Ceilometer network (ALICENET). Aerosol backscatter coefficient ($m^{-1} sr^{-1}$) at 1064 nm (top), and aerosol depolarization in % (bottom).

The comparison of fine and coarse mode particles observed on board the Sky Arrow with aerosol properties at the ground provides evidence for the important role of fine particle photo-nucleation in the MPC Rome, favoured by high radiation and temperatures (Campanelli et al., 2021; Barnaba et al., 2021 in preparation).

The extent and effect of mixing of air masses of different nature observed during the EMeRGe IOP is investigated in more detail elsewhere (Förster et al., 2021 in preparation; Holanda et al., in preparation 2021).

5 Processing of polluted air masses during transport

Chemical and physical processing of MPC emissions during transport has an important impact on the potential to form O_3 and other secondary photochemical oxidants in the outflows. In addition, photochemical processing changes the volatility and hygroscopicity of the aerosol particles and thereby their impact on cloud formation. In this sense, the EMeRGe airborne observations of primary and secondary pollutants and the ratios between species having different chemical lifetime were used as tracers of the degree of processing of the pollution plumes probed.

The NO/NO_y ratio provides information about the reactivity of the air mass but is not a reliable chemical clock due to the complex and rapid chemistry involved in the air masses investigated. Depending on the chemical and physical conditions, the lifetime of NO versus the formation of other reactive nitrogen compounds is of the order of a few hours or less. Internal transformation processes within the family of total reactive nitrogen NO_y do not alter their integrated concentration. However, washout and aerosol formation are loss processes controlling the lifetime of NO_y, which varies between hours and days.

A more robust chemical clock is the NO_y to CO ratio which is generally used to study ageing of an air mass with respect to ozone and nitrogen chemistry (e.g. Stohl et al., 2002). The CO lifetime varies between several weeks

and months (e.g. Emmons et al., 2010). Depending on the distance from the source as well as on the chemical and physical properties of the air mass, the NO_y/CO ratio declines to background values within a few days. As expected within the EMeRGe IOP in Europe, the NO_y/CO values were generally significantly higher for the processed polluted plumes than for the background air masses. For instance, during E-EU-08 discussed in Sect. 4.2, the NO_y to CO ratio was of the order of 0.01 to 0.02 in the air sampled outside the outflow of London and increased up to 0.1 in the London outflow plumes, as the air mass was processed and mixed.

The ratio between VOCs with comparable emission sources but significantly different chemical lifetimes is often used as a chemical clock to study emissions from point sources. This is the case for C_7H_8 and C_6H_6 emitted from gasoline-powered engines used in traffic and industry (Gelencsér et al., 1997; Shaw et al., 2015; Warneke et al., 2001). The atmospheric lifetime of these aromatic hydrocarbons, i.e., 1.9 and 9.4 days, respectively (Garzón et al., 2015), is assumed to be controlled only by the reaction with OH radicals (Atkinson, 2000). Provided that the emission rates are known, the C_7H_8/C_6H_6 ratio is expected to decrease with increasing distance to the pollution source and can be used to estimate the photochemical age of the sampled air (Winkler et al., 2002; Warneke et al., 2007). For EMeRGe, the ratio of C_7H_8/C_6H_6 is a good indicator for the presence of freshly or already processed anthropogenic emissions in the probed air. However, since the emission ratios of distinct VOC sources vary (Barletta et al., 2005), the active plume mixing before sampling as in EMeRGe, limits the use and feasibility of this chemical clock for the determination of the transport time of a specific outflow.

Information about the ageing of the air mass is additionally derived from differences in the chemical composition of aerosol particles. Aerosol mass spectrometer data using organic ions containing oxygen, e.g. CO_2^+ (m/z 44) and $C_2H_3O^+$ (m/z 43), are used to assess photochemical oxidation. Observations from laboratory and field studies indicate that during photochemical processing the ion signal of m/z 43 decreases while that of m/z 44 increases (Ng et al., 2010; Lambe et al., 2011). This metric is used to infer the degree of photochemical processing of organic aerosol in the atmosphere (e.g., Ng et al., 2011; Schroder et al., 2018; de Sa et al., 2018). In that regard, photochemical processing of aerosol particles was evident during the transport of MPC plumes during the EMeRGe IOP.

Since photo oxidation of fresh plumes is fast and mixing of aged plumes with the background occurs, the use of aerosol composition to asses photochemical processing requires complementary information from other measurements to act as a reliable indicator. Figure 37 shows an example of photochemical processing of the gas and the aerosol phases in ageing London plumes as measured by the C-ToF-AMS during E-EU-08. The data are plotted in *f*44-*f*43 space, where *f* denotes the ratio of the respective ion to the total organic ion signal. In these metric, atmospheric processing moves the data points towards the upper left corner of the triangle indicated by the dotted lines (Ng et al., 2010). The simultaneous measurements of CO are used to indicate dilution, while the atmospheric processing is inferred from other gas phase measurements (C_7H_8/C_6H_6 and NO_y/CO colour codes). Lower CO concentrations due to plume dilution along transport correspond to higher photochemical processing in the upper part of the triangle. As NO_y has a shorter lifetime than CO, the NO_y/CO ratio indicates that the processing is taking place in addition to dilution. Therefore, lower NO_y/CO and C_7H_8/C_6H_6 ratios in the upper part of the triangle indicate aged and processed air. In this case, the FLEXTRA backward trajectories revealed that the air masses identified as "background" were transported above the PBL and had no recent contact to the MPC London. The anthropogenically influenced air masses represent a mixture of recent emissions and photochemically processed London outflow as mentioned in 4.2.2 (see Fig. 24 and Fig. 25).

~~a)~~

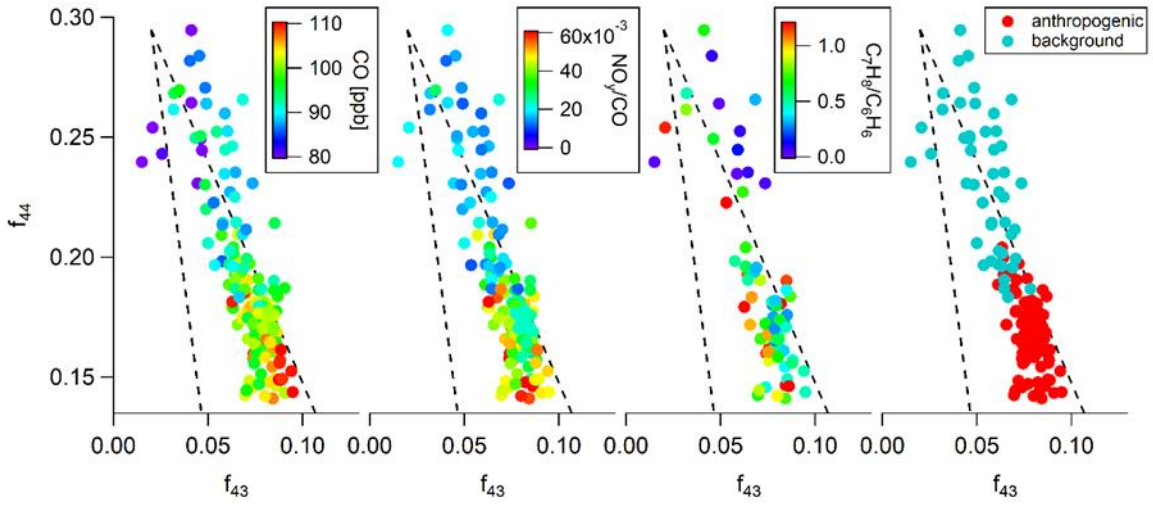

~~b)~~

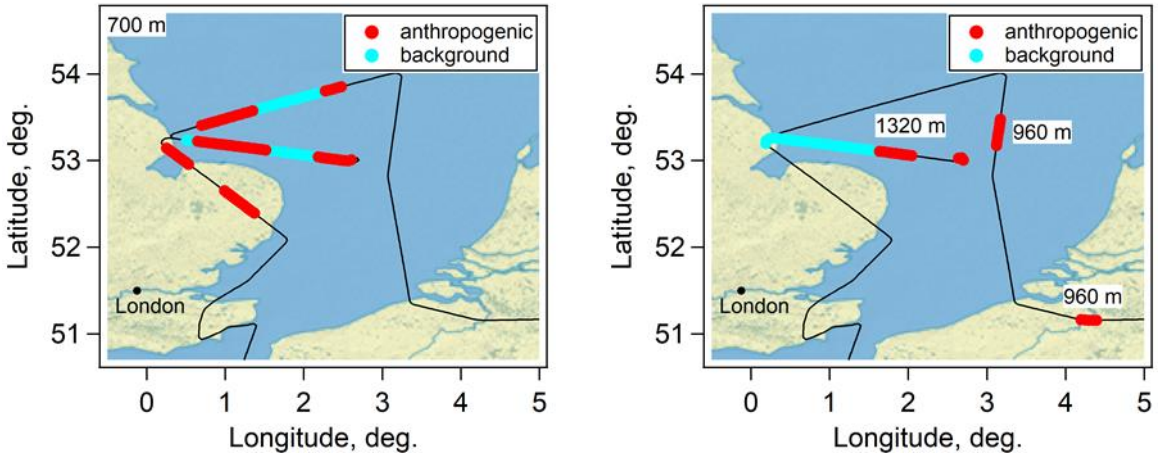

~~**Figure 37:** a) Scatter plots of C-ToF-AMS signal fractions at m/z 44 (f44) and m/z 43 (f43) of the London plume measured during the E-EU-08 on 26 July 2017 between 10:20 and 12:57 UTC. In this metric, the degree of photochemical processing increases to the upper left corner of the triangle which encompasses the range of typical atmospheric observations. The colour code indicates dilution (CO) and processing of the gas phase (NO_y to CO and C_7H_8 to C_6H_6 ratios). The right panel shows the assignment to unpolluted background air and air masses of anthropogenic polluted origin as introduced in Sect. 4.1. b) Spatial distribution of the background and anthropogenic polluted air masses identified in a). The flight altitudes are indicated in the graphs.~~

~~The results presented above confirm the complexity of the air masses as a result of the mixing of sources. Following the ageing of the outflow of a single MPC is challenging. However, the distinction between fresh and aged air is possible and gives a coherent picture for the applied methods and chemical clocks. At large distances from the source, the use of gas and aerosol trace species is insufficient for identifying MPC plumes. In this context, the relevance of PFC tracers and the support of adequate transport models becomes obvious.~~

~~The secondary formation of pollutants as a result of plume processing was further investigated with the support of HYSPLIT plume age simulations. An example is formic acid (HCOOH), the most abundant organic acid in the troposphere. Although HCOOH has primary sources, i.e., the emissions by fossil fuel combustion and biomass burning, the secondary formation from gas phase and aqueous photochemistry has been suggested to be~~

~~dominant in the troposphere (Paulot et al., 2011). During EMeRGe, HCOOH was measured by CI-ITMS by using CO_3^- as reactant ion (Viidanoja et al., 1998). Significantly enhanced volume mixing ratios up to 25 ppb were observed in the pollution plumes of MPCs in Europe, and HCOOH was found to be more abundant in the plumes than sulphur and nitrogen precursor species of inorganic acids (Eirenschmalz et al., in preparation 2021). Figure 38 shows HCOOH enhancements above ambient background relative to CO enhancements in different MPC plumes as a function of plume age. Here, ΔHCOOH and ΔCO are determined from the measurements, and the plume age from HYSPLIT simulations considering CO emissions from EDGAR and the dispersion of the plumes during transport. CO is used as an indicator of the strength of emissions from combustion in the individual MPC plumes and as tracer for the dilution of the plumes for the actual meteorological conditions during the measurements. The ΔHCOOH to ΔCO ratios significantly increase with plume age indicating secondary formation of formic acid to be its main source in the MPC plumes, mainly due to oxidation of C_5H_8 in the plume.~~

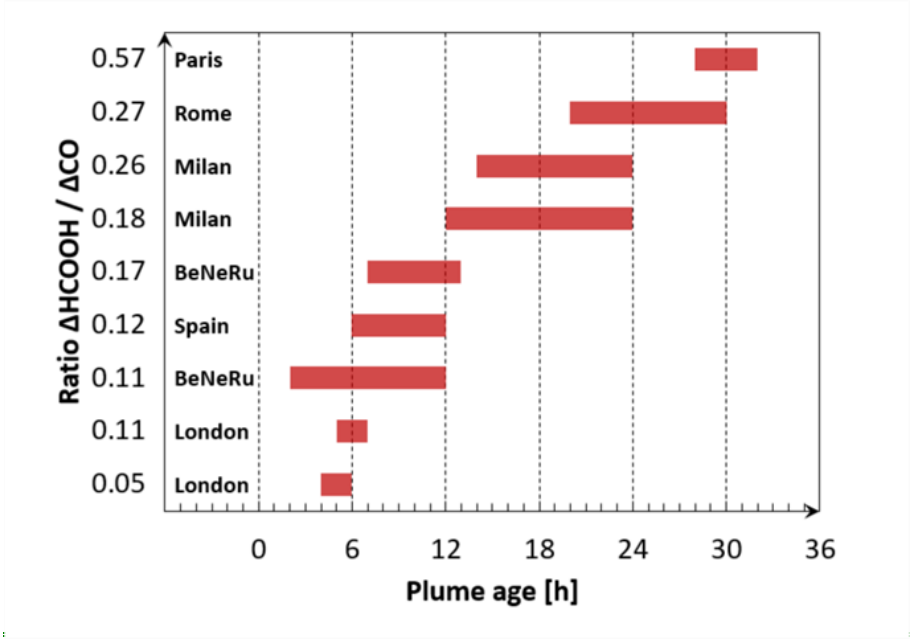

~~**Figure 38:** Observed enhancements of formic acid (ΔHCOOH) in MPC plumes relative to observed CO enhancements (ΔCO) as a function of plume age from HYSPLIT simulations. The corresponding city plume is indicated next to the ratios.~~

- First results of the global/regional chemistry-climate MECO(n) model (Kerkweg & Jöckel 2012, Mertens et al., 2016) indicated that the emissions of NO_x and/or their further processing in the model (deposition, washout, chemical transformation) reasonably agree with the HALO measurements. However, the simulation of complex plume structures would benefit from a higher model spatial resolution.

An example is given in Fig. 37 for the E-EU-05 flight on 17 July 2017, when the London plume was probed over the English Channel. The MECO(n) model (Kerkweg & Jöckel 2012, Mertens et al., 2016)~~**6 Simulating the processing of European MPC emissions with the MECO(n) model**~~

~~Atmospheric modelling is used to place the spatially and temporally limited number of observations during EMeRGe into a broader context, e.g. by analysing long-term trends or temporal and spatial variability in the MPC emissions in Europe.~~

~~The EMeRGe data set offers an opportunity to test whether the transport and transformation of MPC emissions are well captured by state of the art atmospheric models. In this context, simulations with the MECO(n) model (Kerkweg & Jöckel 2012, Mertens et al., 2016) were performed. The model~~ couples a global and a regional chemistry climate model. In the set-up applied here, Central Europe was resolved with up to 7 km horizontal resolution. The model data was sampled along the HALO flight paths with 60 s temporal resolution using the MESSy submodel S4D (Jöckel et al., 2010). These sampled model data are used for a one-by-one comparison with the measurements. The EDGAR 4.3.1 emission inventory for the year 2010 was used (see S15).~~.~~

~~The tagging method by Grewe et al., (2017) was applied as additional model diagnostics. This method decomposes the budget of ozone and ozone related precursors into the contributions of different emission sectors (Mertens et al., 2020a). Out of the 12 applied emission categories, land transport (mainly road traffic) in Europe, anthropogenic (other than traffic) in Europe, shipping, land transport outside Europe, anthropogenic (other than traffic) outside Europe, lightning and biogenic emissions are the most important ones (see Fig. 39b). A detailed description of the model and the source apportionment technique are provided in the supplement (see S12).~~

~~The model results show a positive bias in O_3 and a negative bias in CO with respect to the EMeRGe measurements over Europe. This confirms previous comparisons with other observational data (see Mertens et al.,~~2016, 2020b). Given the complexity of the air masses sampled during EMeRGe, the comparison with the model results was extended by undertaking different sensitivity studies to investigate the impact of specific set-up changes on the simulated mixing ratios.~~

~~An example is given for the E-EU-05 flight on 17 July 2017. The comparison between measured NO_y mixing ratios and MECO(n) results is shown in Fig. 39a, when the London plume was probed over the English Channel.~~

The enhancements of NO_y between 12 and 16 UTC below 900 hPa in Figure 37a are reasonably well simulated by the model except for the measurements at around 15:30 UTC which are strongly overestimated by the model. To address this issue, two plumes marked with '1' and '2' in Fig. 37a~~39a~~ were investigated in more detail.

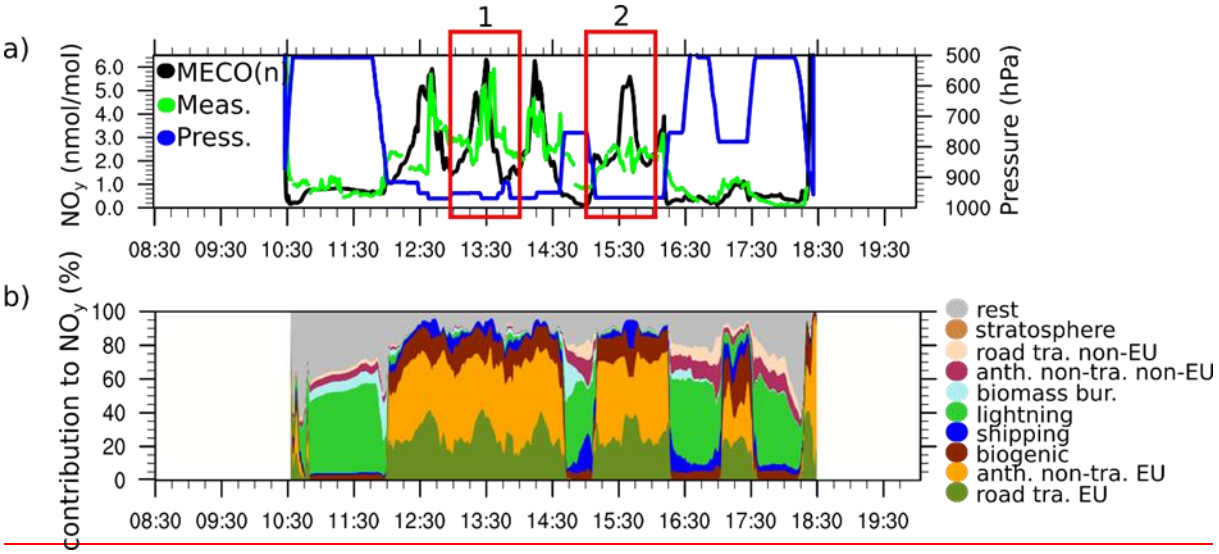

~~**Figure 39:** a) NO_y mixing ratios measured (green) and simulated by the MECO(n) model (black) for E-EU-05 on 17 July 2017. The blue line denotes the pressure altitude of the aircraft (right axis). b) Relative contributions of different emission sectors to the NO_y mixing ratios simulated by MECO(n). Note that the NOy measurements were averaged to 60 s to fit the MECO(n) temporal resolution.~~

The model results and the measurements on the plume marked '1' are shown at 980 hPa and 965 hPa in Fig. 38a~~40a~~. 980 hPa is the pressure of the model layer which is nearest to the HALO flight altitude at 13:30 UTC

while 965 hPa is pressure of one model layer above. The model results show large horizontal and vertical inhomogeneities in the NO_y mixing ratios indicating different mixtures instead of a single London plume. The NO_y enhancement coincides with the London plume (marked with the turquoise square in Fig. 38a~~40a~~).

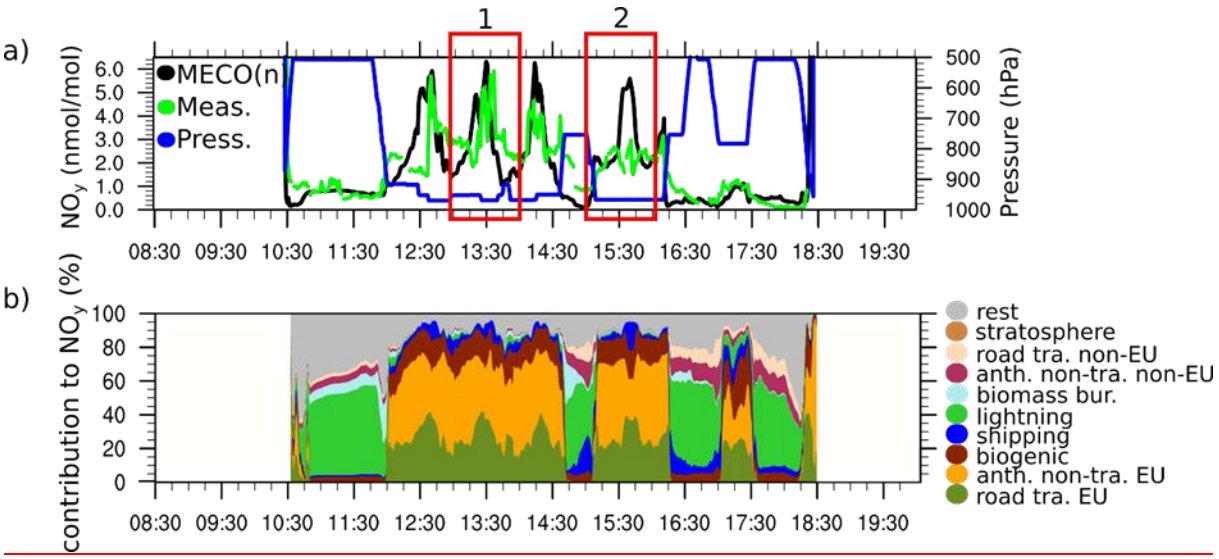

Figure 37: a) NO_y mixing ratios measured (green) and simulated by the MECO(n) model (black) for E-EU-05 on 17 July 2017. The blue line denotes the pressure altitude of the aircraft (right axis); b) Relative contributions of different emission sectors to the NO_y mixing ratios simulated by MECO(n). Note that the NOy measurements were averaged to 60 s to fit the MECO(n) temporal resolution.

Similarly, Figure 38b~~40b~~ shows the model results and measurements for the plume marked '2'. Here, the model shows a large plume remnant~~remanence~~ in the western part (turquoise square in Fig. 38b~~40b~~) leading to the overestimation of mixing ratios around 15:30 UTC. The simulated mixing ratios in a higher model layer are lower and agree better with the observations. These results indicate that a vertical displacement of the plume remnant~~remanence~~ causes the mismatch between measurements and model results around 15:30 UTC.

MECO(n) results showed a positive bias in O_3 and a negative bias in CO with respect to the EMeRGe measurements over Europe. This confirms previous comparisons with other observational data (see Mertens et al., 2016, 2020b) and is investigated for EMeRGe in separate sensitivity studies focusing on the representation of the NOx-VOC-O_3 chemistry and the evaluation of the applied emission data sets.

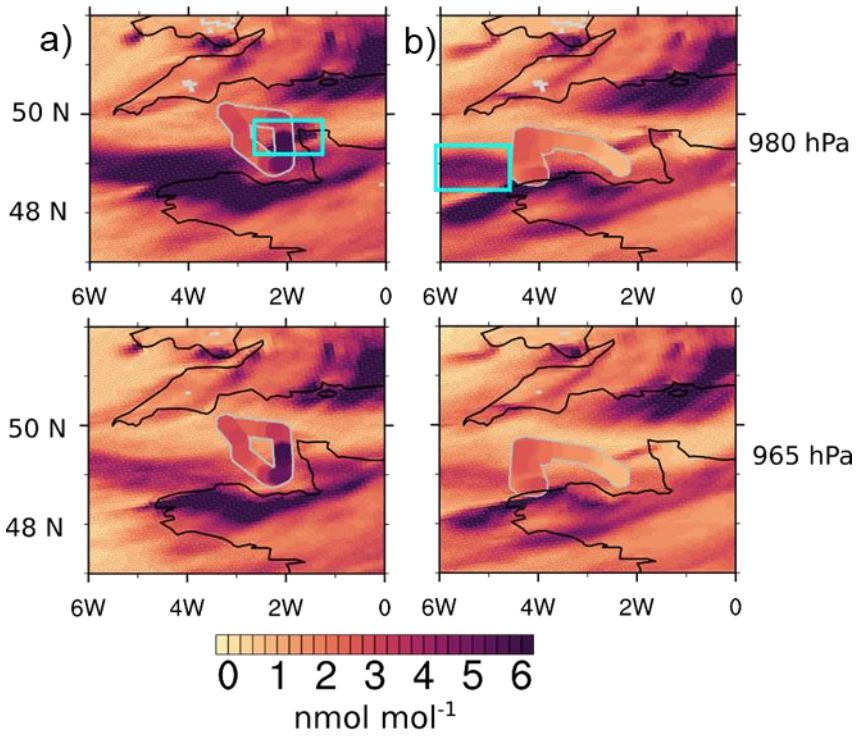

Figure 3840: NO_y mixing ratios as simulated by MECO(n) (background) and measured during E-EU-05. The model results at 980 hPa and 965 hPa are shown. Model results are averaged between a) 13 and 14 UTC, b) 15 and 16 UTC. The measured mixing ratios of NO_y during 13-14 UTC and 15-16 UTC are colour-coded and highlighted by grey contours. Black lines indicate coast lines. The turquoise rectangles highlight the regions discussed in the text.

~~The agreement between the measurements and model results shows that the emissions of NO_x and/or their further processing in the model (deposition, washout, chemical transformation) are reasonably well represented by MECO(n). However, the simulation of complex plume structures would benefit from a higher model spatial resolution.~~

The diagnostic capabilities of MECO(n), e.g. the tagging method by Grewe et al., (2017),~~,~~ were applied to individual EMeRGe flight tracks to investigate~~provide a better understanding of~~ the impact of emissions on the atmospheric chemistry in Europe. Figure 37b~~39b~~ shows the relative contribution of the different emission sectors to the measured NO_y mixing ratios during the E-EU-05 as a stacked graph. According to this, emissions from European road transport, anthropogenic non-traffic and biogenic sectors dominate the NO_y mixing ratios of the London plume with a similar relative contribution in all four plume crossings. For the NO_y measurements in the free troposphere (until 12 UTC approximately) a large relative contribution of lightning emissions is calculated in the model. In these regions, however, the absolute mixing ratios are rather low. As the NO_y lifetime is much longer in the upper troposphere than in the PBL, LRT of NO_y might be more likely than encounters of fresh lightning NO-plumes. A detailed description of the model and the source apportionment technique are provided in the supplement (S15).

~~The MECO(n) model was further evaluated within EMeRGe by similar analysis with different measured chemical species and emission inventories. The combination of the MECO(n) results with HYSPLIT backward trajectories provides good insights into the uncertainty of the model based estimates of the origin of the air masses probed.~~

7 Summary

The present article provides an overview on some of the scientific achievements obtained within the EMeRGe IOP in Europe.

The EMeRGe campaign in Europe focused on the identification and measurement of the plumes of pollution from selected MPCs, i.e. their emissions, transport and transformation. EMeRGe achieved its measurement objectives by exploiting the unique capabilities of the HALO research platform to probe these plumes over a relatively large geographical coverage and by the use of forecasting models and tools.

The results obtained from EMeRGe provide new insights into the transport and transformation of pollution plumes over Europe during the IOP in July 2017:

- EMeRGe provides a unique set of in situ and remote sensing airborne measurements of trace gases and aerosol particles along flight routes in the lower troposphere over Europe. The interpretation of the HALO measurement data is facilitated by the use of collocated ground based and satellite measurements. In that respect, EMeRGe enhances previous pollution studies in Europe by adding an extensive experimental data set in the PBL.
- The selected MPCs are confirmed as pollution hot spots by analysis using the aircraft measurements, backward and forward trajectories, dispersion models, CAMS tracer simulations and satellite observations.
- Distinct aerosol layering is observed over some of the investigated MPCs. Collocated ground based remote sensing instruments improved vertical and temporal resolution as compared to HALO. The synergetic use of these data improves the understanding of the evolution of the airborne observed scenarios and the attribution of the vertical distribution of pollutants probed during the shuttles flights.
- Plumes originating from European MPC outflows are typically observed below the top of the BL at 2000 m and occasionally after being transported over long distances. The location and position of the city plumes are typically well forecasted by the CAMS global, MECO(n) regional and by HYSPLIT dispersion simulations using urban city tracers.
- The composition of the pollution plumes measured along the flight tracks depend on the MPC emissions and the mixing with air from other emission sources. Enhancements in the concentration of selected species, such as CO, NO_y and VOCs such as C_6H_6 and CH_3CN measured on board HALO, enable the identification of anthropogenic and BB signatures in the plumes.
- Isotope measurements in VOC samples collected at MPC ground sites and on board HALO enable the determination of atmospheric residence times and the source apportionment. Different ranges of $\delta^{13}C$ values in VOCs are determined and attributed to MPC sources, e.g. for C_6H_6 in the Po Valley and Rome for the first time.
- Signatures of urban sources of long lived greenhouse gases like CH_4 and CO_2 are identified in the airborne measurements in plumes close to the MPC regions in Europe. The identification of plumes of GHG and the quantification of the MPC contributions to the regional GHG budget are challenging. This results from the long lifetime of these gases which yields a well mixed and large atmospheric background, and the distance from the MPC to the sampling.
- The aerosol inside the MPC plumes is typically dominated by smaller particles which are clearly visible in the total aerosol number concentration for the aerosol radius in the range 0.01 to 3 µm.

- ~~Tagging of polluted air masses in the centre of MPCs by ground based releases of PFC tracers provides a unique opportunity to identify successfully and unambiguously MPC outflows after transport times of between 5 and 26 hours.~~ The tracer experiments during EMeRGe additionally tested~~test~~ the ability of models (HYSPLIT, FLEXPART, FLEXPART-WRF, FALL3D) to simulate the transport and dispersion of the tracer for different meteorological conditions and topography around the release sites. While the simulated position of the PFC plumes agreed~~agrees~~ with the measurements, the tracer mixing ratios calculated by the dispersion models were~~are~~ by a factor 2 to 3 higher than detected. The degree of agreement between the tracer simulations and observations depended~~depends~~ on the parametrisation of dispersion and the representation of the topography in the models, as well as the goodness of tracer sampling in the plume, e.g. matching the maximum PFC concentrations was not always possible due to restrictions by air traffic control and flight endurance. Sensitivity studies with different meteorological datasets (ECMWF's ERA5 and IFS) and advanced turbulence parametrisation options in the PBL highlighted the pivotal role of meteorological input data on transport simulations (Schlager et al., 2021, in preparation).~~EMeRGe is one of the first airborne measurement campaigns to use this air mass tracer approach and has successfully demonstrated its value.~~
- ~~Regional transport of several European MPC outflows is successfully identified and measured: a) London over the English Channel to Central Europe, b) Po Valley either North over the Alps or in a south easterly direction towards the Adriatic, c) Rome over the Apennines into the Adriatic and d) Madrid and Barcelona into the Western Mediterranean.~~
- ~~BB emissions mix frequently with anthropogenic pollution during the transport over Europe. BB signatures are encountered in a large fraction of the pollution plumes probed during the EMeRGe IOP.~~
- ~~BB also contributes significantly to the concentration of pollutants above the PBL and represents an important particle source over Europe, in addition to urban, industrial emissions and mineral dust. BB observed during EMeRGe at altitudes above 5000 m is attributed to be in older masses, which had originated in North American fires, in agreement with models.~~
- ~~Mineral dust is identified in the aerosol size distribution and the optical properties of some of the air masses probed in Southern Europe above the PBL, in agreement with space and ground based observations.~~
- ~~The photochemical activity as indicated by the presence of free radicals varies widely in the plumes. The largest peroxy radical, RO_2^*, mixing ratios are observed below 3000 m in Southern Europe. This is expected and results from higher insolation and temperatures, which accelerate the photochemical processing. The O_3 production rates calculated from the RO_2^* measured on board are in the same order of magnitude as those reported in urban pollution for mixing ratios of NO < 1 ppbv.~~
- ~~HONO mixing ratios detected in the PBL and lower part of the free troposphere often exceed mixing ratios expected from known gas phase reactions as indicated by comparisons with model simulations. Potential mechanisms for the heterogeneous HONO formation are explored using theoretical studies in combination with the gas phase, aerosol composition and radiation observations~~
- ~~The photochemical processing of the MPC outflows during transport is inferred from the airborne measurements. Ratios of species such as NO/NO_y, NO/VOC and C_7H_8/C_6H_6 and observations of oxidation proxies such as peroxy radical concentrations and organic aerosol composition indicate with reasonable agreement that chemical processing of the MPC emissions identified during EMeRGe was substantial.~~

~~Measurements of $\delta^{13}C$ isotopes survey the chemical processing of MPC London plumes and of the MPC Rome outflow during the transit over the Apennines.~~

- ~~The analysis of the aerosol composition during EMeRGe indicates that aerosol photochemical processing is fast under European summer conditions. Chemical processing modifies both the chemical properties and the partitioning between gas and particle phase in the air masses over Europe. Simultaneous measurements of organic ions, CO and C_7H_8/C_6H_6 and NO_y/CO ratios on board enable dilution and processing in the plumes to be discriminated.~~
- ~~PFC tracers and adequate transport models are shown to be of indispensable value to quantify the processing of MPC plumes at large distances from the sources. Mixing of plumes from the release to the observation limits the application of VOC clocks, such as the ratio of C_7H_8 to C_6H_6, for the investigation of the transformation of MPC outflows on large scales.~~
- ~~The precise knowledge of the transport times between the source regions and the HALO sampling sites in the plumes obtained from the PFC experiments and dispersion models enables the analysis of chemical transformations during transport, e.g. oxidation of SO_2 and formation of HCOOH. The photochemical formation of HCOOH is shown to be the main source of HCOOH during the EMeRGe IOP in Europe. HCOOH is found to be more abundant in the plumes than the precursor species of inorganic acids, NO_2 and SO_2.~~

~~Secondary organic aerosol prevails in the polluted air masses probed in Europe above 2000 m. In the free troposphere above 4000 m the direct effect of anthropogenic emissions on the organic and inorganic aerosol components is observed to be small.~~

5 Outlook

EMeRGe contributes to the long history of providing observations facilitating a continuous and incremental progress in the capability to forecast and simulate atmospheric composition and chemistry. The interpretation of the extensive EMeRGe observational data set provides a clear step forward in understanding the complex spatial distribution of trace gases and aerosol particles resulting from mixing, transport and transformation of pollution plumes over Europe. The present work is an overview of the most salient results which are addressed in additional dedicated EMeRGe studies. The lessons learned from a continued analysis of the EMeRGe observations are also expected to be valuable to build upon and to improve airborne measurement strategies for future deployments focusing on pollution in Europe. First of all, the results of EMeRGe confirm the chemical complexity of the air masses over Europe as a result of the mixing of emissions from nearby MPC sources. EMeRGe airborne observations of primary and secondary pollutants and the ratios between species having different chemical lifetime were used as tracers of the degree of processing of the pollution plumes probed. The distinction between fresh and aged air was possible and gave a coherent picture for the applied methods and chemical clocks. However, high specific background measurements close to MPCs are needed and following the ageing of the outflow of a single MPC is challenging. At large distances from the source, the use of gas and aerosol trace species is insufficient for unequivocally identifying MPC plumes. In this context, the relevance of PFC tracers and the support of adequate transport models become obvious. EMeRGe is one of the first airborne measurement campaigns using air mass tracer approaches and has successfully demonstrated its value. For future studies, sampling the same air mass inside a tagged MPC plume at several different aging states, either by following the air mass or by crossing the plume at different distances from the source, would be beneficial to investigate the atmospheric processing of trace gases and organic aerosol as a function of time. For this (quasi-)

Lagrangian approach the combination with either a Zeppelin-based measurement platform or with a small, slow-flying aircraft might be suitable to cope with air traffic control restrictions, in particular for low level flights close to MPCs.

Satellite data have proven useful in assessing the overall pollution patterns and to put measurements during the campaign phase into a long-term perspective. For future campaigns, the new generation of geostationary air quality satellites started with the Korean GEMS instrument providing data at hourly resolution will enable detailed tracing of transport patterns and chemical evolution. For flight planning, satellite observations are best used in combination with models which provide forecasting capability. In the case of EMeRGe, the use of CAMS tracer and full chemistry forecasts facilitated the measurement of several pollution plumes. Subsequent comparisons to the measurements reflect the quality of the forecasts and support the improvement of future model runs. The total column AOT derived from geostationary satellites provided valuable information for the EMeRGe campaign. The integration of satellite total column AOT and model simulated aerosol extinction profile information enables further analysis of the component aerosol near the EMeRGe flight height. An important step to move further is the synergistically use of hyperspectral and multi-spectral satellite instruments for a better understanding of the aerosol component near the flight height and the component AOT (e.g. dust AOT, black carbon AOT).

An interesting aspect of EMeRGe is the high added value from measurements rarely used for the characterisation of urban pollution. In that sense, the measurement of stable carbon isotope ratios in VOC collected on the ground close to or at certain MPCs supported source apportionment and the estimation of integrated residence times of compounds in the air sampled on board HALO. EMeRGe has significantly expanded the very rare coverage of stable carbon isotope data from different locations and atmospheric regions. This and future data sets are valuable to verify model results and to assess the physical and chemical processing of VOCs during transport.

Similarly, the sparse in-situ data available for HCOOH has also been enhanced by EMeRGe. This major organic acid in the troposphere was found to be more abundant in MPC plumes than the sulphur and nitrogen precursor species of inorganic acids. The HCOOH production rates in the pollution plumes as a function of the plume ages during the EMeRGe IOP in Europe differ significantly to those encountered in Asia. Future studies are required to investigate sources and composition of organic compounds with respect to the effect on the formation and the properties of aerosols, clouds and acidity of precipitation in different seasons and for MPCs in different regions of the world. Furthermore, signatures of urban sources of long-lived GHG like CH_4 and CO_2, identified in the airborne measurements in plumes close to the MPC regions in Europe, provided valuable insights on sources and expanded the knowledge on existing top-down studies by confirming urban emission hotspots. An accurate knowledge of GHG sources and sinks in MPCs establishes the link between air quality and climate change. In that respect, the impact of climate change (e.g. increasing number of fires, temperature effect on chemical processing, changes in radiation), and emission reduction strategies or the use of alternative fuels, on the composition and transformation of the outflows along transport requires increasing interest. For a more comprehensive picture, conducting dedicated local flight experiments complemented with coordinated ground-based GHG measurements on several days and in all seasons for the same area is highly desirable. This would show seasonal evolution and emission sources (e.g. residential biomass burning in winter) increase statistics and reinforce the findings.

- Finally, the EMeRGe set of airborne data are particularly expected to support photochemical transport models in assessing:

~~First efforts to simulate observations of the EMeRGe flight tracks were made with the global/regional chemistry climate model MECO(n). Further investigation of small scale effects by complementary model activities with validated data includes the development of a box model to account for fast chemical transformation of pollution in air masses along the flight tracks. The EMeRGe set of airborne data supports photochemical transport models to assess:~~

- the relative contribution of biogenic, BB and anthropogenic sources to the VOC burden over Europe,
- the net ozone production in the investigated MPC outflows in relation to the transport time and mixing of the pollution plumes,
- the adequacy of radiative transfer model calculations and the prediction capabilities of photolysis frequencies,
- the contribution of VOC species such as glyoxal and/or methylglyoxal to secondary aerosol formation in aged pollution plumes,
- the adequacy of Angstrom coefficients, aerosol fine mode fraction products and the geostationary satellite derived AOT to identify aerosol sources and transport features of mixing events of anthropogenic particles and mineral dust, and
- the significance and representativeness of the transport and concentration patterns obtained during EMeRGe in summer 2017, which was a period with anomalous meteorological conditions in Central Europe.

Data availability

The EMeRGe data are available at the HALO data base (https://halo-db.pa.op.dlr.de/) and can be accessed upon registration. Further data can be made available upon request to the corresponding author.

~~The collected data during EMeRGe help to improve the current understanding of the complex spatial distribution of trace gases and aerosol particles resulting from mixing, transport and transformation of pollution plumes over Europe. The wide range of observations presented here is the basis for further work being addressed within dedicated studies. More detailed analyses of individual data sets are provided elsewhere. Prospective deployments of similar characteristics are desirable to consolidate and contextualise the EMeRGe results in Europe.~~

~~The analysis of the EMeRGe data obtained in the second IOP in Asia will be presented in separate publications.~~

Acknowledgements

The authors thank the following teams and individuals, without whom the EMeRGe in Europe IOP would not have been possible:

- HALO flight organisation, permissions and related
  the DLR-FX and the HALO EMeRGe team. Special thanks to Lisa Kaser, Frank Probst, Michael Großrubatscher, Stefan Grillenbeck, Marc Puskeiler, for flight coordination and planning, to Alexander Wolf, and Thomas Leder, the flight engineers and to the BAHAMAS team. The authors also thank- enviscope GmbH in particular of Nicole Brehm and Rolf Maser for the support during the integration and preparation phase of the IOP in Europe.

- Meteorological and chemical composition forecasting
  Michael Gauss and Álvaro Valdebenito (MetNo) for provision of EMEP forecasts for the campaign and CAMS/ECMWF, in particular Johannes Flemming and Luke Jones for providing the atmospheric compositionweather and tracertrace constituent forecasts throughfor the CAMS field campaign support (https://atmosphere.copernicus.eu/scientific-field-campaign-support).. The CAMS-regional modelling team are also acknowledged for providing regional model forecast data for Europe.

- Ground based remote sensing observations
- LIDAR Observations
  EARLINET for providing aerosol LIDAR measurements and DWD, ALICE-net and RMI for ceilometer measurements. The support from AERONET, Service National d'Observation PHOTONS/ AERONET-EARLINET part of the ACTRIS-France research infrastructure and GOA-CF, part of ACTRIS-Spain, for their continuous efforts in providing high-quality measurements and products, and in particular of all PIs and Co-PIs of the AERONET sites contributing to EMeRGe for maintaining their instruments and providing their data to the community is greatly appreciated.

- Luca Ferrero (GEMMA and POLARIS Research Centers, Department of Earth and Environmental Sciences, University of Milano-Bicocca) for the air samples collected at the ground in Milan (Italy) during the HALO flights..

- Tracer releases
  Jonathan E. Murray and Helen Graven and the Imperial College team for releasing the PFC tracer in London.

KK and JohS would like to thank Christiane Schulz and Philipp Schuhmann for support during the integration phase. BAH, OOK, CP, DW, UP and MLP would like to thank Thomas Klimach, Björn Nilius, Jorge Saturno, Oliver Lauer and MeinratMeinradt Andreae for support during the EMeRGe campaign in Europe and during the data analysis.

MDAH, MG, YL and JPB thank Wilke Thomssen for support during the preparation and integration phases of EMeRGe and Heiko Schellhorn for continuous technical support and retrieval of model data during the campaigns.

Funding information

The HALO deployment during EMeRGe was funded by a consortium comprising the German Research Foundation (DFG) Priority Program HALO-SPP 1294, the Institute of Atmospheric Physics of DLR, the Max Planck SocietyPlank Gesellschaft (MPG) and the Helmholtz Association Gemeinschaft.

FK, BS, and KP acknowledge the support given by the DFG through the projects PF 384-16, PF 384-17 and PG 385-19. RK and MK acknowledge DFG funding through the project KR3861 1-1. KB acknowledges additional funding from the Heidelberg Graduate School for Physics. JohS, KK, and SB acknowledge funding through the DFG, project No. 316589531. LE and HS acknowledge support by DFG through project MEPOLL (SCHL1857/4-1). ABKHAH would like to thank DAAD and DLR for a Research Fellowship. HS acknowledge financial support by the DLR TraK (Transport and Climate) project. MS acknowledges support from the EU (GA no. 654109, 778349, 871115 and 101008004) and the Spanish Government (ref. CGL2017-90884-REDT, PID2019-103886RB-I00, RTI2018-096548-B-I00 and MDM-2016-0600).

MG, YL, MDAH and JPB acknowledge financial support from the University of Bremen. FLEXPART simulations were performed on the HPC cluster Aether at the University of Bremen, financed by DFG within the scope of the Excellence Initiative. A.-M. Blechschmidt was partly funded through the CAMS-84 project.

JW acknowledges support from the German Federal Ministry for Economic Affairs and Energy – BMWi (project Digitally optimized Engineering for Services – DoEfS; contract no. 20X1701B)

TK thanks DLR VO-R for funding the young investigator research group "Greenhouse Gases".

MM, PJ, MK acknowledge resources of the Deutsches Klimarechenzentrum (DKRZ) granted by the WLA project ID bd0617 for the MECO(n) simulations and the financial support from the DLR projects TraK (Transport und Klima) and the Initiative and Networking Fund of the Helmholtz Association through the project "Advanced Earth System Modelling Capacity" (ESM).

BAH acknowledges the funding from Brazilian CNPq (process 200723/2015-4).

2358 |

References

AERONET: AERONET aerosol data base, available at: http://aeronet.gsfc.nasa.gov/, last access: 11 December 2020

Alfarra, M. R., Prevot, A. S. H., Szidat, S., Sandradewi, J., Weimer,S., Lanz, V. A., Schreiber, D., Mohr, M., and Baltensperger, U.:Identification of the mass spectral signature of organic aerosols from wood burning emissions, Environ. Sci. Technol., 41, 5770–5777, doi.org/10.1021/es062289b, 2007.

Alvarado, L. M. A., Richter, A., Vrekoussis, M., Hilboll, A., Kalisz Hedegaard, A. B., Schneising, O., and Burrows, J. P: Unexpected long-range transport of glyoxal and formaldehyde observed from the Copernicus Sentinel-5 Precursor satellite during the 2018 Canadian wildfires, Atmos. Chem. Phys., 20, 2057–2072, 2020.

Andreae, M. O., and Rosenfeld, D.: Aerosol–cloud–precipitation interactions. Part 1. The nature and sources of cloud-active aerosols, Earth-Science Reviews 89, 13-41, 2008.

Andreae, M. O. , Afchine, A. Albrecht, R., Holanda, B. A., Artaxo, P., Barbosa, H. M. J., Borrmann, S., Cecchini, M. A., Costa, A., Dollner, M., Fütterer, D., Järvinen, E., Jurkat, T., Klimach, T., Konemann, T., Knote, C., Krämer, M., Krisna, T., Machado, L. A. T., Mertes, S.; Minikin, A. , Pöhlker, C., Pöhlker, M. L., Pöschl, U. Rosenfeld, D., Sauer, D., Schlager, H., Schnaiter, M., Schneider, J., Schulz, C., Spanu, A., Sperling, V. B., Voigt, C., Walser, A., Wang, J., Weinzierl, B., Wendisch, M. , Ziereis, H.: Aerosol characteristics and particle production in the upper troposphere over the Amazon Basin. Atmos. Chem. Phys., 18, 921–961, doi: 10.5194/acp-18-921-2018, 2018.

Andreae, M. O.: Emission of trace gases and aerosols from biomass burning – an updated assessment, Atmos. Chem. Phys., 19, 8523–8546, doi.org/10.5194/acp-19-8523-2019, 2019.

Ashworth, K. et al, Megacity and local contributions to regional air pollution: an aircraft case study over London, Atmos. Chem. Phys., 20, 7193–7216, doi:10.5194/acp-20-7193-2020, 2020.

Atkinson, R.: Atmospheric chemistry of VOCs and NOx, Atmospheric Environment, 34, 2063-2101, 2000.

Barnaba, F. and Gobbi, G. P., Aerosol seasonal variability over the Mediterranean region and relative impact of maritime, continental and Saharan dust particles over the basin from MODIS data in the year 2001. Atmos. Chem. . Phys.. 4, doi:10.5194/acpd-4-4285-2004, 2004.

Barnaba, F., Angelini, F., Curci, G., and Gobbi, G.P.: An important fingerprint of wildfires on the European aerosol load, Atmos. Chem. Phys, 11, 10487-10501, doi: 105194/acp-11-10487-2011, 2011.

Beekmann, M., Prévôt, A. S. H., Drewnick, F., Sciare, J., Pandis, S. N., Denier van der Gon, H. A. C., Crippa, M., Freutel, F., Poulain, L., Ghersi, V., Rodriguez, E., Beirle, S., Zotter, P., von der Weiden-Reinmüller, S.-L., Bressi, M., Fountoukis, C., Petetin, H., Szidat, S., Schneider, J., Rosso, A., El Haddad, I., Megaritis, A., Zhang, Q. J., Michoud, V., Slowik, J. G., Moukhtar, S., Kolmonen, P., Stohl, A., Eckhardt, S., Borbon, A., Gros, V., Marchand, N., Jaffrezo, J. L., Schwarzenboeck, A., Colomb, A., Wiedensohler, A., Borrmann, S., Lawrence, M., Baklanov, A., and Baltensperger, U.: In situ, satellite measurement and model evidence on the dominant regional contribution to fine particulate matter levels in the Paris megacity, Atmos. Chem. Phys., 15, 9577–9591, https://doi.org/10.5194/acp-15-9577-2015, 2015.Beirle, S., Borger, C., Dörner, S., Li A., Hu, Z., Liu, F., Wang, Y., Wagner, T.: Pinpointing nitrogen oxide emissions from space, Sci. Adv. 2019, 5, eaax9800 13 November 2019.

Boeke, N. L., Marshall, J. D., Alvarez, S., Chance, K. V., Fried, A.,. Kurosu, T. P., Rappenglück, B., Richter, D., Walega, J., Weibring, P. and Millet, D.B.: Formaldehyde columns from the Ozone Monitoring Instrument: Urban versus background levels and evaluation using aircraft data and a global model, J. Geophys. Res., 116, D05303, doi:10.1029/2010JD014870, 2011.

Bohn, B., and Lohse, I.: Calibration and evaluation of CCD spectroradiometers for ground-based and airborne measurements of actinic flux densities, Atmos. Meas. Tech., 10, 3151-3174, doi:10.5194/amt-10-3151-2017, 2017.

Bond, T.C., Doherty, S.J., Fahey, D.W., Forster, P.M., Berntsen, T., DeAngelo, B.J., Flanner, M.G., Ghan, S., Kärcher, B., Koch, D., Kinne, S., Kondo, Y., Quinn, P.K., Sarofim, M.C., Schultz, M.G., Schulz, M., Venkataraman, C., Zhang, H., Zhang, S., Bellouin, N., Guttikunda, S.K., Hopke, P.K., Jacobson, M.Z., Kaiser, J.W., Klimont, Z., Lohmann, U., Schwarz, J.P., Shindell, D., Storelvmo, T., Warren, S.G., and Zender, C.S.: Bounding the role of black carbon in the climate system: A scientific assessment, Journal of Geophysical Research: Atmospheres, Vol. 118, 5380-5552, doi: 10.1002/jgrd.50171, 2013.

Brands, M., M. Kamphus, T. Böttger, J. Schneider, F. Drewnick, A. Roth, J. Curtius, C. Voigt, A. Borbon, M. Beekmann, A. Bourdon, T. Perrin, and S. Borrmann: Characterization of a Newly Developed Aircraft-Based Laser Ablation Aerosol Mass Spectrometer (ALABAMA) and First Field Deployment in Urban Pollution Plumes over Paris During MEGAPOLI 2009, Aerosol Sci. Technol., 45, 46-64, doi: 10.1080/02786826.2010.517813, 2011.

Bréon, F.M., Vermeulen, A., and Descloitres J.: An evaluation of satellite aerosol products against sun photometer measurements. Remote Sensing of Environment, doi:10.1016/j.rse.2011.06.017, 2011.

Bréon, F.M., Broquet, G., Puygrenier, V., Chevallier, F., Xueref-Remy, I., Ramonet, M., Dieudonné, E., Lopez, M., Schmidt, M., Perrussel, O., and Ciais, P.: An attempt at estimating Paris area CO_2 emissions from atmospheric concentration measurements, Atmos. Chem. Phys. 2015, 15 (4), 1707–1724. doi~~DOI~~: 10.5194/acp-15-1707-2015, 2015.

Brito, J., and Zahn, A.: An unheated permeation device for calibrating atmospheric VOC measurements, Atmos. Meas. Tech., 4(10), 2143–2152, doi: 10.5194/amt-4-2143-2011, 2011.

Burrows, J.P., Richter A., Dehn A., Deters B., Himmelmann S., Voigt S. and Orphal J.,: Atmospheric remote sensing reference data from GOME: Part 2 temperature dependent absorption cross-sections of O_3 in the 231-794 nm range, Journal of Quantitattive Spectroscopy and Radiative Transfer, Volume: 61 Issue: 4, 509-517, 1999.

Butler, T. M., and Lawrence, M. G.: The influence of megacities on global atmospheric chemistry: A modelling study, Environ. Chem., 6 (3), 219– 225. 2009.

Butler, T.M., Stock, Z.S., Russo, M.R., Denier van der Gon, H.A.C., and Lawrence, M.G.: Megacity ozone air quality under four alternative future scenarios. Atmos. Chem. Phys., 12, 4413–4428, doi: 10.5194/acp-12-4413-2012, 2012.

Campos Braga, R., Rosenfeld, D., Weigel, R., Jurkat, T., Meinrat O. Andreae, M.O., Wendisch, M., Pöschl, U., Voigt, C., Mahnke, C., Borrmann, S., Albrecht, R.I., Molleker, S., Vila, D.A., Machado, L.A.T., and Grulich, L.: Further evidence for CCN aerosol concentrations determining the height of warm rain and ice initiation in convective clouds over the Amazon basin, Atmos. Chem., Phys., 17, 14433-14456, https://doi.org/10.5194/acp-17-14433-2017, 2017.

Cassiani, M., Stohl, A., and Eckhardt S.: The dispersion characteristics of air pollution from world's megacities, Atmospheric Chemistry and Physics, 13, 9975-9996, 2013.

Chan Miller, C., Jacob, D. J., Marais, E. A., Yu, K., Travis, K. R., Kim, P. S., Fisher, J. A., Zhu, L., Wolfe, G. M., Hanisco, T. F., Keutsch, F. N., Kaiser, J., Min, K.-E., Brown, S. S., Washenfelder, R. A., González Abad, G., and Chance, K.: Glyoxal yield from isoprene oxidation and relation to formaldehyde: chemical mechanism, constraints from SENEX aircraft observations, and interpretation of OMI satellite data, Atmos. Chem. Phys., 17, 8725–8738, https://doi.org/10.5194/acp-17-8725-2017, 2017.

Chance, K., Palmer, P. I., Spurr, R. J. D., Martin, R. V., Kurosu, T. P., and Jacob, D.: Satellite observations of formaldehyde over North America from GOME, Geophys. Res. Lett., 27, 3461– 3464, 2000.

Chen H., Winderlich, J., Gerbig, C., Hoefer, A., Rella, C. W., Crosson, E. R., Van Pelt, A. D., Steinbach, J., Kolle, O., Beck, V., Daube, B. C., Gottlieb, E. W., Chow, V. Y., Santoni, G. W., and S. C. Wofsy, High-accuracy continuous airborne measurements of greenhouse gases (CO_2 and CH_4) using the cavity ring-down spectroscopy (CRDS) technique, Atmos. Mes. Tech., 3, 375-386, 2010.

Copernicus Climate Change Service (C3S): ERA5: Fifth generation of ECMWF atmospheric reanalyses of the global climate. Copernicus Climate Change Service Climate Data Store (CDS), 2017.

Crippa, M., DeCarlo, P. F., Slowik, J. G., Mohr, C., Heringa, M. F., Chirico, R., Poulain, L., Freutel, F., Sciare, J., Cozic, J., Di Marco, C. F., Elsasser, M., Nicolas, J. B., Marchand, N., Abidi, E., Wiedensohler, A., Drewnick, F., Schneider, J., Borrmann, S., Nemitz, E., Zimmermann, R., Jaffrezo, J.-L., Prévôt, A. S. H., and Baltensperger, U.: Wintertime aerosol chemical composition and source apportionment of the organic fraction in the metropolitan area of Paris, Atmos. Chem. Phys., 13, 961–981, https://doi.org/10.5194/acp-13-961-2013, 2013.

~~Curci, G., Ferrero, L., Tuccella, P., Barnaba, F., Angelini, F., Bolzacchini, E., et al., : How much is particulate matter near the ground influenced by upper-level processes within and above the boundary layer? A summertime case-study in Milan (Italy) evidences the distinctive role of nitrate. , Atmos. Chem. Phys., 15(5), 2629-2649, 2015~~

De Smedt, I., Stavrakou, T., Hendrick, F., Danckaert, T., Vlemmix, T., Pinardi, G., Theys, N., Lerot, C., Gielen, C., Vigouroux, C., Hermans, C., Fayt, C., Veefkind, P., Müller, J.-F., and Van Roozendael, M.: Diurnal, seasonal and long-term variations of global formaldehyde columns inferred from combined OMI and GOME-2 observations, Atmos. Chem. Phys., 15, 12519–12545, https://doi.org/10.5194/acp-15-12519-2015, 2015.

De Gouw, J. A., Warneke, C., Parrish, D. D., Holloway, J. S., Trainer, M., and Fehsenfeld, F. C.: Emission sources and ocean uptake of acetonitrile (CH_3CN) in the atmosphere, J. Geophys. Res., D11, 108, 4329, doi:10.1029/2002JD002897, 2003.

De Sá, S. S., Palm, B. B., Campuzano-Jost, P., Day, D. A., Hu, W., Isaacman-VanWertz, G., Yee, L. D., Brito, J., Carbone, S., Ribeiro, I. O., Cirino, G. G., Liu, Y., Thalman, R., Sedlacek, A., Funk, A., Schumacher, C., Shilling, J. E., Schneider, J., Artaxo, P., Goldstein, A. H., Souza, R. A. F., Wang, J., McKinney, K. A., Barbosa, H., Alexander, M. L., Jimenez, J. L., and Martin, S. T.: Urban influence on the concentration and composition of submicron particulate matter in central Amazonia, Atmos. Chem. Phys., 18, 12185–12206, doi.org/10.5194/acp-18-12185-2018, 2018.

Diémoz, H., Barnaba, F. Magri, T., Pession, G., Dionisi, D., Pittavino, S., Tombolato, I., Campanelli, M., Della Ceca, L. S., Hervo M., Di Liberto, L., Ferrero, L., Gobbi, G. P.: Transport of Po Valley aerosol pollution to the northwestern Alps – Part 1: Phenomenology. Atmospheric Chemistry and Physics. 19. 3065-3095. 10.5194/acp-19-3065-2019, 2019a.

Diémoz, H, Gobbi, G.P, Magri, T., Pession, G., Pittavino, S. Tombolato, I.K.F., Campanelli, M., and Barnaba, F.: Transport of Po Valley aerosol pollution to the northwestern Alps –Part 2: Long-term impact on air quality, Atmos. Chem. Phys., 19, 10129–10160, 2019b.

Dodman, D.: Blaming cities for climate change? An analysis of urban greenhouse gas emissions inventories. Environ.Urban. 21 (No. 1, April), 185–202, 2009.

Dufour, G., Wittrock, F., Camredon, M., Beekmann, M., Richter, A., Aumont, B., and Burrows, J. P.: SCIAMACHY formaldehyde observations: constraint for isoprene emission estimates over Europe?, Atmos. Chem. Phys., 9, 1647–1664, https://doi.org/10.5194/acp-9-1647-2009, 2009.

European Environmental Agency: Air quality in Europe - 2019 report, No 10/2019; ISBN 978-92-9480-088-6, doi:10.2800/822355, 2019.

European Strategy and Policy Analysis System, ESPAS, Global Trends to 2030: The future of urbanization and Megacities, ESPAS Ideas Paper series, 2018

Finardi et al., Analysis of pollutants exchange between the Po Valley and the surrounding European region, Urban Climate 2014

Fischer, E. V., Jacob, D. J., Yantosca, R. M., Sulprizio, M. P., Millet, D. B., Mao, J., Paulot, F., Singh, H. B., Roiger, A., Ries, L., Talbot, R. W., Dzepina, K., and Pandey Deolal, S.: Atmospheric peroxyacetyl nitrate (PAN): a global budget and source attribution, Atmos. Chem. Phys., 14, 2679–2698, https://doi.org/10.5194/acp-14-2679-2014, 2014.

Fisher, R., Lowry, D., Wilkin, O., Sriskantharajah, S., and Nisbet, E.G.: High-precision, automated stable isotope analysis of atmospheric methane and carbon dioxide using continuous-flow isotope-ratio mass spectrometry, Rapid communications in mass spectrometry: RCM**,** *20* (2), 200–208. doi: 10.1002/rcm.2300, 2006.

Flemming, J., Huijnen, V., Arteta, J., Bechtold, P., Beljaars, A., Blechschmidt, A.-M., Diamantakis, M., Engelen, R. J., Gaudel, A., Inness, A., Jones, L., Josse, B., Katragkou, E., Marecal, V., Peuch, V.-H., Richter, A., Schultz, M. G., Stein, O., and Tsikerdekis, A.: Tropospheric chemistry in the Integrated Forecasting System of ECMWF, Geosci. Model Dev., **8**, 975-1003, doi:10.5194/gmd-8-975-2015, 2015.

Flemming, F., Jones, L., and Blechschmidt, A.-M.: CAMS supports scientific aircraft campaigns, ECMWF Newsletter No. 160, Summer 2019, available online at https://www.ecmwf.int/en/publications/newsletters. 2019

Forzieri, G., Cescatti, A., Batista e Silva, F., Feyen, L.: Increasing risk over time of weather-related hazards to the European population: a data-driven prognostic study, The Lancet Planetary Health, Vol 1, Issue 5, p e-200-e208, 2017.

Freney, E. J., Sellegri, K., Canonaco, F., Colomb, A., Borbon, A., Michoud, V., Doussin, J.-F., Crumeyrolle, S., Amarouche, N., Pichon, J.-M., Bourianne, T., Gomes, L., Prevot, A. S. H., Beekmann, M., and Schwarzenböeck, A.: Characterizing the impact of urban emissions on regional aerosol particles: airborne measurements during the MEGAPOLI experiment, Atmos. Chem. Phys., 14, 1397–1412, https://doi.org/10.5194/acp-14-1397-2014, 2014.

Freutel, F., Schneider, J., Drewnick, F., von der Weiden-Reinmüller, S.-L., Crippa, M., Prévôt, A. S. H., Baltensperger, U., Poulain, L., Wiedensohler, A., Sciare, J., Sarda-Estève, R., Burkhart, J. F., Eckhardt, S., Stohl, A., Gros, V., Colomb, A., Michoud, V., Doussin, J. F., Borbon, A., Haeffelin, M., Morille, Y., Beekmann, M., and Borrmann, S.: Aerosol particle measurements at three stationary sites in the megacity of Paris during summer 2009: meteorology and air mass origin dominate aerosol particle composition and size distribution, Atmos. Chem. Phys., 13, 933–959, https://doi.org/10.5194/acp-13-933-2013, 2013.

Fu, T.-M., Jacob, D. J., Wittrock, F., Burrows, J. P., Vrekoussis, M., and Henze, D. K.: Global budgets of atmospheric glyoxal and methylglyoxal, and implications for formation of secondary organic aerosols, J. Geophys. Res.-Atmos., 113, D15303, https://doi.org/10.1029/2007JD009505, 2008.

Fu, Y., Tai, A. P. K. and Liao, H.: Impacts of historical climate and land cover changes on fine particulate matter (PM2.5) air quality in East Asia between 1980 and 2010, Atmospheric Chemistry and Physics, 16(16), pp. 10369–10383. doi: 10.5194/acp-16-10369-2016, 2016.

Gardi, C.: Urban Expansion, Land Cover and Soil Ecosystem Services, Ed. Taylor & Francis, ISBN 1317504712, 9781317504719, 2017.

Garzon, J.P, Huertas, J. I., Magana, M. Huertas, M.E., Cardenas, B., Watanabe, T., Maeda, T., Wakamatsu, S., Blanco, S.: Volatile organic compounds in the atmosphere of Mexico City, Atmospheric Environment, 119, 425-429, 2015.

Gelencsér, A; Siszler, K; and Hlavay, J: Environmental Science & Technology 31 (10), 2869-2872, doi: 10.1021/es970004c, 1997.

General, S., Pöhler, D., Sihler, H., Bobrowski, N., Frieß, U., Zielcke, J., Horbanski, M., Shepson, P. B., Stirm, B. H., Simpson, W. R., Weber, K., Fischer, C., and Platt, U.: The Heidelberg Airborne Imaging DOAS Instrument (HAIDI) – a novel Imaging DOAS device for 2-D and 3-D imaging of trace gases and aerosols, Atmos. Meas. Tech., 7, 3459-3485, 2014, doi:10.5194/amt-7-3459-2014.

George, M., Andrés Hernández, M. D., Nenakhov, V., Liu, Y., and Burrows, J. P.: Airborne measurement of peroxy radicals using chemical amplification coupled with cavity ring-down spectroscopy: the PeRCEAS instrument, Atmos. Meas. Tech., 13, 2577–2600, https://amt.copernicus.org/articles/13/2577/2020/, 2020.

Gerbig, C., Kley, D., Volz-Thomas, A., Kent, J., Dewey, K., and McKenna, D. S.: Fast response resonance fluorescence CO measurements aboard the C-130: Instrument characterization and measurements made during North Atlantic Regional Experiment 1993, J. Geophys. Res., 101, 29229-29238, 1996.

Gioli, B., Miglietta, F., Vaccari, F. P., Zaldei, A. and De Martino, B.: The Sky Arrow ERA, an innovative airborne platform to monitor mass, momentum and energy exchange of ecosystems. Annals of Geophysics. 49. 10.4401/ag-3159, 2009.

Gioli, B., Carfora, M.F., Magliulo, V., Metallo, M.C., Poli, A.A., Toscano, P., and Miglietta, F.: Aircraft mass budgeting to measure CO_2 emissions of Rome, Italy, Environmental monitoring and assessment, 186 (4), 2053–2066. DOI: 10.1007/s10661-013-3517-4, 2014.

Gkikas, A; Hatzianastassiou, N., Mihalopoulos, N., Katsoulis, V., Kazadzis, S., Pey, J., Querol, X., and Torres, O.: The regime of intense desert dust episodes in the Mediterranean based on contemporary satellite observations and ground measurements, Atmos. Chem. Phys., 13, 12135–12154, doi:10.5194/acp-13-12135-2013, 2013.

Giles, D.M., Sinyuk, A., Sorokin, M.G., Schafer, J.S., Smirnov, A., Slutsker, I., Eck, T.F., Holben, B.N., Lewis, J.R., Campbell, J.R., Welton, E.,J., Korkin, S. V., and Lyapustin, A. I. : Advancements in the Aerosol Robotic Network (AERONET) Version 3 database – automated near-real-time quality control algorithm with improved cloud screening for Sun photometer aerosol optical depth (AOD) measurements, Atmos. Meas. Tech., 12, 169–209, doi.org/10.5194/amt-12-169-2019, 2019.

Goldstein, A. and Shaw, S.: Isotopes of volatile organic compounds: an emerging approach for studying atmospheric budgets and chemistry, Chem. Rev., 103, 5025–5048, doi:10.1021/cr0206566, 2003.

Grewe, V., Tsati, E., Mertens, M., Frömming, C., & Jöckel, P.: Contribution of emissions to concentrations: the TAGGING 1.0 submodel based on the Modular Earth Submodel System (MESSy 2.52), Geoscientific Model Development, 10, 2615–2633, doi: 10.5194/gmd-10-2615-2017, URL https://www.geosci-model-dev.net/10/2615/2017/, 2017.

Grimm, N.B., Faeth, S.H., Golubiewski, N.E., Redman, C.L., Wu, J., Bai, X., Briggs, J.M.: Global change and the ecology of cities. Science 319, 756–760. doi.:10.1126/science.1150195, 2008.

Guerreiro, S. B., Dawson, R. J., Kilsby, C., Lewis, E., and Ford, A.: Future heat-waves, droughts and floods in 571 European cities, Environ. Res. Lett. 13 034009, doi.org/10.1088/1748-9326/aaaad3, 2018.

Haywood, J. and Boucher, O.: Estimates of the direct and indirect radiative forcing due to tropospheric aerosols: A review, Reviews of Geophysics, doi:~~2000,~~ 38.10.1029/1999RG000078, 2000.

Heckel A., Richter, A. Tarsu T., Wittrock, F., Hak C., Pundt I., Junkermann W. and Burrows J.P, :MAX-DOAS measurements of formaldehyde in Po-Valley, Atmospheric Chemistry and Physics, 5, 909-918, 2005.

Helfter, C., Tremper, A.H., Halios, C.H., Kotthaus, S., Bjorkegren, A., Grimmond, C.S.B., Barlow, J.F., and Nemitz, E.: Spatial and temporal variability of urban fluxes of methane, carbon monoxide and carbon dioxide above London, UK, Atmos. Chem. Phys., 16 (16), 10543–10557. DOI: 10.5194/acp-16-10543-2016, 2016.

Hennigan, C. J., Sullivan, A. P., Collett, J. L., and Robinson,A. L.: Levoglucosan stability in biomass burning particles ex-posed to hydroxyl radicals, Geophys. Res. Lett., 37, L09806, doi:10.1029/2010GL043088, 2010.

Hennigan, C. J., Miracolo, M. A., Engelhart, G. J., May, A. A., Presto, A. A., Lee, T., Sullivan, A. P., McMeeking, G. R., Coe, H., Wold, C. E., Hao, W.-M., Gilman, J. B., Kuster, W. C., de Gouw, J., Schichtel, B. A., Collett Jr., J. L., Kreidenweis, S. M., and Robinson, A. L.: Chemical and physical transformations of organic aerosol from the photo-oxidation of open biomass burning emissions in an environmental chamber, Atmos. Chem. Phys., 11, 7669–7686, doi.org/10.5194/acp-11-7669-2011, 2011.

Hilboll, A., Richter, A., and Burrows, J. P.: Long-term changes of tropospheric NO_2 over megacities derived from multiple satellite instruments, Atmos. Chem. Phys., 13, 4145-4169, doi:10.5194/acp-13-4145-2014, 2014

Holanda, B.A., Pöhlker, M.L., Walter, D., Saturno, J., Sörgel, M., Ditas, J., Ditas, F. Schulz, C., et al,: Influx of African biomass burning aerosol during the Amazonian dry season through layered transatlantic transport of black carbon-rich smoke, Atmos. Chem. Phys., 20, 4757–4785, doi.:org/10.5194/acp-20-4757-2020, 2020.

Holanda et al., in preparation 2021: Characteristic correlations between CCN and BC of most relevant aerosol species.

Holben, B.N., Eck, T.F., Slutsker, I., Tanré, D., Buis, J.P., Setzer, A., Vermote, E., Reagan, J.A., Kaufman, Y.J., Nakajima, T., Lavenu, F., Jankowiak, I., and Smirnov, A.: Aeronet—A Federated Instrument Network and Data Archive for Aerosol Characterization. Remote Sensing of Environment, 66, 1-16. doi.org/10.1016/S0034-4257(98)00031-5, 1998.

Hollingsworth, A. R., Engelen, R. J., Textor, C., Benedetti, A., Boucher, O., Chevallier, F., Dethof, A., Elbern, H., Eskes, H., Flemming,Granier, C., Kaiser, J. W., Morcrette, J.-J., Rayner, P., Peuch, V.-H., Rouil, L., Schultz, M. G., Simmons, A. J., and Consortium, T. G.: Toward a monitoring and forecasting system for atmospheric composition: The GEMS project, B. Am. Meteorol. Soc., 89, 1147–1164, 2008.

Hoole, C., Hincks, S. and Rae, A.: The contours of a new urban world? Megacity population growth and density since 1975. Town Planning Review, 90 (6). ISSN 0041-0020,. https://doi.org/10.3828/tpr.2019.41, 2019., ~~2019. https://doi.org/10.3828/tpr.2019.41~~

Hüneke, T., Aderhold, O.-A., Bounin, J., Dorf, M., Gentry, E., Grossmann, K., Grooß, J.-U., Hoor, P., Jöckel, P., Kenntner, M., Knapp, M., Knecht, M., Lörks, D., Ludmann, S., Matthes, S., Raecke, R., Reichert, M., Weimar, J., Werner, B., Zahn, A., Ziereis, H., and Pfeilsticker, K.: The novel HALO mini-DOAS instrument: inferring trace gas concentrations from airborne UV/visible limb spectroscopy under all skies using the scaling method, Atmos. Meas. Tech., 10, 4209–4234, https://doi.org/10.5194/amt-10-4209-2017, 2017.

Huijnen, V., Williams, J., van Weele, M., van Noije, T., Krol, M., Dentener, F., Segers, A., Houweling, S., Peters, W., de Laat, J., Boersma, F., Bergamaschi, P., van Velthoven, P., Le Sager, P., Eskes, H., Alkemade, F., Scheele, R., Nédélec, P., and Pätz, H.-W.: The global chemistry transport model TM5: description and evaluation of the tropospheric chemistry version 3.0, Geosci. Model Dev., 3, 445–473, https://doi.org/10.5194/gmd-3-445-2010, 2010.

Huntrieser, H., and H. Schlager: Air Pollution Export from and Import to Europe: Experimental Evidence, In: The Handbook of Environmental Chemistry, Vol. 4 Air Pollution: Intercontinental Transport of Air Pollution (Ed. A. Stohl), Springer Verlag, pp. 69-98. 2004.

Huntrieser, H., Heland,J., Schlager,H., Forster, C., Stohl, A., Aufmhoff, H., Arnold, F. Scheel, H.E., Campana, M., Gilge, S.,Eixmann, R., and Cooper O. : Intercontinental air pollution transport from North America to Europe: Experimental evidence from airborne measurements and surface observations, J. Geophys. Res., 110, D01305, doi:10.1029/2004JD005045, 2005.

Im, U., Markakis, K., Koçak, M., Gerasopoulos, E., Daskalakis, N., Mihalopoulos, N., Poupkou, A., Kındap, T., Unal, A., and Kanakidou, M.: Summertime aerosol chemical composition in the Eastern Mediterranean and its sensitivity to temperature, Atmos. Environ., 50, 164-173, https://doi.org/10.1016/j.atmosenv.2011.12.044, 2012.

Inness, A., Blechschmidt, A.-M., Bouarar, I., Chabrillat, S., Crepulja, M., Engelen, R. J., Eskes, H., Flemming, J., Gaudel, A., Hendrick, F., Huijnen, V., Jones, L., Kapsomenakis, J., Katragkou, E., Keppens, A., Langerock, B., de Mazière, M., Melas, D., Parrington, M., Peuch, V. H., Razinger, M., Richter, A., Schultz, M. G., Suttie, M., Thouret, V., Vrekoussis, M., Wagner, A., and Zerefos, C.: Data assimilation of satellite-retrieved ozone, carbon monoxide and nitrogen dioxide with ECMWF's Composition-IFS, Atmos. Chem. Phys., **15**, 5275-5303, doi:10.5194/acp-15-5275-2015, 2015.

IPCC, 2014: Climate Change 2014: Synthesis Report. Contribution of Working Groups I, II and III to the Fifth Assessment Report of the Intergovernmental Panel on Climate Change (Core Writing Team, R.K. Pachauri and L.A. Meyer (eds.)). IPCC, Geneva, Switzerland, 151 pp. 2014.

Jacob, D.J., and Winner, D.A.: Effect of climate change on air quality, Atmospheric Environment, 43, 51-63, doi:10.1016/j.atmosenv.2008.09.051, 2009.

Jöckel, P., Kerkweg, A., Pozzer, A., Sander, R., Tost, H., Riede, H., Baumgaertner, A., Gromov, S., & Kern, B.: Development cycle 2 of the Modular Earth Submodel System (MESSy2), Geoscientific Model Development, 3, 717–752, doi: 10.5194/gmd-3-717-2010, URL http://www.geosci-model-dev.net/3/717/2010/, 2010

Jonson, J. E., Schulz, M., Emmons, L., Flemming, J., Henze, D., Sudo, K., Tronstad Lund, M., Lin, M., Benedictow, A., Koffi, B., Dentener, F., Keating, T., Kivi, R., and Davila, Y., The effect of intercontinental emission sources on European air pollution levels. Atmos. Chem. Phys., 18, 13655–13672, https://doi.org/10.5194/acp-18-13655-2018, 2018.

Kaiser, J. W., Heil, A., Andreae, M. O., Benedetti, A., Chubarova, N., Jones, L., Morcrette, J.-J., Razinger, M., Schultz, M. G., Suttie, M., and van der Werf, G. R.: Biomass burning emissions estimated with a global fire assimilation system based on observed fire radiative power, Biogeosciences, 9, 527–554, https://doi.org/10.5194/bg-9-527-2012, 2012.

Kaiser, J., Wolfe, G. M., Min, K. E., Brown, S. S., Miller, C. C., Jacob, D. J., de Gouw, J. A., Graus, M., Hanisco, T. F., Holloway, J., Peischl, J., Pollack, I. B., Ryerson, T. B., Warneke, C., Washenfelder, R. A., and Keutsch, F. N.: Reassessing the ratio of glyoxal to formaldehyde as an indicator of hydrocarbon precursor speciation, Atmos. Chem. Phys., 15, 7571–7583, https://doi.org/10.5194/acp-15-7571-2015, 2015.

Kalivitis, N., Gerasopoulos, E., Vrekoussis, M., Kouvarakis, G., Kubilay, N., Hatzianastassiou, N., Vardavas, I. and Mihalopoulos, N, Dust transport over the eastern Mediterranean derived from Total Ozone Mapping Spectrometer, Aerosol Robotic Network, and surface measurements, Journal of Geophysical Research-Atmospheres 112(D3),). 2007.

Kalnay, E., Kanamitsu, M., Kistler, R., Collins, W., Deaven, D., Gandin, L., Iredell, M., Saha, S., White, G., Woollen, J., Zhu, Y., Leetmaa, A., Reynolds, B., Chelliah, M., Ebisuzaki, W., Higgins, W., Janowiak, J., Mo, K. C., Ropelewski, C., Wang, J., Jenne, R., and Joseph, D. : The NCEP/NCAR 40-year reanalysis project, Bull. Amer. Meteor. Soc., 77, 437-470, 1996.

Kanakidou, M., Mihalopoulos, N., Kindap, T., Im, U.,Vrekoussis, M., Gerasopoulos, E., Dermitzaki, E., Unal, A., Koçak, M., Markakis, K., Melas, D., Kouvarakis, G., Youssef, A.F., Richter, A., Hatzianastassiou, N., Hilboll, A., Ebojie, F., Wittrock, F., von Savigny, C., Burrows, J.P., Ladstaetter-Weissenmayer, A., Moubasher, H.: Megacities as hot spots of air pollution in the East Mediterranean, Atmospheric Environment, 45, 1223-1235, 2011.

Kerkweg, A. & Jöckel, P.: The 1-way on-line coupled atmospheric chemistry model system MECO(n) – Part 2: On-line coupling with the Multi-Model-Driver (MMD), Geoscientific Model Development, 5, 111–128, doi: 10.5194/gmd-5-111-2012, URL http://www.geosci-model-dev.net/5/111/2012/, 2012

Kluge, F., Hüneke, T., Knecht, M., Lichtenstern, M., Rotermund, M., Schlager, H., Schreiner, B., and Pfeilsticker, K.: Profiling of formaldehyde, glyoxal, methylglyoxal, and CO over the Amazon: normalized excess mixing ratios and related emission factors in biomass burning plumes, Atmos. Chem. Phys., 20, 12363–12389, https://doi.org/10.5194/acp-20-12363-2020, 2020.

Klausner, T. M., Aircraft-based in situ measurements of CH_4 and CO_2 downstream of European and Asian urban centres at local to synoptic scales. Dissertation, LMU München: Fakultät für Physik, doi: 10.5282/edoc.26983, 2020.

Klausner, T., Mertens, M., Huntrieser, H., Galkowski, M., Kuhlmann, G., Baumann, R., Fiehn, A., Jöckel P., Pühl, M., and Roitger, A.:. Urban greenhouse gas emissions from the Berlin area: A case study using airborne CO_2 and CH_4 in situ observations in summer 2018. Elem Sci Anth, 8: 15, doi.org/10.1525/elementa.411, 2020.

Kuc, T., Rozanski, K., Zimnoch, M., Necki, J.M., and Korus, A.: Anthropogenic emissions of CO2 and CH4 in an urban environment, Applied Energy ~~2003~~, 75 (3-4), 193–203. DOI: 10.1016/S0306-2619(03)00032-1, 2003.

Kunkel, D., M. G. Lawrence, H. Tost, A. Kerkweg, P. Jöckel, and Borrmann S.: Urban emission hot spots as sources for remote aerosol deposition, Geophys. Res. Lett., 39, L01808, doi: 10.1029/2011GL049634, 2012.

Laborde, M., Crippa, M., Tritscher, T., Jurányi, Z., Decarlo, P. F., Temime-Roussel, B., Marchand, N., Eckhardt, S., Stohl, A., Baltensperger, U., Prévôt, A. S. H., Weingartner, E., and Gysel, M.: Black carbon physical properties and mixing state in the European megacity Paris, Atmos. Chem. Phys., 13, 5831–5856, https://doi.org/10.5194/acp-13-5831-2013, 2013.

Lai, C., Liu, Y., Ma, J., Ma, Q., He, H.: Degradation kinetics of levoglucosan initiated by hydroxyl radical under different environmental conditions, Atmospheric Environment, 91, 32-39, doi.org/10.1016/j.atmosenv.2014.03.054, 2014.

Lambe, A. T., Onasch, T. B., Massoli, P., Croasdale, D. R., Wright, J. P., Ahern, A. T., Williams, L. R., Worsnop, D. R., Brune, W. H., and Davidovits, P.: Laboratory studies of the chemical composition and cloud condensation nuclei (CCN) activity of secondary organic aerosol (SOA) and oxidized primary organic aerosol (OPOA), Atmos. Chem. Phys., 11, 8913–8928, doi.org/10.5194/acp-11-8913-2011, 2011.

Lawrence, M.G., Butler, T.M., Steinkamp, J., Gurjar, B.R., and J. Lelieveld: Regional pollution potentials of megacities and other major population centers, Atmos. Chem. Phys., 7, 3969–3987, doi:10.5194/acp-7-3969-2007, 2007.

Lawrence, M.G., and Lelieveld, J.: Atmospheric pollutant outflow from southern Asia: a review, Atmos. Chem. Phys., 10, 11017–11096, doi:10.5194/acp-10-11017-2010, 2010.

Lelieveld, J., Berresheim, H., Borrmann, S., Crutzen, P.J., Dentener, F.J., Fischer, H., et al.: Global air pollution crossroads over the Mediterranean. Science 298, 794, doi: 10.1126/science.1075457, 2002.

Lelieveld, J., Evans, J., Fnais, M., Giannadaki, D., and Pozzer, A.,: The Contribution of Outdoor Air Pollution Sources to Premature Mortality on a Global Scale, Nature, vol. 525, pp. 367-371, 2015.

Lelieveld, J., Klingmüller, K., Pozzer, A., Burnett, R. T., Haines, A., and Ramanathan, V.: Effects of fossil fuel and total anthropogenic emission removal on public health and climate, P. Natl. Acad. Sci. USA, 116, 7192–7197, https//doi.org/ 10.1073/pnas.1819989116, 2019.

Lelieveld, J., Pozzer, A., Pöschl, U., Fnais, M., Haines, A., and Münzel, T.: Loss of life expectancy from air pollution compared to other risk factors: a worldwide perspective, Cardiovascular Research, 116, 1910-1917, ~~2020,~~ doi: 10.1093/cvr/cvaa025, 2020.

Leung, D. M., Tai, A. P. K., Mickley, L. J., Moch, J. M., Van Donkelaar, A., Shen, L. and Martin, R. V., Synoptic meteorological modes of variability for fine particulate matter (PM2.5) air quality in major metropolitan regions of China, Atmospheric Chemistry and Physics, 18(9), pp. 6733–6748. doi: 10.5194/acp-18-6733-2018, 2018.

Lian, J., Bréon, F.-M., Broquet, G., Zaccheo, T.S., Dobler, J., Ramonet, M., Staufer, J., Santaren, D., Xueref-Remy, I., and Ciais, P.: Analysis of temporal and spatial variability of atmospheric CO2 concentration within Paris from the GreenLITE TM laser imaging experiment, Atmos. Chem. Phys. Discuss. https://doi.org/10.5194/acp-2019-547, 2019~~2019. https://doi.org/10.5194/acp-2019-547, in review~~.

Liu, D., Allan, J. D., Young, D. E., Coe, H., Beddows, D., Fleming, Z. L., Flynn, M. J., Gallagher, M. W., Harrison, R. M., Lee, J., Prevot, A. S. H., Taylor, J. W., Yin, J., Williams, P. I., and Zotter, P.: Size distribution, mixing state and source apportionment of black carbon aerosol in London during wintertime, Atmos. Chem. Phys., 14, 10061–10084, https://doi.org/10.5194/acp-14-10061-2014, 2014.

Mallaun, C., Giez, A. and Baumann, R.: Calibration of 3-D wind measurements on a single engine research aircraft Atmos. Meas. Tech., 8, 3177-3196, doi: 10.5194/amt-8-3177-2015, 2015.

Mar, K.A., Putting the brakes on climate change – it's about more than just CO_2., Climanosco Research Articles 3, https://doi.org/10.37207/CRA.3.1, 2021.

Mayer, M., Wang, C., Webster, M., and Prinn, R. G.: Linking local air pollution to global chemistry and climate, J. Geophys. Res., 105, 22869–22896, 2000.

Mei, L. L., Rozanov, V., Vountas, M., Burrows, J., Levy, R., Lotz, W., Retrieval of aerosol optical properties using MERIS observations: algorithm and some first results, Remote Sensing of Environment,, doi.:10.1016/ j.rse.2016.11.015, 197, 125-140, 2017a

Mei, L. L., Rozanov, V., Vountas, M., Burrows, J., Levy, R., Lotz, W., A Cloud masking algorithm for the XBAER aerosol retrieval using MERIS data, Remote Sensing of Environment doi.: 10.1016/j.rse.2016.11.016,197, 141-160, 2017b

Melchiorri, M.; Florczyk, A.J.; Freire, S.; Ehrlich, D.; Schiavina, M.; Pesaresi, M.; Kemper, T. Megacities Spatiotemporal Dynamics Monitored with the Global Human Settlement Layer. In Proceedings of the REAL CORP 2018 Expanding Cities—Diminishing Space, Wien, Austria, 4–6 April 2018; Schrenk, M.,Popovisch, V.V., Zeile, P., Elisei, P., Beyer, C., Navratil, G., Eds.; CORP: Wien, Austria, 2018; pp. 285–294,2018.

Mertens, M., Kerkweg, A., Jöckel, P., Tost, H., & Hofmann, C.: The 1-way on-line coupled model system MECO(n) – Part 4: Chemical evaluation (based on MESSy v2.52), Geoscientific Model Development, 9, 3545–3567, doi: 10.5194/gmd-9-3545-2016, URL http://www.geosci-model-dev.net/9/3545/2016/, 2016.

Mertens, M., Kerkweg, A., Grewe, V., Jöckel, P., & Sausen, R.: Attributing ozone and its precursors to land transport emissions in Europe and Germany, Atmospheric Chemistry and Physics, 20, 7843–7873, doi: 10.5194/acp-20-7843-2020, URL https://www.atmos-chem-phys.net/20/7843/2020/, 2020.

Mertens, M., Kerkweg, A., Grewe, V., Jöckel, P., & Sausen, R.: Are contributions of emissions to ozone a matter of scale? – a study using MECO(n) (MESSy v2.50), Geoscientific Model Development, 13, 363–383, doi: 10.5194/gmd-13-363-2020, URL https://www.geosci-model-dev.net/13/363/2020/, 2020.

Millán, M.M., Salvador, R., Mantilla, E., Kallos, G.: Photooxidant dynamics in the Mediterranean basin in summer: Results from European research projects, Journal of Geophysical Research, 102, N0. D7, 8811-8823, 1997.

Millán, M. M., Mantilla, E., Salvador, R., Carratalá, A., Sanz, M. J., Alonso, L., Gangoiti, G., and Navazo, M.: Ozone Cycles in the Western Mediterranean Basin: Interpretation of Monitoring Data in Complex Coastal Terrain**.** Journal of Applied Meteorology, 39: 487-508. 2000.

Monks, P. S., Granier, C., Fuzzi, S., Stohl, A., Williams, M. L., Akimoto, H., Amann, M., Baklanov, A., Baltensperger, U., Bey, I., Blake, N., Blake, R. S., Carslaw, K., Cooper, O. R., Dentener, F., Fowler, D., Fragkou, E., Frost, G. J., Generoso, S., Ginoux, P., Grewe, V., Guenther, A., Hansson, H. C., Henne, S., Hjorth, J., Hofzumahaus, A., Huntrieser, H., Isaksen, I. S. A., Jenkin, M . E., Kaiser, J., Kanakidou, M., Klimont, Z., Kulmala, M., Laj, P., Lawrence, M. G., Lee, J. D., Liousse, C., Maione, M., McFiggans, G., Metzger, A., Mieville, A., Moussiopoulos, N. Orlandou, J. J., O'Dowd, C. D., Palmer, P. I., Parrish, D. D., Petzold, A., Platt, U., Pöschl, U., Prévôt, A. S. H., Reeves, C. E., Reimann, S., Rudich, Y., Sellegri, K., Steinbrecher, R., Simpson, D., ten Brink, H., Theloke, J., van der Werf, G. R., Vautard, R., Vestreng, V., Vlachokostas, Ch., von Glasow,R.: Atmospheric composition change-global and regional air quality, Atmospheric Environment, 43, 5268–5350, doi:10.1016/j.atmosenv.2009.08.021, 2009.

Myriokefalitakis, S., Vrekoussis, M., Tsigaridis, K., Wittrock, F., Richter, A., Brühl, C., Volkamer, R., Burrows, JP., and Kanakidou, M: Influence of natural and anthropogenic secondary sources on the glyoxal global distribution, Atmos. Chem. Phys., 8, 4965-4981, 2008.

Ng, N. L., Canagaratna, M. R., Zhang, Q., Jimenez, J. L., Tian, J., Ulbrich, I. M., Kroll, J. H., Docherty, K. S., Chhabra, P. S., Bahreini, R., Murphy, S. M., Seinfeld, J. H., Hildebrandt, L., Donahue, N. M., DeCarlo, P. F., Lanz, V. A., Prévôt, A. S. H., Dinar, E., Rudich, Y., and Worsnop, D. R.: Organic aerosol components observed in Northern Hemispheric datasets from Aerosol Mass Spectrometry, Atmos. Chem. Phys., 10, 4625–4641, doi.org/10.5194/acp-10-4625-2010, 2010.

Ng, N. L., Canagaratna, M. R., Jimenez, J. L., Chhabra, P. S., Seinfeld, J. H., and Worsnop, D. R.: Changes in organic aerosol composition with aging inferred from aerosol mass spectra, Atmos. Chem. Phys., 11, 6465–6474, doi.org/10.5194/acp-11-6465-2011, 2011.

Odendahl, C., Springford, J., Johnson, S. and J. Murray: The big European sort? The diverging fortunes of Europe's regions, Centre for European Reform, www.cer.eu; 2019.

O'Shea, S.J., Allen, G., Fleming, Z.L., Bauguitte, S.J.-B., Percival, C.J., Gallagher, M.W., Lee, J., Helfter, C., and Nemitz, E.: Area fluxes of carbon dioxide, methane, and carbon monoxide derived from airborne measurements around Greater London: A case study during summer 2012, J. Geophys. Res. 119 (8), 4940–4952. doi: 10.1002/2013JD021269, 2014.

Paulot, F., Wunch, D., Crounse, J. D., Toon, G. C., Millet, D. B., DeCarlo, P. F., Vigouroux, C., Deutscher, N. M., González Abad, G., Notholt, J., Warneke, T., Hannigan, J. W., Warneke, C., de Gouw, J. A., Dunlea, E. J., De Mazière, M., Griffith, D. W. T., Bernath, P., Jimenez, J. L., and Wennberg, P. O.: Importance of secondary sources in the atmospheric budgets of formic and acetic acids, Atmos. Chem. Phys., 11, 1989–2013, https://doi.org/10.5194/acp-11-1989-2011, 2011.

Pappalardo et al., EARLINET: towards an advanced sustainable European aerosol lidar network, Atmos. Meas. Tech., 7, 2389-2409, doi:10.5194/amt-7-2389-2014, 2014.

Paz, S., Goldstein, P., Kordova-Biezuner, L. et al. Differences in Benzene Patterns Among Traffic and Industrial Areas and a Prediction Model for Benzene Rates Based on NOx Values. Water Air Soil Pollut 226, 161, doi.org/10.1007/s11270-015-2406-6, 2015.

Pey, J., Querol, X., Alastuey, A., Forastiere, F., and Stafoggia, M.: African dust outbreaks over the Mediterranean Basin during 2001–2011: PM10 concentrations, phenomenology and trends, and its relation with synoptic and mesoscale meteorology, Atmos. Chem. Phys., 13, 1395–1410, doi:10.5194/acp-13-1395-2013, 2013.

Pikridas, M., Vrekoussis, M., Sciare, J., Mihalopoulos, N, Kleanthous, S., and Savvidis, C, Spatial and temporal (short and long-term) variability of submicron, fine and sub-10 μm particulate matter (PM1, PM2.5, PM10) in Cyprus, Atmos. Environ., 191:79–93, 2018. doi:10.1016/j.atmosenv.2018.07.048, 2018.

Pitt, J.R., Allen, G., Bauguitte, S.J.-B., Gallagher, M.W., Lee, J.D., Drysdale, W., Nelson, B., Manning, A.J., and Palmer, P.I.: Assessing London CO2, CH4 and CO emissions using aircraft measurements and dispersion modelling, Atmos. Chem. Phys. 2019, 19 (13), 8931–8945. DOI: 10.5194/acp-19-8931-2019.

Pöhlker, M. L., Pöhlker, C., Ditas, F., Klimach, T., Hrabe de An-gelis, I., Araújo, A., Brito, J., Carbone, S., Cheng, Y., Chi, X.,Ditz, R., Gunthe, S. S., Kesselmeier, J., Könemann, T., Lavriˇc,J. V., Martin, S. T., Mikhailov, E., Moran-Zuloaga, D., Rose, D.,Saturno, J., Su, H., Thalman, R., Walter, D., Wang, J., Wolff,S., Barbosa, H. M. J., Artaxo, P., Andreae, M. O., and Pöschl,U.: Long-term observations of cloud condensation nuclei in theAmazon rain forest – Part 1: Aerosol size distribution, hygro-scopicity, and new model parametrizations for CCN prediction, Atmos. Chem. Phys., 2016.

Pöhlker, M. L., Ditas, F., Saturno, J., Klimach, T., Hrabˇe de Ange-lis, I., Araùjo, A. C., Brito, J., Carbone, S., Cheng, Y., Chi, X.,Ditz, R., Gunthe, S. S., Holanda, B. A., Kandler, K., Kesselmeier,J., Könemann, T., Krüger, O. O., Lavriˇc, J. V., Martin, S. T.,Mikhailov, E., Moran-Zuloaga, D., Rizzo, L. V., Rose, D., Su, H.,Thalman, R., Walter, D., Wang, J., Wolff, S., Barbosa, H. M. J., Artaxo, P., Andreae, M. O., Pöschl, U., and Pöhlker, C.: Long-term observations of cloud condensation nuclei over the Amazon rain~~Amazonrain~~ forest – Part 2: Variability and characteristics of biomass burning~~biomassburning~~, long-range transport, and pristine rain forest aerosols, Atmos. Chem. Phys., 2018.

Pöhlker, C., Walter, D., Paulsen, H., Könemann, T., Rodríguez-Caballero, E., Moran-Zuloaga, D., Brito, J., Carbone, S., Degrendele, C., Després, V. R., Ditas, F., Holanda, B. A., Kaiser, J. W., Lammel, G., Lavrič, J. V., Ming, J., Pickersgill, D., Pöhlker, M. L., Praß, M., Löbs, N., Saturno, J., Sörgel, M., Wang, Q., Weber, B., Wolff, S., Artaxo, P., Pöschl, U., and Andreae, M. O.: Land cover and its transformation in the backward trajectory footprint region of the Amazon Tall Tower Observatory, Atmos. Chem. Phys., 19, 8425–8470, https://doi.org/10.5194/acp-19-8425-2019, 2019.

Pöschl, U.: Atmospheric aerosols: Composition, transformation, climate and health effects, Angew. Chem. Int. Ed., 44(46), 7520–7540, doi:10.1002/anie.200501122, doi: 10.1002/anie.200501122, 2005.

Ramanathan V., Crutzen P. J., Kiehl J. T., Rosenfeld D.: Aerosols, climate, and the hydrological cycle. Science 294:2119–2124, DOI: 10.1126/science.1064034, 2001.

Reddington, C.L., McMeeking G., Mann, G.W. Coe, H., Frontoso M. G, Liu, D., Flynn, M., Spracklen, D.V., and Carslaw, K.S.: The mass and number size distributions of black carbon aerosol over Europe, Atmos. Chem. Phys., 13, 4917-4939, 2013.

Rautenhaus, M., G. Bauer, and A. Dörnbrack,: A web service based tool to plan atmospheric research flights. Geosci. Model Dev., 5, 55–71, doi.org/10.5194/gmd-5-55-2012. 2012.

Ren, Yu, Schlager, H., Martin D.: The Application of TD/GC/NICI–MS with an Al2O3-PLOT-S Column for the Determination of Perfluoroalkylcycloalkanes in the Atmosphere. Chromatographia, 77, pp 309-316. doi: 10.1007/s10337-013-2584-6., 2013.

Ren, Y., Baumann, R., Schlager, H.: An airborne perfluorocarbon tracer system and its first application for a Lagrangian experiment. Atmos. Meas. Tech., 8, 69-80. doi: 10.5194/ amt-8-69-2015, 2015.

Richter, A., Burrows, J. P., Nüß, H., Granier, C, Niemeier, U., Increase in tropospheric nitrogen dioxide over China observed from space, Nature, 437, 129-132, doi: 10.1038/nature04092, 2005.

Richter, A., Begoin, M., Hilboll, A., and Burrows, J. P.: An improved NO_2 retrieval for the GOME-2 satellite instrument, Atmos. Meas. Tech. , 4, 1147-1159, doi:10.5194/amt-4-1147-2011, 2011.

Roiger, A., Aufmhoff, H., Stock, P., Arnold, F., Schlager, H.: An aircraft-borne chemical ionization – ion trap mass spectrometer (CI-ITMS) for fast PAN and PPN measurements. Atmos. Meas.Tech., 4, 173-188. DOI: 10.5194/amt-4-173-2011, 2011.

Rolph, G., Stein, A., and Stunder, B.,: Real-time Environmental Applications and Display sYstem: READY. Environmental Modelling & Software, 95, 210-228, https://doi.org/10.1016/j.envsoft.2017.06, 2017.

Rosenfeld, D., Lohmann, U., Raga, G. B., O'Dowd, C. D., Kulmala, M., Fuzzi, S., Reissell, A., and Andreae, M. O.: Flood or drought: How do aerosols affect precipitation?, Science, 321, 1309-1313, 10.1126/science.1160606, 2008.

Rudolph, J., Czuba, E., and Huang, L.: The stable carbon isotope fractionation for reactions of selected hydrocarbons with OH-radicals and its relevance for atmos-pheric chemistry, J. Geophys. Res., 105, 29329–29346, doi:10.1029/2000JD900447, 2000.

Schneider, J., Weimer, S., Drewnick, F., Borrmann, S., Helas, G., Gwaze, P., Schmid, O., Andreae, M. O. and Kirchner, U.: Massspectrometric analysis and aerodynamic properties of various types of combustion-related aerosol particles, Int. J. Mass. Spec.,258, 37–49, doi.org/10.1016/j.ijms.2006.07.008, 2006.

Schroder, J. C., Campuzano-Jost, P., Day, D. A., Shah, V., Larson, K., Sommers, J. M., et al: ~~. (2018).~~ Sources and secondary production of organic aerosols in the northeastern United States during WINTER. Journal of Geophysical Research: Atmospheres, 123, 7771– 7796. doi.org/10.1029/2018JD028475, 2018.

Schulz, C., Schneider, J., Holanda, B. A., Appel, O., Costa, A., de Sá, S.S., Dreiling, V. Fütterer, D., Jurkat-Witschas, T., Klimach, T., Knote, C., Krämer, M., Martin, S.T., Mertes, S., Pöhlker, M.L., Sauer, D., Voigt, C., Walser, A., Weinzierl, A.B., Ziereis, H., Zöger, M., Andreae, M.O., Artaxo, P., Machado, L-A.T., Pöschl, U., Wendisch, M., and S. Borrmann, Aircraft-based observations of isoprene-epoxydiol-derived secondary organic aerosol (IEPOX-SOA) in the tropical upper troposphere over the Amazon region. Atmos. Chem. Phys., 18, 14979–15001, ~~2018, https://~~doi.org/ 10.5194/acp-18-14979-2018, 2018.

Schumann, U.: Measurement and model data comparisons for the HALO-FAAM formation flight during EMeRGe on 17 July 2017, DLR FB 2020-48, doi.:10.5281/zenodo.4427965, 2020.

Schwarz, J. P., Gao, R.S., Spackman,J.R., Watts, L.A., Thomson, D.S., Fahey, D.W., Ryerson, T.B., Peischl, J., Holloway, J.S., Trainer, M., Frost, G.J., Baynard, T., Lack, D.A., de Gouw, J.A., Warneke, C., and Del Negro, L.A.: Measurement of the mixing state, mass, and optical size of individual black carbon particles in urban and biomass burning emissions, Geophys. Res. Lett., 35, L13810, doi:10.1029/ 2008GL033968, 2008.

Shaw, M. D., Lee, J. D., Davison, B., Vaughan, A., Purvis, R. M., Harvey, A., Lewis, A. C., and Hewitt, C. N.: Airborne determination of the tempo-spatial distribution of benzene, toluene, nitrogen oxides and ozone in the boundary layer across Greater London, UK, Atmos. Chem. Phys., 15, 5083–5097, doi.org/10.5194/acp-15-5083-2015, 2015.

Silver, B., Reddington, C.L., Arnold, S.R., and Spracklen: Substantial changes in air pollution across China during 2015-2017, Environ. Res. Lett. 13, 114012, 2018.

Simpson, I. J., Akagi, S. K., Barletta, B., Blake, N. J., Choi, Y., Diskin, G. S., Fried, A., Fuelberg, H. E., Meinardi, S., Rowland, F. S., Vay, S. A., Weinheimer, A. J., Wennberg, P. O., Wiebring, P., Wisthaler, A., Yang, M., Yokelson, R. J., and Blake, D. R.: Boreal forest fire emissions in fresh Canadian smoke plumes: C1-C10 volatile organic compounds (VOCs), CO_2, CO, NO_2, NO, HCN and CH_3CN, Atmos. Chem. Phys., 11, 6445–6463, https://doi.org/10.5194/acp-11-6445-2011, 2011.

Speidel, M., Nau, R., Arnold, F., Schlager, H., A. Stohl, Sulfur dioxide measurements in the lower, middle and upper troposphere: Deployment of an aircraft-based chemical ionization mass spectrometer with permanent in-flight calibration, Atmospheric Environment, 41, 2427-2437, doi:10.1016/j.atmosenv. 2006.07.047. 2007.

Stein, A.F., Draxler, R.R, Rolph, G.D., Stunder, B.J.B., Cohen, M.D., and Ngan, F.: NOAA's HYSPLIT atmospheric transport and dispersion modeling system, Bull. Amer. Meteor. Soc., 96, 2059-2077, doi.org/10.1175/BAMS-D-14-00110.1, 2015.

Stohl, A., Wotawa, G. Seibert, P. and Kromp-Kolb H.: Interpolation errors in wind fields as a function of spatial and temporal resolution and their impact on different types of kinematic trajectories. J. Appl. Meteor. 34, p. 2149-2165, 1995.

Stohl, A., Haimberger, L., Scheele, M.P. and Wernli, H.: An intercomparison of results from three trajectory models. Meteorol. Applications 8, 127-135, 1999.

Stohl, A., Eckhardt, S., Forster, C., James, P., and Spichtinger, N.: On the pathways and timescales of intercontinental air pollution transport. J. Geophys. Res., 107(D23), 4684, doi:10.1029/2001JD001396, 2002.

Stohl, A., Forster, C., Eckhardt, S., Spichtinger, N., Huntrieser, H., Heland, J., Schlager, H., Wilhelm, S., Arnold, F., and Cooper, O.: A backward modeling study of intercontinental pollution transport using aircraft measurements. J. Geophys. Res., 108(D12), 4370, doi:10.1029/2002JD002862, 2003.

Tan, Z., Fuchs, H., Lu, K., Hofzumahaus, A., Bohn, B., Broch, S., Dong, H., Gomm, S., Häseler, R., He, L., Holland, F., Li, X., Liu, Y., Lu, S., Rohrer, F., Shao, M., Wang, B., Wang, M., Wu, Y., Zeng, L., Zhang, Y., Wahner, A., and Zhang, Y.: Radical chemistry at a rural site (Wangdu) in the North China Plain: observation and model calculations of OH, HO2 and RO2 radicals, Atmos. Chem. Phys., 17, 663–690, https://doi.org/10.5194/acp-17-663-2017, 2017.

Taraborrelli, D., Cabrera-Perez, D., Bacer, S., Gromov, S., Lelieveld, J., Sander, R., and Pozzer, A.: Influence of aromatics on tropospheric gas-phase composition, Atmos. Chem. Phys. Discuss., https://doi.org/10.5194/acp-2020-461, 2020.

Thieuleux, F., Moulin, C., Bréon, F. M. , Maignan, F., Poitou, J. , and Tanré, D.: Remote Sensing of Aerosols over the oceans using MSG/SEVIRI Imagery, Ann. Geophys., 23, 3561-3568, doi:10.5194/angeo-23-3561-2005, 2005.

Titos, G., Ealo, M., Román, R., Cazorla, A., Sola, Y., Dubovik, O., Alastuey, A., Pandolfi, M.: Retrieval of aerosol properties from ceilometer and photometer measurements: long-term evaluation with in situ data and statistical analysis at Montsec (southern Pyrenees), Atmos. Meas. Tech., https://doi.org/10.5194/amt-12-3255-2019.

Turco, M. et al., : Exacerbated Fires in Mediterranean Europe Due to Anthropogenic Warming Projected with Non-Stationary Climate-Fire Models, Nature Communications 9, no. 1, ~~(December 2018):~~ 3821, https://doi.org/10.1038/s41467-018-06358-z, 2018.

United Nations, Department of Economic and Social Affairs, Population Division World Urbanization Prospects: The 2018 Revision (ST/ESA/SER.A/420). New York: United Nations, 2019.

United Nations Environment Programme (UNEP), World Meteorological Organization (WMO), Integrated Assessment of Black Carbon and Tropospheric Ozone, ISBN:92-807-3141-6, 2011.

Viidanoja, J., Reiner, T. and Arnold, F: Laboratory investigations of negative ion molecule reactions of formic and acetic acids: Implications for atmospheric measurements by Ion Molecule Reaction Mass Spectrometry, Int. J. Mass Spectrom., 181, 31-41, 1998.

Volz-Thomas, A., Xueref, I., and Schmitt, R.: Automatic gas chromatograph and calibration system for ambient measurements of PAN and PPN, Environ. Sci. Poll. Res., 9, 72-76, 2001.

von der Weiden-Reinmüller, S.-L., Drewnick, F., Zhang, Q. J., Freutel, F., Beekmann, M., and Borrmann, S.: Megacity emission plume characteristics in summer and winter investigated by mobile aerosol and trace gas

measurements: the Paris metropolitan area, Atmos. Chem. Phys., 14, 12931–12950, https://doi.org/10.5194/acp-14-12931-2014, 2014.

Vrekoussis, M., Wittrock, F., Richter, A., Burrows, J.P: Temporal and spatial variability of glyoxal as observed from space" Atmos. Chem. Phys., 9, 4485-4504, 2009.

Vrekoussis, M., Richter, A., Hilboll, A., Burrows, J. P., Gerasopoulos, E., Lelieveld, J., Barrie, L., Zerefos, C., and Mihalopoulos, N. Economic crisis detected from space: Air quality observations over Athens/Greece, Geophys. Res. Lett., 40, 458– 463, doi:10.1002/grl.50118. 2013.

Whalley, L. K., Stone, D., Dunmore, R., Hamilton, J., Hopkins, J. R., Lee, J. D., Lewis, A. C., Williams, P., Kleffmann, J., Laufs, S., Woodward-Massey, R., and Heard, D. E.: Understanding in situ ozone production in the summertime through radical observations and modelling studies during the Clean air for London project (ClearfLo), Atmos. Chem. Phys., 18, 2547–2571, https://doi.org/10.5194/acp-18-2547-2018, 2018.

Whalley, L. K., Slater, E. J., Woodward-Massey, R., Ye, C., Lee, J. D., Squires, F., Hopkins, J. R., Dunmore, R. E., Shaw, M., Hamilton, J. F., Lewis, A. C., Mehra, A., Worrall, S. D., Bacak, A., Bannan, T. J., Coe, H., Percival, C. J., Ouyang, B., Jones, R. L., Crilley, L. R., Kramer, L. J., Bloss, W. J., Vu, T., Kotthaus, S., Grimmond, S., Sun, Y., Xu, W., Yue, S., Ren, L., Acton, W. J. F., Hewitt, C. N., Wang, X., Fu, P., and Heard, D. E.: Evaluating the sensitivity of radical chemistry and ozone formation to ambient VOCs and NOx in Beijing, Atmos. Chem. Phys., 21, 2125–2147, https://doi.org/10.5194/acp-21-2125-2021, 2021.

Warneke, C., van der Veen, C., Luxembourg, S., de Gouw, J.A,. Kok A.: Measurements of benzene and toluene in ambient air using proton-transfer-reaction mass spectrometry: calibration, humidity dependence, and field intercomparison, International Journal of Mass Spectrometry, Volume 207, Issue 3, doi.org/10.1016/S1387-3806(01)00366-9, 2001.

Warneke, C., McKeen, S. A., de Gouw, J. A., Goldan, P. D., Kuster, W. C., Holloway, J. S., Williams, E. J., Lerner, B. M., Parrish, D. D., Trainer, M., Fehsenfeld, F. C, Kato, S, Atlas, E. L, Baker, A, and Blak, D. R.: Determination of urban volatile organic compound emission ratios and comparison with an emissions database, J. Geophys. Res., 112, D10S47, doi:10.1029/2006JD007930, 2007.

Warneke, C., Froyd, K. D., Brioude, J., Bahreini, R., Brock, C. A., Cozic, J. , de Gouw, J. A., Fahey, D. W., Ferrare, R., Holloway, J. S., Middlebrook, A. M., Miller, L., Montzka, S., Schwarz, J. P., Sodemann, H., Spackman, J. R., and Stohl, A.: An important contribution to springtime Arctic aerosol from biomass burning in Russia, Geophys. Res. Lett., 37, L01801, doi:10.1029/2009GL041816, 2010.

Wendisch, M., et al.: The ACRIDICON-CHUVA campaign: Studying tropical deep convective clouds and precipitation over Amazonia using the new German research aircraft HALO, Bull. Amer. Meteorol. Soc., 97, 1885-1908, doi: 10.1175/BAMS-D-14-00255, 2016.

Wennberg, P. O., Bates, K. H., Crounse, J. D., Dodson, L. G., Mc-Vay, R. C., Mertens, L. A., Nguyen, T. B., Praske, E., Schwantes, R. H., Smarte, M. D., St Clair, J. M., Teng, A. P., Zhang, X., and Seinfeld, J. H.: Gas-Phase Reactions of Isoprene and Its Major Oxidation Products, Chem. Rev., 118, 3337–3390, doi.:10.1021/acs.chemrev.7b00439, 2018.

Winkler J., Blank, P., Glaser, K., Gomes, J.A.G., Habram, M., Jambert, C., Jaeschke, W-. Konrad, S., Kurtenbach, R., Lenschow, P., Lörzer, J.C., Perros, P.E., Pesch, M., Prümke, H.J., Rappenglück, B., Schmitz, Th., Slemr, F., Volz-Thomas, A., and Wickert, B.: Ground-Based and Airborne Measurements of Nonmethane Hydrocarbons in BERLIOZ: Analysis and Selected Results, Journal of Atmospheric Chemistry 42: 465–492, 2002.

Wintel, J., Hösen, E., Koppmann, R., Krebsbach, M., Hofzumahaus, A., and Rohrer, F.:Stable carbon isotope ratios of toluene in the boundary layer and the lower free troposphere, Atmos. Chem. Phys., 13, 11059-11071, doi:10.5194/acp-13-11059-2013, 2013.

World Health Organization (WHO), Review of evidence on health aspects of air pollution – REVIHAPP Project. WHO Regional Office for Europe, Copenhagen, Denmark, 2013.

Zahn, A., Weppner, J., Widmann, H., Schlote-Holubek, K., Burger, B., Kühner, T., Franke, H.: A fast and precise chemiluminescence ozone detector for eddy flux and airborne application, Atmos. Meas. Tech., 5 (2), 363–375. doi:10.5194/amt-5-363-2012, 2012.

Zhang, Y. H., Su, H., Zhong, L. J., Cheng, Y. F., Zeng, L. M., Wang, X. S., Xiang, Y. R., Wang, J. L., Gao, D. F., Shao, M., Fan, S. J., and Liu, S. C.: Regional ozone pollution and observation-based approach for analyzing ozone–precursor relationship during the PRIDE-PRD2004 campaign, Atmos. Environ., 42, 6203–6218, https://doi.org/10.1016/j.atmosenv.2008.05.002, 2008.

Zhu, T., Melamed, M., Parrish, D. Gauss, M., Gallardo Klenner, L., Lawrence, M., Konare, A. and Liousse, C.: Impacts of Megacities on air pollution and climate, WMO/ IGAC, GAW Report No.205, 2012.

Ziereis, H., Minikin, A., Schlager, H., Gayet, J.F., Auriol, F., Stock, P., Baehr, J., Petzold, A., Schumann, U., Weinheimer, A., Ridley, B., and Ström, J.: Uptake of reactive nitrogen on cirrus cloud particles during INCA, Geophys. Res. Lett., 31(5), 2004.

Zimnoch, M., Necki, J., Chmura, L., Jasek, A., Jelen, D., Galkowski, M., Kuc, T., Gorczyca, Z., Bartyzel, J., and Rozanski, K.: Quantification of carbon dioxide and methane emissions in urban areas: Source apportionment based on atmospheric observations, Mitig Adapt Strateg Glob Change 2019, 24 (6), 1051–1071. DOI: 10.1007/s11027-018-9821-0, 2019.